

REPORT PAPERS IN—

analytical techniques

economic geology

engineering hydrology

experimental hydrology

geochemistry

geochronology

geomorphology

geophysics

glaciology

herpetology

photography

stratigraphy

physical properties
of rocks

tertiary geology

quality of water

stratigraphy

structural geology

surface water

technical illustrations

theoretical hydrology

GEOLOGICAL SURVEY RESEARCH 1965

Chapter B

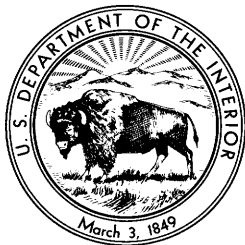


GEOLOGICAL SURVEY RESEARCH 1965

Chapter B

GEOLOGICAL SURVEY PROFESSIONAL PAPER 525-B

Scientific notes and summaries of investigations prepared by members of the Geologic, Water Resources, and Publications Divisions in geology, hydrology, and related fields



UNITED STATES GOVERNMENT PRINTING OFFICE, WASHINGTON: 1965

UNITED STATES DEPARTMENT OF THE INTERIOR

STEWART L. UDALL, Secretary

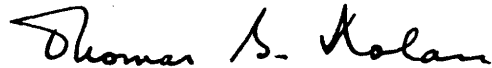
GEOLOGICAL SURVEY

Thomas B. Nolan, Director

FOREWORD

This collection of 41 short papers is the first of a series to be released as chapters of Geological Survey Research 1965. The papers report on scientific and economic results of current work by members of the Geologic, Publications, and Water Resources Divisions of the U.S. Geological Survey. Some of the papers present results of completed parts of continuing investigations; others announce new discoveries or preliminary results of investigations that will be discussed in greater detail in reports to be published in the future. Still others are scientific notes of limited scope, and short papers on techniques and instrumentation.

Chapter A of this series will be published later in the year, and will present a summary of results of work done during the present fiscal year.



THOMAS B. NOLAN,
Director.

CONTENTS

	Page
Foreword -----	III
GEOLOGIC STUDIES	
Geophysics	
The basalt-eclogite transformation and crustal structure in the Western United States, by L. C. Pakiser-----	B1
Geophysical evidence of a caldera at Bonanza, Colo., by D. E. Karig-----	9
Hawaiian seismic events during 1963, by R. Y. Koyanagi and E. T. Endo-----	13
Economic geology	
Correlation of zinc abundance with stratigraphic thickness variations in the Kingsport Formation, West New Market area, Mascot-Jefferson City mining district, Tennessee, by Helmuth Wedow, Jr., and J. R. Marie-----	17
Mercury-bearing antimony deposit between Big Creek and Yellow Pine, central Idaho, by B. F. Leonard-----	23
Suggestions for prospecting for evaporite deposits in southwestern Virginia, by C. F. Withington-----	29
Low-volatile bituminous coal of Mississippian age on the Lisburne Peninsula, northwestern Alaska, by I. L. Tailleux-----	34
Distribution of gravel in the Patuxent Formation in the Beltsville quadrangle, Prince Georges and Montgomery Counties, Md., by C. F. Withington-----	39
Structural geology and stratigraphy	
Structure of the Timber Mountain caldera, southern Nevada, and its relation to basin-range structure, by R. L. Christiansen, P. W. Lipman, P. P. Orkild, and F. M. Byers, Jr.-----	43
The Clinchport thrust fault—a major structural element of the southern Appalachian Mountains, by L. D. Harris-----	49
Correlation of Cretaceous and lower Tertiary rocks near Livingston, Mont., with those in other areas of Montana and Wyoming, by A. E. Roberts-----	54
Paleontology	
An Upper Cretaceous deposit in the Appalachian Mountains, by R. H. Tschudy-----	64
Classification of the superfamily Healdiacea and the genus <i>Pseudophanasymmetria</i> Sohn and Berdan, 1952 (Ostracoda), by I. G. Sohn-----	69
Stratigraphic distribution of the Late Cambrian mollusk <i>Matthevia</i> Walcott, 1885, by E. L. Yochelson, J. F. McAllister, and Anthony Reso-----	73
Petrology and petrography	
A classification for quartz-rich igneous rocks based on feldspar ratios, by J. T. O'Connor-----	79
Gold Flat Member of the Thirsty Canyon Tuff—a pantellerite ash-flow sheet in southern Nevada, by D. C. Noble-----	85
Precipitation and recycling of phosphate in the Florida land-pebble phosphate deposits, by Z. S. Altschuler-----	91
Geochemistry	
Distribution of tantalum in some igneous rocks and coexisting minerals of the Southern California batholith, by David Gottfried and J. I. Dinnin-----	96
Metallic copper in stony meteorites, by M. B. Duke and Robin Brett-----	101
Geochronology	
K-Ar and Rb-Sr ages of biotite from the Middle Jurassic part of the Carmel Formation, Utah, by R. F. Marvin, J. C. Wright, and F. G. Walthall-----	104
Potassium-argon ages of some plutonic rocks, Tenakee area, Chichagof Island, southeastern Alaska, by M. A. Lanphere, R. A. Loney, and D. A. Brew-----	104
Geomorphology and Pleistocene geology	
A large transitional rock glacier in the Johnson River area, Alaska Range, by H. L. Foster and G. W. Holmes-----	112
Dissected gravels of the Río Copiapó valley and adjacent coastal area, Chile, by Kenneth Segerstrom-----	117
Earth cracks—a cause of gullyng, by William Kam-----	122
Glacial deposits of Nebraskan and Kansan age in northern Kentucky, by M. M. Leighton and L. L. Ray-----	126
Age and origin of the Puget Sound trough in western Washington, by D. R. Crandell, D. R. Mullineaux, and H. H. Waldron-----	132

Glaciology

- | | |
|--|--------------|
| Rate of ice movement and estimated ice thickness in part of the Teton Glacier, Grand Teton National Park, Wyo., by J. C. Reed, Jr..... | Page
B137 |
|--|--------------|

Physical properties of rocks

- | | |
|---|-----|
| Use of magnetic susceptibility and grain density in identification of basalt flows at the Nevada Test Site, by K. A. Sargent..... | 142 |
| The best value of porosity of lapilli tuff from the Nevada Test Site, by G. E. Manger..... | 146 |

Analytical techniques

- | | |
|---|-----|
| Gamma activation device for low-level beryllium analysis, by W. W. Vaughn, W. G. Cramer, and W. N. Sharp..... | 151 |
| Use of X-ray fluorescence in determination of selected major constituents in silicates, by H. J. Rose, Jr., Frank Cuttitta, and R. R. Larson..... | 155 |
| The problem of automatic plate reading and computer interpretation for spectrochemical analysis, by A. W. Helz..... | 160 |
| A platinum-lined bomb for the high-temperature decomposition of refractory minerals, by Irving May, J. J. Rowe, and Raymond Letner..... | 165 |

HYDROLOGIC STUDIES**Quality of water**

- | | |
|---|-----|
| Rapid field and laboratory determination of phosphate in natural water, by M. J. Fishman and M. W. Skougstad..... | 167 |
| Leachable silica and alumina in streambed clays, by E. C. Mallory, Jr..... | 170 |

Surface water

- | | |
|--|-----|
| Growth of salt cedar (<i>Tamarix gallica</i>) in the Pecos River near the New Mexico-Texas boundary, by R. U. Grozier..... | 175 |
| Effect of Great Swamp, N.J., on streamflow during base-flow periods, by E. G. Miller..... | 177 |

Engineering hydrology

- | | |
|---|-----|
| Shortening and protrusion of a well casing due to compaction of sediments in a subsiding area in California, by J. F. Poland and R. L. Ireland..... | 180 |
|---|-----|

Experimental and theoretical hydrology

- | | |
|--|-----|
| Use of sodium iodide to trace underground water circulation in the hot springs and geysers of the Daisy geyser group, Yellowstone National Park, by J. J. Rowe, R. O. Fournier, and G. W. Morey..... | 184 |
| The algebra of stream-order numbers, by A. E. Scheidegger..... | 187 |

PUBLICATION TECHNIQUES**Technical illustrations**

- | | |
|--|-----|
| Photographic copying using reflection-transmission illumination, by E. P. Krier..... | 190 |
|--|-----|

INDEXES

- | | |
|----------------------|-----|
| Subject | 193 |
| Author | 195 |

THE BASALT-ECLOGITE TRANSFORMATION AND CRUSTAL STRUCTURE IN THE WESTERN UNITED STATES

By L. C. PAKISER, Denver, Colo.

Work done in part under Advanced Research Projects Agency Order 193-64

Abstract.—Comparison of geothermal gradients, crustal structure, and pressure-temperature relations for the basalt-eclogite transformation leads to the conclusion that the transformation zone may occur mainly within the crust in much of the Eastern United States and entirely within the mantle in much of the Western United States. The primitive crust that evolved from the mantle may have been silicic, later to have been made progressively more mafic.

The nature of the Mohorovicic discontinuity (M-discontinuity) and its relation to the basalt-eclogite phase transformation have been subjects of much speculation and debate for many years. Wyllie (1963a, 1963b) summarized the status of the debate and presented a compromise based on the idea that the M-discontinuity represents the basalt-eclogite phase transformation in some places (for example, mountain belts) and a chemical discontinuity between basalt and peridotite in others (for example, ocean basins and continental shields). Wyllie's compromise seems to have merit, but it is based in part on the idea that the crust is thin in shields and other stable continental regions and relatively thick in orogenic belts and other active continental regions. Seismic-refraction studies have shown that, in the conterminous United States at least, the opposite is true: as a whole the crust is thick in stable continental regions and relatively thin in active continental regions (Tatell and Tuve, 1955; Steinhart and Meyer, 1961; Pakiser, 1963; Stuart and others, 1964; Pakiser and Steinhart, 1964). The terms "M-discontinuity" and "base of the crust" are used interchangeably in the discussion that follows, and crustal thickness is identical with depth of the M-discontinuity below the surface of the earth.

In this paper, I will attempt to relate the crustal and upper-mantle structure in part of the Western United States to modern data from geochemistry and high-

pressure rock physics: a proposed compositional model for the upper mantle (Ringwood, 1962a, 1962b), recent experimental data on the basalt-eclogite phase transformation (Kennedy, 1959; Boyd and England, 1959; Yoder and Tilley, 1962; Ringwood and Green, 1964), and rock velocities under high pressures (Birch, 1961). Correlation of these data leads to the suggestion that the basalt-eclogite phase-transformation zone may be within the upper mantle where the crust is thin and within the lower crust and probably also within the upper mantle where the crust is thick. This suggestion was developed through discussions and (or) correspondence with Jerry P. Eaton and John H. Healy, of the U.S. Geological Survey, Frank Press, of the California Institute of Technology, George A. Thompson, of Stanford University, and John S. Steinhart, of the Carnegie Institution of Washington. I am, of course, alone responsible for any factual or interpretive errors that may be contained in this paper.

PETROLOGIC AND GEOPHYSICAL EVIDENCE

Ringwood (see also Clark and Ringwood, 1964) proposed a petrologic model for the upper mantle which is the equivalent of a mixture of about 4 parts peridotite and 1 part basalt. He called this rock "pyrolite," of which there are high-pressure and low-pressure phases analogous to eclogite and basalt. The high-pressure phase, called "garnet pyrolite" by Ringwood and "garnet peridotite" by Wyllie, is a mixture composed principally of peridotite and eclogite. The low-pressure phase, called "plagioclase pyrolite" by Ringwood and "feldspathic peridotite" by Wyllie, is a mixture composed principally of peridotite and basalt.

These two types of mantle rock are at least qualitatively consistent with observed variations in the velocity of compressional waves in the upper mantle (Herrin

and Taggart, 1962; Pakiser, 1963; Stuart and others, 1964; Pakiser and Steinhart, 1964). The plagioclase in a basaltic fraction of the low-pressure phase would tend to reduce the velocity, whereas the garnet in an eclogitic fraction of a high-pressure phase would have little effect on the velocity of a mixture in which peridotite predominates. Ringwood (1962a) estimated the compressional-wave velocity for the mixture peridotite-eclogite to be 8.0 kilometers/second and for the mixture peridotite-basalt 7.8 km/sec. Seismic observations suggest that 8.2 km/sec may be the normal velocity for the upper-mantle rocks east of the Rocky Mountains and that 7.8 km/sec may be the normal velocity for the upper-mantle rocks west of the Rocky Mountains. The velocity 8.2 km/sec would be appropriate for a mixture of peridotite and eclogite, and the velocity 7.8 km/sec would be appropriate for a mixture of peridotite and basalt.

It is recognized, however, that factors other than change of phase—for example, elevated temperatures, changes in bulk composition including hydrous mineral assemblages, partial serpentinization of peridotite—may also influence velocity. The resulting uncertainties have been summarized recently by Boyd (1964). In particular, Boyd pointed out that rocks of basaltic composition are quite commonly interstratified with kyanite schists in metamorphic sequences, but in the form of amphibolite rather than anhydrous gabbro or eclogite. This association implies water vapor pressure sufficiently high to mask the basalt-eclogite transition. If, therefore, much water is present at great depths in the crust and in the upper mantle, the transformation of basalt to eclogite might not take place at all.

Approximate stability fields for basalt, eclogite, and liquid, together with the basalt-eclogite transformation and melting zones, were plotted (fig. 1) from data in Kennedy (1959) and Boyd and England (1959) as summarized by Yoder and Tilley (1962), and from Ringwood and Green (1964). As discussed by Boyd (1964), the stability fields of basalt and eclogite have not yet been adequately determined, especially with regard to the width of the transition zone and its slope. The assumed geothermal gradients for the Basin and Range and Great Plains provinces are virtually the same as those assumed by Ringwood and Green for eastern and western Australia, respectively. Temperature at the M-discontinuity in the Great Plains (depth, 50 km) would be 525°C, and in the Basin and Range province (depth, 34 km) 590°C. Heat flow in the early Precambrian shield of western Australia is about 1 microcalorie per square centimeter per second, a rate probably about the same as that in the Great Plains; heat flow in mountainous eastern Australia is about 2 microcal/cm²/sec,

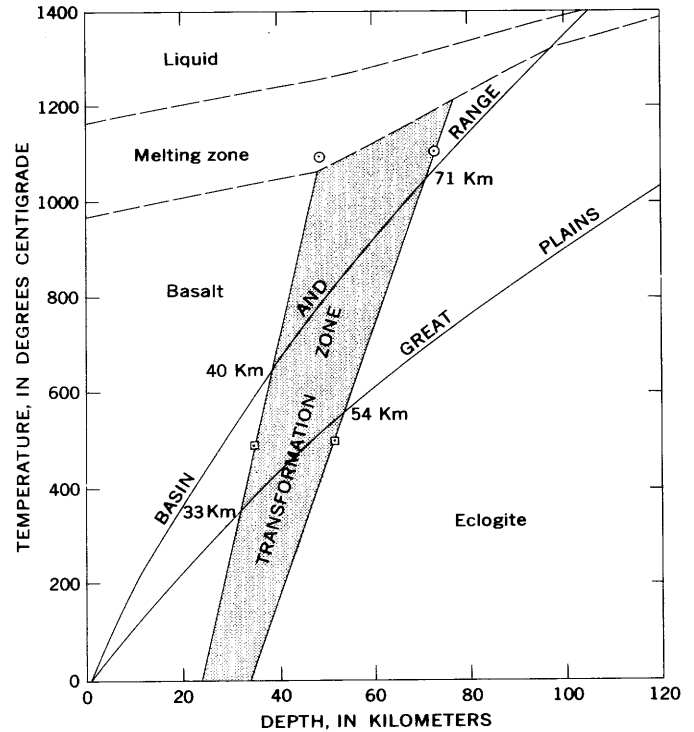


FIGURE 1.—Approximate stability fields of basalt, eclogite, and liquid, based on Kennedy (1959) and Boyd and England (1959) as summarized by Yoder and Tilley (1962); and Ringwood and Green (1964). Geothermal gradients for the Basin and Range and Great Plains provinces are assumed. Sources of data on transformation zone: circle, Ringwood and Green (1964); square, Kennedy (1959).

a rate probably about the same as that in the Basin and Range province. Heat-flow determinations in the Western United States are few, but the values above are consistent with the most recently available data (Roy, 1963).

For the Basin and Range province, radiogenic heat production in a crust consisting of 22½ km silicic rock and 11½ km mafic rock would be 1.0 microcal/cm²/sec. This determination is based on a heat production of 4×10^{-13} cal/cm³/sec for silicic rock and 1×10^{-13} cal/cm³/sec for mafic rock; both values are reasonable averages. If heat flow from the mantle is 0.6 microcal/cm²/sec, the total heat flow at the surface would be 1.6 microcal/cm²/sec, which value is conservative for the province. This heat flow and a thermal conductivity of 6×10^{-3} cal/cm/sec/°C for crustal rocks (a reasonable average) would produce the geothermal gradient assumed for the Basin and Range province.

The average heat production of crustal rocks for a 50-km crust in the Great Plains province can be no greater than 1.2×10^{-13} cal/cm³/sec if the surface heat flow is 1.2 microcal/cm²/sec and the heat flow from the mantle is 0.6 microcal/cm²/sec. This heat production is about that of average basalt, and is seemingly too low

for a crust with a significant silicic fraction. If heat flow from the mantle is significantly less than 0.6 microcal/cm²/sec, or if the total surface heat flow is greater than 1.2 microcal/cm²/sec, heat production in the crust can be assumed to increase toward values appropriate for a more silicic crust. Surface heat flow of 1.2 microcal/cm²/sec and a thermal conductivity of 8×10^{-3} cal/cm/sec/°C (a seemingly high estimate) would produce the geothermal gradient assumed for the Great Plains.

For the geothermal gradient that is assumed for the Great Plains, basalt would be stable to a depth of 33 km; the basalt-eclogite transformation zone, if it exists, would extend to 54 km; and eclogite would be stable at greater depths (fig. 1). For the geothermal gradient assumed for the Basin and Range province, basalt would be stable to a depth of 40 km; the basalt-eclogite transformation zone, if it exists, would extend to 71 km; and eclogite would be stable at greater depths. The transformation zone under these conditions would, therefore, be mainly in the lower crust in the Great Plains, where crustal thickness is about 50 km, and entirely in the upper mantle in the Basin and Range province, where crustal thickness is about 34 km.

CRUSTAL STRUCTURE

A crustal section extending from central Nevada to southeastern Nebraska was prepared (fig. 2) from a number of sources, summarized in part by Stuart and others (1964). The section is similar to that presented by Pakiser (1963), except that the deep root under the Rocky Mountains has been moved eastward to a point near the Rocky Mountains-Great Plains border. Steinhart and Meyer (1961, p. 338) stated that explosion-seismology results in western Montana "indicate the surprising result that the crust is thinner in the Northern Rocky Mountains than it is on the flanks of the Rockies." A similar result was obtained recently in the Middle Rocky Mountains of Idaho, Utah, and Wyoming by C. R. Willden, of the U.S. Geological Survey (written communication, 1964), and recordings along an unreversed profile extending into the Southern Rocky Mountains from southeastern Colorado, discussed by Pakiser, are interpreted to indicate that the crust does not thicken much, if any, westward from the Great Plains. A preliminary interpretation by W. H. Jackson, of the Geological Survey (written communication, 1964), of recordings of seismic waves along the highest part of the Southern Rocky Mountains north of Climax, Colo., indicates that the thickness of the crust is about the same there as it is in the Great Plains of eastern Colorado.

Seismic evidence supporting the separation of the crust into a silicic upper crust and a mafic lower crust

is strong in the Basin and Range province and much of the intermontane plateaus, but is weak in the Great Plains. (See Pakiser and Steinhart, 1964, for a discussion of the problem of the variation of velocity with depth.) All available evidence, however, indicates that compressional-wave velocity increases either continuously or discontinuously with depth at all places along the section of figure 2. The line separating the silicic upper crust from the mafic lower crust should not be taken as necessarily a discontinuity, but rather as a line that separates generally silicic rock (velocity 5.8–6.4 km/sec) above the line from generally mafic rock (velocity 6.6–7.6 km/sec) below.

The depth interval appropriate for the basalt-eclogite transformation zone for the assumed Basin and Range and Great Plains geothermal gradients, when plotted on the crustal section, is wholly within the mantle under the Basin and Range province, crosses the M-discontinuity under the Colorado Plateau and Rocky Mountains, and is mainly in the lower crust in the Great Plains (fig. 2). The upper-mantle region suggested as consisting of peridotite and basalt (plagioclase pyrolite) and the suggested basalt-eclogite transformation zone under the intermontane plateaus is very similar to the upper-mantle region of low density and velocity in the Basin and Range province discussed by Pakiser (1963). The geometric configuration of the suggested basalt-eclogite transformation zone in the crustal section seems to explain, at least qualitatively, the observed distribution of crustal and upper-mantle velocities in the Western United States.

If the geothermal gradient assumed for the Basin and Range province is approximately correct, a basaltic fraction of the upper-mantle rocks would begin to melt at a depth of about 100 km (fig. 1), which is consistent with the Gutenberg low-velocity channel in the upper mantle deduced from a shadow zone for body waves and the dispersion of surface waves (Gutenberg, 1959; Press, 1959). If the geothermal gradient in the Basin and Range province is a little steeper, and this may be so in local hot spots, the melting zone for the basaltic fraction would merge with the basalt-eclogite transformation zone, and a melting zone for a silicic fraction of the crust might be developed. Such a phenomenon might explain the severe attenuation of seismic waves in the Basin and Range province. Under the Great Plains, the melting zone would presumably lie at great depths and a pronounced low-velocity channel would not be expected.

VELOCITY-DEPTH MODELS

Velocity-depth models for the crust and upper mantle in the Basin and Range and Great Plains provinces were constructed from averages based on long-range

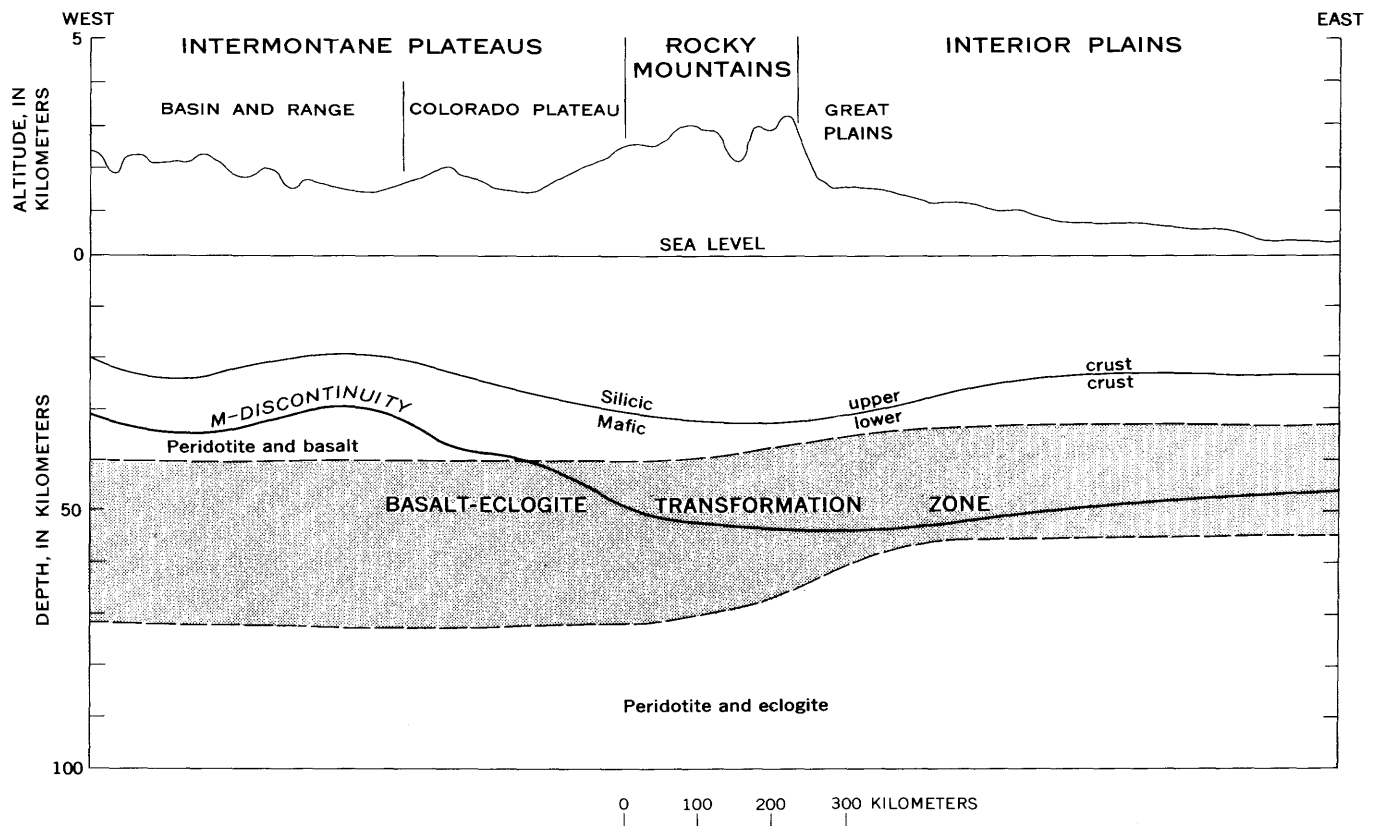


FIGURE 2.—Section showing the crustal and upper-mantle structure and the inferred basalt-eclogite transformation zone (fig. 1) from the Basin and Range province to the Great Plains. Section extends from central Nevada to southeastern Nebraska.

seismic-refraction profiling as summarized by Steinhart and Meyer (1961), Pakiser (1963), Stuart and others (1964), and Pakiser and Steinhart (1964), and from velocities determined in the laboratory and summarized by Birch (1961). The values adopted for pressures ranging from 1 atmosphere to 10 kilobars are given in the accompanying table.

Crustal thickness and velocity in the Basin and Range and Great Plains provinces

Thickness or velocity	Basin and Range province	Great Plains province
Thickness of silicic upper crust (km)---	22½	22½
Thickness of mafic lower crust (km)---	11½	27½
Total crustal thickness (km)-----	34	50
Velocity in silicic upper crust (km/sec) (Birch, 1961, average for granitic rocks)-----	5.0-6.4	5.0-6.4
Velocity in mafic lower crust (km/sec) (Birch, 1961, average for diabase, gabbro, norite)-----	6.4-7.1	6.4-7.1
Upper-mantle velocity (km/sec)-----	7.8	8.2

Velocities in the depth interval appropriate for the basalt-eclogite transformation zone, where within the crust, were assumed to range linearly from 7.1 km/sec (basalt) to 8.0 km/sec (eclogite). Velocities in the

transformation zone interval, where within the mantle, were assumed to range linearly from 7.8 km/sec (peridotite and basalt) to 8.2 km/sec (peridotite and eclogite). The M-discontinuity was assumed to be sharp. The silicic upper crust and mafic lower crust were assumed to be separated by a velocity transition zone 5 km deep.

Representative velocity-depth models in the Basin and Range and Great Plains provinces based on these data and assumptions are plotted graphically (fig. 3). The Basin and Range velocity-depth model may be compared with the model of Roller and Healy (1963, fig. 10). Roller and Healy represented the silicic upper crust and mafic lower crust as separated by a sharp discontinuity, but otherwise the two models are virtually the same. The Great Plains velocity-depth model may be compared with that for eastern Montana in Steinhart and Meyer (1961, fig. 9.15). Steinhart and Meyer represented the crust by layers of uniform velocity, but otherwise the two models are virtually equivalent. The apparent failure of such a thick crust to produce high radiogenic heat suggests a crust even more mafic than that indicated by the velocity-depth model.

High velocities in the deepest crust near those predicted for the basalt-eclogite transformation zone (7.7 km/sec on fig. 3) have been reported by several investi-

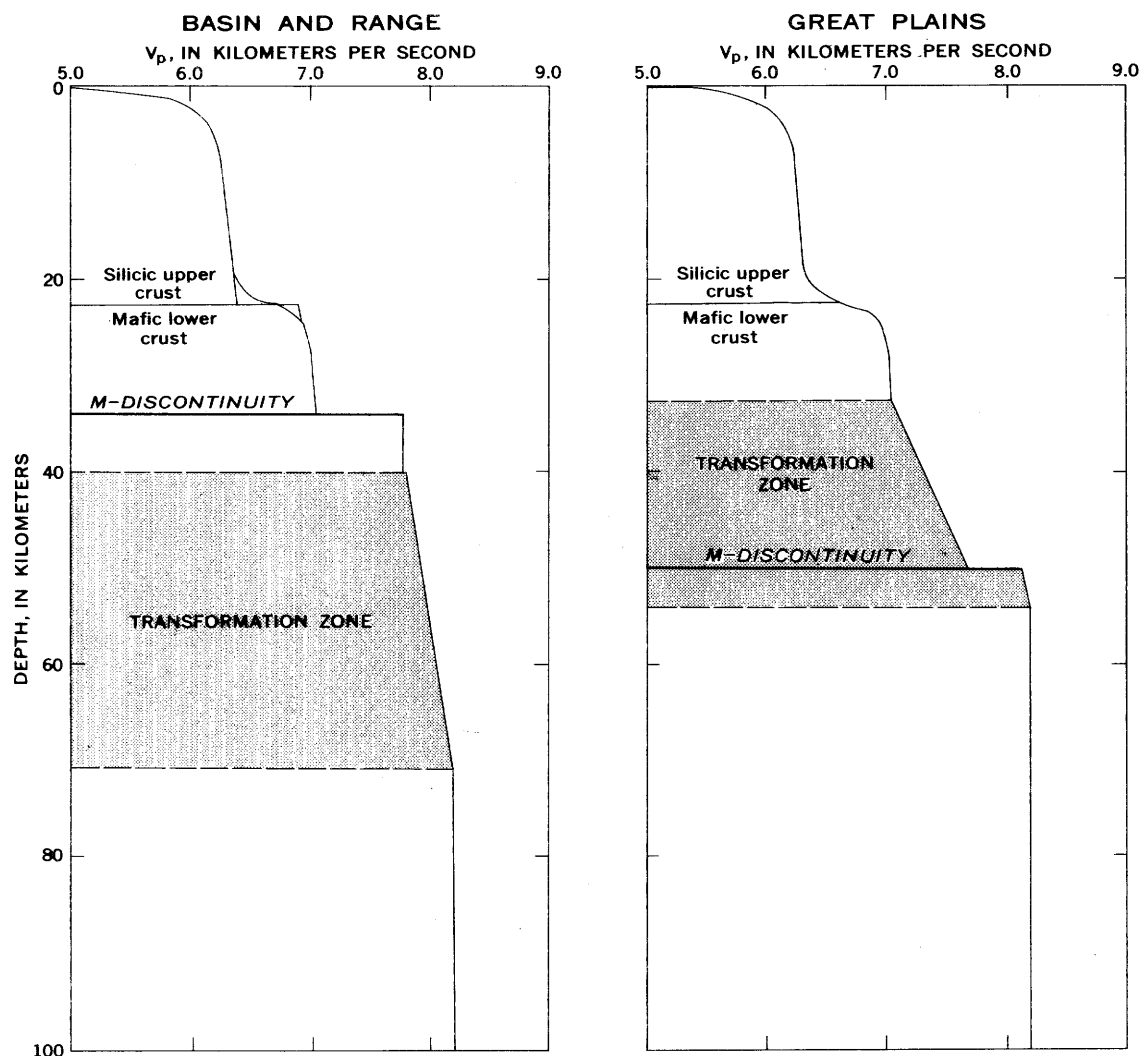


FIGURE 3.—Postulated velocity structure in the Basin and Range and in the Great Plains provinces, based on figures 1 and 2 and Birch (1961). Rocks in silicic upper crust are assumed to be average granitic rocks. Rocks in mafic lower crust are assumed to be average of diabase, gabbro, and norite, and their equivalents in the transformation zone.

gators, but they are based mainly on traveltimes of secondary arrivals. Steinhart and Meyer reported a velocity of 7.58 km/sec for the lower 10 to 20 km of the crust in eastern Montana. McCamy and Meyer (1964) reported velocities as high as 7.8 km/sec in eastern Montana and 7.3 km/sec in the thinner crust of the Arkansas-Missouri region. The trend in explosion-seismology research is toward detailed field experiments such as those using fixed arrays and moving shot points, and toward various array-processing techniques for phase identification, such as those reported by McCamy and Meyer (1964) and Ryall (1964). Hopefully, these experiments will lead to more confident estimates of velocities in the lower crust.

If velocities as high as 7.7 to 7.8 km/sec. in the lower crust are substantiated, the problem of separating the

lower crust from the upper mantle by the M-discontinuity may become rather arbitrary. However, in the area east of the Rocky Mountains, where velocities in the deep crust may be high, the upper-mantle velocity is high (greater than 8.0 km/sec), and in the area west of the Rocky Mountains, where velocities in the lower crust are generally significantly lower, velocities in the upper mantle are also low (typically 7.8 km/sec). Therefore, it is probable that a velocity contrast sufficient for detection exists at the M-discontinuity in all or most of the United States, and that the M-discontinuity can be regarded as a chemical discontinuity separating crustal rocks of predominantly mafic composition from upper-mantle rocks of predominantly ultramafic composition.

TECTONIC IMPLICATIONS

Distinct differences in the seismic properties of the crust and upper mantle east and west of the Rocky Mountain System suggest that the conterminous United States is divided by the Rocky Mountains into two crustal and upper-mantle superprovinces (Pakiser and Steinhart, 1964). In the eastern superprovince, the velocity of compressional waves in the upper-mantle rocks is everywhere greater than 8 km/sec, the mean crustal velocity is generally greater than 6.4 km/sec, and the crust is generally thicker than 40 km. In the western superprovince, the velocity of compressional waves in the upper-mantle rocks is everywhere less than 8 km/sec (except along the margin of the Pacific Ocean Basin), the mean crustal velocity is generally less than 6.4 km/sec., and the crust is generally thinner than 40 km. These are, of course, generalized averages, and there are important regional variations within both superprovinces. For example, the mean crustal velocity in the Coastal Plain (eastern superprovince) is less than 6.4 km/sec because of the thick section of low-velocity sedimentary deposits; the root of the Sierra Nevada Mountains of California (western superprovince) extends to a depth of more than 40 km, and the mafic lower crust in the Snake River Plain of Idaho (western superprovince) extends to, or very near to, the surface.

Late Mesozoic and Cenozoic diastrophism, plutonism, and volcanism have been widespread in the western superprovince, whereas the eastern superprovince has been relatively stable and quiescent during the past 100 million years or so. The crust and upper mantle in the western superprovince can be thought of as youthful—still in the process of evolution. The crust and upper mantle in the eastern superprovince can be thought of as mature. The crust of the west is now receiving mafic material from the mantle, whereas the crust of the east has already been extensively intruded with material from the mantle.

According to the foregoing analysis, the depth zone for the basalt-eclogite transformation is entirely within the upper mantle in the western superprovince, and the upper mantle there probably consists largely of the mixture peridotite-basalt overlying a zone extending from about 40 to 70 km in which the basaltic fraction is gradually transformed to eclogite. The mantle probably consists largely of the mixture peridotite-eclogite at greater depths. In the eastern superprovince, the depth zone for the basalt-eclogite transformation is mainly within the lower crust in areas of very thick crust, and the upper mantle there (except the uppermost part, which is in the transformation depth zone)

probably consists largely of the mixture peridotite-eclogite. This relation has important tectonic implications, as discussed by Ringwood (1962a), Wyllie (1963a, 1963b), and others.

Ringwood (1962a) estimated the phase transformation from garnet pyroxene to plagioclase pyroxene to have been accompanied by an increase of 3 percent in volume. This would have produced a vertical uplift of about $\frac{1}{2}$ km for the model of figure 2 if the expansion were vertical only, and much less if the expansion were 2- or 3-dimensional, provided that the low-pressure peridotite-basalt phase formerly existed as the high-pressure peridotite-eclogite phase, which is by no means certain. For the sake of discussion, I will assume an expansion of 6 percent because of added thermal effects (including partial melting) and possibly also conversion of some peridotite to serpentine, as suggested by Hess (1955). This expansion and conversion would produce a maximum vertical uplift of 1 km. This uplift is still seemingly not enough to account for the Late Cretaceous and more recent uplift in the western superprovince, which in many places exceeds 2 km. In the Rocky Mountains and Sierra Nevada, uplift exceeds 4 km. The western part of the Great Plains province, which is in the eastern superprovince, has been uplifted as much as 1 km since Late Cretaceous time, and the basalt-eclogite transformation seems totally inadequate to explain this uplift.

Gilluly (1963) suggested that uplift of the Colorado Plateau could be explained by the "subcrustal transfer of sial from other areas, perhaps the present area of the Basin Range province." Unless the upper-mantle zone of expansion is extended through a greater depth zone than that of figure 2, some such kinematic process involving, in my opinion, subcrustal and intracrustal transfer of molten basalt over a broader area seems necessary to explain the uplift of the mountains and high plateaus of the western superprovince and the maintenance of isostatic equilibrium. If the geothermal gradient in the Basin and Range province is as high or higher than that of figure 1, partial melting of a basaltic fraction of the upper mantle could provide a source for the Cenozoic basalt flows of the province. Partial melting of a silicic fraction of crustal rocks would require a much more severe geothermal gradient. Intrusive and extrusive silicic rocks of Late Cretaceous and Cenozoic times are widespread in the western superprovince.

SPECULATION CONCERNING CRUSTAL EVOLUTION

The mean crustal velocity of the conterminous United States is less than what it would be if the average com-

position of the crust were that of basalt (Pakiser and Steinhart, 1964), unless it is possible to break down basalt in such a way that the average velocity of large volumes of the separate components is substantially reduced. The processes of weathering, transport of weathered materials, and their reconstitution as porous sedimentary deposits do produce rocks of substantially lower velocity than their source rocks, but the effect of porosity on seismic velocities is generally eliminated by pressure at depths greater than a few kilometers. The silicic upper crust constitutes more than half the volume of the crust in much of the western superprovince, and a significant fraction of the crust in the eastern superprovince (fig. 2). Therefore, the average composition of the continental crust is probably significantly more silicic than basaltic.

If the crust of the eastern superprovince is, as was suggested, mature in the sense that it has already been extensively intruded with mafic material from the mantle, and the crust of the western superprovince is youthful in the sense that it is now receiving mafic material from the mantle, then the crust has been becoming increasingly more mafic with time. This process suggests that the primitive continental crust was silicic and that addition of mafic material from the mantle and removal of silicic material by erosion has made the crust progressively more mafic with time. This suggestion is supported by the higher mean crustal velocity of the rocks of the eastern superprovince, the lower heat flow, and the higher mean crustal density indicated by laboratory measurements of density and seismic velocity (Birch, 1961) and considerations of isostasy (Pakiser, 1963).

Many thermal models indicate that the earth was getting progressively hotter during much of its history (MacDonald, 1963); this heat increase might have resulted in the early mobilization of low-melting and (or) water-soluble components in the upper mantle that, following upward migration, may have been reconstituted as a primitive silicic crust. As the earth heated, a basaltic fraction could readily have been melted in the upper mantle and added, by intrusion and extrusion, to the primitive silicic continental crust, a process that may still be occurring in the western superprovince. A silica-enriched continental crust also could be explained either by the emplacement of the crust in one episode and the settling of an ultramafic fraction which became an addition to the upper mantle, or by a variety of kinematic processes involving lateral and (or) vertical transfer of silicic and mafic material. Current geologic processes and geologic history suggest, in any event, that crustal evolution is a continuing process. Localiza-

tion of the continents may have been the result of compositional inhomogeneities in the mantle of the primitive earth.

REFERENCES

- Birch, Francis, 1961, The velocity of compressional waves in rocks to 10 kilobars, pt. 2: *Jour. Geophys. Research*, v. 66, no. 7, p. 2199-2224.
- Boyd, F. R., 1964, Geological aspects of high-pressure research: *Science*, v. 145, no. 3627, p. 13-20.
- Boyd, F. R., and England, J. L., 1959, Experimentation at high pressures and temperatures: *Carnegie Inst. Washington Yearbook*, v. 58, p. 82-89.
- Clark, S. P., Jr., and Ringwood, A. E., 1964, Density distribution and constitution of the mantle: *Rev. Geophys.*, v. 2, p. 35-88.
- Gilluly, James, 1963, The tectonic evolution of the Western United States: *Quart. Jour. Geol. Soc. London*, v. 119, p. 133-174.
- Gutenberg, Beno, 1959, The asthenosphere low-velocity layer: *Am. Geofis. Rome*, v. 12, p. 439-460.
- Herrin, Eugene, and Taggart, James, 1962, Regional variations in P_n velocity and their effect on the location of epicenters: *Seismol. Soc. America Bull.*, v. 52, no. 5, p. 1037-1046.
- Hess, H. H., 1955, Serpentine, orogeny, and epeirogeny, in Poldervaart, Arie, ed., *Crust of the Earth—a symposium*: *Geol. Soc. America Spec. Paper* 62, p. 391-407.
- Kennedy, G. C., 1959, The origin of continents, mountain ranges, and ocean basins: *Am. Scientist*, v. 47, no. 4, p. 491-504.
- McCamy, Keith, and Meyer, R. P., 1964, A correlation method of apparent velocity measurement: *Jour. Geophys. Research*, v. 69, no. 4, p. 691-699.
- MacDonald, G. J. F., 1963, The deep structure of continents: *Rev. Geophys.*, v. 1, p. 587-665.
- Pakiser, L. C., 1963, Structure of the crust and upper mantle in the Western United States: *Jour. Geophys. Research*, v. 68, no. 20, p. 5747-5756.
- Pakiser, L. C., and Steinhart, J. S., 1964, Explosion seismology in the Western Hemisphere, in Odishaw, Hugh, ed., *Research in Geophysics*; v. 2, *Solid earth and interface phenomena*: Cambridge, Massachusetts Inst. Technology Press, p. 123-147.
- Press, Frank, 1959, Some implications on mantle and crustal structure from G waves and Love waves: *Jour. Geophys. Research*, v. 64, no. 5, p. 565-568.
- Ringwood, A. E., 1962a, A model for the upper mantle, pt. 1: *Jour. Geophys. Research*, v. 67, no. 2, p. 857-867.
- 1962b, A model for the upper mantle, pt. 2: *Jour. Geophys. Research*, v. 67, p. 4473-4477.
- Ringwood, A. E., and Green, D. H., 1964, Experimental investigations bearing on the nature of the Mohorovicic discontinuity: *Nature*, v. 201, no. 4919, p. 566-567.
- Roller, J. C., and Healy, J. H., 1963, Seismic-refraction measurements of crustal structure between Santa Monica Bay and Lake Mead: *Jour. Geophys. Research*, v. 68, no. 20, p. 5837-5849.
- Roy, R. F., 1963, Heat-flow measurements in the United States: Harvard Univ. Ph. D. thesis, 76 p., 2 appendices.
- Ryall, Alan, 1964, Improvement of array seismic recordings by digital processing: *Seismol. Soc. America Bull.*, v. 54, no. 1, p. 277-294.

- Steinhart, J. S., and Meyer, R. P., 1961, Explosion studies of continental structure: Carnegie Inst. Washington Pub. 622, 409 p.
- Stuart, D. J., Roller, J. C., Jackson, W. H., and Mangan, G. B., 1964, Seismic propagation paths, regional traveltimes and crustal structure in the Western United States: *Geophysics*, v. 29, p. 178-187.
- Tatel, H. E., and Tuve, M. A., 1955, Seismic exploration of a continental crust, *in* Poldervaart, Arie, ed., *Crust of the Earth—a symposium*: Geol. Soc. America Spec. Paper, 62, p. 35-50.
- Wyllie, P. J., 1963a, The nature of the Mohorovicic discontinuity, a compromise: *Jour. Geophys. Research*, v. 68, p. 4611-4619.
- 1963b, The Mohorovicic discontinuity and the orogenic cycle: *Trans. Am. Geophys. Union*, v. 44, no. 4, p. 1064-1071.
- Yoder, H. S., Jr., and Tilley, C. E., 1962, Origin of basalt magmas; an experimental study of natural and synthetic rock systems: *Jour. Petrology*, v. 3, p. 342-532.



GEOPHYSICAL EVIDENCE OF A CALDERA AT BONANZA, COLORADO

By DANIEL E. KARIG, Denver, Colo.

Abstract.—A gravity survey of the San Luis Valley region of Colorado has revealed a closed gravity low that is interpreted as the expression of a middle Tertiary caldera. The suspected collapse caldera is centered near Bonanza, at the northeast corner of the San Juan volcanic field. Available geologic and gravity evidence suggests that the structure has an elliptical outline with axes of 8 and 10 miles, and is filled with about 8,000 feet of low-density material.

A regional gravity survey made in and around the San Luis Valley, Colo., during the summer of 1963 revealed a gravity low over volcanic rocks in the Bonanza mining district. Available geologic evidence supports an interpretation that the gravity low marks a caldera center.

The Bonanza district lies at the northeast corner of the San Juan volcanic field, and at the north end of the San Luis Valley. The major tectonic unit with which these features is associated is the Rio Grande trough, a rift system that extends from the upper Arkansas Valley and San Luis Valley of Colorado, across New Mexico, and into northern Mexico. The Rio Grande trough is a complex graben, broken along its length into many separate en echelon basins. Middle Tertiary to Recent volcanism associated with the trough has resulted in many local accumulations of lava and pyroclastic rocks.

The San Luis basin, which lies near the north end of the trough, is shown by recent unpublished gravity studies to be broken into a complex of buried en echelon horsts and grabens. Immediately to the west of the San Luis Valley lies the San Juan volcanic pile, one of several volcanic fields flanking the rift zone. Recognition of caldera structures as volcanic sources in these fields has become fairly common. The Valles caldera has been recognized in the Jemez volcanic field in New Mexico (Smith and others, 1961). Other calderas in

Colorado have been described near Silverton and Lake City (Burbank, 1933; Luedke and Burbank, 1963) and Creede (Steven and Ratté, 1960; Steven and Ratté, 1963) in the San Juan Mountains.

GEOLOGIC EVIDENCE

Burbank (1932) described the Bonanza district as a volcanic dome and collapse structure. No detailed geologic study has been made of the district since the concept of caldera structures became well known. Exploratory geologic work done by the Bear Creek Mining Co. (Cook, 1960) suggested a caldera structure, but mapping was too local in extent to substantiate the idea.

Volcanic rocks in the Bonanza area lie unconformably on a rugged topographic surface cut on older Paleozoic and Mesozoic sedimentary rocks and Precambrian crystalline rocks. Larson and Cross (1956) dated the volcanic rocks as pre-Potosi (middle Miocene), but Cook (1960) considers them to be of Oligocene age and contemporaneous with the Silverton Volcanic Group of middle and late Tertiary age. A post-Oligocene Tertiary age is suggested by pollen analysis of specimens from plant-rich lake beds found at the base of the volcanic rocks about 12 miles northwest of Bonanza (E. B. Leopold, written communication, 1964). The locality from which this pollen collection was taken has been assigned U.S. Geological Survey paleobotany locality No. D3343.

The volcanic rocks range from andesite to rhyolite in composition, and have been estimated to be at least 5,000 feet thick (Burbank, 1932). If the gravity low marks a caldera, the underlying volcanic rocks could be much thicker.

Reconnaissance geologic study, by the author, of the poorly mapped west flank of the Bonanza district during the gravity survey, combined with Burbank's (1932) and Cook's (1960) data, shows the following:

1. Volcanic rocks on the flanks generally dip radially away from the center of the gravity low (fig. 1).
2. A circular belt of peaks, with an average diameter of about 7 miles, surrounds a topographic basin in the vicinity of the gravity low. Although this pattern resulted in part from erosion, it may reflect original structural relief.
3. Precambrian and Paleozoic rocks are exposed north, east, and south of the gravity low at altitudes substantially higher than the base of the volcanic rocks within the low. Considered with the outward dips on the outer flanks of the volcanic pile, this outcrop pattern suggests that the central area may be displaced downward, perhaps along faults between the Precambrian and volcanic rocks. Limited data indicate that such faults lie both inside and outside the ring of peaks.
4. The volcanic units include welded tuffs and lava flows. Certain of the more viscous, siliceous flow units (for example, Porphyry Peak Rhyolite and Hayden Peak Latite) are restricted to small areas on the margins of the gravity low, and are suggestive of peripheral volcanic accumulations around the margin of a collapsed area.

GRAVITY EVIDENCE

About 50 gravity stations were established in and immediately adjacent to the Bonanza district. Most of them were located at bench marks and spot elevations; however, lack of vertical control west and south of Bonanza made necessary the use of altimeters for the determination of altitude at 15 percent of the stations. Gravity readings were reduced to the Bouguer anomaly, on the basis of a slab density of 2.67 g/cm^3 . Topographic corrections were applied for a radial distance of about 18 miles from the stations.

The Bonanza gravity low, as defined by the -286 -milligal contour (fig. 1), is subcircular with a definite northwest elongation. It has at least 12 mgal of closure. Gravity relief, relative to the low, ranges from more than 70 mgal on the south to slightly more than 20 mgal on the east. The most negative Bouguer-anomaly value measured in the Bonanza district is -296 mgal, and the steepest gradient bounding the low is about 10 mgal/mile. The area enclosed by the -286 mgal contour is broken into a series of north-northwest-trending highs and lows with amplitudes of 4 to 6 mgal. Relatively large gravity highs bound the Bonanza low on the north and south, and a gravity ridge flanks it on the east. The gravity field to the west has not been mapped.

Detailed quantitative analysis of the Bonanza low is difficult because of the many variables involved. How-

ever, an approximate interpretation can be made by assuming that the top of the anomalous mass is at the ground surface, and that the significant density contrast is between the low-density fill and the Precambrian rocks. Cook (1960) has reported that the Precambrian rocks, most of which are biotite granite gneiss, have an average density of 2.70 g/cm^3 . The volcanic rocks range in density from 2.00 to 2.62 g/cm^3 depending on lithology and degree of alteration. An average density of 2.50 g/cm^3 was assigned to the volcanic rocks and also to the Paleozoic strata. This gives a density contrast of 0.20 g/cm^3 between the low-density fill and the surrounding Precambrian rocks.

A solid-angle graticule (Lachenbruch, 1957) was used to compute the theoretical gravity anomaly produced by a three-dimensional mass distribution chosen to approximate the proposed Bonanza caldera. This mass distribution was altered until its computed anomaly agreed with the observed anomaly. A distribution that satisfies the observed anomaly is an elliptical cylinder centered about 2 miles northwest of Bonanza with a maximum radius of about 5 miles trending northwest and a minimum radius of about 4 miles. This model can be regarded as an elliptical structure filled with materials less dense than the surrounding Precambrian rocks. Figure 2 shows a vertical section through this mass distribution. If the density contrast is 0.20 g/cm^3 , the low-density fill would be about 8,000 feet thick. Small changes in the density contrast result in relatively large changes in the thickness of low-density material required to produce the observed anomaly; a contrast of 0.10 g/cm^3 would require a low-density material thickness of only 4,000 feet. The measured thickness of the volcanic rocks exposed in fault blocks (Burbank, 1932) is 5,000 feet, which suggests that a depth of 8,000 feet is reasonable.

Low-amplitude anomalies enclosed by the -286 -mgal contour may be explained as the expression of horsts and grabens which result from post-subsidence doming (Smith and others, 1961). The pattern suggests that a second series of ring faults might lie within the ring of peaks at a radius of about 3 miles. The area within this ring appears to be a dome with a bisecting central graben trending nearly parallel to the long axis of the caldera.

CONCLUSIONS

Although the accumulated geologic evidence does not conclusively demonstrate that the volcanic center at Bonanza is a caldera, it does, when augmented by gravity evidence, support such an interpretation. The number of known caldera structures in areas of Cenozoic volcanic rocks of the Western United States is

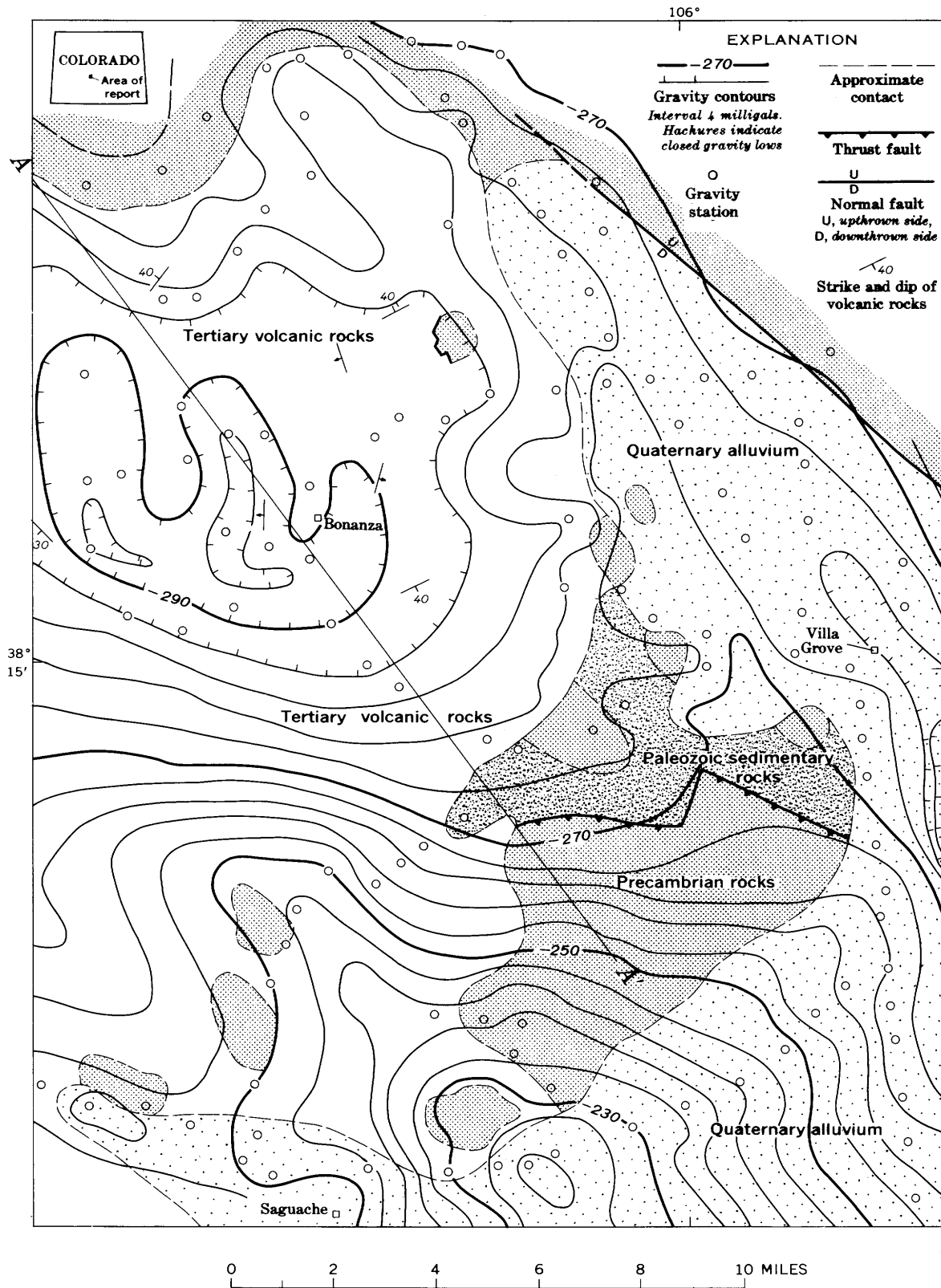


FIGURE 1.—Combined gravity and geologic map of the Bonanza region, Colorado. Geology from Burbank (1932), Cook (1960), and reconnaissance made by the author at the time of the gravity survey.

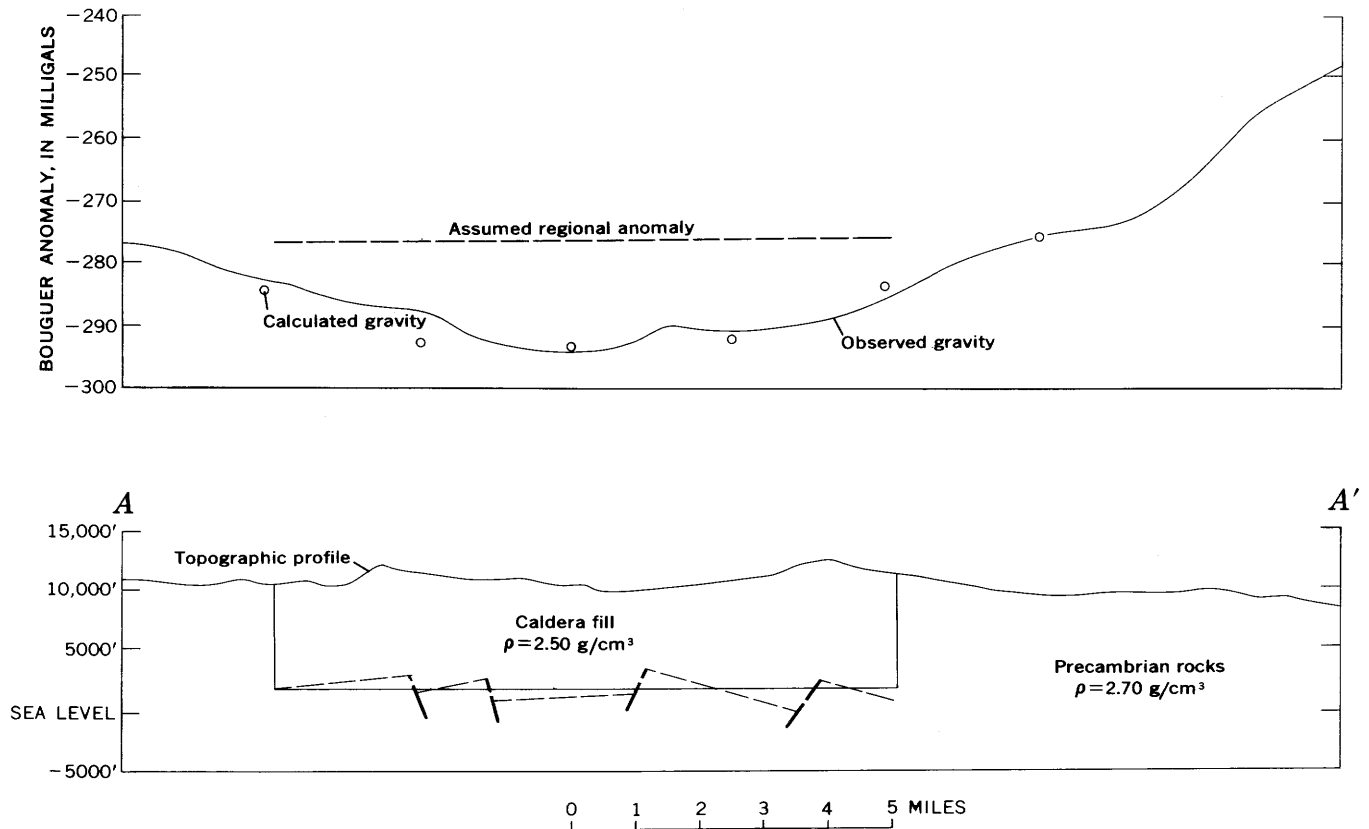


FIGURE 2.—A section through a mass distribution that will produce the gravity anomaly observed across the Bonanza district along profile A-A' (fig. 1).

increasing as detailed mapping proceeds. Gravity studies may prove to be a quick and possibly diagnostic method of indicating the presence of caldera structures in areas where cover or other factors make geologic interpretation difficult.

REFERENCES

- Burbank, W. S., 1932, Geology and ore deposits of the Bonanza mining district, Colorado: U.S. Geol. Survey Prof. Paper 169, 166 p.
- , 1933, Vein systems of the Arrastre Basin and regional geologic structure in the Silverton and Telluride quadrangles, Colorado: Colorado Sci. Soc. Proc., v. 13, p. 135-214.
- Cook, D. R., 1960, Bonanza project, Bear Creek Mining Company: Am. Inst. Mining Metall. Engineers Trans., Mining sect., p. 285-295.
- Lachenbruch, A. H., 1957, Three-dimensional heat conduction in permafrost beneath heated buildings: U.S. Geol. Survey Bull. 1052-B, p. 51-69.
- Larson, E. S., Jr., and Cross, Whitman, 1956, Geology and petrology of the San Juan region, southwestern Colorado: U.S. Geol. Survey Prof. Paper 258, 303 p.
- Luedke, R. G., and Burbank, W. S., 1963, Tertiary volcanic stratigraphy in the western San Juan Mountains, Colorado: U.S. Geol. Survey Prof. Paper 475-C, p. C39-C44.
- Smith, R. L., Bailey, R. A., and Ross, C. S., 1961, Structural evolution of the Valles caldera, New Mexico, and its bearing on the emplacement of ring dikes: Art. 340 in U.S. Geol. Survey Prof. Paper 424-D, p. D145-149.
- Steven, T. A., and Ratté, J. C., 1960, Relation of mineralization to caldera subsidence in the Creede District, San Juan Mountains, Colorado: U.S. Geol. Survey Prof. Paper 400-B, p. B14-B17.
- , 1963, Resurgent cauldrons in the Creede area, San Juan Mountains, Colorado [abs.]: Am. Geophys. Union Trans., v. 44, no. 1, p. 112-113.



HAWAIIAN SEISMIC EVENTS DURING 1963

By ROBERT Y. KOYANAGI and ELLIOT T. ENDO,
Hawaiian Volcano Observatory

Abstract.—Six hundred and seventy-three earthquakes of magnitudes 2.0 to 5.3 were recorded and located beneath the Hawaiian Ridge during 1963. The Kaoiki fault system, the Kalapana Trail region, the east rift zone of Kilauea, and a zone 30 km beneath Kilauea Caldera were regions of concentrated earthquake activity.

This report extends the coverage of "Hawaiian Seismic Events during 1962" (Koyanagi, 1964) and complements Summaries 29–32 of the Hawaiian Volcano Observatory for 1963 (Koyanagi and others, 1964a, 1964b; Krivoy and others, 1964; Okamura and others, 1964). Methods and limitations of epicenter locations were similar to those described in the report of 1962 events. To facilitate comparison of events the organization of that report has been retained. Figure 1 shows the geologic features and volcanic systems of the island of Hawaii.

The earthquakes plotted were those of magnitude 2.0 and greater which were recorded on the Hawaiian Volcano Observatory seismic net and located along the Hawaiian Ridge within the geographical coordinates lat 18°–23° N. and long 154°–161° W. The thoroughness of our interpretation depended in large part on the degree of concentration of seismic activity. Thus, the May 9–12, July 1–5, and August 3–5 seismic crises; the August 21–23 and October 5–6 Kilauea flank eruptions; and the August 26, September 21, and October 23 Kaoiki fault earthquake series were periods of such intense seismic activity that the arrival times of some earthquake phases were difficult to determine.

CHRONOLOGY OF EVENTS IN 1963

A swarm of about 150 earthquakes occurred 30 kilometers beneath the summit of Kilauea during January 8–9. The largest of these (magnitudes 4.3 and 4.2) occurred on January 8 and were felt throughout the island. Magnitudes of the others ranged down to less than 1. The largest earthquake recorded in the first

quarter of 1963 (magnitude 4.5) occurred under the south flank of Mauna Kea on March 24 (fig. 2).

The second quarter (fig. 2) was characterized by the seismic crisis of May 9–12. Thousands of small, shallow earthquakes occurred along the 10-km-long east-trending Koaie fault system immediately south of Kilauea Caldera. Although several quakes were felt in the Kilauea summit region during this episode, most of them were less than magnitude 2. Cracking of the ground was observed in the epicentral zone, and a moderate collapse of the Kilauea summit was indicated by tiltmeter readings.

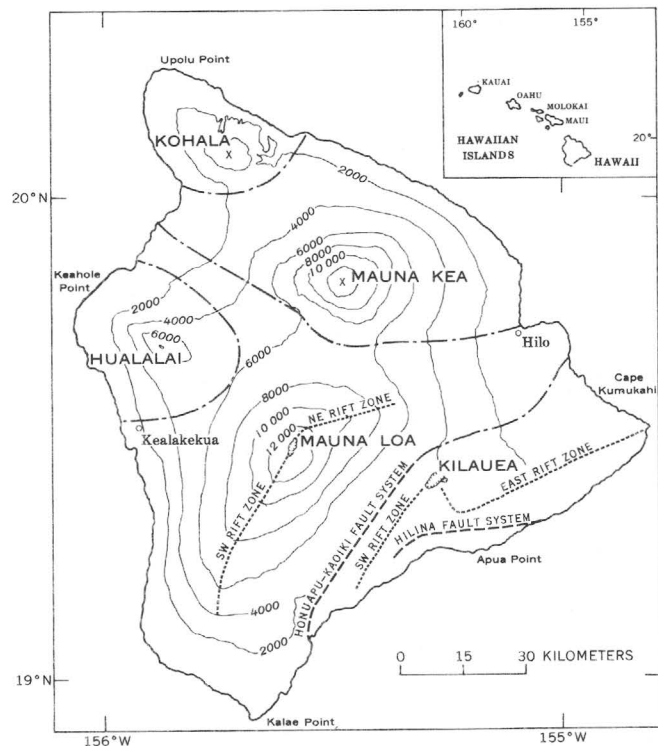


FIGURE 1.—Map of the island of Hawaii, showing geologic features. The five volcanic systems are after Macdonald (1956). Contour interval is 2,000 feet; datum is mean sea level. Dot-and-dash lines are boundaries of volcanic systems.

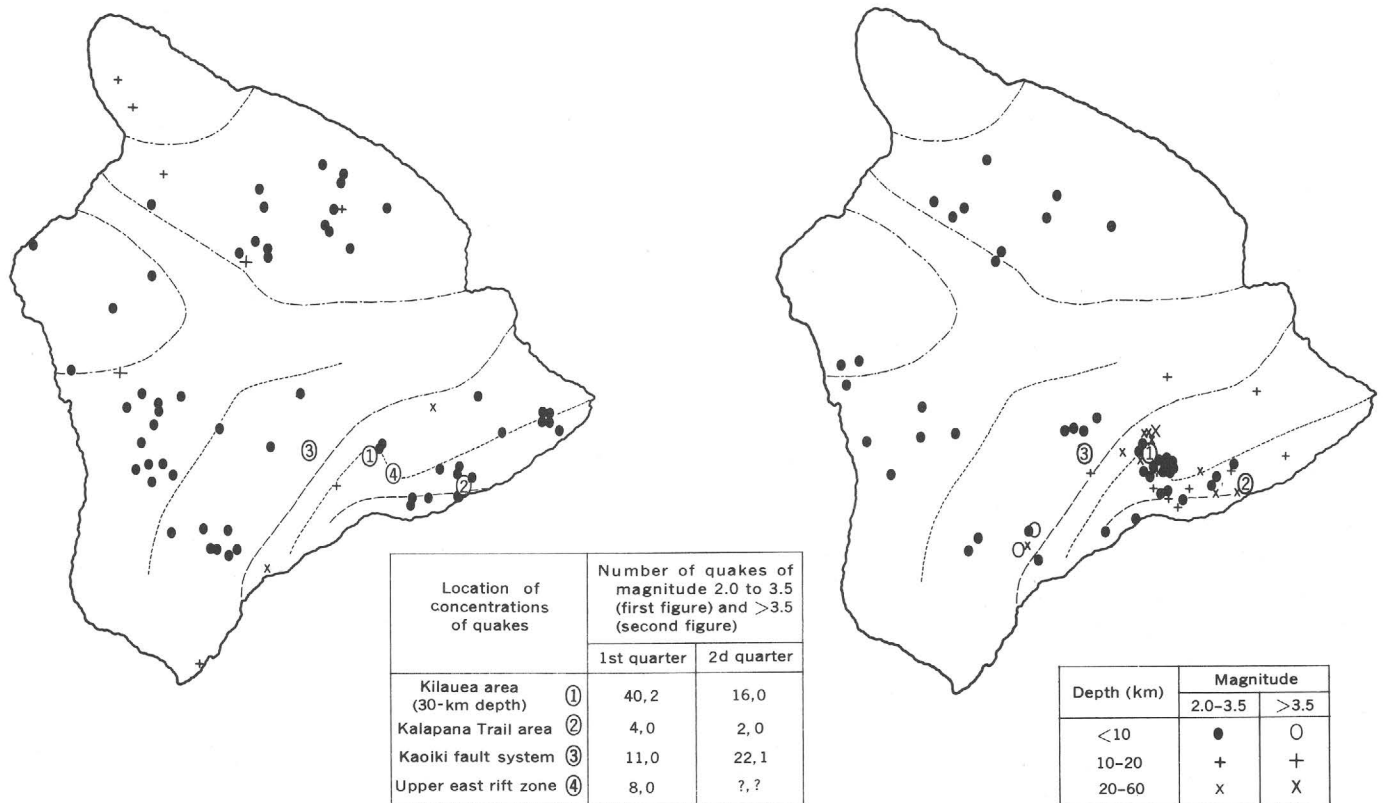


FIGURE 2.—Epicenters of earthquakes of magnitude 2.0 and greater for the first quarter (*left*) and second (*right*) of 1963. The number symbols identify concentrations of quakes that are listed in the left-hand table because they are too numerous to plot separately, and represent the following areas: (1) Kilauea, at a depth of 30 km; (2) along the Kalapana Trail, which extends south of Kilauea's east rift; (3) along the Kaoiki fault system; and (4) along the upper east rift zone of Kilauea. Geographic names are shown on figure 1. The number of earthquakes in the upper east rift and including the adjacent Koaie fault system was difficult to determine accurately during the May 9-12, July 1-5, and August 3-5 seismic crises, and the August 21-23 Kilauea east rift eruption because of the complexity of the seismograms.

The cumulative activity of the following five events distinguished the third quarter (fig. 3) as the most active period of the year seismically: (1) July 1-5, Kilauea collapse; (2) August 3-5, Kilauea seismic episode; (3) August 21-23, Kilauea eruptions along the east rift; (4) August 26, Kaoiki earthquakes series; and (5) September 21, Kaoiki earthquake series.

The July 1-5 collapse of the Kilauea summit was accompanied by many small, shallow earthquakes and resulted in the cracking of the ground along the upper east rift zone of Kilauea. Collapse of the Kilauea summit was indicated by tiltmeter readings.

The August 3-5 seismic episode consisted of 2 hours of strong seismic activity along Kilauea's upper east rift zone, much like the event of July 1-5 but of shorter duration. It was followed by a flurry of Kilauea quakes at a depth of 30 km.

The August 21-23 eruption on the east rift of Kilauea was marked by small, shallow earthquakes, and har-

monic tremor was recorded throughout the eruptive period. Collapse of the Kilauea summit was indicated by tiltmeter readings.

On August 26 an earthquake of magnitude 4.9 occurred at a shallow depth along the Kaoiki fault system. It was followed by hundreds of small aftershocks in the next several days.

On September 21 there was another earthquake, of magnitude 4.8, along the Kaoiki fault system, which also was followed by hundreds of small aftershocks.

The most significant event during the fourth quarter (fig. 3) was the October 5-6 eruption on the east rift zone of Kilauea. It was characterized by small, shallow earthquakes, harmonic tremor, and collapse of the Kilauea summit. On October 23 an earthquake of magnitude 5.3 occurred at a shallow depth along the Kaoiki fault system; it was followed by several hundred small aftershocks.

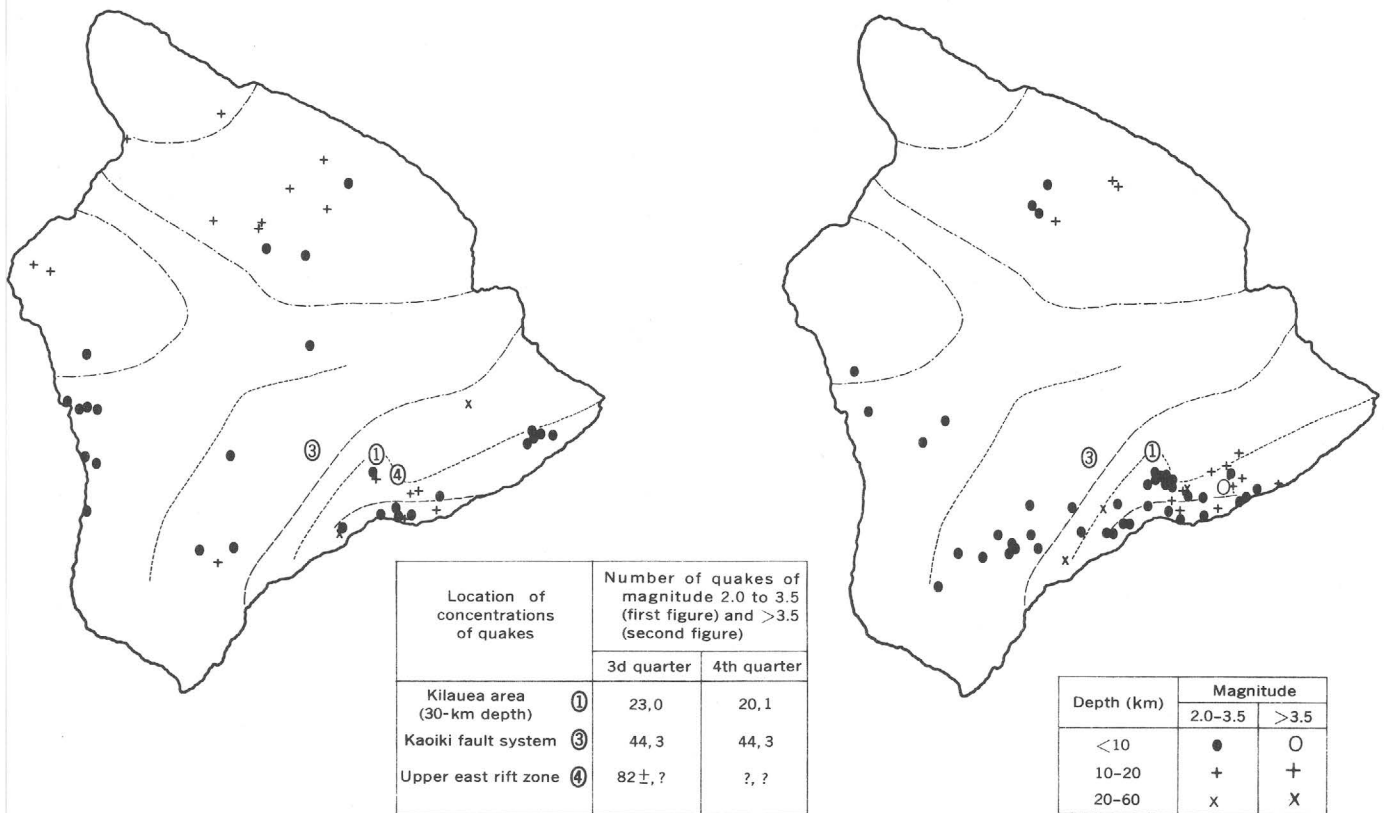


FIGURE 3.—Epicenters of earthquakes of magnitude 2.0 and greater for the third quarter (left) and fourth quarter (right) of 1963. The number symbols identify concentrations of quakes that are listed in the left-hand table because they are too numerous to plot separately, and represent the following areas: (1) Kilauea, at a depth of 30 km; (3) along the Kaoiki fault system; and (4) along the upper east rift of Kilauea. No quakes of this magnitude were reported for the Kalapana Trail area (location 2, fig. 2). Geographic names are shown on figure 1. The number of earthquakes in the upper east rift during the October eruption on the east rift of Kilauea was difficult to determine accurately because of the complexity of the seismograms.

SUMMARY

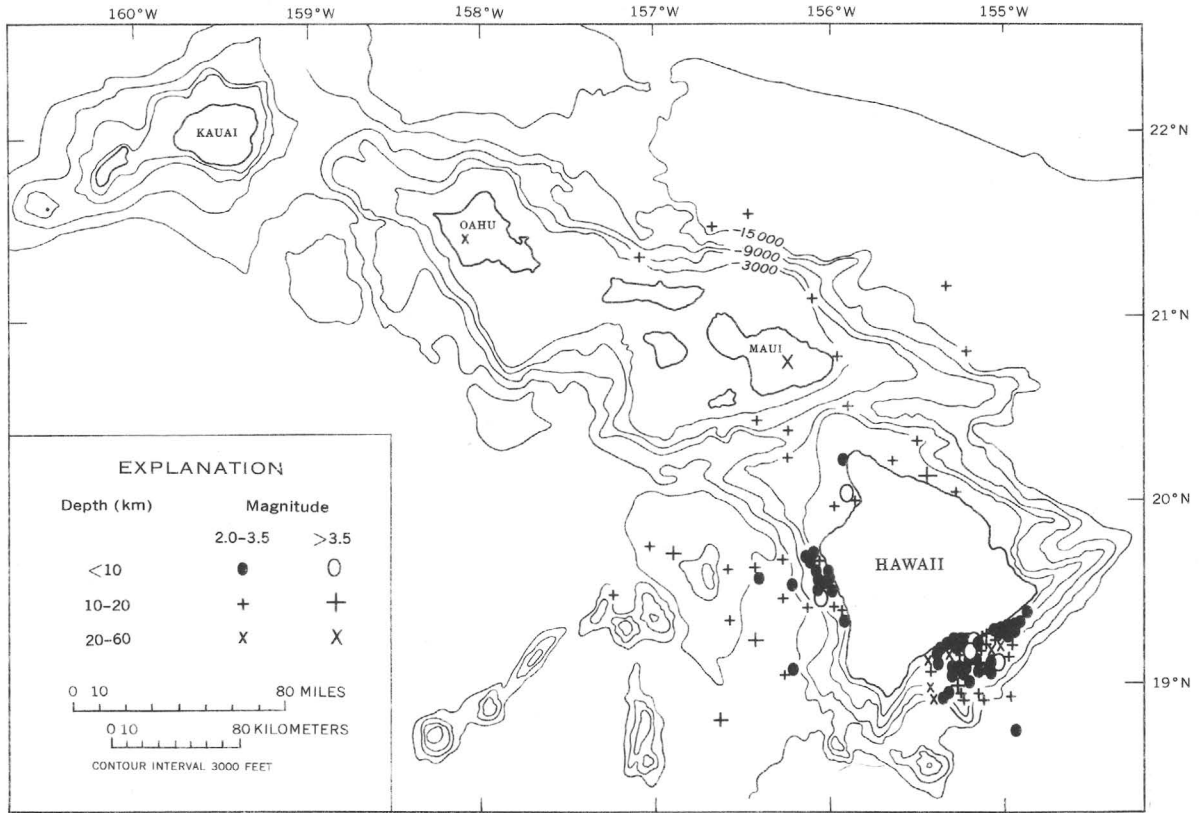
Earthquakes in Hawaii during 1963 were most numerous on the southeast end of the Hawaiian Ridge, mostly on the island of Hawaii (fig. 4). As documented for the period April 1958 to September 1959 (Eaton, 1962) and for 1962 (Koyanagi, 1964), seismic activity was greatest near and beneath the two active volcanic systems, Kilauea and Mauna Loa, and less in the dormant systems, Mauna Kea, Hualalai, and Kohala (fig. 5). Of the earthquakes of magnitude 2 and greater which were recorded and located in 1963, 47 percent were beneath Kilauea, 29 percent beneath Mauna Loa, 6 percent beneath Mauna Kea, 1 percent beneath Hualalai, 1 percent beneath Kohala, and the remaining 16 percent were offshore. Seventy-six percent of the earthquakes occurred beneath the active volcanic systems of Kilauea and Mauna Loa. Most of the recorded quakes were smaller than 2 in magnitude; of that group, most were

less than 1. Many of these took place at shallow depths beneath Kilauea Caldera, where earthquake counts of hundreds per day were not uncommon.

Both of the outbreaks on the flank of Kilauea in 1963 were characterized by several hours of shallow but intense pre-eruption seismic activity in the summit region, harmonic tremor for the duration of the eruptive period, and marked deflation of the summit.

Focal depths of earthquakes ranged from near surface to 45 kilometers. With the exception of earthquakes that occurred in the highly seismic zone 30 kilometers beneath the Kilauea Caldera region, most earthquakes had focal depths of less than 15 kilometers.

About 100 earthquakes of magnitudes 3-5 were reported felt on the island of Hawaii during 1963. Some shallow quakes of less than magnitude 3, along the east rift zone of Kilauea near the residential area of Pahoehoe, were reported felt by inhabitants.



Base from U.S. Navy Hydrographic Office Preliminary Sheet BC 04N

FIGURE 4.—Map of the Hawaiian Ridge showing epicenters of earthquakes during 1963 of magnitude 2.0 and greater located off the island of Hawaii.

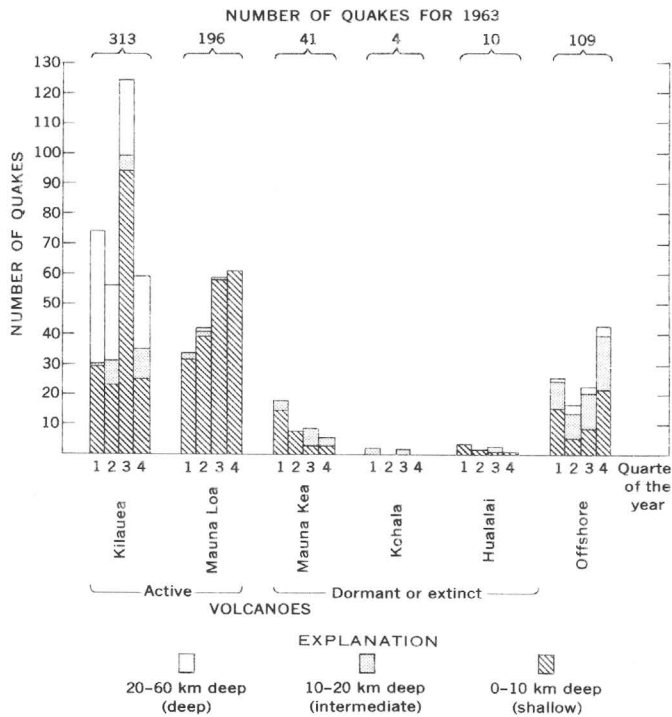


FIGURE 5.—Bar graph showing earthquakes of magnitude 2.0 and greater which occurred along the Hawaiian Ridge during 1963.

REFERENCES

Eaton, J. P., 1962, Crustal structure and volcanism in Hawaii, in Macdonald, G. A., and Kuno, Hisashi, eds., Crust of the Pacific Basin: Am. Geophys. Union, Geophys. Mon. 6, p. 13-29.

Koyanagi, R. Y., 1964, Hawaiian seismic events during 1962, Art. 144 in U.S. Geol. Survey Prof. Paper 475-D, p. D112-D117.

Koyanagi, R. Y., Okamura, A. T., Krivoy, H. L., and Yamamoto, A., 1964a, Hawaiian Volcano Observatory summary: U.S. Geol. Survey Hawaiian Volcano Observatory Summary 29 (Jan., Feb., and March 1963).

Koyanagi, R. Y., Okamura, A. T., Kinoshita, W. T., and Powers, H. A., 1964b, Hawaiian Volcano Observatory summary: U.S. Geol. Survey Hawaiian Volcano Observatory Summary 31 (July, Aug., and Sept. 1963). [In press]

Krivoy, H. L., Okamura, A. T., and Koyanagi, R. Y., 1964, Hawaiian Volcano Observatory summary: U.S. Geol. Survey Hawaiian Volcano Observatory Summary 30 (Apr., May, and June). [In press]

Macdonald, G. A., 1956, The structure of Hawaiian volcanoes: Gravenhage, K. Nederlandsch Geol.-Mijn. Genootschap Verh. Geol. Ser., Deel 16, p. 274-295.

Okamura, A. T., Koyanagi, R. Y., Kinoshita, W. T., and Powers, H. A., 1964, Hawaiian Volcano Observatory summary: U.S. Geol. Survey Hawaiian Volcano Observatory Summary 32 (Oct., Nov., and Dec. 1963). [In press]



**CORRELATION OF ZINC ABUNDANCE
WITH STRATIGRAPHIC THICKNESS VARIATIONS
IN THE KINGSPORT FORMATION, WEST NEW MARKET AREA,
MASCOT-JEFFERSON CITY MINING DISTRICT, TENNESSEE**

By HELMUTH WEDOW, JR., and JAMES R. MARIE,
Knoxville, Tenn., Alexandria, La.

Abstract.—The stratigraphic thickness of the upper dolomite member of the Kingsport Formation varies inversely with that of the lower limestone member of the Kingsport at the rate of about 1:–3 in the West New Market area. Zinc abundance coefficients of the Kingsport, as calculated from drill-hole assay data, vary directly but logarithmically with the inverse thickness relation. Ten-fold increments occur in the abundance coefficients for changes of +42 feet and –25 feet in the respective thicknesses of the upper and lower members. These numerical relations suggest that a fracture porosity, created by collapse dilatation of the upper dolomite member where the lower member had been thinned by solution removal of limestone, became clogged by deposits from migrating zinc-bearing fluids.

The West New Market area lies in the heart of the Mascot-Jefferson City mining district, Tennessee (fig. 1). Large reserves of zinc ore were discovered in this area during the 1950's by the American Zinc Co. of Tennessee (Oder, 1958), with government assistance through a loan supplied by the Defense Minerals Exploration Administration of the U.S. Department of the Interior. In 1960, Tri-State Zinc, Inc., conducted additional drilling in the West New Market area in advance of its joint venture with American Zinc to develop part of the West New Market ores. The wealth of data gained as a result of these exploration drilling programs is so immense that it is almost unwieldy. Accordingly, the U.S. Geological Survey has in progress a project to reduce some of these data, as well as some from other exploration programs in the East Tennessee zinc districts, to more manageable and comprehensible form through the application of mathematical and statistical techniques. The present paper is a preliminary report on several of the more significant statistical patterns that have emerged in the course of developing electronic-computer programs to handle the multiplicity of data and calculations. The authors wish to thank

the American Zinc Co. of Tennessee and the New Market Zinc Co. for permission to use selected drilling data from the West New Market area for this statistical analysis.

Initial study of the West New Market drill logs, structure sections, and isochore maps indicated qualitatively that the host Kingsport Formation¹ of the Lower Ordovician part of the Knox Group is thinner where penetrated by ore and shine holes than where penetrated by trace and barren holes.² The local thinning of the Kingsport appears to be due to the thinning of its lower limestone member; the upper fine-grained dolomite member has a tendency to thicken concomitantly, but not sufficiently for complete compensation. This qualitative relation is exemplified by the cross section of figure 1. In the 20 drill holes of this section, mean thicknesses of the lower and upper members are 82.1 and 175.4 feet, respectively. If the 20 holes are divided into two groups: barren and trace holes on the one hand, and shine and ore holes on the other, the resulting mean thickness for each member in each group (see table 1) clearly indicates that zinc is in greater abundance in areas where the lower member thins and the upper member thickens.

¹ In this paper the Kingsport Formation is considered to be the strata subtended by horizons G-192 above and G-(–)62 below; the G-28 horizon marks the division of the formation into the upper dolomite and lower limestone members (Oder and Miller, 1945, table 2; Oder and Ricketts, 1961, pl. 1). The lower limestone member is also considered to be the equivalent of the "R" and "S" beds of Crawford (1945, p. 413, 414, and fig. 1) in the Jefferson City area.

² An ore hole is one which has cut at least one interval of zinc-bearing material of minable grade and thickness. A shine hole shows strongly mineralized rock but contains no minable interval attaining ore grade. A trace hole is but weakly mineralized with a few scattered traces (specks) of sphalerite. Barren is used to designate a hole in which no sphalerite was noted during normal visual core logging and, thus, was not studied in greater detail nor assayed chemically; doubtless, a more thorough study of the "barren" core, particularly with optical aids, would have upgraded some of the barren holes to the trace category.

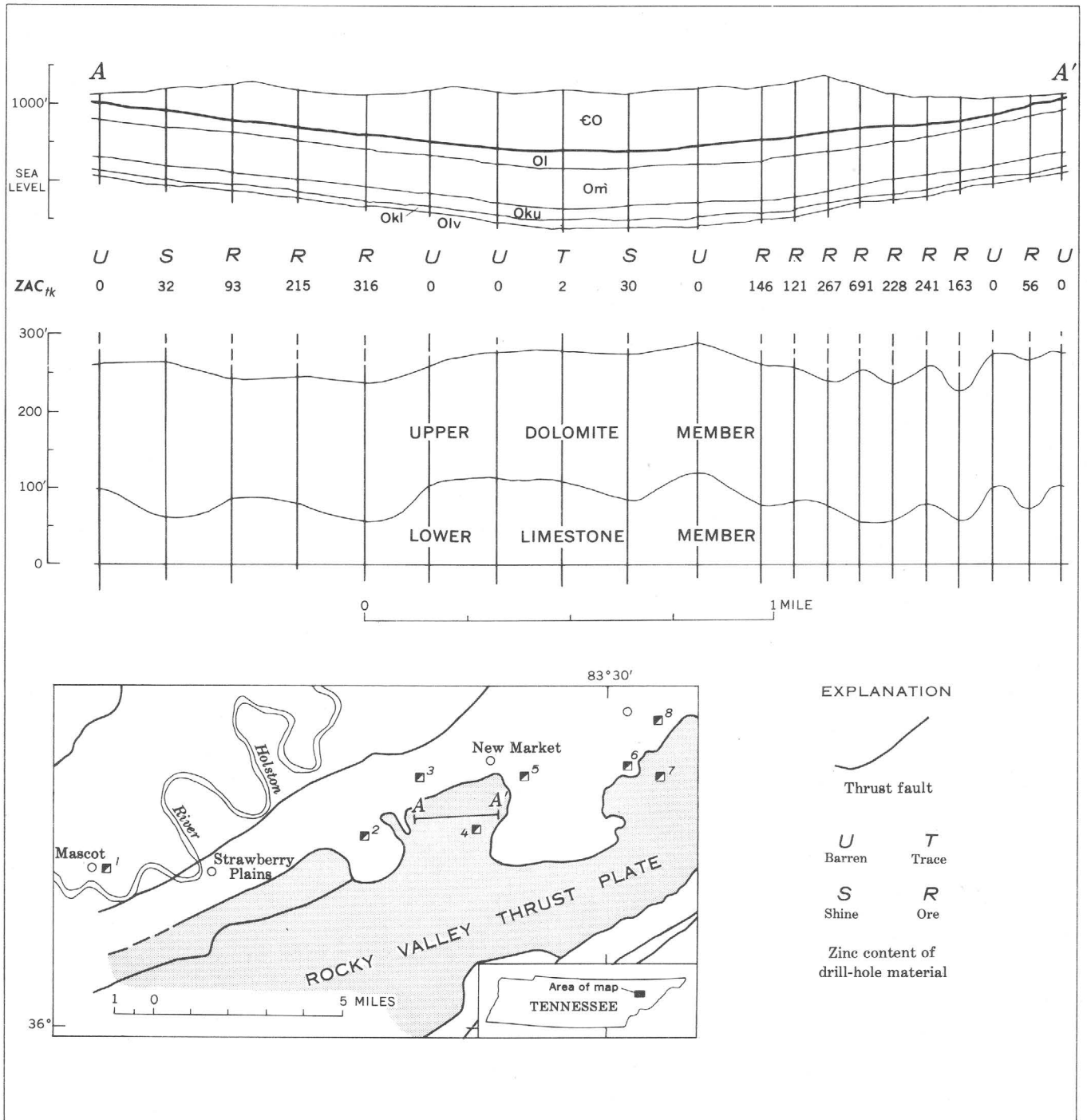


FIGURE 1.—Geologic section A-A' in the West New Market area, Mascot-Jefferson City zinc district, Tennessee. Upper section, with no vertical exaggeration, shows present structure. CO, Cambrian and Ordovician formations in hanging-wall block of Rocky Valley thrust fault; Ol, Lenoir Limestone; Om, Mascot Dolomite; Oku, Kingsport Formation, upper dolomite member; Okl, Kingsport Formation, lower limestone member; Olv, Longview Dolomite. Lower section, with $\times 10$ vertical exaggeration and base of Kingsport Formation as zero datum, shows relative thickness variations of the upper and lower members of the Kingsport Formation. R, S, T, and U indicate ore, shine, trace, and barren (see footnote 2 for definitions) categories, respectively, in a semiquantitative classification of the amount of zinc found in the drill holes (vertical lines). ZAC_{tk}, zinc abundance coefficients (see footnote 3 for derivation) of the Kingsport Formation in drill holes. Mine locations on index map: 1, Mascot No. 2; 2, Young; 3, North Friends Station; 4, New Market; 5, Grasselli; 6, Davis-Bible; 7, Jefferson City; and 8, Coy.

TABLE 1.—Mean thickness, in feet, of the Kingsport Formation in the 20 drill holes of geologic section A-A' in figure 1

	Barren and trace holes (7)	Ore and shine holes (13)	All holes (20)
Upper member	167.4	179.7	175.4
Lower member	105.1	69.7	82.1
Total	272.5	249.4	257.5

Of the more than 350 holes drilled in the 10-square-mile West New Market area, 150 representing all holes in the central 4 square miles of the area were selected for a preliminary quantitative study of the thickness variations and their bearing on zinc abundance. Stratigraphic thickness data were derived by correcting drill-hole penetration thickness for dip, although as most dips in this area are less than 10° this correction is relatively insignificant and does not appreciably modify the statistics. Quantity of zinc in the Kingsport Formation in each drill hole is expressed numerically by a zinc abundance coefficient.³ Both thickness data and zinc abundance coefficients were rounded to the nearest whole number, except for the low coefficients of less than 0.5 but more than zero, which were upgraded to unity. The data thus derived comprise four variables for each drill hole: the stratigraphic thicknesses (in feet) of (1) the Kingsport Formation and its (2) lower limestone and (3) upper dolomite members, and (4) the zinc abundance coefficient for the total Kingsport; for convenience these variables are designated TK , LK , UK , and ZAC_{tk} , respectively. Table 2 presents the respective frequency distributions of the variables. Means, sample standard deviations (s), and the relative measures of skewness, α_3 , based on the third moment about the mean (Croxtton and Cowden, 1955, p. 229–232), are also listed in table 2. The univariate distributions of LK , UK , TK , and $\log ZAC_{tk}$ are also shown by histograms on figure 2. Chi-square values (to show

“goodness-of-fit” to normal distributions with the same means and standard deviations) and the calculated normal curves are also given with the histograms.

The statistics show that although the frequencies of TK can be considered to approximate a normal distribution, the distributions of LK and UK are nowhere near normal. The distribution of LK is bimodal and appears to be somewhat left skewed, whereas that of UK has but a single mode and is strongly right skewed. The combination of the thicknesses of the two members into that for the total formation (TK) tends to cancel out the opposing skewnesses, so as to develop a more normal distribution, although a hint of the slightly left skewed bimodal character of LK is retained.

The distribution of ZAC_{tk} (table 2) is clearly the least normal of the variables considered herein. It is extremely right skewed ($\alpha_3 = +2.13$) and is thus probably log-normal. Consequently, log transformations of the ZAC_{tk} values were used for further study of the variation of zinc abundance and its relation to variations in the stratigraphic thickness of the members of the Kingsport Formation (see $\log ZAC_{tk}$, table 2). The distribution of $\log ZAC_{tk}$ is distinctly different from ZAC_{tk} , having two strong modes and a much lower skewness coefficient. The chi-square value (fig. 2) shows that it is less normal than any of the thickness variables considered above. The impression of right skewness, in spite of a relatively low value for α_3 , is caused by arbitrarily cramming all zero values of ZAC_{tk} into the lowest log class interval (1.5–0.0). The frequency distribution of ZAC_{tk} is probably about equally divided into two log-normal subpopulations with high and low mean⁴ abundance coefficients of less than 1 and about 70, respectively. If these distributions are log-normal, it can be reasoned that the “barren” holes contain slight traces of sphalerite which are below the threshold of “measurement” in visual core logging. Obviously, actual chemical data, from which the lower values of the abundance coefficients can be calculated precisely, will be necessary for a better understanding of univariate distribution of this variable.

The inverse correlation of UK with LK , suggested by the opposing skewnesses of their univariate distributions and by the approach to normalcy when they are summed into the distribution of TK , is clearly seen in their bivariate frequency distribution (fig. 3). The standard statistical test for correlation by the product moment method yields an r_{xy} coefficient of -0.42 . This value is considered highly significant, as the critical value of r_{xy} for significance at the 1-percent level is 0.21

³ Zinc abundance coefficients (ZAC) are calculated by summing the foot-percent (that is, the length of the assay run, in feet, times the zinc content, in percent) values of all chemical assays in the total thickness interval of the stratigraphic unit for which a coefficient is desired, in this case the Kingsport Formation. The semiquantitative visual designations of “shine” and “trace,” which are not assayed chemically in normal company practice, are each given the arbitrary low foot-percent values of 0.4 and 0.2, respectively. In the few instances where chemical assays of weakly mineralized runs were not made, the original visually estimated grades are used directly. An example of the calculation of ZAC for a hypothetical drill hole follows:

Depth (feet)	Zinc content	Foot-percent values
750	Trace ZnS	0.2
782	Trace ZnS2
771	Shine ZnS4
808–812	4 ft at 5.6 percent	22.4
812–817	5 ft at 3.3 percent	16.5
820–822	2 ft at $\frac{3}{4}$ percent (estimated)	1.5
Zinc abundance coefficient (ZAC)		41.2

It is immediately apparent from the above that the low zinc abundance coefficients are based primarily on estimated values, whereas high coefficients are dominated by the more precise chemical assays.

⁴ Geometric mean, that is, the antilog of the arithmetic mean of the log values.

TABLE 2.—Univariate frequency distributions of stratigraphic thickness variables and zinc abundance coefficients of the Kingsport Formation in a sample of 150 drill holes from the West New Market area

[*LK*, thickness of lower limestone member; *UK*, thickness of upper dolomite member; *TK*, thickness of total Kingsport Formation; ZAC_{tk} , zinc abundance coefficient of Kingsport Formation; *f*, frequency; *s*, sample standard deviation; α_3 , skewness coefficient of sample frequency distribution (based on third moment about the mean)]

	<i>LK</i> (feet)		<i>UK</i> (feet)		<i>TK</i> (feet)		ZAC_{tk}		Log ZAC_{tk}	
	Class interval	<i>f</i>	Class interval	<i>f</i>	Class interval	<i>f</i>	Thickness × percentage of zinc			
							Class interval	<i>f</i>	Class interval	<i>f</i>
	<60	9	<150	6	<230	7	0	56	1.5-0.0-	56
	60-69	12	150-159	16	230-239	12	1-100	64	0.0-0.5-	19
	70-79	26	160-169	54	240-249	21	101-200	17	0.5-1.0-	5
	80-89	26	170-179	38	250-259	28	201-300	8	1.0-1.5-	12
	90-99	24	180-189	15	260-269	26	301-400	3	1.5-2.0-	27
	100-109	31	190-199	12	270-279	30	401-500	1	2.0-2.5-	26
	110-119	22	>199	9	280-289	18	501-600	0	2.5-3.0-	5
					>289	8	601-700	1		
Σ -----		150		150		150		150		150
Mean-----	89.5		172.0		261.6		97.3		0.86	
<i>s</i> -----	17.3		14.0		17.9		106.9		1.05	
α_3 -----	-0.27		+0.60		-0.16		+2.13		+0.25	

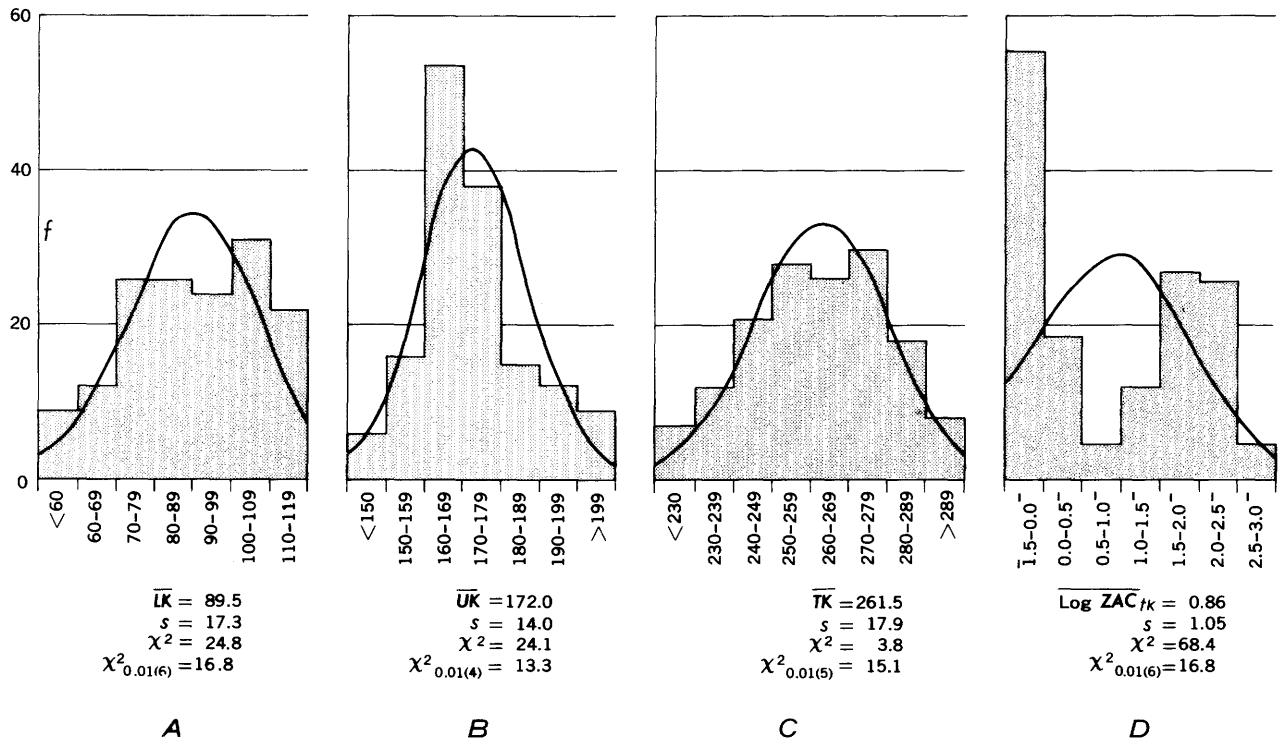


FIGURE 2.—Histograms showing frequency distributions of the variables *LK* (A), *UK* (B), *TK* (C), and log ZAC_{tk} (D) in a sample of 150 drill holes from the West New Market area. Arithmetic means (symbols with overhead bars), sample standard deviations (*s*) for these distributions, and the chi-square values (χ^2) (to indicate relative "goodness-of-fit" to normal curves derived from these statistics) are also given. Subscripts of the χ^2 values indicate levels of significance with their respective degrees of freedom in parentheses. The respective curves for normal distributions having the same means and standard deviations are plotted over the histograms.

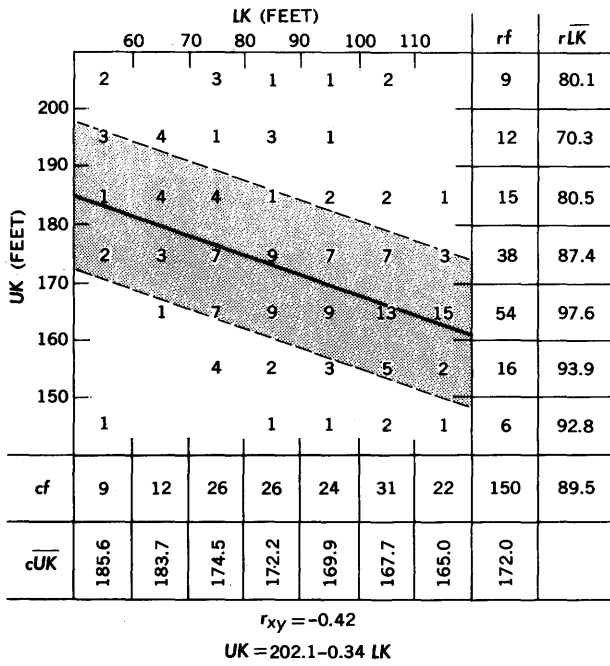


FIGURE 3.—Combination bivariate frequency distribution table and linear regression diagram, showing relation of stratigraphic thickness of upper dolomite member (UK) to that of the lower limestone member (LK) of the Kingsport Formation, from drill-hole data in the West New Market area. Numbers in body of figure indicate hole frequencies in 10-foot by 10-foot cells. Stippled zone is 1 standard error of estimate (68-percent confidence). rf and cf are row and column frequencies, respectively. rLK and cLK are row and column means, respectively. r_{xy} is product-moment correlation coefficient.

for an N of 150 (by interpolation, Dixon and Massey, 1957, table A-30a, p. 468). The slope coefficient in the linear regression equation of UK on LK ,

$$UK = 202.1 - 0.34 LK,$$

was tested against the hypothesis that it may be zero (that is, $H: B=0$). As the calculated value of t (Dixon and Massey, 1957, p. 196) is -4.6 and the critical region of t at the 1-percent level of significance is -2.6 to $+2.6$, there is excellent reason to believe that UK is dependent on LK .

Figure 4 demonstrates the exponential relations of ZAC_{tk} to the thicknesses of the two members of the

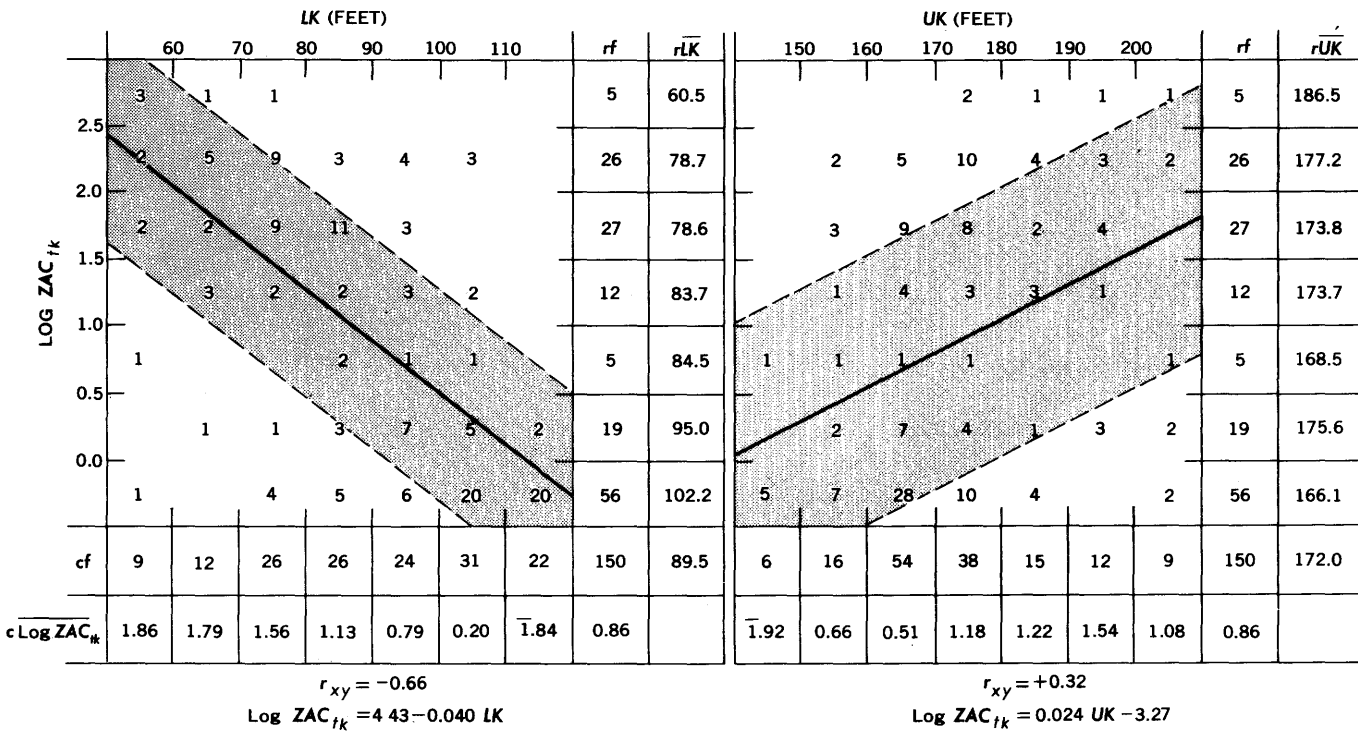


FIGURE 4.—Combination bivariate frequency distribution tables and linear regression diagrams, showing relation of $log ZAC_{tk}$ to LK and UK , respectively, from drill-hole data in the West New Market area. Numbers in body of figure indicate hole frequencies in $1/2$ -log-cycle by 10-foot cells. Stippled zones are 1 standard error of estimate (68-percent confidence). rf and cf are row and column frequencies, respectively. rLK and rUK are row means of the lower and upper members, respectively, of the Kingsport Formation. $cLog ZAC_{tk}$ is the column mean of the log of the abundance coefficient. r_{xy} is the product-moment correlation coefficient.

Kingsport Formation. The variation is inverse with the lower member and direct with the upper. The linear correlations of $\log ZAC_{tk}$ to LK and to UK having r_{xy} values of -0.66 and 0.32 , respectively, are also considered significant at the 1-percent level (critical value 0.21 for an N of 150). Tests of the regression coefficients in the equations

$$\log ZAC_{tk} = 4.43 - 0.040 LK$$

$$\log ZAC_{tk} = 0.024 UK - 3.27$$

were made against the hypotheses that they may equal zero. The calculated value of t_{lk} is -10.7 and of t_{uk} is $+4.1$. With the critical region of t in both cases being -2.6 to $+2.6$ at 1-percent significance, dependence of $\log ZAC_{tk}$ on LK and UK is indicated.

It is concluded from the foregoing statistics derived from the drilling data in the West New Market area that within the limits of the data the upper dolomite member of the Kingsport Formation thickens about a third of a foot for every foot of thinning in the lower limestone member. Furthermore, there is a 10-fold increase in zinc abundance, as compiled from assay data, for every 25 feet of thinning of the lower member and for every 42 feet of thickening of the upper member. It is conjectured that, during the development of an extensive karst terrane on the Knox Group in early Middle Ordovician time (Wedow, 1961; Hoagland and others, 1964), stresses were created in the upper dolomite member of the Kingsport Formation by the solution removal of limestone from the lower member. Such stresses were relieved concomitantly by sag, rupture, and collapse, vertically dilating the upper member (Wedow and Marie, 1964). As this increase in the thickness of the upper member is not sufficient to compensate completely for the thinning of the lower member, further

evidence of dilatancy and accompanying mineralized breccias may be anticipated in the overlying Mascot Dolomite. Correlation of zinc abundance with the inverse relation between the thicknesses of the two members of the Kingsport can follow, where the fracture porosity created by collapse dilatation has been lessened or destroyed by the cementing effect of deposits from migrating zinc-bearing fluids.

REFERENCES

- Crawford, Johnson, 1945, Structural and stratigraphic control of zinc deposits in East Tennessee: *Econ. Geology*, v. 40, p. 408-415.
- Croxton, F. E., and Cowden, D. J., 1955, Applied general statistics: New York, Prentiss-Hall, Inc., 843 p.
- Dixon, W. J., and Massey, F. J., Jr., 1957, Introduction to statistical analysis: New York, McGraw-Hill Book Co., Inc., 488 p.
- Hoagland, A. D., Hill, W. T., and Fulweiler, R. E., 1964, Observations relating to the genesis of the East Tennessee zinc deposits [abs.]: *Geol. Soc. America Spec. Paper* 76, p. 80, 81.
- Oder, C. R. L., 1958, How American Zinc's Tennessee DMEA program proved 35,000,000 tons ore: *Mining World*, v. 20, no. 7, p. 50-53.
- Oder, C. R. L., and Miller, H. W., 1945, Stratigraphy of the Mascot-Jefferson City zinc district [Tenn.]: *Am. Inst. Mining and Metallurgical Engineers Tech. Pub.* 1818, *Mining Technology* v. 9, no. 3, 9 p.
- Oder, C. R. L., and Ricketts, J. E., 1961, Geology of the Mascot-Jefferson City zinc district, Tennessee: Tennessee Dept. Conserv. and Commerce, Div. Geology, Rept. Inv. 12.
- Wedow, Helmuth, Jr., 1961, Structures underlying prominent Early and Middle Paleozoic erosion surfaces in the southern Appalachian Valley [abs.]: *Tennessee Acad. Sci. Jour.*, v. 36, p. 140, 141.
- Wedow, Helmuth, Jr., and Marie, J. R., 1964, Statistical analysis of solution-collapse structures [abs.]: *Geol. Soc. America Spec. Paper* 76, p. 262.



MERCURY-BEARING ANTIMONY DEPOSIT BETWEEN BIG CREEK AND YELLOW PINE, CENTRAL IDAHO

By B. F. LEONARD, Denver, Colo.

Abstract.—A stibnite deposit accidentally found in the spring of 1964 contains appreciable cinnabar. The mercury content of selected samples is 0.5–5 percent. The ore is in a sheared, silicified zone in granodiorite cut by Miocene (?) dikes. Mercury was not previously known from central Idaho mineral deposits having this geologic setting. The discovery of this workable ore body refocuses attention on the mineral potential of extensive silicified zones in the region.

Mercury was discovered in an antimony deposit in the Big Creek mining district in September 1964. The antimony deposit itself had been found only a few months before, when high-grade stibnite was accidentally uncovered on the B and B claims by Ray Nissula while bulldozing an access road to other claims in the Profile Summit area. The stibnite find was partly explored by stripping, and by late summer a modest tonnage of antimony ore had been trucked to a custom mill at Yellow Pine for treatment. Later in September, the operator found that "red mud" from overburden at the southwest end of the workings contained mercury (Ray Nissula, 1964, oral communication). Independently and almost simultaneously, cinnabar was identified by the U.S. Geological Survey from specimens of the antimony ore.

No reliable estimate of the expectable size or average grade of the deposit could be made from the sparse data available when I examined the property in September. However, the showing was of considerable promise, considering the accessibility of the deposit, presence of a mill at Yellow Pine, and current local price of 38 cents per pound of contained antimony. The presence of mercury in the ore, not known at the time of my examination, September 4, 1964, should enhance its value considerably if both mercury and antimony can be satisfactorily recovered.

The following preliminary account, based on observations made on the above date is presented because (1) the cinnabar-bearing stibnite deposit itself is of immediate economic interest, (2) mercury has not previously

been reported from the Big Creek district, and (3) an intimate association of stibnite and cinnabar, said to be common in nondomestic deposits of this character, is rare in the adjoining Yellow Pine district, which has been a major producer both of antimony and of mercury from discrete deposits containing those metals.

The cinnabar-bearing stibnite deposit on the B and B claims is the only new body of antimony ore to be exploited in the Big Creek-Yellow Pine area in 20 years, and the first find of mercury ore outside the narrow limits of the Cinnabar-Fern area of the Yellow Pine district.

LOCATION

The B and B group of unpatented claims is northeast of Profile Summit, the pass crossed by the graded forest road from Yellow Pine to Big Creek, Valley County, Idaho. The mercury-antimony deposit described in this report is on the B and B No. 4 claim, 1.1 miles by road from Profile Summit toward Big Creek, at elevation 7,270 feet, NW $\frac{1}{4}$ NW $\frac{1}{4}$ sec. 19, T. 20 N., R. 9 E., in Payette National Forest. An access road 250 feet long extends from the graded road to the prospect. The topographic map for the area is the Big Creek 15-minute quadrangle, scale 1:62,500. The B and B claims are held by Frank Callender and Ray Nissula, Cascade, Idaho. The antimony deposit is being worked by Ray Nissula.

Access to this mountainous area is relatively good for central Idaho. Profile Summit is open to traffic from June to November, and the rest of the forest road is open longer. The road distance from Yellow Pine to the prospect is about 15 miles, and from Big Creek settlement about 8 miles. Both settlements are served by graded roads maintained by the U.S. Forest Service and airstrips maintained by the Idaho Department of Aeronautics. McCall and Cascade are the nearest villages served by highway and railroad.

GEOLOGIC SETTING

The mercury-bearing antimony deposit is in a major system of silicified zones that accompanies the Profile dike swarm near the heart of the Idaho batholith. The Profile swarm, shown on figure 3 of Shenon and Ross (1936, following p. 12), is part of a larger swarm that extends northward for 11 miles through the Big Creek quadrangle from Middle Lake to the head of the north fork of Smith Creek. (To locate the B and B deposit on Shenon and Ross' figure 3, plot a point 200 feet southwest of the old prospect shown at the road edge, on the contact between "moraine" and "Idaho batholith," 2,500 feet northeast of Profile Summit, the "Profile Gap" of their map.) Most of the dikes are granitic porphyries. Because similar dikes elsewhere cut the Challis Volcanics of Eocene(?), Oligocene, and Miocene(?) age, they are thought to be approximately of Miocene age. In the Profile Summit area, the silicified zones are mainly in a slightly contaminated facies of felsic granodiorite of the Idaho batholith. These silicified zones are replacements, fissure fillings, and stockworks within a mylonitized, sheared, and brecciated belt of granodiorite. At the undeveloped Red Bluffs scheelite-huebnerite deposit, the sheared part of the silicified material is pre-dike in age, while the undeformed quartz, scheelite, huebnerite, and accessory sulfides of copper, lead, and zinc are either syn- or more likely post-dike. The ore-quartz relations may be similar at the mercury-antimony deposit on the B and B claims, since both deposits occur in the same dike swarm and scattered stibnite prospects, some of them close to scheelite prospects, are present in similar though not continuous silicified zones near Yellow Pine and Big Creek settlements. However, the relation of the newly discovered cinnabar-stibnite deposit to nearby showings of stibnite and scheelite, such as those reported by Shenon from the present Syringa and adjoining Glasgow claims (Shenon and Ross, 1936, p. 24), is still to be determined.

The geologic setting of the B and B deposit is similar in its essential features to that of the antimony-gold-tungsten deposit at the Yellow Pine mine at Stibnite described by White (1940) and Cooper (1951), but different from that of the mercury deposits at the Hermes (Cinnabar) and Fern mines described by Larsen and Livingston (1920), Ross (Schrader and Ross, 1926, p. 156-163), and Bradley (1943). In the Stibnite-Cinnabar area, the minerals stibnite and cinnabar have been found together only at the Sugar Creek prospect (Cooper, 1951, p. 188). Cooper's observation has subsequently been confirmed by Ernest Oberbillig (1963, oral communication), a mining engineer familiar with the antimony and mercury deposits of the region.

The discovery of mercury and antimony ore on the B and B claims reemphasizes the mineral potential of the extensive shear zones in the Big Creek and Yellow Pine districts and should stimulate prospecting for similar deposits in this environment.

STRUCTURE

The B and B cinnabar-bearing stibnite deposit is in a sheeted quartz "vein" that strikes N. 30°-40° E. and dips perhaps 75°-80° SE. On September 4, ore was intermittently exposed for a length of 40 feet. The southwest end was covered by mud washed in from the low bench above; the northeast end was still concealed beneath undisturbed colluvial and glacial debris. The single good exposure across the vein showed a width of 5 feet of ore. The height between the 2 exploratory benches was 8-10 feet. The estimated grade of the ore was 14 percent stibnite by volume, equivalent to about 15 percent antimony by weight. The mercury content was unknown.

Several factors that affect the apparent attitude and dimensions of the exposed ore body are discussed below.

The strike, based on intermittent exposures, is obvious; the dip is not. Subparallel stibnite veinlets within the sheeted quartz vein strike N. 35°-40° E. and dip 75°-80° SE. The hanging wall of ore exposed on September 4 was a scaly surface striking N. 30° E. and dipping 55°-80° SE. For want of better information the inferred attitude of the ore body is therefore N. 30°-40° E., 75°-80° SE., perhaps dipping more gently in places.

The hanging wall exposed on September 4 was a surface only, about to be tested in the third dimension by drilling. The area to the southeast was muck covered.

The position of the footwall is somewhat better known. Intermittent exposures on the bench floor northwest of the ore body showed a 28-foot width of vein quartz, locally with coarse muscovite and perhaps a little relict granodiorite. This quartz contained disseminated pyrite specks but only a few very small knots of stibnite. Farther west the bench was muck covered.

Two features suggest that the ore body might be a plunging shoot within the silicified zone. The hanging wall exposed on September 4 showed striae generally raking 15°-20° NE., but locally steeper; the striae are nearly parallel to the trace of a set of coarse, gently dipping joints. Groups of stibnite veinlets within the quartz vein seemed to form pods raking about 70° NE. This scanty information is enough to suggest that the hypothesis of shoot structure should be kept in mind as exploration advances. Shoots plunging about 30° N. were present in gold-antimony ore at the Meadow Creek and Yellow Pine mines near Stibnite (Cooper, 1951, p.

182 and pl. 44; pl. 42, section A-A'), and mercury ore at the Hermes mine may have been confined to a gently plunging shoot (Bradley, 1943, p. 41-42). The presence of shoot structure in these neighboring ore bodies emphasizes the possibility of there being a similar disposition of ore at the B and B deposit.

Possible right-lateral offset and repetition of the ore body by faulting is suggested by scale structure accompanying the striae on the apparent hanging wall of the exposed ore. The steps of the scales or flakes indicate that relative movement along this surface was west side north and down. If the apparent hanging wall is the true hanging wall, and if significant movement occurred along that surface after deposition of the stibnite, one might be prompted to seek a ruptured part of the stibnite body—in effect, a new ore body—southwest of the present exposure and on the southeast side of the projected hanging-wall surface. The amount of possible right-lateral offset cannot be predicted from the data at hand; consequently, prospecting for an inferred repetition of the known ore body would be somewhat hazardous.

MINERALOGY

The principal ore mineral is stibnite. Associated metallic minerals—all relatively sparse, fine grained, and disseminated—are cinnabar, pyrite, arsenopyrite(?), sphalerite, boulangerite(?), and covellite(?). The last three are too sparse to warrant further comment in this report. Quartz is the chief gangue mineral; several generations are present. Barite is common in cinnabar-bearing specimens. Purple sericite is rare. Alteration products are mainly orange, yellow, green, and white antimony oxides, locally accompanied by limonite, scorodite(?), minute crystals of quartz, and a bit of white clay. These secondary minerals were conspicuous, though quantitatively negligible, in ore piled for shipment; they were sparse at the mine face. Presumably they are largely or wholly supergene. Unidentified powdery black material is present locally; it may be an antimony oxide. Its status as a secondary mineral is doubtful. Secondary mercury minerals, if present, have not been recognized.

Stibnite, mostly fine grained but in part coarsely bladed and locally vuggy, forms patches, veinlets, and irregular masses in quartz. The larger veinlets are one-half inch to several inches thick and a few feet long, subparallel to the vague sheeting in the quartz host and scattered at close intervals throughout it, possibly as plunging podlike(?) bodies. Much of the stibnite is a replacement of quartz, but some small veinlets are fissure fillings. Other veinlets show a combination of these features, one wall being sharply defined and unreplaced, each projection of the wall corresponding to an inden-

tation in the stibnite, the other wall being fuzzy and bordered with islands of quartz in stibnite. A little stibnite occurs as small clots of finely disseminated grains, or as clusters of prisms a few millimeters long. One specimen shows thicker stibnite veinlets slightly displaced by an oblique fracture along which barite and second-generation stibnite have been introduced, largely as a replacement of the quartz host.

Cinnabar, the common form of mercury sulfide, occurs sporadically in stibnite and quartz as groups of discrete granules, as patches of coalescing granules, and as coatings of very small crystals. Each granule and crystal is a millimeter or less in diameter (less than $\frac{1}{16}$ inch). Once identified, the mineral is easily recognized by its red color and finely granular habit. Even where sparse, it is conspicuous in association with quartz or orange and yellow antimony oxides, but it is readily overlooked in massive stibnite, where it may be undetected until the specimen is cut by a rock saw. Cinnabar replaces both quartz and stibnite, and some thin veinlets of second(?) -generation stibnite are cut by hairlike veinlets of cinnabar. In all specimens showing a quartz-stibnite contact, cinnabar is close to the contact and concentrated in either the quartz or the stibnite. Commonly cinnabar is accompanied by medium-grained barite and by minute pyrite cubes. One specimen shows sparse crystals of cinnabar deposited on stibnite in a narrow, vuggy space between a barite vein and the gray quartz host. Part of this quartz has been brecciated and then cemented by the barite.

The quantity of cinnabar in the ore is difficult to estimate because of fine grain size and spotty distribution. Several specimens containing conspicuous cinnabar have about 0.5-1 percent of it by volume; the richest one contains about 7 percent. (One volume percent cinnabar is roughly equivalent to 1 weight percent mercury in antimony ore of average grade.) In some specimens, very sparse cinnabar was detectable only after sawing. Presumably cinnabar is absent from some of the antimony ore. Nevertheless, the sketchy data suggest that, under current economic conditions, the antimony ore from this deposit is also an ore of mercury. (See accompanying chemical data.)

Cinnabar is the only red mineral identified so far, although other red minerals resembling cinnabar—such as kermesite ($\text{Sb}_2\text{S}_2\text{O}$), some antimony oxides, realgar (AsS), and perhaps gerstleyite (complex hydrous sulfosalt containing Sb and As)—might be expected in an ore of this type. The identification of cinnabar, based on qualitative optical properties and microchemical tests (Hg and S positive, Sb and As negative), has been confirmed by an X-ray powder diffraction pattern made by Fred A. Hildebrand, Geological Survey.

Pyrite and arsenopyrite(?) are of interest because of their possible association with gold. For example, Cooper (1951, p. 167) states that the pyrite-arsenopyrite flotation concentrates from the Yellow Pine mine, Stibnite, Idaho, contained 1.5 to 2.5 ounces of gold per ton. The gold content of pyrite, arsenopyrite(?), and their oxidation products in ore from the B and B deposit has not yet been determined.

Tungsten minerals have not been identified in ore from this deposit, though small showings of scheelite are present on nearby claims of the Syringa group.

A mineral that might be expected in a deposit of this sort is livingstonite, the mercury-antimony sulfide. This rare mineral has not been identified from the B and B deposit. Outwardly the mineral looks like stibnite, from which it can perhaps be distinguished in the field by its darker, almost brownish-black color and slightly adamantine luster, and by the reddish tint of its black streak. Positive identification of livingstonite requires study of its optical properties in polished section or analysis of the powder by X-ray diffraction. Any of the stibnite ore that shows a high mercury content but little visible cinnabar or secondary mercury minerals may be suspected of containing livingstonite or metacinnabar (black mercury sulfide) and should be subjected to appropriate tests.

CHEMICAL DATA

Analytical data are given in the accompanying table. The data are for individual specimens selected to show a range in antimony and mercury content. The quantitative determinations of antimony are not yet available. Those of mercury (Hg) indicate that mercury-bearing material of ore grade is indeed present in the antimony ore.

Mercury was determined spectrophotometrically after suitable dilution. The concentrations are considerably higher than those which the method was devised to measure; accordingly, the reported numbers should be regarded as good approximations rather than absolute values (F. N. Ward, Geological Survey, 1964, oral communication).

Silver (Ag) is present. Its concentration is highest in the stibnite-rich sample. Since the amount of stibnite in samples 1 and 3 can be estimated by eye, the ratio of stibnite to contained silver can be approximated. If we assume that the silver is closely associated with stibnite and likely to be concentrated with it during beneficiation, as it was at the Meadow Creek and Yellow Pine mines (Cooper, 1951, p. 170), high-purity stibnite concentrates prepared from these 2 samples should contain roughly 4 to 5 ounces of silver per ton. This is considerably less than the silver concentration reported for

TABLE 1.—Mercury content and semiquantitative spectrographic analyses of associated elements in selected samples, B and B deposit

[Weight percent. Analyses from laboratories of the Geological Survey. Mercury determined by J. B. McHugh, semiquantitative spectrographic analysis by R. G. Havens]

	1	2	3
Field No.....	L/64/SR7	L/64/SR13	L/64/SR14
Lab. No.....	D115188	D115189	D115190
Quantitative determinations			
Hg.....	0.5	5	0.4
Semiquantitative spectrographic analyses¹			
Si.....	M	M	M
Al.....	.7	1.5	3
Fe.....	.15	.3	1
Mg.....	.05	.07	.15
Ca.....	.07	.15	.15
Na.....	.05	.05	.07
K.....	0	0	1.5
Ti.....	.015	.02	.05
P.....	0	0	0
Mn.....	.002	.003	.015
Ag.....	.015	.001	.002
B.....	.0015	.0015	.003
Ba.....	.2	M	7
Be.....	0	0	.0002
Cr.....	.0002	.0005	.00015
Cu.....	.015	.003	.005
Ga.....	0	.0003	.001
Ge.....	.003	.001	.001
Hg.....	(?)	(?)	(?)
Pb.....	.05	.01	.01
Sb.....	>3	>3	>3
Sr.....	.001	.07	.02
Zn.....	.3	.3	.07
Zr.....	.002	.002	.005

Looked for, but found to be below the limits of spectrographic detection: As, Au, Bi, Cd, Ce, Co, Hf, In, La, Li, Mo, Nb, Ni, Pd, Pt, Re, Sc, Sn, Ta, Te, Th, Tl, U, V, W, Y, Yb.

1. High-grade antimony ore. Massive stibnite, slightly oxidized, with subordinate quartz. Cinnabar not visible until specimen was cut with a rock saw.
2. High-grade mercury ore, poor in antimony. Cinnabar-barite vein in stibnite-bearing quartz.
3. Antimony ore, roughly of average antimony grade but with more antimony oxides and more conspicuous cinnabar than most specimens. Hand specimen selected for study of cinnabar. Not intended to represent the deposit.

¹ M, major. 0, looked for but not detected. Other results are reported in percent to the nearest number in the series 1, 0.7, 0.5, 0.3, 0.2, 0.15, and 0.1, and so forth; these numbers represent approximate midpoints of group data on a geometric scale. The assigned group for semiquantitative results will include the quantitative value about 30 percent of the time.

² Detected. See separate determination at head of table.

stibnite concentrates from the Meadow Creek and Yellow Pine mines, but the crude nature of the estimate and the small number of samples of B and B ore should be kept in mind.

Gold (Au) is reported as zero in the spectrographic analyses. However, sensitivity for this element is low. Gold concentrations less than 0.002 percent, equivalent to 0.58 troy ounce per ton, would not be detected.

The selenium (Se) content of the samples, determined by Kam Leong, Geological Survey, is less than 1 part per million—much less than that of samples of anti-

mony ore from the Yellow Pine mine, as reported by Davidson (1960, p. 11).

OTHER OCCURRENCES

Other occurrences of stibnite are known in the Big Creek quadrangle. Information on most of these is scanty. Mercury minerals have not been recognized in any of them and are perhaps not to be expected in some, though it would be imprudent to prejudge them on this point. The occurrences are listed by number from south to north and referred to the appropriate ninth of the quadrangle. All except 1, 7, and 8 are in or near the silicified zones associated with the Profile-Smith Creek dike swarm. The locations given (fig. 1) are the best available at this time.

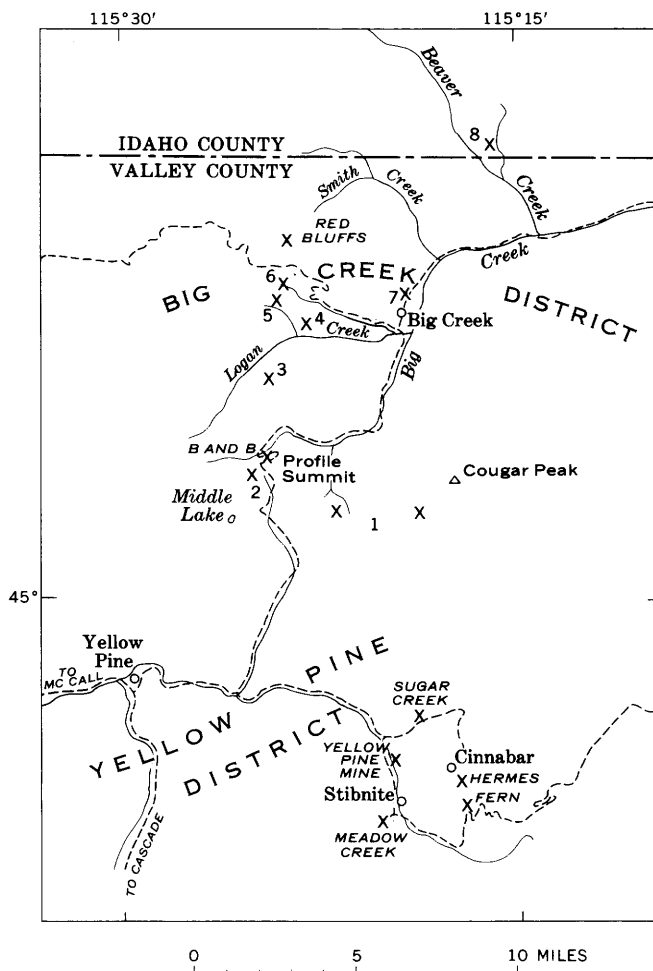


FIGURE 1.—Index map of parts of the Big Creek and Yellow Pine districts, Idaho. Location of prospects 1, 4, 6, 7, and 8 is approximate.

(1) Prospects near the head of Belvidere Creek, south-central ninth (Bert Fisher, 1954, oral communication; Robin McRae, 1964, oral communication), and near Cougar Peak, southeast ninth (Robin McRae, 1964,

oral communication). Presumably in area of Challis Volcanics.

(2) Occurrences on the present Syringa and Glasgow claims described by Shenon (Shenon and Ross, 1936, p. 24–25).

(3) Stibnite in float several hundred feet northeast of the Moore tunnel of the Moscow mine, NW $\frac{1}{4}$ sec. 6, T. 20 N., R. 9 E., central ninth (Shenon *in* Shenon and Ross, 1936, p. 26).

(4) Showing of stibnite and pyrite in quartz-veined garnet-hornblende skarn at the Logan Copper Hill prospect of Axel Falkenburg, northeast of the forks of Logan Creek, central ninth (C. P. Ross, 1944, written communication).

(5) Prospects on the Golden West claims staked in 1942 by the late Evert Potter and at one time claimed as the Palo Alto group by Jack Roberson, James and Vera Cahill, and others. The claims are on the north side of the north fork of Logan Creek, central ninth, about N. 55° E. from Dixie Mountain, elevation about 7,200 feet. The principal adit followed a N. 25° E. zone of gouge and sheared granitic rock for 150 feet to a zone of stibnite-bearing silicified, sericitized granodiorite that strikes N. 80° E. and dips 60° N. This zone was explored for about 50 feet and was stoped locally. Ore is said to have been shipped to Stibnite for treatment. Sparse scheelite is present in a silicified zone explored by an adit about 1,000 feet west-northwest.

(6) Stibnite deposit of Erik Dokka, from which 17 tons of ore assaying 39.6 percent antimony was produced in 1941. Location uncertain; possibly 4 miles up Government Creek from Big Creek, on the north side of the creek (D. E. White, 1942, written communication).

(7) Prospect on claim formerly held by John Routson, $\frac{3}{4}$ mile north of Big Creek store, east ninth (D. E. White, 1942, written communication). Presumably in old metavolcanic rocks (Leonard, 1962) near prospects of Elliott Mining Co.

(8) Prospects in Beaver Creek area, northeast ninth, on claims formerly held by Noel Routson and by Roberson and Chambers (D. E. White, 1942, written communication; Jack Roberson, 1956, oral communication). Presumably in syenite of the Ramey Ridge Complex (Leonard, 1963), north of Beaver Creek and west of Mulligan Creek, north or northeast of adits on Roberson's Golden claims.

Most of the occurrences of stibnite in the adjacent Yellow Pine quadrangle are listed in the reports of White (1940) and Cooper (1951); those of cinnabar are described by Ross (Schrader and Ross, 1926).

REFERENCES

- Bradley, Worthen, 1943, The Hermes quicksilver mine: Mining Congress Jour., v. 29, no. 11, p. 32-34; no. 12, p. 40-44.
- Cooper, J. R., 1951, Geology of the tungsten, antimony, and gold deposits near Stibnite, Idaho: U.S. Geol. Survey Bull. 969-F, p. 151-197.
- Davidson, D. F., 1960, Selenium in some epithermal deposits of antimony, mercury, and silver and gold: U.S. Geol. Survey Bull. 1112-A, 16 p.
- Larsen, E. S., and Livingston, D. C., 1920, Geology of the Yellow Pine cinnabar-mining district, Idaho: U.S. Geol. Survey Bull. 715, p. 73-83.
- Leonard, B. F., 1962, Old metavolcanic rocks of the Big Creek area, central Idaho: Art. 5 in U.S. Geol. Survey Prof. Paper 450-B, p. B11-B15.
- 1963, Syenite complex older than the Idaho batholith, Big Creek quadrangle, central Idaho: Art. 204 in U.S. Geol. Survey Prof. Paper 450-E, p. E93-E97.
- Schrader, F. C., and Ross, C. P., 1926, Antimony and quicksilver deposits in the Yellow Pine district, Idaho: U.S. Geol. Survey Bull. 780-D, p. 137-164.
- Shenon, P. J., and Ross, C. P., 1936, Geology and ore deposits near Edwardsburg and Thunder Mountain, Idaho: Idaho Bur. Mines and Geology Pamph. 44, 45 p.
- White, D. E., 1940, Antimony deposits of a part of the Yellow Pine district, Valley County, Idaho: U.S. Geol. Survey Bull. 922-I, p. 247-279.



SUGGESTIONS FOR PROSPECTING FOR EVAPORITE DEPOSITS IN SOUTHWESTERN VIRGINIA

By C. F. WITHINGTON, Washington, D.C.

Abstract.—Salt and gypsum are produced from deposits in the Maccrady Shale (Mississippian), in southwestern Virginia, from the only known economic deposits of these minerals in the South Atlantic States. The Maccrady is generally 50 to 100 feet thick, but locally is as much as 2,000 feet thick, probably as a result of flowage of the evaporites during thrust faulting. On the assumption that the evaporites acted as a lubricant along the thrust surfaces, new deposits of evaporites can reasonably be sought near the fault traces. Anomalously high concentrations of sulfate in water from springs near the faults are suggested as a potential aid in prospecting for concealed deposits.

Although salt and gypsum are plentiful in the United States, in the South Atlantic States these important minerals are known to occur only in southwestern Virginia, in deposits that crop out along the valley of the North Fork of the Holston River between Plasterco, in Washington County, and Locust Cove, about 20 miles to the northeast, in Smyth County (fig. 1). Salt has been produced commercially at Saltville, by brine methods, since the late 1700's. Gypsum was first mined about 1830 near Plasterco, and since then has been mined at many places between Plasterco and Locust Cove. One gypsum mine is now in operation at Plasterco, and a second is being opened at Locust Cove (Mineral Industries Journal, 1963). Because these deposits supply only a fraction of the salt and gypsum used in the South Atlantic States the discovery of additional sources of either mineral would be of benefit to the economy of the area. The purpose of this report is to describe briefly the geologic setting of the evaporites in Smyth and Washington Counties and to suggest other areas in southwestern Virginia where additional deposits might be found.

GEOLOGIC SETTING OF THE EVAPORITE DEPOSITS

The evaporites in Virginia are found locally in the Maccrady Shale of Mississippian age, which consists chiefly of red and yellow mudstone, soft shale, and thin beds of sandstone and dolomite. The formation is gen-

erally between 50 and 100 feet thick, but undisturbed thicknesses of 800 feet have been reported (Butts, 1940, p. 354.) Underlying the Maccrady is the Price Sandstone of Mississippian age, a resistant unit that consists of fine-grained yellow sandstone and beds of shale. Overlying the Maccrady is the Little Valley Limestone which is here reinstated to former usage. It is of Mississippian age and consists predominantly of argillaceous limestone, with some beds of sandstone and shale. Although exposures of the Maccrady in Virginia are generally poor, the formation can be traced in narrow bands, seldom more than a mile wide, northeastward for about 120 miles from the Virginia-Tennessee line, through Scott, Washington, Smyth, Wythe, and Pulaski Counties, to a point about 3 miles west of Blacksburg, in Montgomery County (fig. 1). Faults, which come to the surface south of the Maccrady Shale through much of this belt, have thrust older rocks over the Maccrady. Another outcrop belt of the Maccrady is in Lee, Wise, and Scott Counties, but because the Maccrady here is thin and more clastic than that at Saltville (Stose, 1923, p. 53), and because evaporites probably are not present, this outcrop is not included on figure 1.

An understanding of the effect of the Saltville thrust on the Little Valley Limestone and the Maccrady Shale, which can be demonstrated at Plasterco, may be helpful in finding additional evaporite deposits in Virginia. The Little Valley Limestone has been folded into an overturned northeast-trending syncline by the Saltville fault, which has thrust Cambrian rocks over Mississippian rocks. Northeast of Saltville, the Cambrian rocks rest directly on the Maccrady and make up the uplands on the southeast side of the valley of the North Fork of the Holston River. Little Mountain on the northwest side of the Valley is formed by the resistant Price Sandstone. The Saltville fault dips southeastward at angles that range from 20° to 60°. A hole drilled about a mile southeast of Plasterco passed through the fault into the Maccrady at a depth of 2,400 feet (Nelson, 1958). A

sandstone which is presumably the Price Sandstone was cut below the Maccrady at Plasterco by a drill hole in the mine, according to Mr. H. D. Decker, of the U.S. Gypsum Co. (oral communication, 1957). These relations are shown on a schematic cross section through Plasterco (fig. 1).

At Plasterco the Maccrady was thickened to at least 2,000 feet, and consists of both bedded and jumbled, detached masses or blocks of gypsum, anhydrite, salt, sandstone, and limestone in a matrix of red and green mudstone and shale. The amount of salt increases with depth; below about 1,500 feet it makes up most of the Maccrady. Cooper (1964, p. 93-95) comments on the tremendous thickening of the Maccrady and other formations within the Greendale syncline northwest of the Saltville fault, and attributes this thickening at Saltville and Locust Cove to downfolding during deposition of the Mississippian rocks. At least part of the thickening of the Maccrady is evidently due to plastic flowage of salt and calcium-sulfate rocks, however, for both rocks are known to thicken considerably along the axes of folds.

Surface indications of the evaporites are sparse. Salt is found in salt springs and salt licks near Saltville, and gypsum in isolated outcrops in the Maccrady along the North Fork from Plasterco northeastward to Locust Cove. In the subsurface, bedded calcium sulfate occurs at the top of the Maccrady both under the Saltville fault on the southeast side of the valley and under the Little Valley Limestone on the northwest side of the valley (fig. 1). Within the upper part of the Maccrady the calcium sulfate, sandstone, limestone, and salt are in blocks typically 50 feet long, 20 feet high, and 15 feet wide. The blocks of gypsum, which are elongated northeastward parallel to the outcrops of the Maccrady, are randomly distributed through the clay matrix, and finding new blocks is difficult. The calcium sulfate is mainly gypsum down to a depth of about 1,000 feet; below that depth anhydrite predominates. The gypsum is white, is medium to fine grained, and is either massive or laminated with shale; the gypsum laminae are as much as 5 mm thick and the shale laminae as much as 1 mm. The laminae are original bedding features within the gypsum. Masses of petroliferous shale and black magnesian limestone occur at places within the gypsum.

ORIGIN OF THE EVAPORITES

The origin of the evaporites in southwestern Virginia has been the subject of much speculation. Several early writers regarded the gypsum as an alteration product of limestone, possibly of very recent age (Rogers, 1884, p. 141-142, reprinted from a report of 1836; Lesley,

1862; and Stevenson, 1885). Eckel (1903, p. 406) concluded that both the salt and gypsum were formed as part of the original depositional sequence through the evaporation of sea water, and he gave an early Carboniferous age to the deposits. Stose (1913) described the evaporite-bearing beds and named them the Maccrady Shale from exposures near Maccrady (McCready on fig. 1), a town northeast of Saltville. He believed that the evaporites were derived from calcareous-argillaceous sediments that originally contained finely disseminated gypsum and salt which had been precipitated in a partly enclosed arm of the sea during the deposition of the Maccrady Shale, and that the evaporites were later further enriched as ground waters dissolved calcium carbonate and carried it away. Since Stose published his report in 1913, the evaporites have been better exposed and better explored. Because laminated gypsum, typical of bedded gypsum deposits, has been found in the isolated gypsum blocks, it is now certain that the salt and calcium sulfate, probably in the form of anhydrite, were deposited as part of the original depositional sequence.

On the basis of stratigraphic conditions elsewhere it can be assumed that near Plasterco and Saltville the Maccrady originally consisted of bedded calcium sulfate, salt, shale, and thin sandstone in a unit that was about 100 feet thick. The Maccrady acted as a lubricated mass over which the thrust plate glided. In the process of thrusting, the overriding mass squeezed the Maccrady before it, concentrating the calcium sulfate and salt by plastic flowage, and thickening the formation. At this time, limestone and other impurities were included in the evaporites. Then, as Cullison (1938, p. 36) has suggested, the thrust distorted the rocks and broke them to form the isolated blocks. Fragments of the Little Valley Limestone and probably of the underlying Price were also broken off and included in the jumbled mass of the Maccrady. The bedded gypsum found in the Plasterco mine at the top of the Maccrady was little disturbed by the overriding mass; evidently most of the action of the thrust took place east and southeast of Plasterco.

AREAS AND METHODS OF PROSPECTING

Only in the 20-mile-long belt that extends northeastward from Plasterco is it certain that evaporites exist. Rogers (1884, p. 141) stated that gypsum extends northward from Plasterco along the North Fork of the Holston River into the Walker Creek valley, a distance of 40 miles, but there is no record that exposures of gypsum or salt have been found beyond Locust Cove. The basin in which the evaporites were deposited probably covered much more of southwestern

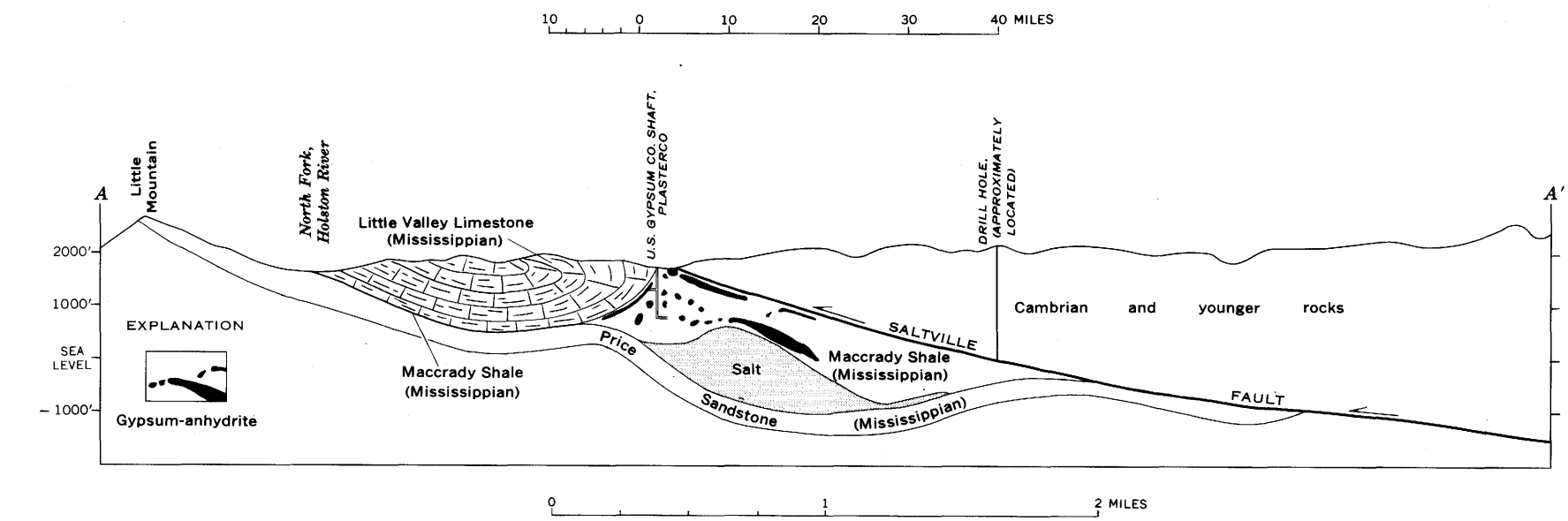
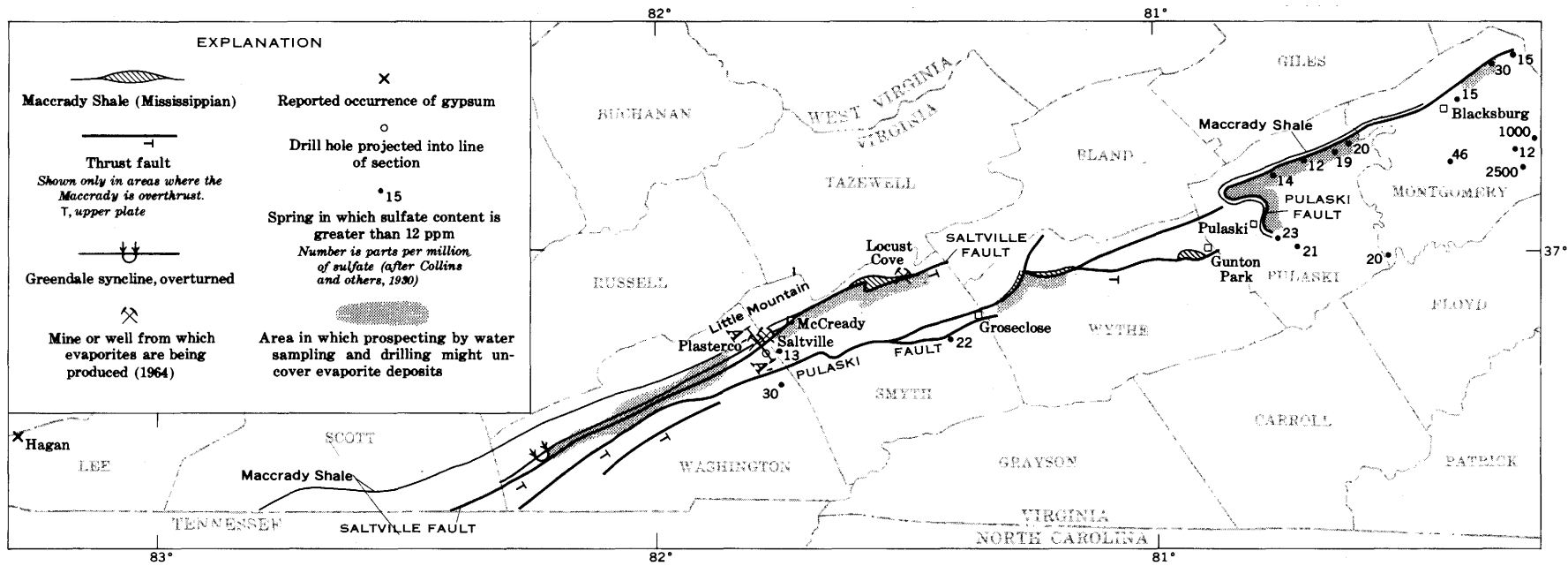


FIGURE 1.—Map of southwestern Virginia, showing outcrop area of the evaporite-bearing Maccrady Shale of Mississippian age (after Calver, 1963). Schematic section A-A' shows relation of the Maccrady Shale to the Saltville fault (after Cullison, 1938; Nelson, 1958; topographic profile from Saltville and Glade Springs 7½' topographic maps).

Virginia than is now known to contain evaporites, but because of the soluble nature of both gypsum and salt very little evidence of their existence would be found on the surface. An 8-foot bed of gypsum in the Newman Limestone of Mississippian age, exposed in a railroad tunnel between Harlan County, Ky., and Hagan, Lee County, Va. (fig. 1), about 75 miles due west of Saltville (R. L. Miller, oral communication, 1964), encourages the belief that evaporites may be found elsewhere in southwestern Virginia. This occurrence is a few hundred feet stratigraphically above the Maccrady.

Study of the analyses of water from more than 225 springs in southwestern Virginia (Collins and others, 1930) suggests that gypsum is more widespread than is now known. On the basis of concentration of sulfate the analyses can be classified in two groups; in one the samples contain less than 8 parts per million of sulfate, and in the other they contain 12 ppm or more. Nearly 75 percent of the analyses show less than 8 ppm of sulfate, and 20 percent of them contain 12 ppm or more. These springs, which are mostly in Wythe, Pulaski, and Montgomery Counties, flow from the Cambrian rocks that have been thrust over the Maccrady Shale by the Pulaski or Saltville faults. Few of the analyses above 12 ppm of sulfate are from springs north of the Saltville fault. The locations of the springs yielding water that contained more than 12 ppm of sulfate are shown on figure 1. Among the 17 sulfate values shown, 15 range from 12 to 46 ppm, one is 1,000 ppm, and one is 2,500 ppm. It is not certain, of course, that the anomalous sulfate in the analyses comes from the solution of calcium sulfate, nor are there corresponding increases of sodium and chloride in the analyses. The fact that most of the springs with the higher concentrations of sulfate flow from the Cambrian rocks that have overridden the Maccrady strongly suggests that the sulfate in the ground water is derived from gypsum in the Maccrady. The absence of anomalous amounts of chloride in the analyses is not surprising, because any salt exposed to ground water would have long since been removed. The very high concentrations of sulfate are thought to reflect a relatively short distance of travel of the solution; the lower values probably are due to longer travel and greater dilution by ground water.

Even where all traces of evaporites have been removed from the outcrop, and where only a poorly defined collapse-breccia remains, deposits might still be found in the subsurface. Figure 1, which is from the geologic map of Virginia (Calver, 1963), shows where the Maccrady has been overridden by older rocks along the Saltville fault, which is in Smyth and Washington

Counties, or along the Pulaski fault, the trace of which runs northeastward from Washington County to Montgomery County. Analyses of water from springs near faults should be examined for above-average concentrations of calcium sulfate. To be significant these concentrations need not be especially high, for both the salt and gypsum are encased in clay which, where it is particularly impermeable, must protect these relatively soluble minerals from attack by ground water. Drilling should be done southeast of the outcrop of the Maccrady, and even southeast of the trace of the faults, because the thickest part of the Maccrady is downdip from the undisturbed outcrop along the North Fork of the Holston River (fig. 1). Care should be taken not to drill too far southeast of the trace of the fault, however, for the action of the thrust probably squeezed all the salt before it, so that within a mile or so southeast of the trace, all that remains of the Maccrady is likely to be a jumbled mass of clay, sandstone, and limestone.

The areas shown on figure 1, in which prospecting might be successful, include: (1) Smyth and Washington Counties south of the outcrop of the Maccrady and south of the Saltville fault; (2) Smyth and Wythe Counties south of the Pulaski fault, from Groseclose in Smyth County to Gunton Park in Wythe County; (3) an area from Pulaski northward and thence eastward into Montgomery County where the Maccrady is overthrust by the Pulaski fault; and (4) an area northeast of Blacksburg, in Montgomery County, in which the Maccrady does not crop out, but where spring water south of the Pulaski fault contains as much as 30 ppm of sulfate.

REFERENCES

- Butts, Charles, 1940, *Geology of the Appalachian Valley in Virginia*: Virginia Geol. Survey Bull. 52, pt. 1, 568 p.
- Calver, J. L., 1963, *Geologic map of Virginia*: Virginia Dept. Conserv. and Econ. Devel., Div. Mineral Resources; scale 1:500,000.
- Collins, W. D., Foster, M. D., Reeves, Frank, and Meacham, R. P., 1930, *Springs of Virginia*: Virginia State Comm. on Conserv. and Devel., Div. Water Res. and Power Bull. 1, 55 p.
- Cooper, B. N., 1964, *Relation of stratigraphy to structure in the southern Appalachians*, in *Tectonics of the southern Appalachians*: VPI [Virginia Polytech. Inst.] Dept. Geol. Mem. 1, p. 81-114.
- Cullison, J. S., 1938, *Mineral deposits in the vicinity of the Buffalo Fork of Holston River*: Knoxville, Tennessee Valley Authority, Div. Water Control Planning, Geologic Br., 44 p.
- Eckel, E. C., 1903, *Salt and gypsum deposits of southwestern Virginia*, in *Contributions to economic geology, 1902*: U.S. Geol. Survey Bull. 213, p. 406-416.
- Lesley, J. P., 1862, *Gypsum deposits*: Am. Philos. Soc. Proc., v. 9, no. 67, p. 33-35.

- Mineral Industries Journal, 1963, Saltville, Virginia, geology and mineral industries: Virginia Polytech. Inst., v. 10, no. 2, p. 7.
- Nelson, W. A., 1958, A further discussion of the Saltville fault in Smyth and Washington Counties, Virginia [abs.]: Virginia Acad. Sci., v. 9 (new ser.), no. 4, p. 426.
- Rogers, W. B., 1884, The plaster banks, *in* On the Geology of the Virginias: New York, D. Appleton and Co., repr., p. 140-142.
- Stevenson, J. J., 1885, The salt and gypsum deposits of the Holston Valley, Virginia, *in* The Virginias: Staunton, Va., v. 6, no. 4, p. 53-55.
- Stose, G. W., 1913, Geology of the salt and gypsum deposits of southwestern Virginia: U.S. Geol. Survey Bull. 530-N, p. 248-255.
- 1923, Pre-Pennsylvanian rocks, *in* Eby, J. G., The geology and mineral resources of Wise County and the coal-bearing portion of Scott County, Virginia: Virginia Geol. Survey Bull. 24, p. 22-62.



LOW-VOLATILE BITUMINOUS COAL OF MISSISSIPPIAN AGE ON THE LISBURNE PENINSULA, NORTHWESTERN ALASKA

By IRVIN L. TAILLEUR, Menlo Park, Calif.

Abstract.—Near the middle of the west coast of the Lisburne Peninsula, in a formation that extends 30 miles or more along the west side of the Lisburne Hills, a thick section of moderately to strongly deformed quartzite, fine-grained clastic rocks, and coal having a flora of Early Mississippian age contains 13 coal seams 2½ feet or more thick and about 70 feet in aggregate thickness. Analyses (on an as-received basis) of representative samples of the low-volatile bituminous coal reveal 13 to 21 percent volatile matter, 68 to 80 percent fixed carbon, 3 to 16 percent ash, 11,800 to 14,300 Btu, and 1.4 to 1.5 specific gravity. This apparently good-quality coal is, at least, a potential local source of fuel for Point Hope village.

Low-volatile bituminous coal exposed in sea cliffs south of Cape Lisburne has been known for more than 60 years. Although originally reported (Collier, 1906) as having an economic potential worth further investigation, the coal has not been prospected thoroughly. On detailed examination of some of the exposures during regional mapping,¹ this writer found the original evaluation to be valid and concluded that the existence of these deposits of fuel of an apparent high quality warrants further published description.

Historically, coal was the earliest resource in northwestern Alaska to be recognized and utilized. Coal in sea cliffs east of Cape Lisburne was discovered in 1826 by Beechey's expedition (Beechey, 1831), and it became a refueling source for the ships, particularly the whalers and the U.S. revenue cutters, that followed into the Arctic Ocean during the nineteenth century.

Coal of Carboniferous age was shown on the first geologic map compiled for the region (Grewingk, 1848-49), but it represented the coal east of Cape Lisburne, which is a high-volatile Mesozoic coal that had been correlated with beds containing late Paleozoic fossils at the cape. The occurrence of coals of two ages in the region was not noted until the older, harder coal exposed south of Cape

Lisburne was recognized in 1900 (A. G. Maddren, written communication, *in* Schrader, 1904, p. 113-114).

Collier's (1906) report, based on fieldwork in 1904, includes analyses of the coal, identification of the associated flora as Mississippian in age, and the opinion that the deposits probably contain appreciable quantities of good-quality coal. Some use of the coal at the time was observed. Records of subsequent examinations have not been found. A later report (Smith and Mertie, 1930, p. 292-296) repeats Collier's observation in detail, but regards the potential of the deposits somewhat conservatively. On the recent map of the coal fields of Alaska (Barnes, 1961), the coal is shown as three isolated occurrences of Carboniferous bituminous coal of unknown extent.

OCCURRENCE

The formation containing the coal extends from Cape Dyer on the west coast to Cape Thompson on the south coast, a distance of more than 25 miles along the flank of the Lisburne Hills. It is also present in several fault blocks within the hills north of Cape Dyer (fig. 1). The formation was mapped from the Kukpuk River to Cape Thompson by Campbell (1961, fig. 354.1, rock unit *Ms*) in 1959 and 1960. The writer measured sections and mapped the formation north from the Kukpuk River with the assistance of D. R. Currey in 1961, of G. S. Anderson in 1963, and of T. P. Miller and Anderson in 1964.

Significant amounts of coal were seen on the Kukpuk River and to the north, but the coal at Cape Thompson reported to Collier (1906, p. 45) was not located. Coal seams or float were found at Kukpuk on the lower Kukpuk River, along sea cliffs south of Cape Dyer and Kapaloak Creek, along a stretch of beach bluffs between Kiliktukgot Creek and Cape Dyer, and at Niak Creek. Coal is therefore present in the formation at several points in a belt as much as 30 miles long.

¹ Support in the field was furnished in part by the U.S. Atomic Energy Commission in 1961 and by the Arctic Research Laboratory in 1963.

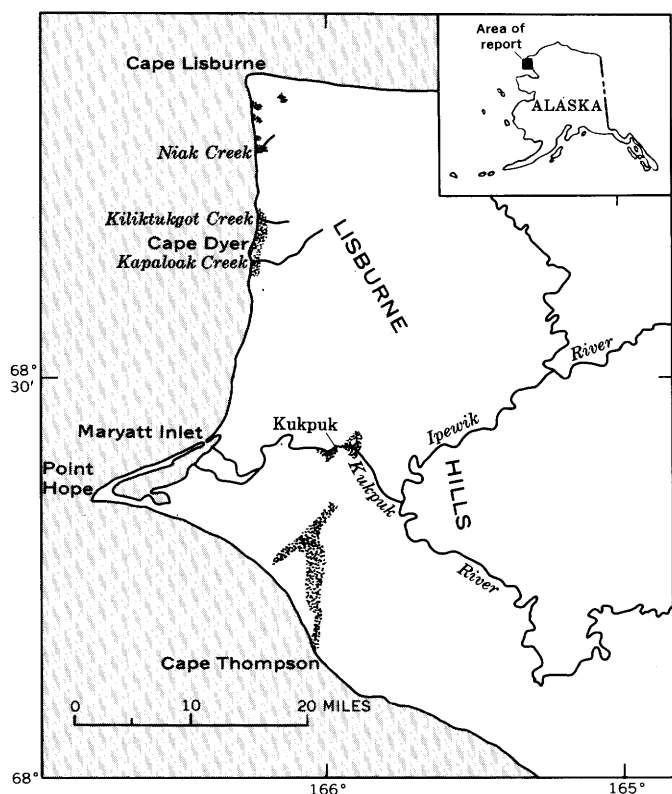


FIGURE 1.—Mapped occurrences (stippled) of the Mississippian coal-bearing formation on the Lisburne Peninsula.

Collier (1906, p. 43-44) described the three coastal localities. He treated the Kiliktukgot Creek (Cape Lewis) locality in greatest detail, implying that the deposits there were most promising. Perhaps exposures have changed as a result of erosion of the cliffs since Collier's work, but more coal is now exposed near Kapaloak Creek. The nearly complete cross section provided by the mile of low cliffs south of Kapaloak Creek permitted detailed study and measurement of the rocks.

As is shown on the sketch of the Kapaloak cliffs (fig. 2), beds dip moderately to steeply northward in the southern two-thirds of the cliffs; in the northern third of the exposure they dip southward, but this is because

the beds have been overturned. Lateral persistence of beds for a few hundred feet is indicated by the bedding traces on the surface in back of the cliffs. Sharp flexures and overturning, and shearing and flowage of the coal, reflect intense disturbance locally. The rocks seem to form the north flank of an anticline.

Nearly 2,200 feet of section was measured between the bottom of the exposed beds at the south end of the cliffs and the uppermost beds just above seam 13 at the north end. An undetermined amount of the upper part of the formation is not exposed. The measured section seems to be free of major repetitions, but the possibility of repetition of beds cannot be excluded; repeated sections could be dissimilar, and remain unrecognized, owing to lateral variations during deposition.

Approximately 300 feet of strata at the bottom of the measured section, in the ridge shown at the south end of figure 2, is not coaly. These beds consist of dark, partly calcareous, fine-grained rocks that may be marine in origin.

The remaining strata, approximately 1,900 feet thick, consist of orthoquartzite, shale, and mudstone in sets of beds of variable thickness, and of clay and seams or zones of coal. These rocks were deposited largely, if not wholly, in a nonmarine environment. Plant remains collected from zones about 500, 900, 1,100, and 1,400 feet above the base of the measured section were identified by S. H. Mamay (written communication, 1963) and correlated by him with floral zones I and II of the (Early) Mississippian (Read and Mamay, 1960).

Coal seams present throughout the upper 1,900 feet range in thickness from a fraction of an inch to 11 feet. Thirteen seams in the upper 1,200 feet are 2½ feet or more thick and have an aggregate thickness of about 70 feet. Detailed sections of these thicker seams are given in table 1. Most of these thicker seams are separated, one from another, by about a hundred feet of barren beds and thinner seams. Figure 3 illustrates the appearance, in the cliffs, of many of the seams.

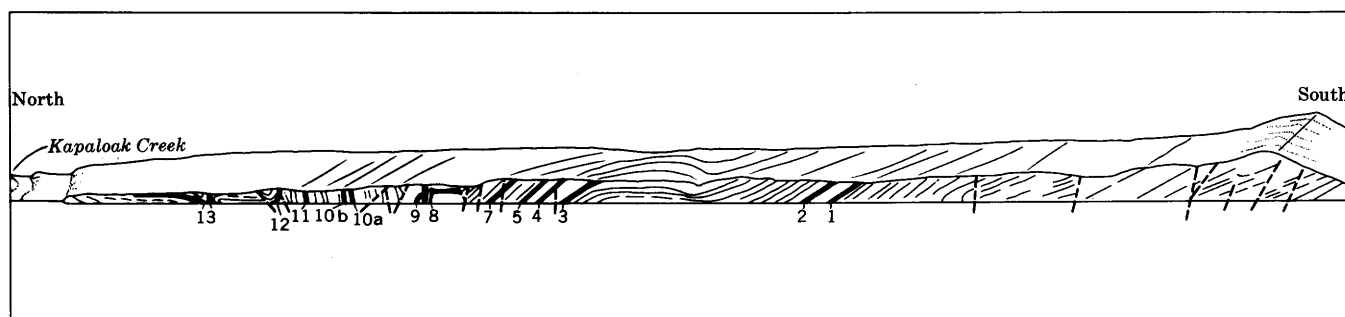


FIGURE 2.—Sketch showing coal seams (thick lines), faults (dashed lines), and bedding traces (thin lines) along sea cliffs south of Kapaloak Creek. Horizontal distance is about 5,500 feet. Sketch from low-altitude aerial photograph. Numbers refer to coal seams listed in table 1.

TABLE 1.—Description of coal seams at Kapaloak Creek

Seam No.	Distance above base of measured section (feet)	Detailed section of seam (U.S. Bureau of Mines lab sample No. from table 2 shown by number)		
		Lithology	Thickness (feet)	
13	2163. 2–2166. 4	H24246	Mudstone.....	4. 0
			Coal.....	2. 6
			Ferruginous nodules.....	. 1
			Coal.....	. 5
			Mudstone.....	1. 3
12	2080. 5–2086. 5		Quartzite (sheared).....	19. 0
			Mudstone.....	. 5
			Coal.....	1. 9
			Clay, coaly clay (impure coal).....	1. 7
			Coal.....	2. 4
11	1944–1955		Mudstone.....	1. 5
			Clay, coaly.....	. 1
			Coal, sheared.....	1. 1
			Coal, impure.....	. 5
			Coal.....	. 7
			Mudstone, carbonaceous.....	. 4
			Mudstone, gray.....	1. 0
			Shale and clay, carbonaceous.....	. 8
			Clay, coaly.....	. 8
			Coal; thin pyrite lens.....	3. 9
			Gouge, coaly, sandy.....	. 1
10b	1809. 5–1818. 3	H24244	Coal; streaks of yellow bloom.....	1. 6
			Quartzite.....	3. 0
			Mudstone.....	5±
			Coal.....	2. 0
			Coal, impure.....	1. 3
			Mudstone, clay.....	. 9
			Clay, coaly.....	. 6
			Coal.....	3. 5
			Clay.....	. 2
			Coal, sheared.....	. 3
			Mudstone.....	6. 5
10a	1797. 1–1800. 8		Mudstone.....	2. 5
			Coal, impure, pyritic.....	. 2
			Coal.....	1. 0
			Coal, impure.....	. 1
			Clay.....	. 2
			Coal, impure.....	. 1
			Coal.....	. 1
			Clay.....	. 4
			Coal.....	. 4
			Coal, impure.....	. 3
			Clay.....	. 2
Coal, impure.....	. 1			
Coal; thin pyrite lens.....	. 6			
Mudstone.....	7. 0			
9	1603. 0–1613. 7	H24243	Mudstone, sheared; possibly thickened tectonically.....	7. 0
			Covered (coal?).....	3. 0
			Coal.....	1. 0
			Limonitic mud.....	. 2
			Coal.....	5. 4
			Limonitic mud.....	. 1
			Coal.....	1. 0
			Mudstone.....	2±

TABLE 1.—Description of coal seams at Kapaloak Creek—Con.

Seam No.	Distance above base of measured section (feet)	Detailed section of seam (U.S. Bureau of Mines lab sample No. from table 2 shown by number)					
		Lithology	Thickness (feet)				
8	1582. 7–1585. 3	H24242 H26280	Quartzite.....	15. 0			
			Mudstone.....	1. 0			
			Coal; thin pyrite stringer.....	. 6			
			Coal.....	1. 5			
			Coal, impure.....	. 1			
			Coal.....	. 4			
			Mudstone.....	1. 3			
			Sandstone.....	9. 0			
			7	1491–1493. 5		Shale and sandstone.....	2. 0
						Coal.....	2. 5±
Covered.....	1. 0						
5	1379. 6–1387. 7		Mudstone.....	6±			
			Coal.....	. 7			
			Gouge, sandy.....	. 1			
			Coal.....	1. 0			
			Clay, coaly.....	1. 0			
			Coal.....	3. 6			
			Coal, impure.....	. 2			
			Coal.....	1. 5			
			Mudstone.....	1. 0			
			4	1289. 5–1297. 0	H24241	Mudstone.....	1. 6
Coal; impure streaks 1 ft above base.....	3. 6						
Clay.....	. 9						
Coal, sheared.....	. 5						
Clay.....	. 5						
Coal, sheared.....	2±						
Mudstone.....	4±						
3	1268. 6–1272. 8		Shale.....	5±			
			Clay, coaly.....	. 1			
			Coal.....	1. 5			
			Clay.....	. 1			
			Coal.....	. 2			
			Clay.....	. 3			
			Coal; clay streaks.....	. 6			
			Clay; yellow bloom.....	. 2			
			Coal, sheared.....	1. 0			
			Clay, carbonaceous.....	. 2			
			Mudstone.....	4±			
2	1005. 4–1011. 5		Quartzite.....	1±			
			Shale; coaly sandstone.....	. 1			
			Coal.....	. 1			
			Mudstone, carbonaceous.....	. 2			
			Coal.....	1±			
			Clay.....	. 1			
			Coal.....	3. 2			
			Coal, impure.....	. 2			
1	943. 2–952. 8	H24240	Coal.....	1. 2			
			Clay(?).....	1. 5			
			Mudstone.....	6±			
			Coal; 4 streaks of impurities; may be thickened tectonically.....	3. 5			
			Coal, impure.....	. 5			
			Coal.....	1. 6			
			Clay.....	. 2			
			Coal.....	1. 4			
			Clay, carbonaceous; streaks of yellow bloom.....	. 3			
			Coal; impure streaks.....	1. 2			
			Coal and coaly shale.....	. 9			
Mudstone, sheared(?).....	6±						

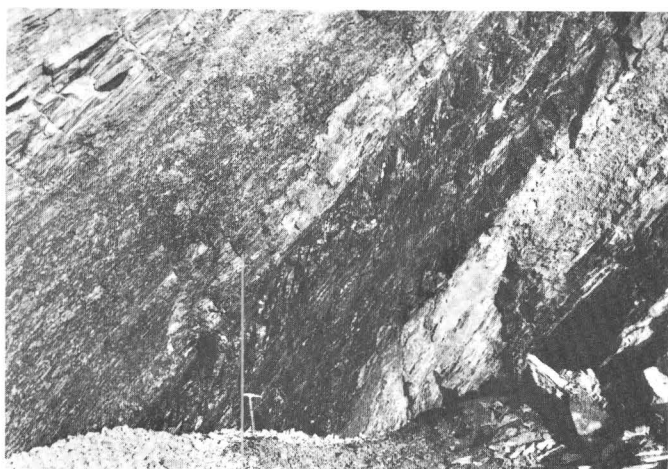


FIGURE 3.—Exposure of seam 3 (shown by hammer) in Kapaloak sea cliff. The coal seam is overlain by quartzite and plant-bearing shale and is underlain by clay and mudstone.

CHARACTER OF THE COAL

Separate channel samples of pure and impure parts of the thicker seams were collected and stored in bags in 1961. Seam 8 was resampled in 1963, and the sample was stored in a sealed can to permit approximation of the original bed-moisture content. Analyses of seven representative samples by the U.S. Bureau of Mines laboratory, Pittsburgh, Pa., are listed in table 2, together with the analyses reported by Collier (1906, p. 43-45). Specific gravities of small lumps from seams 3, 7, and 11 were determined to be 1.4, 1.4, and 1.5 respectively, similar to two determinations by Collier (1906, p. 46) that averaged 1.37.

Although the analyses all represent outcrop samples and hence do not reflect true bed-moisture content, the high ratio of fixed carbon to volatile matter, the hardness, and the relatively high specific gravity suggest that all the coal is probably of low-volatile bituminous rank. The coal should be a good-quality fuel because similar coals elsewhere serve extensively for domestic heating and steam generation (W. H. Oppelt, U.S. Bureau of Mines, written communication, 1963).

RESERVES AND POTENTIAL USE

Reliable estimates of the amount of coal present will require prospecting away from the beaches or riverbanks. Because the amount of coal in the exposed sections is probably fairly representative of the coal content of the formation in adjoining areas, significant deposits of coal are believed to underlie the thin cover of rubble inland from the beaches at the Kapaloak and Kiliktukgot localities. Strong deformation at the Niak Creek locality precludes reliable estimation of the extent of the coal there. On the Kukpuk River, where

there is only one seam of appreciable thickness, most of the outcrops are quartzite and the extent of the coal cannot be determined. The area from the west coast to the Kukpuk River has not been examined in sufficient detail to determine the distribution of coal there.

Physical conditions of the region are adverse for exploitation of the coal, largely because of the Arctic setting: (1) The region is remote from centers of potential heavy use. (2) The climate is severe, and permafrost probably prevades the ground away from the shorelines. (3) The navigation season lasts only from late June to the end of September. (4) The coast is exposed and the Kukpuk River is extremely shoal at times. (5) Maryatt Inlet is the only nearby protected anchorage, and it is suitable only for vessels of 10-foot draft or less. Practical access to the deposits at present is limited to landings by umiak (Eskimo skin boat) chartered at Point Hope village, or to landings on gravel bars near Kukpuk in a light airplane chartered at Kotzebue, 150 miles to the southeast.

Rights to the coal localities may be another factor of significance. The recorded claims noted in 1930 (Smith and Mertie, 1930, p. 292) do not appear to have been maintained, but evidence of recent and ancient habitation is abundant near each locality of exposed coal. As natives have inhabited the area continuously for at least the last several hundred years (Rainey, 1947), the possibility of native rights exists and needs to be taken into account.

At the present time, a small work force is available locally for mining, and small quantities of the coal might be substituted for imported fuel in the coastal villages and installations, but local and regional markets can use only a small part of the potential production from the deposits. However, prospects are good for the development of large-scale metal-mining operations on the upper Kobuk River, 150 miles east of Kotzebue, which would create a large demand for energy, and possibly a large market for these coal deposits.

The writer believes that the coal has an important potential as a local source of fuel for the village of Point Hope, only 30 miles from the closest deposits. Despite the village's proximity and its tradition of making maximum use of available resources, this fuel of apparently high quality is not utilized in the village. Instead, oil and coal are imported from the conterminous United States for fuel. Residents of the village say that the local coal will not burn. However, the coal is combustible; probably it was not tested in the village under conditions suited to its hardness. Maddren (Schrader, 1904, p. 113) noted that the coal burned in the galley stove but was too hard to burn under the ship's boilers without forced draft. In 1963 the U.S. Geological Sur-

TABLE 2.—*Analysis of Mississippian coals from the Lisburne Peninsula, Alaska*

[U.S. Bureau of Mines analyses by F. E. Walker, 1962, 1963; others by W. T. Schaller, 1905? (Collier, 1906, p. 43-49). Condition of sample: 1, as received; 2, moisture free; 3, moisture and ash free]

Sample No. (U.S. Bureau of Mines) or other sample designation	Sample location and description	Condition of sample	Equilibrium moisture (ASTM-D 1412-56T)	Moisture (percent)	Volatile matter (percent)	Fixed carbon (percent)	Ash (percent)	Sulfur (percent)	Heating value (Btu)
H24240	Kapaloak, seam 1, upper 4.0 ft; streaks of impurities; 0.5 ft impure coal at base.	1	12.4	3.0	12.8	68.2	16.0	0.9	11,800
		2	-----	-----	13.2	70.4	16.4	1.0	12,160
		3	-----	-----	15.8	84.2	-----	1.1	14,560
H24241	Kapaloak, seam 4, upper 3.6 ft; impure streak 1 ft above base.	1	3.6	3.0	14.1	80.0	2.9	.6	14,010
		2	-----	-----	14.6	82.4	3.0	.6	14,450
		3	-----	-----	15.0	85.0	-----	.7	14,890
H24242	Kapaloak, seam 8; entire 2.6-ft thickness; streak of sulfide near top and of impure coal near base.	1	2.6	2.0	15.0	79.0	4.0	.5	14,280
		2	-----	-----	15.3	80.7	4.0	.5	14,570
		3	-----	-----	15.9	84.1	-----	.6	15,180
H62680	Kapaloak, seam 8; analysis made for bed moisture.	1	-----	4.7	-----	-----	-----	-----	-----
H24243	Kapaloak, seam 9; lower 6.5 ft; sheared, 0.1 ft limonite streak 1 ft above base.	1	3.3	2.0	15.4	79.4	3.2	.8	14,140
		2	-----	-----	15.7	81.0	3.3	.8	14,430
		3	-----	-----	16.2	83.8	-----	.8	14,920
H24244	Kapaloak, seam 10b; 3.5 ft, 0.5 ft above base.	1	17.0	2.1	12.5	75.7	9.7	.6	13,150
		2	-----	-----	12.7	77.4	9.9	.7	13,420
		3	-----	-----	14.1	85.9	-----	.7	14,900
H24245	Kapaloak, seam 11; lower 5.6 ft; sulfide lens 4.4 ft above base.	1	4.1	2.9	13.5	80.1	3.5	.8	13,760
		2	-----	-----	13.9	82.5	3.6	.8	14,170
		3	-----	-----	14.4	85.6	-----	.8	14,700
H24246	Kapaloak, seam 13; entire 3.2-ft thickness, including layer of nodules 0.5 ft above base.	1	4.0	2.3	15.9	71.6	10.2	.5	12,860
		2	-----	-----	16.3	73.3	10.4	.6	13,160
		3	-----	-----	18.2	81.8	-----	.6	14,690
Collier (1906)	Niak Creek-----	1	-----	3.77	15.64	77.65	2.94	-----	13,887 (Calculated average)
	Kiliktukgot Creek-----	1	-----	5.51	21.16	70.33	3.00	.96	
	Kapaloak Creek-----	1	-----	1.71	15.62	79.86	2.81	-----	

vey field quarters were heated with the coal. Conditions of firebox, grate, and draft necessary for effective domestic use of the coal in the village should be determined by experiment. Then the deposits could be investigated as a practical source of fuel. Substitution of local fuel for imported fuel would be economically beneficial because nearly one-fifth of the relatively meager cash income of the village is now spent on imported fuel (D. C. Foote, U.S. Atomic Energy Commission, written communication, 1961). Because not much of this cash would be needed to exploit the local coal, the money available for nonsubsistence purchases would be increased by nearly 50 percent. In addition, the economy would become even more self sustaining, thereby enhancing the preservation of the unusual blend of Eskimo and modern cultures that now exists in the village.

REFERENCES

Barnes, F. F., 1961, Coal fields of the United States, sheet 2, Alaska: U.S. Geol. Survey, scale 1: 5,000,000.

- Beechey, F. W., 1831, A narrative of a voyage to the Pacific and Beering's Strait: London, Henry Colburn and Richard Bentley, v. 1.
- Campbell, R. H., 1961, Thrust faults in the southern Lisburne Hills, northwest Alaska: U.S. Geol. Survey Prof. Paper 424-D, p. D194-D196.
- Collier, A. J., 1906, Geology and coal resources of the Cape Lisburne region, Alaska: U.S. Geol. Survey Bull. 278, 54 p.
- Grewingk, Constanin, 1848-49, Beitrag zur Kenntniss der orthographischen und geognostischen Beschaffenheit der Nordwest Kuste Amerikas mit den anliegenden Inseln: Russ.-K. Mineralog. Gesell. zu St. Petersburg Verh., p. 76-342.
- Rainey, F. G., 1947, The whale hunters of Tigara: Am. Mus. Nat. History Anthropol. Papers, v. 41, pt. 2.
- Read, C. B., and Mamay, S. H., 1960, Upper Paleozoic floral zones of the United States: U.S. Geol. Survey Prof. Paper 400-B, p. B381-B382.
- Schrader, F. C., 1904, A reconnaissance in northern Alaska, across the Rocky Mountains, along Koyukuk, John, Anaktuvuk, and Colville Rivers and the Arctic coast to Cape Lisburne, in 1901: U.S. Geol. Survey Prof. Paper 20, 139 p.
- Smith, P. S., and Mertie, J. B., Jr., 1930, Geology and mineral resources of northwestern Alaska: U.S. Geol. Survey Bull. 815, 351 p.



DISTRIBUTION OF GRAVEL IN THE PATUXENT FORMATION IN THE BELTSVILLE QUADRANGLE, PRINCE GEORGES AND MONTGOMERY COUNTIES, MARYLAND

By C. F. WITHINGTON, Washington, D.C.

Abstract.—In the Beltsville quadrangle, the Patuxent Formation of Early Cretaceous age is chiefly sand and clay but contains economically important deposits of gravel. A contour map of the ratio of gravel to sand and clay suggests that the gravel was deposited in south- and southwest-trending channels in an alluvial plain. Erosion of the gently dipping formation left the gravel deposits in hilltops. Searching along extensions of the mapped channels, especially where pieces of iron-cemented gravel occur in colluvium, offers the greatest chance of finding new gravel deposits.

The most important mineral resource in the Beltsville quadrangle, Montgomery and Prince Georges Counties, Md., is gravel in the Patuxent Formation of Early Cretaceous age (fig. 1), which is used extensively for aggregate throughout the northern part of the Washington metropolitan area. This report describes the occurrence of the Patuxent gravel and offers guides for prospecting for new deposits. Younger gravels, which are not extensive and which contain fragments of deleterious material such as chert and friable sandstone, are unimportant and are not discussed.

The Patuxent Formation ranges in thickness from a knife edge near its western edge to as much as 100 feet in the subsurface in the southeastern part of the quadrangle (fig. 2). The rocks dip southeastward at the rate of 60 to 80 feet per mile. Erosion has removed much of the formation, especially along the present valleys, so that the Patuxent is found only on the hills and the distribution of its gravel bears no relation to the present drainage pattern.

The Patuxent consists predominantly of sand and clay with lesser amounts of gravel. The sand is coarse to fine and yellow to purple. It consists chiefly of subangular to subrounded quartz grains but is locally micaceous. It is in crossbedded layers. The clay occurs as beds and lenses throughout the formation. Most of it is white, although some is red or yellow. The gravel is generally poorly sorted and consists of subrounded to rounded

quartz and quartzite particles and very minor amounts of sandstone and chert. The stones range from 2-mm granules to elongate cobbles as much as 25 cm (about 10 inches) long; their average size by weight is about 10 mm. The sand fraction (0.074–2 mm; average about 0.5 mm) makes up as much as 80 percent of some samples but averages about 30 percent. Clay and silt (finer than 0.074 mm) together amount to only about 1 percent of the material by weight.

The gravel deposits occur stratigraphically throughout the formation. In places the entire thickness of the formation is predominantly gravel; in other places the gravel alternates with sand and clay. Thicknesses of more than 50 feet of gravel have been exposed in some gravel pits.

Iron oxide which cements much of the upper part of the formation is concentrated as a cap at the contact of the Patuxent with the clay of the overlying Patapsco Formation. It seems likely that the iron cement was deposited contemporaneously with the sediment, much as it is being deposited at present along the Mullica River in southern New Jersey (Lang, 1961). There, ground water containing more than 11 parts per million of iron moves upward toward the river, where the iron is oxidized and precipitates in the near-surface layers of bed material. In the Patuxent Formation, gravel commonly contains a thicker layer of iron than sand, presumably because larger volumes of iron-bearing ground water flowed through the more permeable materials. Thus, where the upper part of the formation is sand the cement is thin and friable, but where the upper part is gravel the cement is thick and hard. Moreover, the thicker and more permeable the gravel, the thicker the cemented layer. It is interesting to note that in the Beltsville quadrangle, the iron-cemented layers are found almost exclusively in the Patuxent Formation.

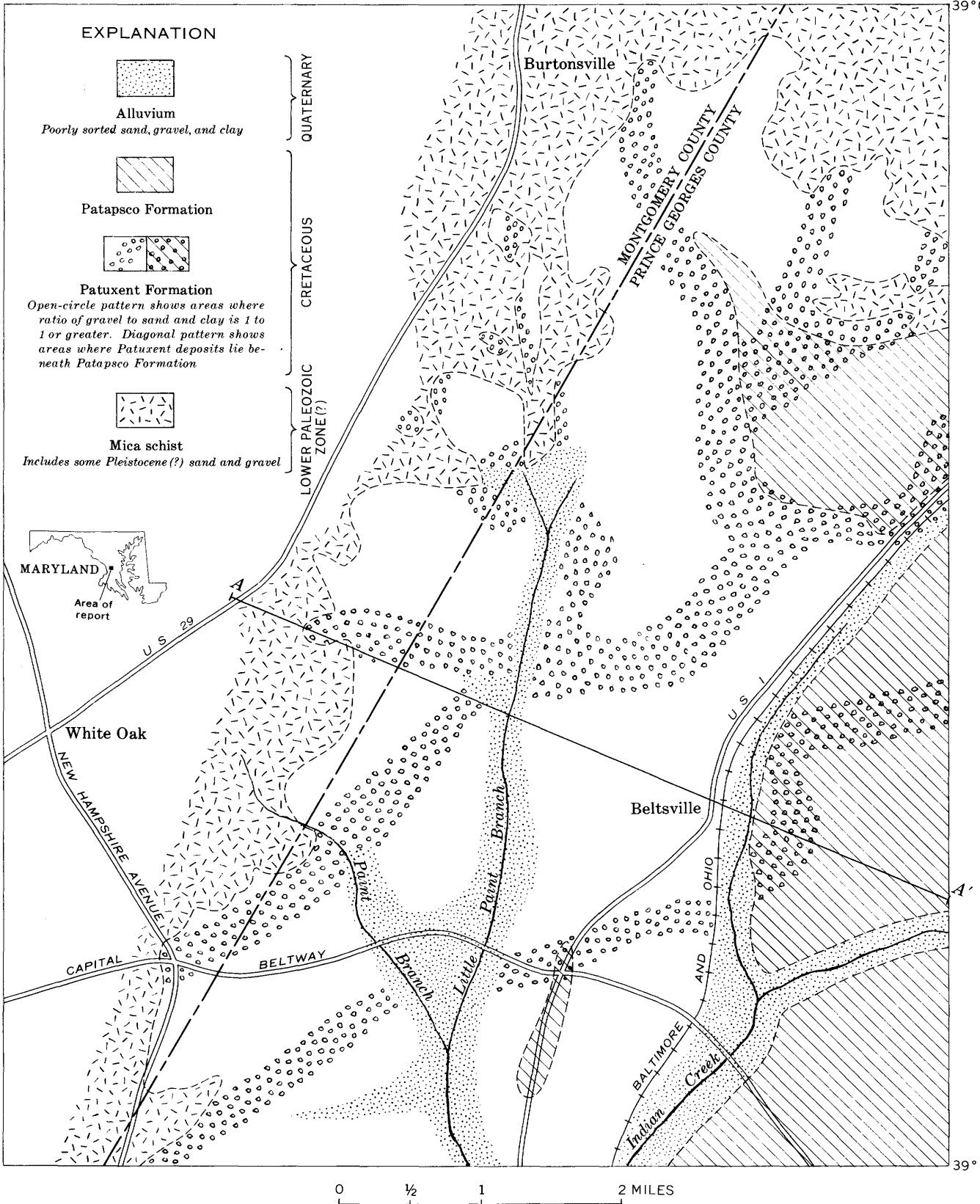


FIGURE 1.—Areal distribution of gravel in the Patuxent Formation in the Beltsville quadrangle, Maryland (after Withington, 1964).

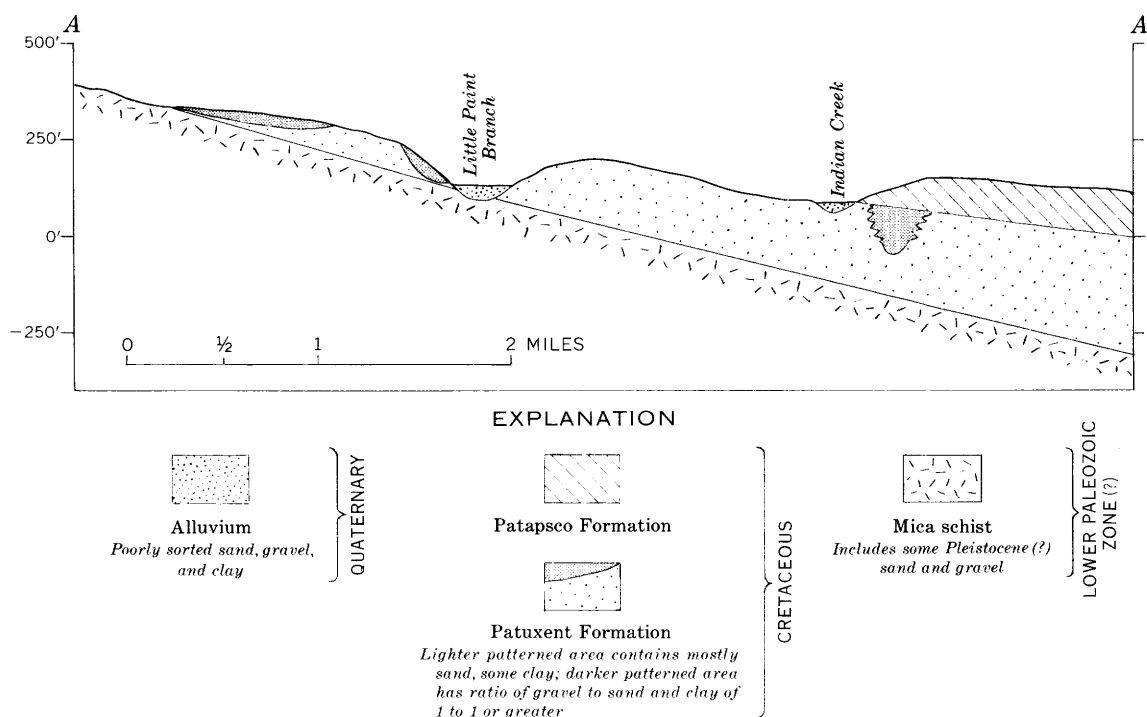


FIGURE 2.—Geologic section showing stratigraphic relations of the Patuxent Formation in the Beltsville quadrangle, Maryland. Location of section is shown on figure 1.

The shapes of the gravel bodies, the depositional trends indicated by the foreset beds exposed in gravel pits, and the areal distribution of the gravel units suggest that these sediments represent channel fills of an ancient river system in the Patuxent Formation. In order to confirm the presence of this apparent system and to determine the distribution of the gravel deposits, especially where they are covered by colluvium, ratios of the amount of gravel to that of sand and clay in many vertical sections were estimated, and lines that limit what may be channel boundaries were drawn to connect points of equal ratios of gravel to sand and clay. Data from drill-hole logs were used in addition to field observations made in gravel and sand pits and other exposures. Because the thickest gravel deposits invariably occur within the inferred channels, a ratio of 1:1 was assumed to represent the boundary of an actual channel. The gravel, of course, is not evenly distributed within the channels because the rivers meandered and their transporting power varied within the channels. Cross beds and directions of deposition as shown in channel axes were measured wherever possible and were plotted on a detailed map to establish the direction of streamflow (Withington, 1964). A summary map (fig. 1) constructed from that detailed map shows the location of the deposits of a Cretaceous river system that drained south and southwest across the quadrangle. The surface drainage during Patuxent time had not pre-

viously been established for the Beltsville area; Darton and Keith (1901, p. 6) mentioned that although there was apparently a shoreline east of Washington during Early Cretaceous time, the nature of the surface drainage is not known.

It is evident that the source rocks were not to the west of the Beltsville area, for certainly some of the sandstones of the Newark Series would be included in the Patuxent gravels. Thus Clark and others (1911, p. 80-81) observed that the Patuxent contained no fragments of sandstone of the Newark Group, which is now exposed less than 10 miles west of the Beltsville area. Nevertheless, they believed that the drainage in Patuxent time was from the west, and suggested that rocks of the Newark Group were less resistant than they are now and hence did not survive transport together with the harder quartz and quartzite, or that the rocks of the Newark Group were then covered by water. The gravel in the Patuxent Formation contains neither mica nor fragments of the sandstones of the Newark Group, both of which are present in younger gravels in this area. It therefore seems unlikely that the source rocks lay to the west of the Beltsville area. Thus, although we cannot identify a source of the stones in the gravel it appears most probable that the source lay north of this area and east of the Newark basin.

The rivers that deposited the gravel flowed in shoe-string-shaped channels across a surface of low relief

on the mica schists of the Piedmont province. Although the sand in the interstream areas is locally micaceous, that in the river channels is not; therefore, it is assumed that little material was contributed to the channels from the interstream areas. Little gravel is found outside the channels, and it seems evident that the material contributed to the interchannel areas was deposited only during periods of flooding. Because it contains little deleterious material such as soft sandstone or chert, this gravel is particularly valuable for all construction uses.

Any prospecting for new deposits of gravel should be done along the extension of the channels in the Beltsville quadrangle as well as in the adjoining quadrangles. The presence of fragments of iron-cemented gravel in the colluvium is a useful indicator of concealed gravel. The possible presence of gravel deposits in the Patuxent

where it is overlain by a thin cover of clay of the Patapsco Formation should not be overlooked.

REFERENCES

- Clark, W. B., Bibbons, A. B., and Berry, E. W., 1911, The lower Cretaceous deposits of Maryland: Maryland Geol. Survey Geol. Rept. 4, p. 23-98.
- Darton, N. H., and Keith, Arthur, 1901, Description of the Washington [D.C.] quadrangle: U.S. Geol. Survey Geol. Atlas, Folio 70, 7 p.
- Lang, S. M., 1961, Natural movement of ground water at a site on the Mullica River in the Wharton Tract, southern New Jersey: Art. 313 in U.S. Geol. Prof. Paper 424-D, p. D52-D54.
- Withington, C. F., 1964, Gravel resources in the Patuxent Formation of Cretaceous age in the Beltsville quadrangle, Prince Georges and Montgomery Counties, Maryland: U.S. Geol. Survey open-file report, 6 p.



STRUCTURE OF THE TIMBER MOUNTAIN CALDERA, SOUTHERN NEVADA, AND ITS RELATION TO BASIN-RANGE STRUCTURE

By ROBERT L. CHRISTIANSEN, P. W. LIPMAN, PAUL P. ORKILD, and F. M. BYERS, JR., Denver, Colo.

Work done in cooperation with the U.S. Atomic Energy Commission

Abstract.—The Timber Mountain volcanic structure formed in three stages: early broad doming, caldera collapse, and resurgent doming of the caldera floor. As the early dome developed, its extended roof was downdropped along a zone of concentric faults, and subsequent caldera collapse occurred along roughly the same zone. Regional normal faults contemporaneous with the volcanic structure were adapted to it, and some of them were utilized in extension of the early dome and in caldera collapse.

The Timber Mountain caldera is a large collapsed volcanic structure in the Nevada Test Site area of southern Nevada (fig. 1). It lies at the edge of the Walker Lane, a transitional zone in the basin-range region between the dominantly parallel structural and topographic trends of the central Great Basin and the more varied trends to the southwest (Locke and others, 1940). Although topography in the Timber Mountain area is generally more subdued than in the surrounding region, the dominant structures form a characteristic basin-range pattern of antithetic fault blocks. Recent geologic mapping in the region has shown that development of basin-range structure in this area was strongly influenced by the simultaneous development of the Timber Mountain volcanic structure.

An area of about 2,500 square miles surrounding Timber Mountain is a much faulted and eroded plateau consisting almost entirely of upper Tertiary volcanic deposits. Large basin-range faults have outlined such features as the Kawich and Belted Ranges, Yucca Flat, Crater Flat, and Bare Mountain around the edges of this plateau. The less faulted inner part of the plateau has been partly preserved on Pahute Mesa, Rainier Mesa, Shoshone Mountain, and Yucca Mountain. Timber Mountain is an isolated structural and topographic

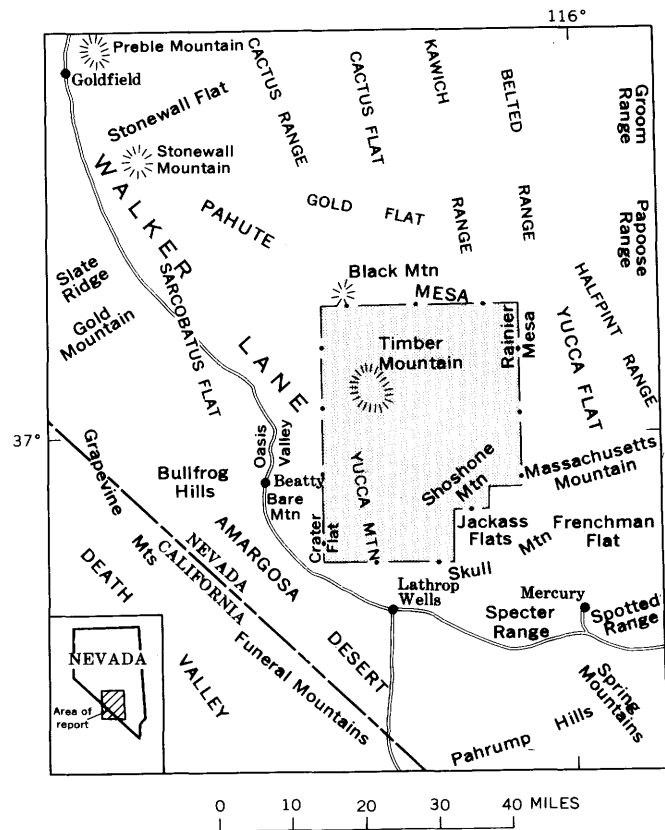


FIGURE 1.—Index map of part of Nevada and California, showing area of figure 2 (stippled).

high in the center of this disrupted plateau, within a roughly circular depressed area about 18 by 20 miles across. This depression is a caldera formed by collapse during and after eruption of a large volume of ash-flow tuff from vents in the Timber Mountain area (Byers

and others, 1963). The Rainier Mesa Member, an ash-flow cooling unit of the Timber Mountain Tuff, is the product of these eruptions. The Paintbrush Tuff, an older ash-flow sequence from another center, makes a good stratigraphic datum for resolving the structural history of the Timber Mountain area. As the upper part of the Paintbrush Tuff and the Timber Mountain Tuff are both early Pliocene, on the basis of K-Ar dating of 20 samples of biotite and sanidine by R. W. Kistler (*in* P. P. Orkild, report in preparation), the Timber Mountain volcanic structure is also Pliocene.

This paper is based on the observations of the authors and their coworkers in the mapping of nine 7½-minute quadrangles covering the area of figure 2. Eight of these quadrangles were mapped at a scale of 1:24,000. The remaining quadrangle, in the southwestern corner of the area, was mapped geologically at a scale of 1:48,000.

BASIN-RANGE FAULTS

The basin-range faults of the region around Timber Mountain are normal, with dips between 60° and 90° and average trends about due north (fig. 2). Most large faults of this system are relatively downthrown to the west, and the intervening blocks are tilted to the east, but smaller faults are both synthetic and antithetic to the major faults. The few large faults relatively downthrown to the east occur in two distinct settings closely related to the Timber Mountain volcanic structure, as discussed later.

Almost no basin-range faulting predating the Paintbrush Tuff can be recognized around Timber Mountain, although some can be demonstrated in nearby areas. Major faulting discernible in the Timber Mountain area is of post-Paintbrush age and largely predates the post-collapse rhyolites on the south rim of the caldera; later movements on these faults were minor. Consequently, basin-range faulting was occurring contemporaneously with development of the Timber Mountain volcanic structure.

STRUCTURES RELATED TO THE CALDERA

A broad domical swell developed in the Timber Mountain area before the climactic ash-flow eruptions and related collapse. Evidence of this broad doming is clearest on the south side of the structure. Outward dips of the dome are preserved in the Paintbrush Tuff on and near Yucca Mountain, although modified by tilting of the basin-range fault blocks. The edge of the dome is marked by a hinge line concentric with the caldera and having a radius of about 14 miles (fig. 2). Outside this hinge, the pretilting attitudes were horizontal.

Evidence for the precollapse age of the broad doming comes from several features. Some geometrical relations of the basin-range faults to the broad dome discussed later clearly indicate that these two structural features developed largely contemporaneously, and in a number of places the tuffs of the caldera-forming Rainier Mesa eruptions are unconformable on these basin-range faults. At the edge of Crater Flat, the Rainier Mesa Member is relatively flat lying on the tilted blocks of Paintbrush Tuff that mark the edge of the dome. Stratigraphic evidence indicates that the Rainier Mesa Member was never deposited on the highest part of Yucca Mountain, although these ash flows extended for many tens of miles to the west, north, and east. Thus, the broadly domed portion of Yucca Mountain inside the hinge already was high topographically when the Rainier Mesa tuffs were erupted. The underlying, easily erodible, uppermost 5 feet of the topmost member of the Paintbrush is, however, widely preserved. Further evidence for the precollapse age of the broad doming is the presence of pre-Rainier Mesa rhyolitic lavas that were extruded through faults related to the doming north and northeast of Crater Flat.

A set of circumferential faults is exposed on the southern caldera rim. The outermost have a radius of about 10 miles. Due south of the center of the caldera they are nearly at right angles to the regional basin-range fault trends, but they follow the arc of the caldera rim for about 90°. All the circumferential faults are normal. Some are relatively downthrown to the north, others to the south, but the cumulative displacement of the blocks, which are partially self supporting in keystone fashion, is downward to the north. The regional basin-range fault trends are tangential to the caldera on the east and west sides of the structure, and here the outermost movements of the circumferential fault zone were on basin-range faults.

The circumferential faults just described are not the principal caldera-forming faults, although they are geometrically related. Mapping clearly shows that the circumferential faults on the south side of the structure postdate the Paintbrush Tuff but predate most, and perhaps all, of the Timber Mountain Tuff. Relations described later between circumferential faults and basin-range faults indicate that these outer circumferential faults were formed during the early broad doming and probably accommodated extension of the roof of the dome although they may have been reactivated in part during caldera collapse.

The eroded wall of the caldera which formed by collapse of the central area of the broad dome during and after eruption of the Rainier Mesa ash flows is largely preserved around nearly 270° of arc from the south-

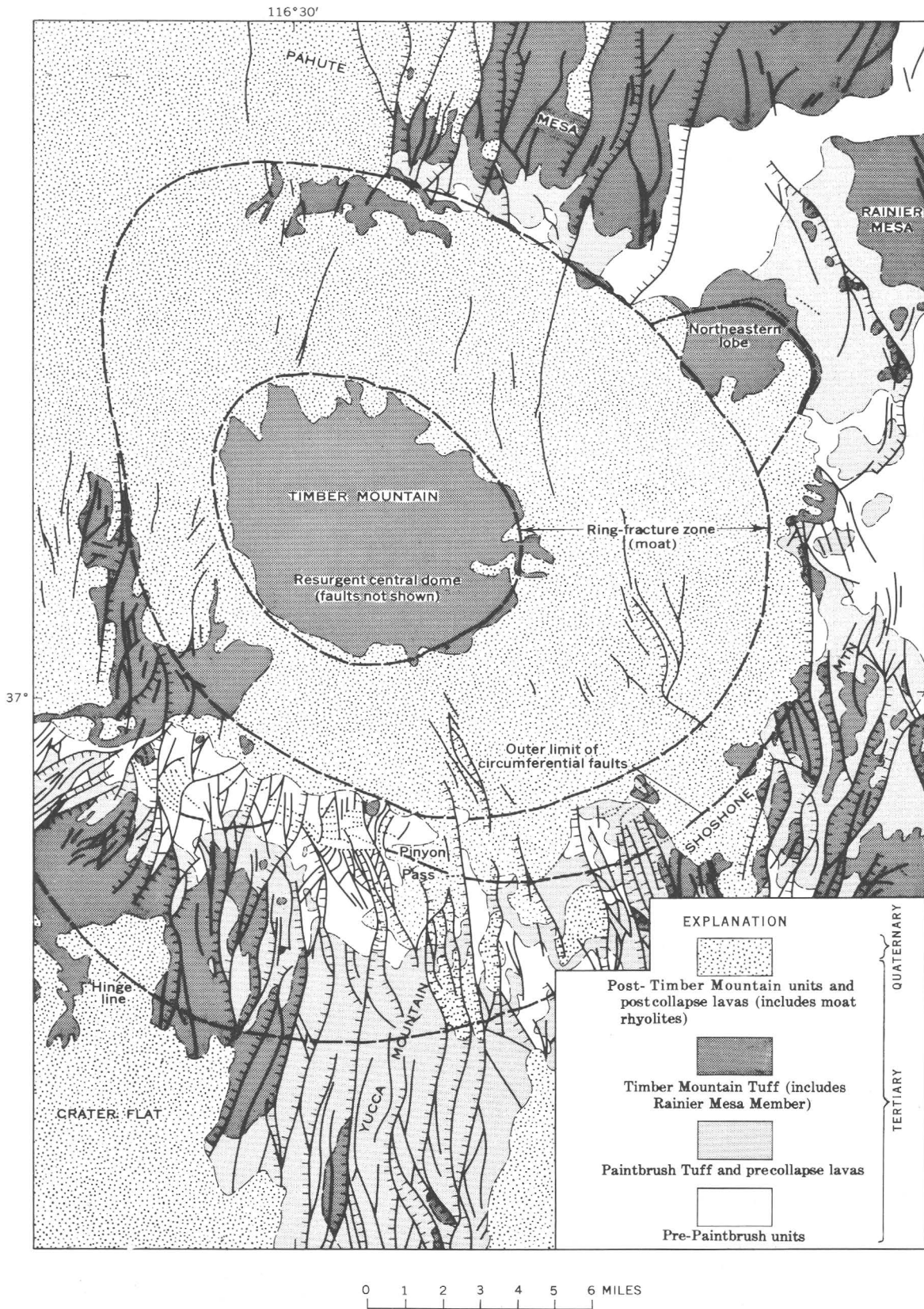


FIGURE 2.—Generalized geologic map of the Timber Mountain area, Nevada. Line symbols: all contacts dashed; hachured lines, major basin-range faults, with hachures on downthrown side; solid lines, minor basin-range faults; dotted lines, circumferential faults.

western to the northern side. The northwestern part of the wall is buried under younger ash-flow tuffs that also partly fill the caldera moat. All units within the caldera consist of young rocks either equivalent to others outside the rim at high elevations or restricted to the caldera and emplaced into it after it formed.

The Timber Mountain caldera is characterized by an outer depression or moat and a central dome and is thus classed as a resurgent cauldron (Smith and Bailey, 1962). The moat contains the fault zone along which the caldera floor collapsed. Although the moat is largely buried by later volcanic and sedimentary rocks, it can be demonstrated that the caldera collapsed as a nearly undisturbed central core bounded by a distinct ring-fracture zone in the present moat area. Most of the faults of the central area are linear graben faults related to its resurgent doming and not to collapse (Carr, 1964); only the reactivated inner edge of the ring-fracture zone is exposed around the outermost southeastern flank of the central dome. The presence of a ring-fracture zone beneath the moat is indicated not only by the general structural pattern just described but also by a group of postcollapse rhyolitic lava domes within the moat area, encircling the central dome.

A mechanical analysis by David Cummings (written communication, 1964) based on a model from elastic plate theory has related positions of the hinge line, the zone of circumferential faults, and the central initially unfaulted area to stresses developed during broad doming.

The moat rhyolites, a few relatively small rhyolitic bodies on the central dome, the flows related to early broad doming, and a group of postcollapse flows along the southern caldera rim are the only rhyolitic lava flows directly related to the Timber Mountain volcanism; they were all localized by major elements of the volcanic structure.

Early broad doming and accompanying circumferential faulting which preceded caldera formation occurred sometime during the period between emplacements of the Paintbrush Tuff and the Rainier Mesa Member of the Timber Mountain Tuff, a period of about 1.5 million years (based on K-Ar dating of sanidine and biotite by R. W. Kistler, written communication, 1963). This process probably was continuous up to the time of eruption of the Rainier Mesa Member. Large-scale collapse of the structure, related to the Rainier Mesa ash flows, was probably very rapid, perhaps catastrophic. Oversteepened walls slumped into the caldera both as large shattered but coherent blocks and as debris flows and unsorted colluvium. One large lobate block on the northeast side of the caldera is a virtually coherent piece of the slumped outer wall bounded by faults that cross

the basin-range fault trends. The third major stage of evolution of the Timber Mountain structure, resurgent doming, appears to have continued, perhaps intermittently, over an appreciable span of geologic time. Ash-flow tuffs were emplaced in the moat about 3.5 million years after collapse (on the basis of K-Ar dating of sanidine) and after resurgent doming had formed the moat; they have been uplifted and tilted eastward on the east flank of the central dome.

RELATIONS BETWEEN BASIN-RANGE FAULTS AND THE TIMBER MOUNTAIN VOLCANIC STRUCTURE

The overall structure and history of the Timber Mountain caldera are similar to those of the Valles caldera of New Mexico (Smith and others, 1961). The greater complication of the Timber Mountain structure results largely from the contemporaneous regional block faulting.

Stratigraphic relations and certain geometric features of the faults indicate that basin-range faulting and early broad domical swelling of the Timber Mountain area occurred at roughly the same time. It has been shown that both the broad doming and much of the basin-range faulting are of post-Paintbrush Tuff and pre-Rainier Mesa Member age. There are also a number of ways in which the basin-range faults on the outer flank of the Timber Mountain structure reflect the concurrent doming and extension. The hinge line bounding the broad dome is a narrow zone in which displacements on most faults are at a minimum and from which both the number of faults and their displacements increase in both directions. The maximum displacement is at the outer limit of circumferential faulting. South of the hinge, outside the domed area, many faults show notable drag, but to the north, most of the faults have little or no drag.

Fault intersections along the south rim of the caldera indicate that the circumferential and basin-range fault systems developed in part contemporaneously. Basin-range faults offset circumferential faults in some places, are offset by them in some others, and terminate against them in yet others. It is apparent, however, that broad doming and circumferential faulting had begun before some of the largest basin-range faults became active. Several large faults belonging to a complex graben near Pinyon Pass terminate against the southernmost circumferential fault. This curved fault concentric with the caldera has an exposed strike length of about 2½ miles and an average downthrow to the north of about 600 feet. Only 2 of 12 basin-range faults mapped up to it from the south offset it, and none of those terminating against it are offset to new positions on the north side. Clearly this fault formed a boundary against

which movement of the fault blocks to the south was taken up. This zone of fault intersections became the locus for eruption of both precollapse and postcollapse rhyolitic lavas along the southern rim area. These relations, along with those described between basin-range faults and the early broad dome, show the concentric fault zone to be a part of the broad dome rather than part of the caldera-forming-fracture zone.

Within the hinge line, the basin-range faults change from regional northerly trends to become radial to the volcanic structure. These are not true radial faults directly resulting from doming; there are, for example, no east-west faults either east or west of the caldera. They do, however, indicate a mechanical influence of the broad dome with its circumferentially faulted roof on the basin-range fault pattern. An analysis of the stress field resulting from interaction between the volcanic structure and regional normal faulting has shown that these changing fault trends are to be expected (David Cummings, written communication, 1964).

On the outer flanks of the broad dome south of the caldera a few large normal faults of the basin-range set have displacements opposite to the dominant regional sense and produce parallel complex grabens in the flanks of the dome. The profile of the early swell is approximately preserved in the dips of the Paintbrush Tuff on the north end of Yucca Mountain, although modified by tilting of the fault blocks. Attitudes in the grabens, however, continue north from the hinge line at the same regional gradient as in the rocks to the south. These grabens partially collapse the flank of the Timber Mountain volcanic structure beyond the edge of the caldera along linear troughs parallel to the regional tectonic trend. They are volcanic sector grabens as described by Williams (1941, p. 309-311). At least two of the major faults responsible for producing such grabens are scissor faults which near the hinge line change in displacement from the dominant regional sense to the opposed sense.

On the southwest side of the caldera, large normal faults also have displacements opposite to the dominant regional ones. They mark the outer limit of circumferential and tangential faulting by downdropping blocks toward the caldera, opposite to the regional sense. By contrast, on the east side of the caldera the dominant regional downdropping along normal faults is the same as that required to accommodate extension of the roof of the broad dome and caldera collapse; the tangential faults here have the regional sense. On this side, however, the walls slumped extensively along preexisting faults after the caldera formed. The faults along which these blocks slumped were apparently opened as surficial gashes, and some of them filled with coarse colluvial de-

bris. In addition, the principal fault blocks are tilted westward, toward the caldera, even though the fault throws are also to the west.

Relatively few basin-range faults occur within the Timber Mountain caldera, despite demonstrable post-collapse displacements on several faults outside the caldera. Some faults do displace caldera rim rocks and continue into the moat only to lose displacement or break into an echelon series and die out, probably reflecting the boundary effects of the circumferential and ring faults and of shattering within the caldera during collapse.

The relations between basin-range faulting and the Timber Mountain volcanic structure are summarized below.

- (1) Before the voluminous ash-flow eruptions and subsequent collapse, a broad structural dome developed over an area larger than the later caldera. Extension of the roof of this broad dome was accommodated by concentric normal faults along which the roof was down-dropped.

- (2) Regional block faulting and tilting were largely contemporaneous with the broad doming but have continued since. The regional faulting was adjusted to the zone of extension resulting from early doming. The number of faults and the displacement on each increased toward the center from a minimum at the edge of the broad dome to a maximum at the outer edge of the zone of circumferential faults. Basin-range faults near the outer edge of the circumferential fault zone tended to be deflected to trends radial to the dome because of the mechanical influence of the faulted roof. Both before and after caldera collapse, the intersection between these fault systems became a locus of extrusion of rhyolitic lavas. Several sector grabens extended outward along the regional fault trends from the outer concentric faults, downdropping segments of the broad dome. Basin-range faults tangential to the structure on the west and east were utilized as parts of the zone of circumferential extension.

- (3) Catastrophic collapse of the Timber Mountain caldera, related to eruption of the Rainier Mesa ash flows, occurred along a well defined ring-fracture zone approximately coincident with the earlier zone of circumferential extension faults. Formation of the caldera retarded development of regional normal faults within the collapsed area.

- (4) Resurgent doming uplifted the floor of the caldera inside the ring-fracture zone, with concurrent development of a set of extension faults, shallow intrusion of granite, and extrusion of rhyolitic lavas on this central dome (Carr, 1964). Rhyolitic lavas were also

erupted through the ring-fracture zone into the caldera moat.

REFERENCES

- Byers, F. M., Jr., Orkild, P. P., Carr, W. J., and Christiansen, R. L., 1963, Timber Mountain caldera, Nevada Test Site and vicinity—a progress report [abs.]: *Am. Geophys. Union Trans.*, v. 44, p. 113.
- Carr, W. J., 1964, Structure of part of the Timber Mountain dome and caldera, Nye County, Nevada, *in* Geological Survey Research 1964: U.S. Geol. Survey Prof. Paper 501-B, p. B16-B19.
- Locke, Augustus, Billingsley, Paul, and Mayo, E. B., 1940, Sierra Nevada tectonic pattern: *Geol. Soc. America Bull.*, v. 51, p. 513-540.
- Smith, R. L., and Bailey, R. A., 1962, Resurgent cauldrons; their relation to granitic ring complexes and large-volume ash-flow fields [abs.]: *Internat. Assoc. Volcanol. Symposium Abstracts, Japan*, p. 67-68.
- Smith, R. L., Bailey, R. A., and Ross, C. S., 1961, Structural evolution of the Valles caldera, New Mexico, and its bearing on the emplacement of ring dikes: Art. 340 *in* U.S. Geol. Survey Prof. Paper 424-D, p. D145-D149.
- Williams, Howel, 1941, Calderas and their origin: *California Univ. Pubs., Dept. Geol. Sci. Bull.*, v. 25, p. 239-346.



THE CLINCHPORT THRUST FAULT— A MAJOR STRUCTURAL ELEMENT OF THE SOUTHERN APPALACHIAN MOUNTAINS

By LEONARD D. HARRIS, Knoxville, Tenn.

Abstract.—Mapping and detailed facies studies of Cambrian rocks in key areas suggest that the trace of the Clinchport thrust fault, parts of which have previously been named the St. Clair, Honaker, Whiteoak Mountain, and Taylor Ridge faults, extends from Virginia to Georgia. In Tennessee the Clinchport fault overrides and buries two thrust plates—the Wallen Valley and Hunter Valley. Maximum displacement is unknown, but locally movement has been as much as 6 miles.

Structure of the southern Appalachian Mountains is dominated by a series of linear northeast-trending thrust faults. Several of these faults, such as the Saltville, Pulaski, and Great Smoky–Holston Mountain, are of great length and persist as entities for hundreds of miles from Virginia to Georgia. In contrast there are many shorter thrusts that begin and end in much less distance. In the past the Clinchport thrust has been assumed to be one of these shorter faults. As originally mapped by Campbell (1894, 1899) the Clinchport fault was shown both at Clinchport and Dungannon, Va., as a series of discontinuous en echelon thrust faults. Butts (1940, p. 460–461) accepted the discontinuous nature of the Clinchport fault, but suggested that it was linked to the St. Clair and Honaker faults and formed a continuous fault zone 170 miles long in Virginia and West Virginia. In northeast Tennessee, Rodgers (1953a, fig. 5) interpreted the Clinchport as a minor fault within the Hunter Valley thrust plate. The Hunter Valley is the first extensive thrust northwest of the Clinchport, in southwest Virginia (fig. 1). Near the Tennessee and Virginia border just east of Sneedville, Tenn., Rodgers showed the Clinchport fault merging with the Hunter Valley; however, southwest of the point of merger, two large “fault slices” lie in front of his Hunter Valley fault. Rodgers (1953a, p. 131) suggested the possibility that the Hunter Valley and Clinchport faults might divide around these slices, but he surmised that the Hun-

ter Valley was dominant because he discontinued the name Clinchport at the point of merger and referred to the fault throughout the rest of Tennessee as the Hunter Valley or Whiteoak Mountain thrust fault. In another paper (1953b, fig. 1) he postulated that the Hunter Valley–Whiteoak Mountain thrust is a principal fault that joins the St. Clair thrust in southwestern Virginia and West Virginia to form a continuous fault about 380 miles long from Virginia to Georgia.

Mapping by Harris and Miller (1958, 1963) and Brent (1963) demonstrated that the Clinchport fault at Clinchport, Va., is not two minor en echelon thrust faults as shown by Campbell (1894); rather the Clinchport is continuous throughout the Clinchport area. However, a relatively minor fault is present north of the Clinchport thrust in the adjacent Hunter Valley thrust plate (fig. 2). Similarly, recent reconnaissance mapping near Dungannon, Va., by the author indicates that Campbell's interpretation of the discontinuous nature of the Clinchport thrust is incorrect. The Clinchport thrust plate is warped in the area where Campbell thought the fault died out or was interrupted. The warp caused the Clinchport fault to change its stratigraphic position from low in the Rome Formation (Lower Cambrian) to the basal part of the Rutledge Limestone (Middle Cambrian). By chance, north-dipping beds of the Rutledge in an anticline in the Clinchport plate were brought in contact across the thrust plane with north-dipping beds of the Rutledge in a syncline in the Hunter Valley thrust plate—thereby producing a pseudo syncline-anticline couple (fig. 3). Campbell apparently observed this relationship and erroneously assumed that the Clinchport fault was decreasing in displacement and dying out in a fold.

After tracing the Clinchport fault northeastward from Clinchport through the Dungannon area, the author realized that northeast of Dungannon, as suggested

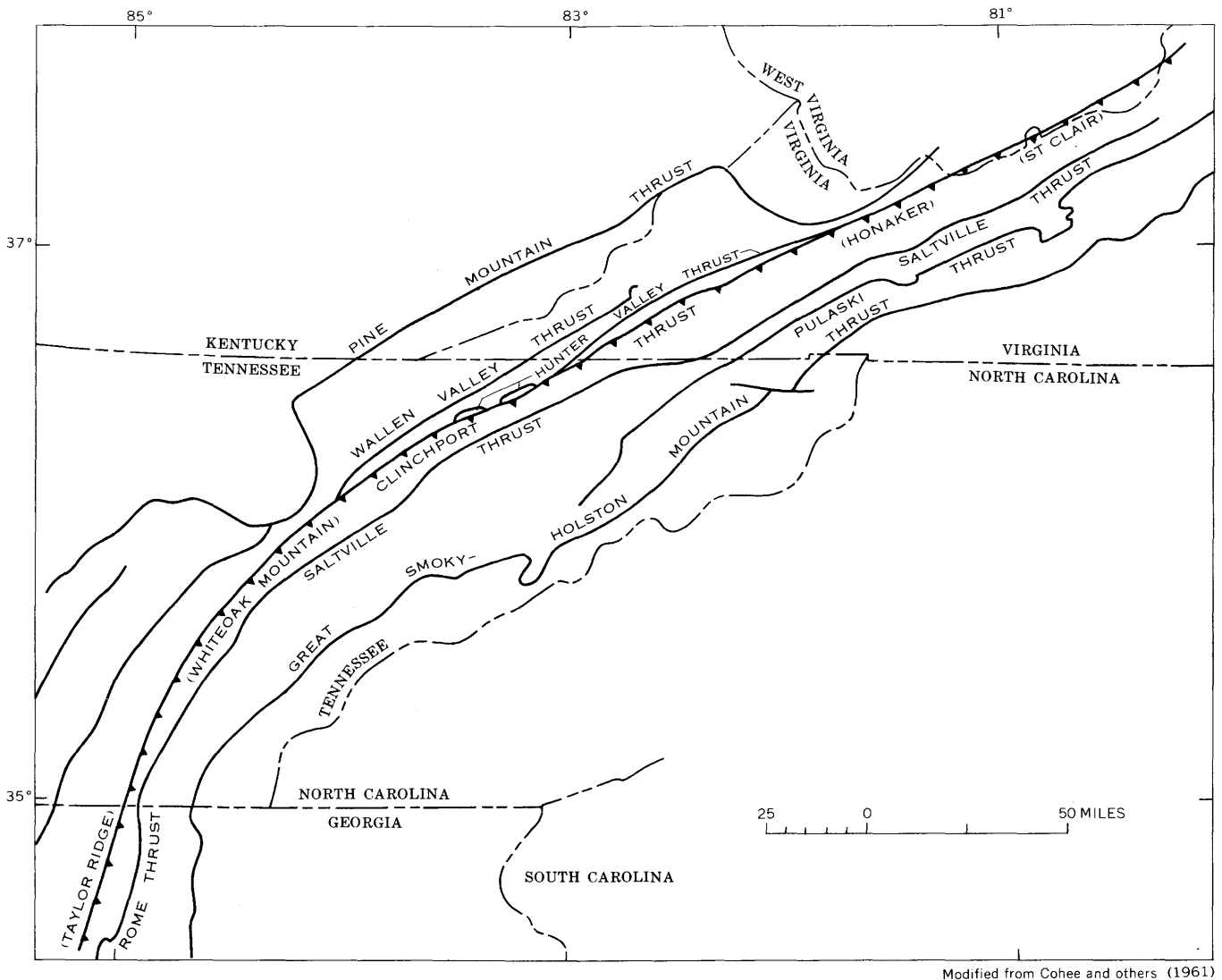


FIGURE 1.—Major thrust faults of the southern Appalachian Mountains. Names in parentheses are those previously used for parts of what is here considered the Clinchport thrust fault. Sawteeth are on upper plate of the Clinchport fault.

by Butts (1940, p. 460–461), the trace of the Clinchport is continuous with the previously named and mapped Honaker and St. Clair thrust faults (fig. 1). The trace of this major fault extends about 140 miles northeast of Dungannon through parts of West Virginia and finally dies out in an anticline in Alleghany County, Va.

Recognition that the Clinchport is a major structural element in Virginia suggested to the author the possibility that in Tennessee the Clinchport fault overrode and buried the Hunter Valley fault plate, instead of merging with the Hunter Valley thrust as suggested by Rodgers (1953a, p. 131). According to such an interpretation, the two large areas referred to as “fault slices” in the Hunter Valley plate by Rodgers would be remnants of that fault projecting from beneath the Clinchport fault plate.

Previous work by several geologists, including the author, in parts of Virginia and Tennessee has suggested that displacement along major thrust faults probably amounts to a number of miles. The displacement tends to obscure regional facies changes by burying large segments of the section and by bringing into juxtaposition facies which accumulated in separate parts of the original basin of deposition. Thus, rocks of the same formation tend to show abrupt and marked changes in lithology and thickness in very short distances from plate to plate. In contrast, rocks of the same formation commonly show gradual and progressive changes in lithology and thickness along strike within a fault plate. Both the marked local changes and the regional progressive changes are illustrated on figure 2 by rocks of the Conasauga Group in two

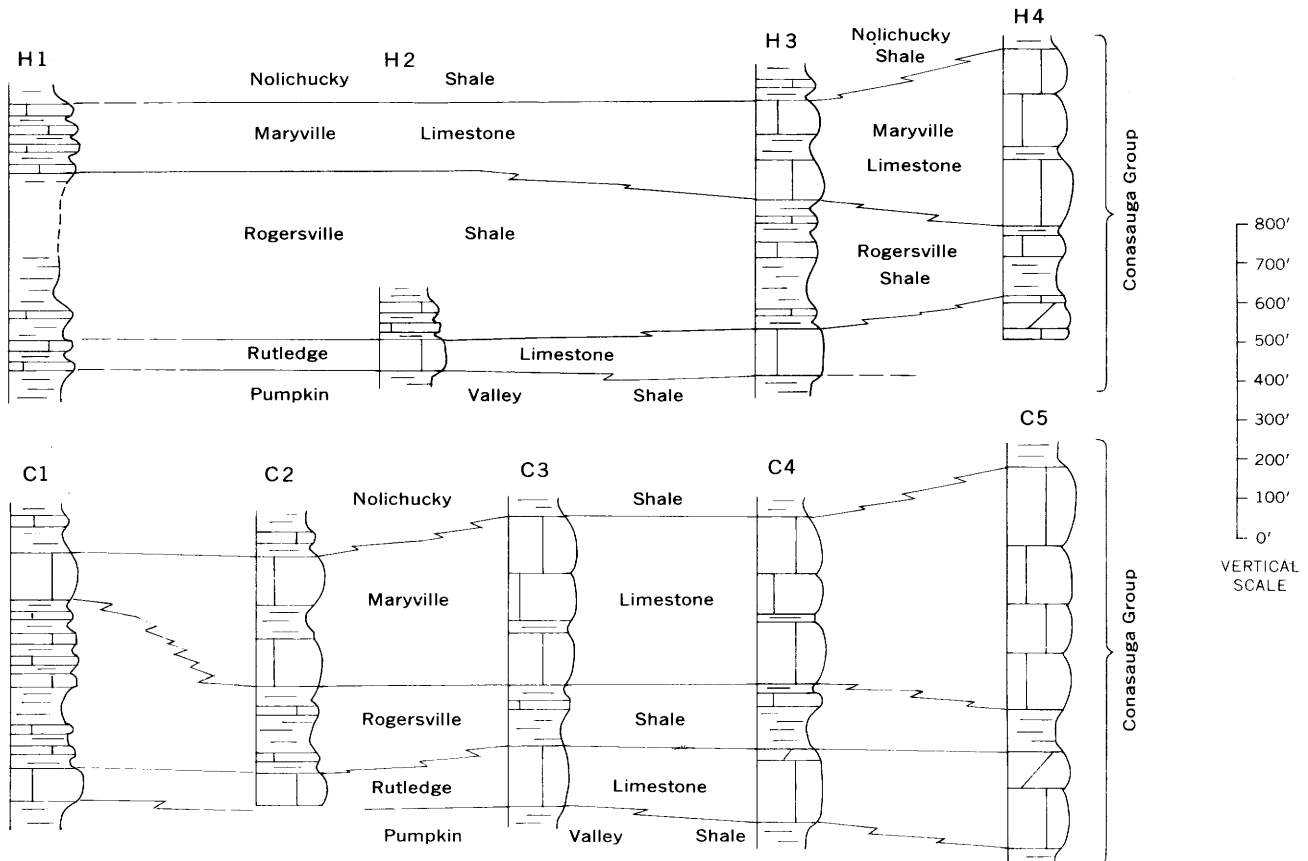
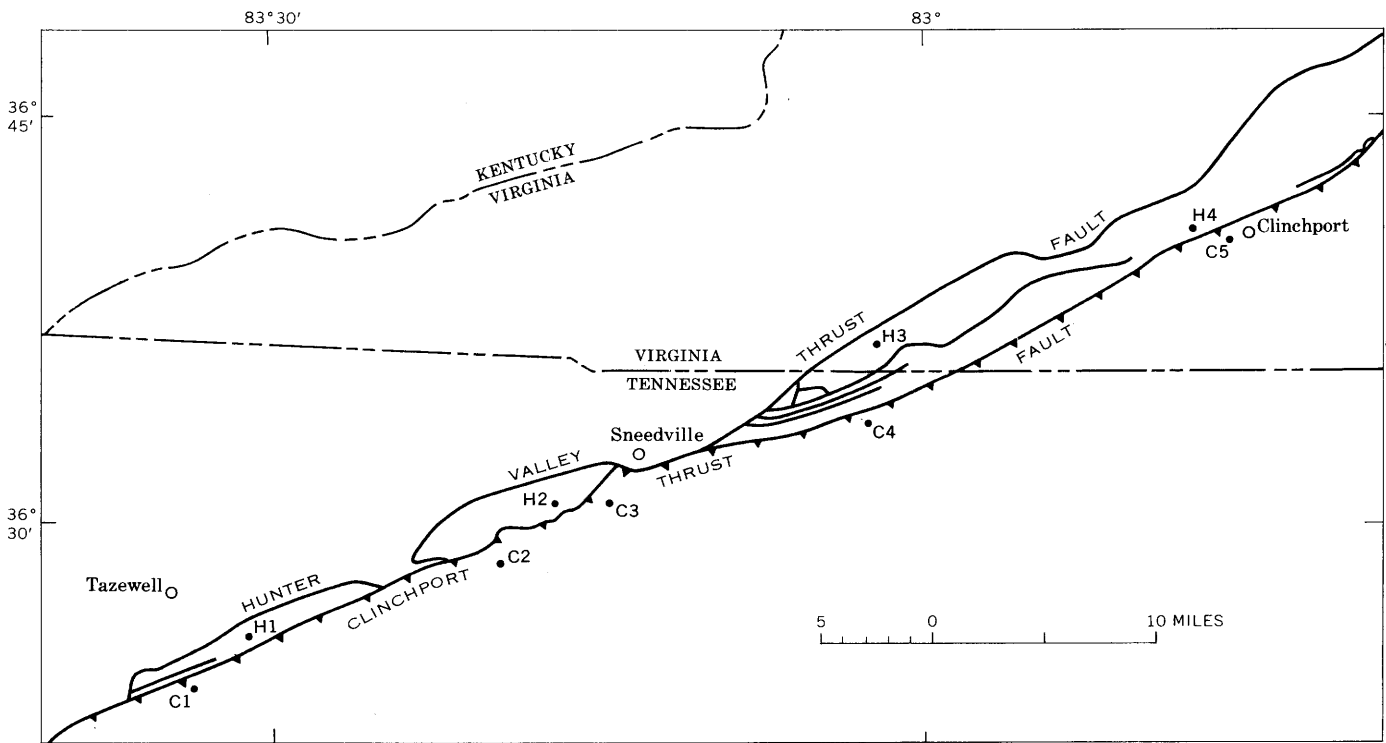


FIGURE 2.—Index map and facies diagram of the area between Tazewell, Tenn., and Clinchport, Va. The map shows thrust faults and location of measured sections; sawteeth are on upper plate of the Clinchport fault. The facies diagram shows changes in formations of the Conasauga Group in the Hunter Valley and Clinchport thrust plates.

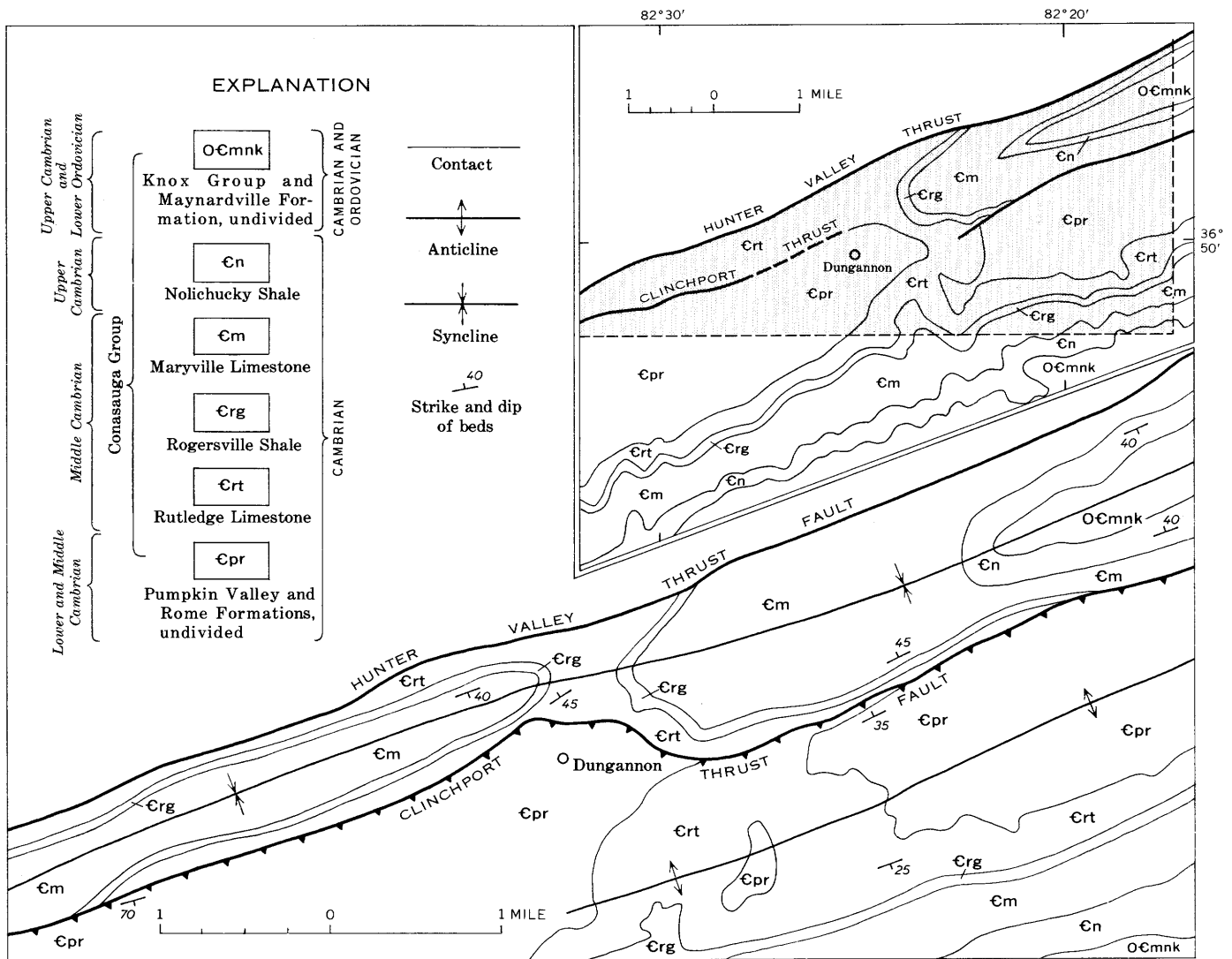


FIGURE 3.—Comparison of Campbell's (1894, 1899) geologic map (inset) of the Dungannon, Va., area and recent mapping by the author in part of the area where Campbell showed a break in the trace of the Clinchport thrust fault. Shaded area on inset map indicates area shown below at larger scale. Sawteeth are on the upper plate of the Clinchport fault of this report.

thrust plates in the area between Clinchport, Va., and Tazewell, Tenn. In this area the Rutledge and Maryville Limestones show a progressive and orderly thinning to the southwest, and the intervening Rogersville Shale shows a corresponding thickening in both the Clinchport and Hunter Valley thrust plates. In contrast, a comparison of stratigraphic sections across the plates normal to the thrust faults demonstrates that the limestones consistently thicken abruptly to the southeast in a relatively short distance (sections H3 and C4). The rocks in the two fault slices between Tazewell and Sneedsville (fig. 2) show a much greater similarity to the rocks of the Hunter Valley plate northeast of Sneedsville than to the rocks of the Conasauga Group exposed immediately to the southeast of

the fault slices in the Clinchport fault plate. Considering these data, the writer concludes that the rocks in the fault slices are isolated parts of the Hunter Valley plate projecting northwestward from below the main mass of the Clinchport plate. Thus, the Clinchport thrust is the major thrust in this area, which increased in displacement from northeast to southwest and overrode and buried the Hunter Valley plate in the area between Sneedsville and Tazewell.

About 35 miles southwest of the remnants of the Hunter Valley thrust sheet, Rodgers (1953a, p. 131) suggested that his Hunter Valley fault (the Clinchport fault of this paper) appeared to merge with the next fault to the north—the Wallen Valley (fig. 1). Southward from the point of apparent merger he called

the fault the Whiteoak Mountain. It seems unlikely that the Clinchport would override the intervening Hunter Valley sheet to merge with the next succeeding fault, the Wallen Valley. Rather it seems more likely that the Clinchport overrode and buried in turn the Hunter Valley and the Wallen Valley sheets. From the point of override the Clinchport (Whiteoak Mountain) can apparently be traced southwestward into the Taylor Ridge fault in north Georgia where it ends in an area of complex faulting.

The existence and to a great degree the extent of the Clinchport fault and component segments (Whiteoak Mountain, Honaker, St. Clair, and Taylor Ridge) have been known since the late 19th century; however, lack of detailed information in key areas delayed recognition of the Clinchport thrust as a continuous major structural element in the southern Appalachians. The Clinchport thrust can be traced for about 380 miles through parts of West Virginia, Virginia, Tennessee, and Georgia. Along its course between West Virginia and Georgia it completely overrides and buries two thrust sheets. The total width of these buried sheets is on the order of 6 miles, which suggests a minimum

displacement for the Clinchport fault. Certainly the Clinchport ranks with such other major thrust faults of the southern Appalachians as the Saltville and Pulaski.

REFERENCES

- Brent, W. B., 1963, Geology of the Clinchport quadrangle, Virginia: Virginia Div. of Mineral Resources, Rept. Inv. no. 5. 47 p.
- Butts, Charles, 1940, Geology of the Appalachian Valley in Virginia: Virginia Geol. Survey Bull. 52. 568 p.
- Campbell, M. R., 1894, Description of the Estillville quadrangle [Kentucky-Virginia-Tennessee]: U.S. Geol. Survey Geol. Atlas, Folio 12.
- 1899, Description of the Bristol quadrangle [Tennessee-Virginia]: U.S. Geol. Survey Geol. Atlas, Folio 59.
- Cohee, G. V., and others, 1961, Tectonic map of the United States: U.S. Geol. Survey and Am. Assoc. Petroleum Geologists.
- Harris, L. D., and Miller, R. L., 1958, Geology of the Duffield quadrangle: U.S. Geol. Survey Geol. Quad. Map GQ-111.
- 1963, Geology of the Stickleyville quadrangle: U.S. Geol. Survey Geol. Quad. Map GQ-238.
- Rodgers, John, 1953a, Geologic map of East Tennessee with explanatory text: Tennessee Div. Geology Bull. 58, pt. 2.
- 1953b, The folds and faults of the Appalachian Valley and Ridge province: Kentucky Geol. Survey, Ser. 9, Spec. Pub. 1, p. 150-166.



CORRELATION OF CRETACEOUS AND LOWER TERTIARY ROCKS NEAR LIVINGSTON, MONTANA, WITH THOSE IN OTHER AREAS OF MONTANA AND WYOMING

By ALBERT E. ROBERTS, Denver, Colo.

Abstract.—Cretaceous and lower Tertiary rocks exposed in the vicinity of Livingston, in southwestern Montana, comprise a marine and continental sequence of sedimentary and volcanic rocks 17,000 feet thick. From recent studies of structure, facies relations, paleontology, and nomenclature, the following units (in ascending order) are correlated with rocks in other areas of Montana and Wyoming: Kootenai Formation, Thermopolis Shale, Mowry Shale, Frontier Formation, Cody Shale, Telegraph Creek Formation, Eagle Sandstone, Cokedale Formation, Miner Creek Formation, Billman Creek Formation, Hoppers Formation, and Fort Union Formation.

Lateral variation in lithology and thickness of rocks assigned to the Cretaceous and lower Tertiary of southwestern Montana presents many problems in correlation. Brief descriptions and a correlation chart are presented here to summarize the writer's interpretation of these stratigraphic relations of the Cretaceous and lower Tertiary rocks of the Livingston area, in southwestern Montana, with other areas in Montana and Wyoming.

REGIONAL STRATIGRAPHY OF CRETACEOUS AND LOWER TERTIARY ROCKS

In Late Jurassic time, the Ellis sea that covered most of Montana withdrew northward into northern Canada, and continental deposition prevailed into the Early Cretaceous. During this time of nonmarine deposition, the Upper Jurassic Morrison Formation and Lower Cretaceous Kootenai Formation and their stratigraphic equivalents were deposited. Near the middle of the Early Cretaceous the southward transgressing arctic sea again covered most of Montana. The depositional history during Colorado and Montana time along the western edge of the Cretaceous Interior basin of Montana includes several westward transgressive stages and several eastward regressive stages. Oscillations of the Cretaceous epicontinental sea that formed these stages probably resulted from a gradual filling and sinking of the trough of the basin to the east. The lower and

upper sandstone members of the Thermopolis Shale, the Frontier Formation, the Eldridge Creek Member of the Cody Shale, and the Eagle, Miner Creek, and Hoppers Formations or their stratigraphic equivalents represent the Cretaceous regressions in southwestern Montana. In very Late Cretaceous (post-Eagle) and Paleocene time the area north of the Beartooth Range and east of the Bridger Range gradually warped downward, forming the Crazy Mountains basin (fig. 1).

STRATIGRAPHY OF CRETACEOUS AND LOWER TERTIARY ROCKS NEAR LIVINGSTON

The Cretaceous System and Paleocene Series near Livingston, Mont., comprise a sedimentary rock sequence that overlies the Morrison Formation of Late Jurassic age. This 17,000-foot-thick sequence includes, in ascending order, the Kootenai Formation, Thermopolis Shale, Mowry Shale, Frontier Formation, Cody Shale, Telegraph Creek Formation, Eagle Sandstone, Cokedale Formation, Miner Creek Formation, Billman Creek Formation, Hoppers Formation, and the lower part of the Fort Union Formation. The correlation and stratigraphic relations of the Cretaceous rocks of the Livingston area, Montana, with those of other areas in Montana and Wyoming are shown on figure 2. The Paleocene Series near Livingston includes sedimentary rocks of the middle and upper parts of the Fort Union Formation.

Volcanism occurred intermittently throughout Cretaceous and early Tertiary time, and volcanic material, which in many sections includes beds of bentonite, is conspicuous in the sediments of nearly all the formations near Livingston.

Lower Cretaceous formations

The Lower Cretaceous Series near Livingston consists of the Kootenai Formation, the Thermopolis Shale, and the Mowry Shale. The Lower Cretaceous Series is

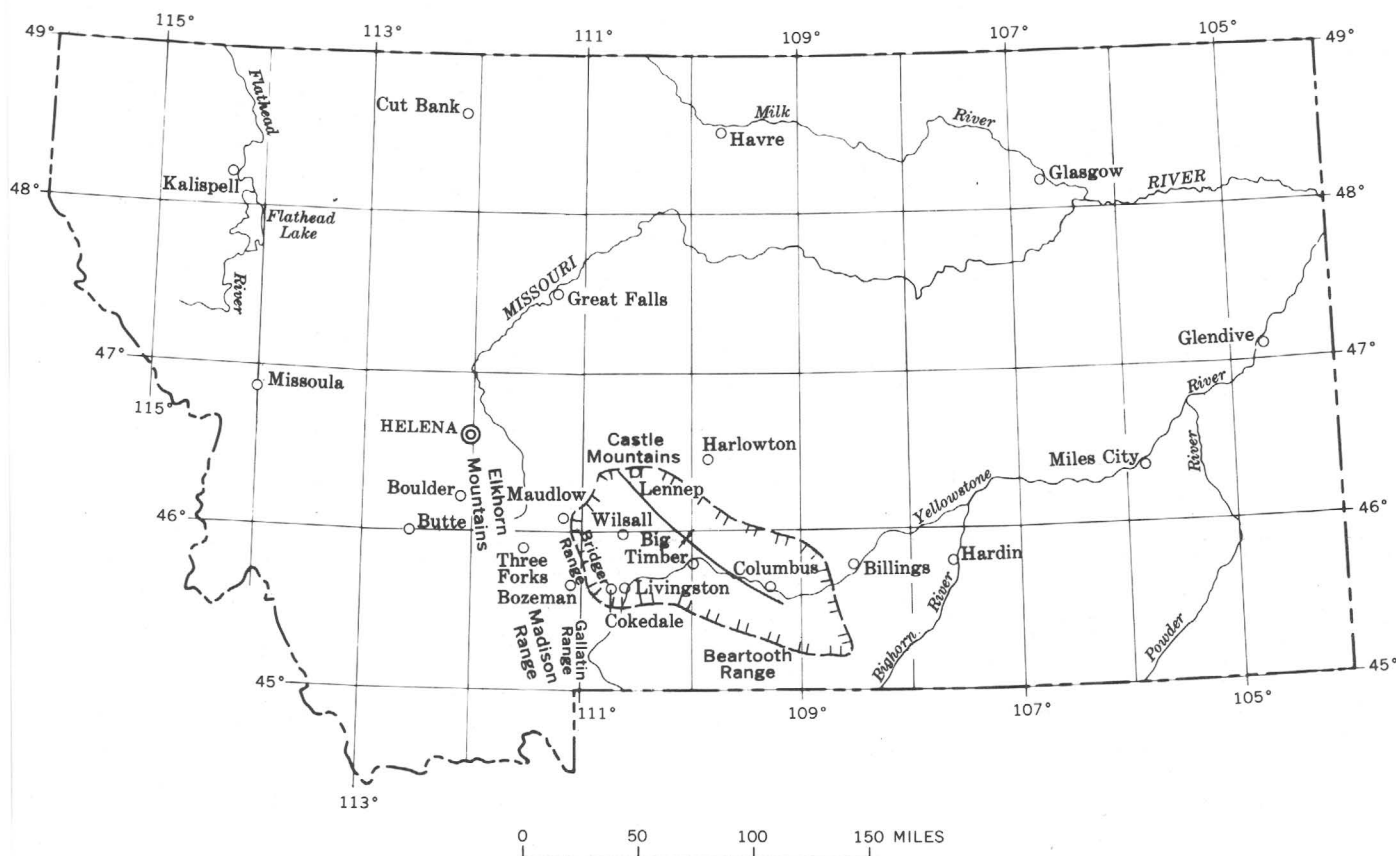


FIGURE 1.—Index map of Montana, showing Crazy Mountains basin (approximate limits indicated by hachured line) relative to area discussed.

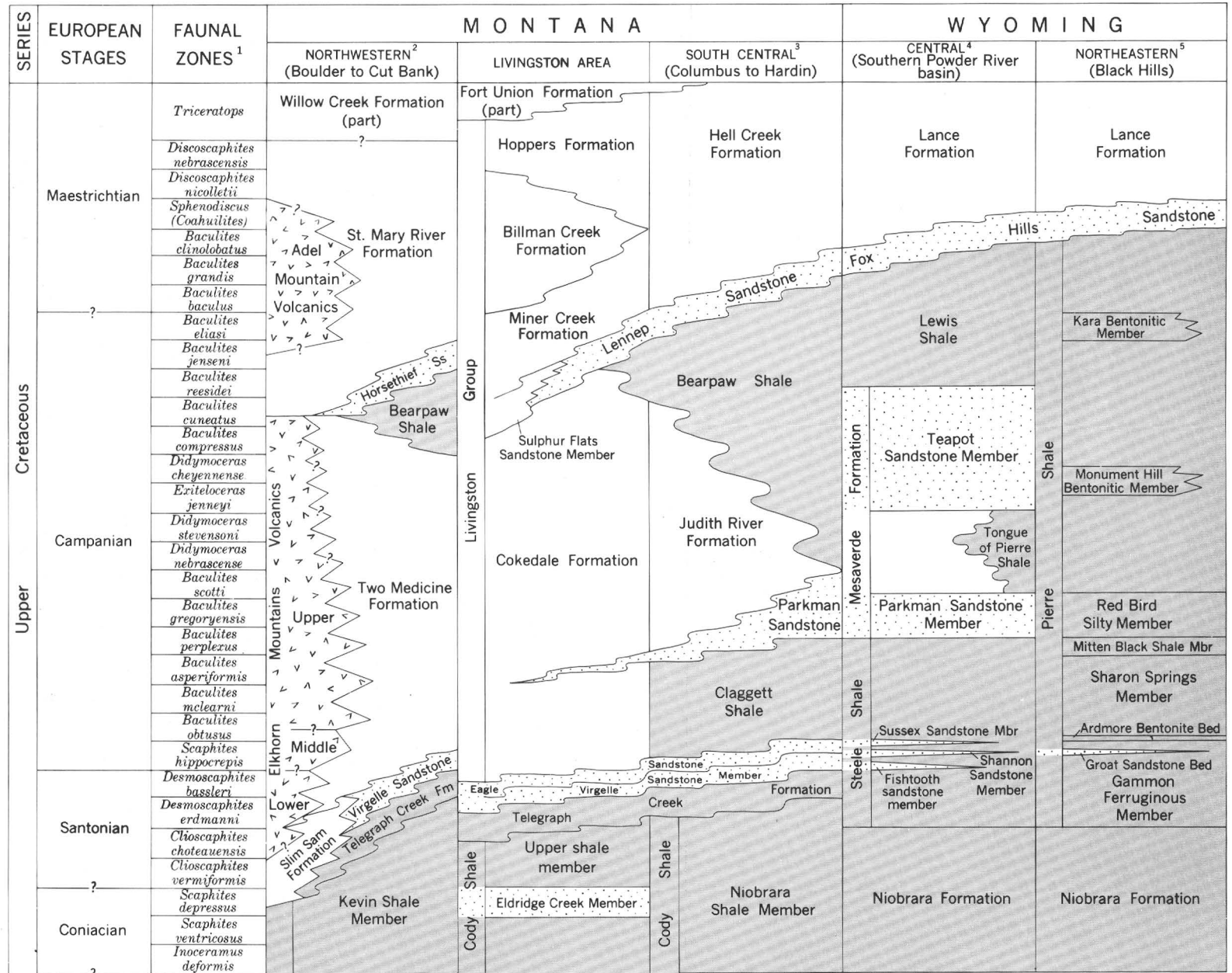
1,250 feet thick and consists of dark-gray and brownish-gray shale and claystone with interbedded quartzose sandstone.

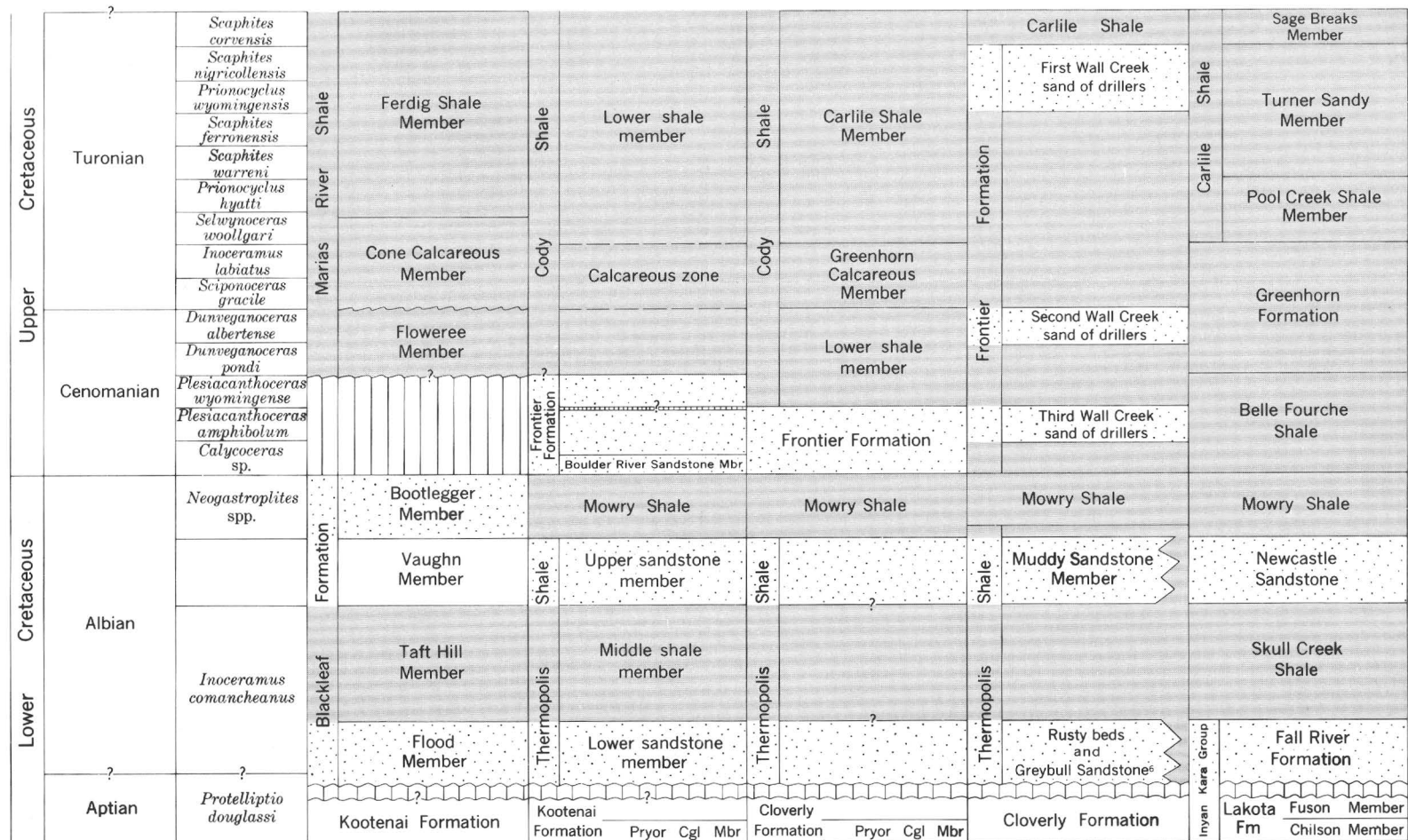
The base of the Cretaceous sequence in the Livingston area of southwestern Montana is marked by the massive bed of indurated chert pebbles newly assigned in this paper to the Pryor Conglomerate Member. The Pryor is the basal member of the Kootenai Formation and unconformably overlies the Upper Jurassic Morrison Formation. Exposures of the continental sequence of the Kootenai Formation in the vicinity of Livingston suggest deposition over an extensive lowland bordered on the west by a highland area. Streams from the west during early deposition of the Kootenai dropped their sediment to create alluvial fans, channel sandstones, and flood-plain deposits. During the remainder of the deposition of the Kootenai the area was predominantly lacustrine, with deposition of very fine grained clastic sediments, predominantly of volcanic origin, and a few limestones. The Kootenai is 245 to 295 feet thick, including the 24- to 37-foot Pryor Conglomerate Member. The Kootenai Formation at Livingston is probably equivalent to the Lakota Formation of northeastern Wyoming and the Cloverly Forma-

tion of south-central Montana and central Wyoming, where the name Cloverly is restricted to Cretaceous rocks (fig. 2).

The Thermopolis Shale overlies the Kootenai Formation and is subdivided into the lower sandstone member, middle shale member, and upper sandstone member. In areas of good exposures these members would be of formation rank; however, in the northern part of the Gallatin Range, valleys with very few outcrops are developed on these units. The Thermopolis Shale is 490 to 530 feet thick and is predominantly soft dark-gray to black marine shale with prominent sandstone ridges or ledges formed by the lower and upper members.

The lower sandstone member rests unconformably on the Kootenai Formation, in many places filling depressions in its upper part. The hiatus between the Kootenai Formation and the lower sandstone member of the Thermopolis Shale is presumed to be small because the index fossil *Protelliptio douglassi* occurs immediately above and below the widespread disconformity separating the two formations (W. A. Cobban, oral communication, 1963). The lower member is a clean quartzose sandstone that in local areas of intense fold-





¹ Modified from Cobban (1958), Zapp and Cobban (1960), and Cobban (1962a, 1962b).

² Modified from Lyons (1944), Klepper, Weeks, and Ruppel (1957), Cobban and others (1959), Schmidt and Zubovic (1961), W. A. Cobban (oral communication, 1962), M. R. Klepper (oral communication, 1962), and R. G. Schmidt (oral communication, 1964).


³ Modified from Hancock (1918) and Richards (1955).

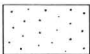
⁴ Modified from Horn (1955) and Cobban (1958).


⁵ Modified from Spivey (1940), Cobban (1958), Robinson, Mapel, and Cobban (1959), Gill and Cobban (1961, 1962), and Knechtel and Patterson (1962).

⁶ As used by Eicher (1960).

EXPLANATION

 Predominantly offshore marine

 Predominantly nearshore marine and brackish water

 Predominantly nonmarine

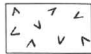
 Predominantly volcanic rock

FIGURE 2.—Correlation and stratigraphic relations of the Cretaceous rocks of the Livingston area, Montana, with rocks of other areas in Montana and Wyoming.

ing is a quartzite; it ranges in thickness from 35 to 50 feet. The lower sandstone member of the Thermopolis Shale is probably equivalent to the Greybull Sandstone and Rusty beds of north-central Wyoming, the Fall River Formation of the Black Hills area of northeastern Wyoming, and the Flood Member of the Blackleaf Formation of northwestern Montana (fig. 2).

The middle shale member conformably overlies the lower sandstone member of the Thermopolis Shale. The middle shale member is a black marine shale ranging in thickness from 350 to 390 feet. The lower 100 feet contains numerous thin beds of siltstone and very fine grained sandstone. The member contains a spore and pollen assemblage similar to that of the Skull Creek Shale of north-central Wyoming (G. O. W. Kremp, written communication, 1960). The middle shale member is also correlative with the Taft Hill Member of the Blackleaf Formation of northwestern Montana (fig. 2).

The upper sandstone member overlies the middle shale member, probably conformably. The upper sandstone member is a fine-grained arkosic sandstone with some interbedded shale in the middle part; it contains a large proportion of heavy minerals and in this it differs from the lower sandstone member. It ranges in thickness from 90 to 105 feet, and generally only the lower part is exposed. Glauconite is present in the upper part of the upper sandstone member. The member is probably equivalent to the Muddy Sandstone Member of north-central Wyoming, the Newcastle Sandstone of the Black Hills area of northeastern Wyoming, and the Vaughn Member of the Blackleaf Formation in northwestern Montana.

The Mowry Shale conformably overlies the upper sandstone member of the Thermopolis Shale. The Mowry is a dark-gray to brownish-gray marine and nonmarine claystone with interbedded siltstone and sandstone throughout. Its thickness ranges from 430 to 500 feet. Septarian concretions are common in the lower part of the formation, and conspicuous greenish-gray claystone with red specks of heulandite is present in the upper 100 feet of the formation. The Mowry at Livingston is probably equivalent to the Bootlegger Member of the Blackleaf Formation in northwestern Montana.

To distinguish the Thermopolis Shale from the Mowry Shale in the Livingston area, emphasis may be given to lithology, fabric, and color. The Thermopolis is predominantly shale (fissile), while the Mowry is predominantly claystone (nonfissile). Also, the Thermopolis Shale is dark gray, weathers to light gray, and is not very tuffaceous; on the other hand the Mowry Shale is brownish gray, weathers to yellowish gray,

and is very tuffaceous. Porcelanitic sandstones are present only in the upper 200 feet of the Mowry.

Upper Cretaceous formations

The Upper Cretaceous Series near Livingston consists of the Frontier Formation, Cody Shale, Telegraph Creek Formation, Eagle Sandstone, Cokedale Formation, Miner Creek Formation, Billman Creek Formation, Hoppers Formation, and the basal part of the Fort Union Formation. The Upper Cretaceous Series is 10,830 feet thick, it consists of dark-gray shale with interbedded siltstone and sandstone in the lower part, and of elastic material derived from Precambrian metamorphic and metasedimentary, Paleozoic and Mesozoic sedimentary, and Cretaceous volcanic rocks in the upper part.

Massive indurated ridge-forming sandstones of the Frontier Formation overlie the Mowry Shale and are probably conformable upon it. The boundary between the Mowry Shale and the Frontier Formation is the base of the lowest well-defined sandstone of the Boulder River Sandstone Member above the Mowry Shale. These sandstones contain an abundant heavy-mineral suite, and their general appearance is that of "salt and pepper" sands. The Frontier contains spores, pollen, and a few shallow-water mollusks (both marine and brackish-water forms); its thickness ranges from 350 to 415 feet. East of the Livingston area, Richards (1957, p. 415) named a prominent 100-foot-thick sandstone unit exposed along the west side of the Boulder River valley near McLeod, Mont., the Boulder River Sandstone Member of the Colorado Shale. This unit, which represents the basal part of the Frontier Formation of the McLeod area and of adjacent areas, is here redesignated as the basal member of the Frontier Formation. At Livingston the Boulder River Sandstone Member is 120 feet thick. At its top is an excellent persistent marker bed of mottled sandstone. The mottling is due to crystallization clusters of analcite in the cementing material, which give the weathered surface the appearance of a small-pebble conglomerate. Siltstone and shale with streaks of coal are present near the middle of the Frontier. Approximately 100 feet from the top of the Frontier is a persistent thin bed of chert-pebble conglomerate. The Frontier Formation at Livingston is approximately equivalent to the Belle Fourche Shale of northeastern Wyoming (fig. 2).

The Cody Shale overlies the Frontier Formation and is subdivided into three units, the lower shale member, the Eldridge Creek Member, and the upper shale member. The Cody Shale at Livingston is 1,285 to 1,375 feet thick and is predominantly a dark-gray marine shale.

Overlying the Frontier Formation, apparently conformably, is 400 to 590 feet of dark-gray to dark-brown marine shale with interbedded siltstone throughout. This shale unit, the lower shale member of the Cody Shale, is correlative with the Greenhorn Formation, the Carlile Shale, and the lower part of the Niobrara Formation of northeastern Wyoming (fig. 2). In the lower part of the lower shale member is a persistent calcareous zone that is correlative with the Greenhorn Calcareous Member of the Cody Shale of south-central Montana.

A persistent thin-bedded greenish-gray fine-grained sandstone named the Eldridge Creek Member of the Cody Shale (Roberts, 1964c) overlies the lower shale member with apparent conformity. This excellent marker bed contains a shallow-water marine middle Niobrara fauna (W. A. Cobban, written communication, 1958) and is very glauconitic. The Eldridge Creek Member ranges in thickness from 90 to 120 feet.

The upper shale member conformably overlies the Eldridge Creek Member and consists of 500 to 845 feet of dark-gray to brown marine shale and siltstone with interbedded very fine grained sandstone. The member gradually increases in total sand content in the younger beds. This upper shale member is correlative with the upper part of the Niobrara Formation of northeastern Wyoming (fig. 2).

The Montana Group equivalent in the Livingston area consists of the Telegraph Creek Formation, Eagle Sandstone, Cokedale Formation, Miner Creek Formation, Billman Creek Formation, and part of the Hoppers Formation. The Telegraph Creek Formation is of shallow-water marine origin; the Eagle Sandstone is of littoral or brackish-water origin; and the Cokedale, Miner Creek, Billman Creek, and Hoppers Formations are predominantly of nonmarine origin.

The Telegraph Creek Formation consists of thin beds of calcareous sandy siltstone and sandstone that contain abundant biotite and a heavy-mineral suite similar to that in the Eagle Sandstone. The Telegraph Creek is approximately 275 feet thick at Cokedale, Mont., 9 miles west of Livingston, and at Livingston it is 295 feet thick. Weed (1893, p. 16) referred to the steeply dipping small ledges in this part of his stratigraphic section at Cokedale as the Tombstone Sandstone. In the Cokedale-Livingston area the Telegraph Creek Formation is transitional in grain size between the very fine grained clastic material of the upper shale member of the Cody Shale and the fine- to medium-grained clastic material of the Eagle Sandstone. The base of the Telegraph Creek is generally covered by Quaternary deposits; in the few localities where the lower part of the formation is exposed, its contact with the Cody Shale is arbitrarily placed at the lowermost biotitic sandstone bed.

The Eagle Sandstone conformably overlies the Telegraph Creek Formation, and the boundary between the two formations is gradational. The Eagle consists of 515 to 860 feet (average about 600 feet) of sandstone with intercalated beds of coal and carbonaceous siltstone. A massive, light gray, arkosic sandstone 110 feet thick at its base is called the Virgelle Sandstone Member. The coal beds, some of which are of commercial quality, are usually lenticular with rapid lateral changes; however, the zones in which they occur are laterally persistent (Roberts, 1957, p. 45). According to W. A. Cobban (written communication, 1961), faunas collected from the Eagle Sandstone 50 miles south of Livingston indicate that the top of the Eagle in this area is no younger than the lower part of the Eagle of central Montana and that an even older age is possible (fig. 2).

Late in the Santonian Stage of Late Cretaceous time, epeirogenic arching began in western Montana, and the Eagle seas regressed to the east. This period of orogeny and erosion was accompanied by volcanism that formed the thick Elkhorn Mountains volcanic pile (Klepper and others, 1957, p. 31-41). Following withdrawal of the Upper Cretaceous Eagle seas in western Montana, the area east of the Bridger Range and north of the Beartooth Range was gradually warped downward forming the Crazy Mountains basin.

The Crazy Mountains basin is elongated northwest and is approximately 40 to 70 miles wide and 130 miles long (fig. 1). The basin is asymmetrical, with more than 13,000 feet of sedimentary rock derived predominantly from andesitic volcanic rock of the Elkhorn Mountains deposited in the deeper (western) part of the basin during the remainder of Upper Cretaceous and Paleocene time (Roberts, 1963, p. B86). The stratigraphic sequence for this part of the basin indicates that deposition was continuous and that the rocks grade laterally to the east and northeast into finer grained marine and nonmarine beds. The nonmarine sequence near Livingston, Mont., has been subdivided into the Livingston Group, which includes the Cokedale, Miner Creek, Billman Creek, and Hoppers Formations of Late Cretaceous age, and the Fort Union Formation of Late Cretaceous and Paleocene age (Roberts, 1963). The Livingston Group represents rapid vertical and lateral variations in lithology commensurate with part of the Laramide orogeny.

The type Cokedale Formation is a nonmarine unit 1,550 feet thick comprised of siltstone and sandstone with lesser amounts of claystone, tuff, bentonite, and coal in the lower part. The Cokedale is correlated eastward with the Claggett Shale, the Judith River Formation, and the Bearpaw Shale, and in northwestern Montana

with the Two Medicine Formation (fig. 2). The Cokedale rests conformably on the Eagle Sandstone at the type section at Cokedale, Mont. The difference in the lithologies of the Eagle Sandstone (predominantly quartz grains) and the Cokedale Formation (predominantly andesite fragments) is considerable. However, the boundary is not represented by an abrupt change in lithology. The contact is placed at the top of the arkosic sandstone that overlies the uppermost minable coal bed in the Eagle Sandstone (Roberts, 1963, p. B90).

The Miner Creek Formation conformably overlies the Cokedale Formation. The type section is 1,350 feet thick. The Miner Creek consists largely of alternating beds of nonmarine siltstone and sandstone; the Sulphur Flats Sandstone Member, a 160-foot-thick unit that forms prominent ridges, is at its base. The Miner Creek Formation is correlated eastward with the lower part of the Hell Creek Formation, and the Sulphur Flats Sandstone Member is the nonmarine facies of the marine Lennep Sandstone and the Horsethief Sandstone (fig. 2).

The type Billman Creek Formation is a nonmarine unit, 2,590 feet thick comprised of red, purple, and green tuff, bentonite, and claystone with a few intercalated beds of sandstone. Claystone constitutes about 65 percent of the formation; three samples of the claystone averaged 40 percent montmorillonite, 50 percent mixed-layer montmorillonite-illite-vermiculite, 5 percent illite, and 5 percent chlorite (L. G. Schultz, oral communication, 1962). A 20-foot continuous sandstone unit 96 feet above the base of the Billman Creek Formation contains abundant spherical calcareous sandstone concretions, generally 1 to 2 feet in diameter, and is an excellent marker bed. The Billman Creek Formation is correlated northward and eastward with the middle part of the Hell Creek Formation (fig. 2). The Billman Creek rests conformably on the Miner Creek Formation at the type section on Billman Creek, near Cokedale, Mont.

The type Hoppers Formation is a nonmarine unit, 965 feet thick, comprised of sandstone and conglomerate with some interbedded siltstone, claystone, and tuff. The basal 140 feet of the Hoppers is a conspicuous yellowish-gray, crossbedded, cliff-forming sandstone that is conglomeratic in many places. The sandstones are generally banded by layers of ferromagnesian minerals. The Hoppers Formation is correlated northward and eastward with the upper part of the Hell Creek Formation (fig. 2).

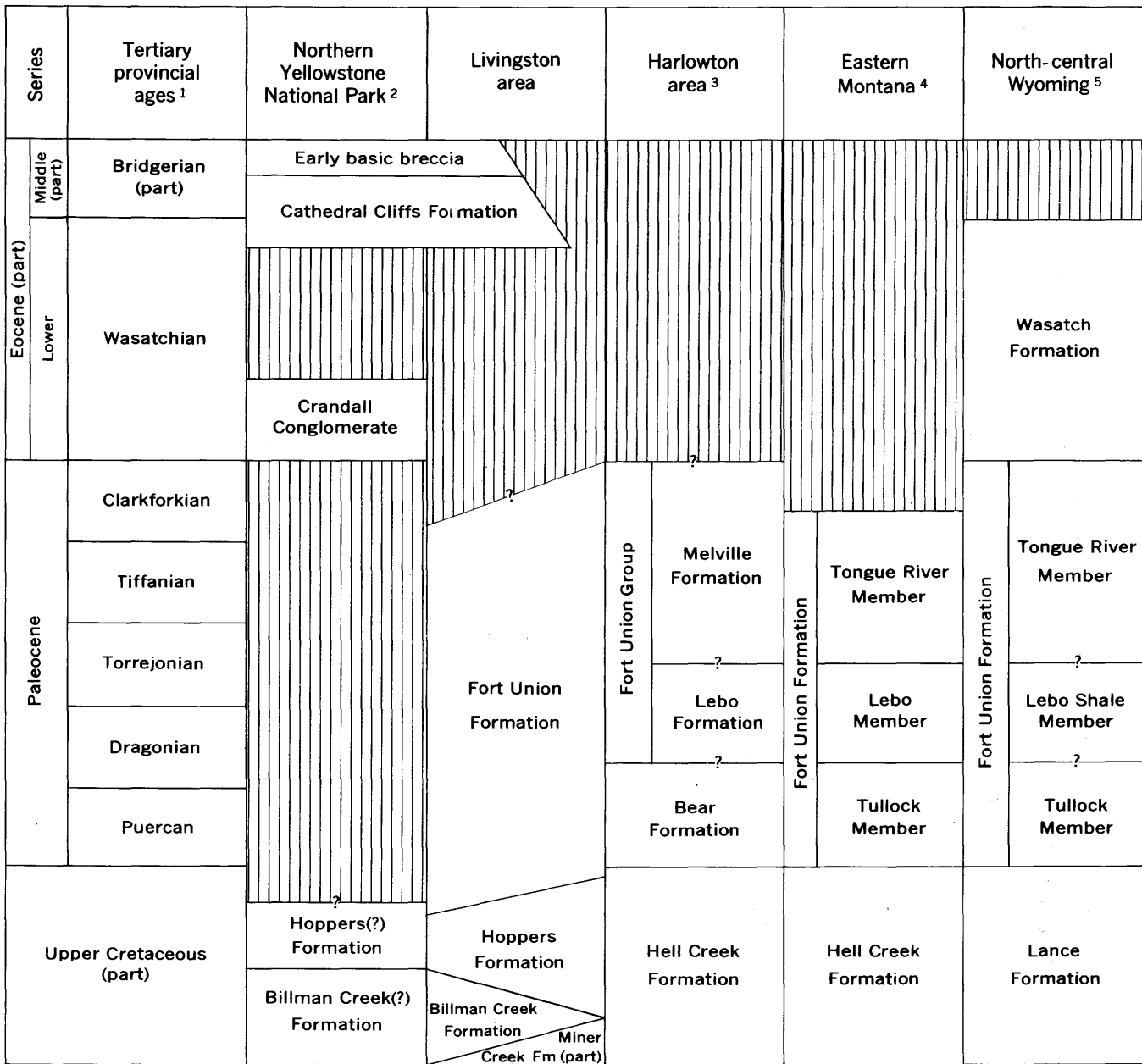
Upper Cretaceous and Paleocene formation

The Livingston Group at Cokedale, Mont., is overlain by a nonmarine sequence of sandstone and conglomerate alternating with siltstone and claystone which is

6,615 feet thick and is assigned to the Fort Union Formation (fig. 3). The Fort Union includes three lithologic units: a lower conglomeratic sandstone member 975 feet thick, a middle member of sandstone and claystone 3,840 feet thick, and an upper conglomeratic sandstone member 1,800 feet thick. There is an erosion surface at the top. Evidence from fossils, stratigraphic position, and tectonic history as interpreted from the types of rock in the unit indicates that the lower member is of Late Cretaceous age. Conglomerate in the Livingston Group consists chiefly of Cretaceous volcanic-rock fragments, whereas the conglomerate in the overlying Fort Union contains igneous, metamorphic, and sedimentary rocks derived from Precambrian, Paleozoic, and Mesozoic formations. The position of the boundary between rocks of Late Cretaceous and Paleocene age is uncertain but may lie somewhere in the lower 800 feet of the middle member of the Fort Union, as these beds contain a flora shown by plant microfossils to be transitional between Cretaceous and Paleocene (R. H. Tschudy, written communication, 1962). Approximately 3,100 feet above the base of the formation the writer collected part of a jawbone with teeth that was identified by C. L. Gazin (written communication, 1958) as *Tetraclaeonodon* cf. *symbolicus* Gidley, a middle Paleocene fossil which has been described from the Lebo Member of the Fort Union Formation.

Eocene formations

The northern part of the Gallatin Range continued to undergo erosion during deposition of the Fort Union Formation in the southwestern part of the Crazy Mountains basin. Later this area was covered by Tertiary flows, flow breccias, and related sedimentary deposits. At the northern extent of these rocks, near Chimney Rock, Mont. (Roberts, 1964e); the post-Fort Union stratigraphic section consists predominantly of conglomerates, flow breccias, agglomerates, and mud flows similar to the types of rocks deposited near the periphery of large volcanic piles. At the base of the section is 160 feet of cliff-forming coarse conglomerate composed predominantly of dacitic volcanic rock but with lesser amounts of Precambrian igneous and metamorphic rocks and Paleozoic and Mesozoic sedimentary rocks. A carbonaceous claystone found locally at the base of this conglomerate (W. J. McMannis, written communication, 1962), contains plant spores and pollen identified by R. H. Tschudy (written communication, 1962), as Wasatchian provincial age of Wood and others (1941) of the Eocene. The cliff-forming conglomerate is overlain by 60 feet of loosely consolidated, slope-forming conglomerate that contains only volcanic rock (generally andesitic). A sequence of several thousand feet of andesitic flows, flow breccias, agglomerates, and mud



¹ Modified from Wood and others (1941).
² Modified from Pierce (1963).
³ Modified from Simpson (1937).
⁴ Modified from Brown (1962).
⁵ Modified from Mapel and others (1959).

FIGURE 3.—Correlation and stratigraphic relations of part of the lower Tertiary rocks of the Livingston area, Montana, with rocks of other areas in Montana and Wyoming.

flows overlies the slope-forming conglomerate. The Wasatchian provincial age of the claystone at the base of the section and petrographic comparisons of the overlying rocks with those in the Absaroka Range indicate that the lower conglomerate is a lateral facies of part of the "early acid breccia" of Hague (1899) in the Absaroka Range or Reese Formation of Calvert (1912) in

the southern part of the Gallatin Range, or the Cathedral Cliffs Formation of Pierce (1963) in the Clarks Fork area of northwestern Wyoming; and that the upper conglomerate and overlying rocks are equivalent to the "early basic breccia" of Hague (1899) of Bridgerian provincial age of the northern Absaroka Range and Yellowstone National Park area, Wyoming.

Post-Fort Union tectonic history

The Bridger Range on the west edge of the Crazy Mountains basin is the result of uplift and basinward (eastward) thrusting, and the Beartooth Range on the south edge is the result of uplift and basinward (north-eastward) thrusting. The uplift was gradual during deposition of the Livingston Group and Fort Union Formation, and the thrusting postdates these units. The Livingston area was relatively stable in comparison with the Bridger Range to the west and the Beartooth Range to the southeast. As the Bridger and Beartooth uplifts were forced basinward the area between Bozeman and Livingston developed into an area of arcuate, northwest-trending, en echelon folds, each of which is convex toward the southwest and parallels the axis of the Crazy Mountains basin (Roberts, 1964a, b, c, d, e, f, g, and h). Folding in the Livingston area continued until the major anticlines became asymmetric, with the steeper dips on the southwest flanks. The Canyon Mountain anticline progressed until it became recumbent on its southwest flank.

The crustal forces continued until failure of the folds occurred and large thrust or high-angle reverse (depending on degree of dip) faults were developed in a similar en echelon arrangement paralleling the folds. Field relations of these faults suggest that deformation was shallow seated. The general dip on the plane of these faults was west or south, depending on proximity to the Bridger or Beartooth Ranges. Mapping of the southwest flank of the Canyon Mountain anticline indicated several pulses of thrusting with intervening periods of erosion (Roberts, 1964 a and b).

Compressive forces continued to move the Bridger block eastward and the Beartooth block northward, and folding continued in the Livingston area but with less magnitude than previously. The thrust plates were folded at this time, changing the general dip of the fault planes to a basinward or north-to-east direction.

Extensive erosion accompanied the folding, and by Late Cretaceous time the Bridger and Beartooth uplifts were truncated to expose Precambrian rocks. The basal conglomerate of the Fort Union Formation in the Livingston area, which is of very Late Cretaceous age, contains rock fragments derived from Precambrian (including the Belt Series), Paleozoic, and Mesozoic rocks (Roberts, 1963, p. B89).

REFERENCES

- Brown, R. W., 1962, Paleocene flora of the Rocky Mountains and Great Plains: U.S. Geol. Survey Prof. Paper 375, 106 p.
- Calvert, W. R., 1912, The Electric coal field, Park County, Montana: U.S. Geol. Survey Bull. 471-E, p. 50-66.
- Cobban, W. A., 1958, Late Cretaceous fossil zones of the Powder River basin, Wyoming and Montana, in Wyoming Geol. Assoc. Guidebook 13th Ann. Field Conf., Powder River basin: p. 114-119.
- 1962a, New Baculites from the Bearpaw Shale and equivalent rocks of the western interior: Jour. Paleontology, v. 36, no. 1, p. 126-135.
- 1962b, Baculites from the lower part of the Pierre Shale and equivalent rocks in the western interior: Jour. Paleontology, v. 36, no. 4, p. 704-718.
- Cobban, W. A., Erdmann, C. E., Lemke, R. W., and Maughan, E. K., 1959, Revision of Colorado Group on Sweetgrass Arch, Montana: Am. Assoc. Petroleum Geologists Bull., v. 43, no. 12, p. 2786-2796.
- Eicher, D. L., 1960, Stratigraphy and micropaleontology of the Thermopolis Shale: Peabody Mus., Yale Univ. Bull. 15, 121 p.
- Gill, J. R., and Cobban, W. A., 1961, Stratigraphy of lower and middle parts of the Pierre Shale, northern Great Plains: Art. 352 in U.S. Geol. Survey Prof. Paper 424-D, p. D185-D191.
- 1962, Red Bird Silty Member of the Pierre Shale, a new stratigraphic unit: Art. 8 in U.S. Geol. Survey Prof. Paper 450-B, p. B21-B24.
- Hague, Arnold, 1899, Geology of the Yellowstone National Park; pt. 2, Descriptive geology, petrography, and paleontology: U.S. Geol. Survey Mon. 32, 893 p.
- Hancock, E. T., 1918, Geology and oil and gas prospects of the Lake Basin field, Montana: U.S. Geol. Survey Bull. 691-D, p. 101-147.
- Horn, G. H., 1955, Geologic and structure map of the Sussex and Meadow Creek oil fields, Johnson and Natrona Counties, Wyoming: U.S. Geol. Survey Oil and Gas Inv. OM-164.
- Klepper, M. R., Weeks, R. A., and Ruppel, E. T., 1957, Geology of the southern Elkhorn Mountains, Jefferson and Broadwater Counties, Montana: U.S. Geol. Survey Prof. Paper 292, 82 p.
- Knechtel, M. M., and Patterson, S. H., 1962, Bentonite deposits of the northern Black Hills district, Wyoming, Montana, and South Dakota: U.S. Geol. Survey Bull. 1082-M, p. 893-1027.
- Lyons, J. B., 1944, Igneous rocks of the northern Big Belt Range, Montana: Geol. Soc. America Bull., v. 55, p. 445-472.
- Mapel, W. J., Robinson, C. S., and Theobald, P. K., 1959, Geologic and structure contour map of the northern and western flanks of the Black Hills, Wyoming, Montana, and South Dakota: U.S. Geol. Survey Map OM-191.
- Pierce, W. G., 1963, Cathedral Cliffs Formation, the Early Acid Breccia Unit of northwestern Wyoming: Geol. Soc. America Bull., v. 74, no. 1, p. 9-22.
- Richards, P. W., 1955, Geology of the Bighorn Canyon-Hardin area, Montana and Wyoming: U.S. Geol. Survey Bull. 1026, 93 p.
- 1957, Geology of the area east and southeast of Livingston, Park County, Montana: U.S. Geol. Survey Bull. 1021-L, p. 385-438.
- Roberts, A. E., 1957, Coal-bearing rocks and mines at Cokedale, Park County, Mont., in Billings Geol. Soc. Guidebook 8th Ann. Field Conf., Crazy Mountain Basin, Montana, 1957: p. 39-47.
- 1963, The Livingston Group of south-central Montana: Art. 22 in U.S. Geol. Survey Prof. Paper 475-B, p. B86-B92.
- 1964a, Geologic map of the Brisbin quadrangle, Montana: U.S. Geol. Survey Geol. Quad. Map GQ-256.
- 1964b, Geologic map of the Chimney Rock quadrangle, Montana: U.S. Geol. Survey Geol. Quad. Map GQ-257.

- Roberts, A. E., 1964c, Geologic map of the Hoppers quadrangle, Montana: U.S. Geol. Survey Geol. Quad. Map GQ-258.
- 1964d, Geologic map of the Livingston quadrangle, Montana: U.S. Geol. Survey Geol. Quad. Map GQ-259.
- 1964e, Geologic map of the Maxey Ridge quadrangle, Montana: U.S. Geol. Survey Misc. Geol. Inv. Map I-396.
- 1964f, Geologic map of the Fort Ellis quadrangle, Montana: U.S. Geol. Survey Misc. Geol. Inv. Map I-397.
- 1964g, Geologic map of the Mystic Lake quadrangle, Montana: U.S. Geol. Survey Misc. Geol. Inv. Map I-398.
- 1964h, Geologic map of the Bozeman Pass quadrangle, Montana: U.S. Geol. Survey Misc. Geol. Inv. Map I-399.
- Robinson, C. S., Mapel, W. J., and Cobban, W. A., 1959, Pierre Shale along western and northern flanks of Black Hills, Wyoming and Montana: Am. Assoc. Petroleum Geologists Bull., v. 43, no. 1, p. 101-123.
- Schmidt, R. G., and Zubovic, Peter, 1961, Cobern Mountain overthrust, Lewis and Clark County, Montana: Art. 211 in U.S. Geol. Survey Prof. Paper 424-C, p. C175-C177.
- Simpson, G. G., 1937, The Fort Union of the Crazy Mountain field, Montana and its mammalian faunas: U.S. Natl. Mus. Bull. 169, 287 p.
- Spivey, R. C., 1940, Bentonite in southwestern South Dakota: South Dakota Geol. Survey Rept. Inv. 36, 56 p.
- Weed, W. H., 1893, The Laramie and the overlying Livingston Formation in Montana: U.S. Geol. Survey Bull. 105, 68 p.
- Wood, H. E., 2d, and others, 1941, Nomenclature and correlation of the North American continental Tertiary: Geol. Soc. America Bull., v. 52, no. 1, p. 1-48.
- Zapp, A. D., and Cobban, W. A., 1960, Some late Cretaceous strand lines in northwestern Colorado and northeastern Utah: Art 112 in U.S. Geol. Survey Prof. Paper 400-B, p. B246-B249.



AN UPPER CRETACEOUS DEPOSIT IN THE APPALACHIAN MOUNTAINS

By ROBERT H. TSCHUDY, Denver, Colo.

Abstract.—Samples of a black sandy clay from the Appalachian Mountains region near Chambersburg, Pa., yielded a suite of Late Cretaceous pollen and spores. Evidence from known stratigraphic ranges of some forms and from the number and percentage of triporate pollen found indicates an extreme age range extending from early Turonian through middle Campanian, with a probable age for the deposit of late Turonian through early Campanian. The discovery is approximately 80 miles west of the nearest known Upper Cretaceous outcrop.

Preliminary palynological examination of a sample of black sandy clay submitted by K. L. Pierce from the vicinity of Chambersburg, Pa., indicated a Late Cretaceous age. The discovery, approximately 80 miles west of the nearest known Upper Cretaceous outcrop, necessitated further confirmation. R. M. Kosanke, of the U.S. Geological Survey, obtained six additional samples from separate parts of the original mine dump. All the samples provided by Kosanke yielded pollen and spore assemblages almost identical in composition with the assemblage in the original sample and with each other.

The dominant element of the spore and pollen flora is bisaccate coniferous pollen with probable podocarpaceous affinities. Secondary elements are monosulcate, probably araucarian pollen; and fern spores including representatives of the genera *Cicatricosisporites* and *Appendicisporites*. Angiosperm pollen of the tricolpate and tricolporate types is common, and triporate pollen is rare.

The palynological taxa discussed in this account are a small part of the complete assemblage. Thorough taxonomic treatment would involve description of some new taxa and emendation of others; the complete assemblage of more than 60 different palynomorphs will be the subject of a taxonomic paper at a later date.

SOURCE OF MATERIAL

All samples were obtained from an old mine dump, referred to hereafter as the Pond Bank deposit. The samples were uniform in appearance and consisted of a black, organic sandy clay. Lignite from the original mine could not be obtained. The mine shaft is located

8 miles southeast of Chambersburg, Pa., 1,250 feet north of lat 39°52'30" N. and 11,150 feet west of long 77°30' W. On the Scotland 7½ minute quadrangle, Pennsylvania, the location is 2,600 feet S. 37° W. of the lookout tower on Little Mountain. It is on the east side of the Greenwood–Mount Alto road, between the junction of the English Valley road and the Pennsylvania Railroad crossing, and is 1.6 miles south of Greenwood and U.S. Route 30.

METHODS

The exterior of large consolidated pieces of the samples was removed to lessen the possibility of contamination by recent pollen. The material was then broken up and treated with 10-percent potassium hydroxide, followed by heavy-liquid flotation with zinc bromide. No modern contaminants were observed in any of the preparations.

STRATIGRAPHIC DISTRIBUTION OF FOSSILS

Some of the more significant plant microfossils found in the Pond Bank material are shown on figure 1. The forms figured provide the principal basis for the age determination. The knowledge of the known stratigraphic ranges of some of the forms discussed below has been supplemented by unpublished data accumulated in the U.S. Geological Survey palynological laboratory at the Denver Federal Center.

Appendicisporites (fig. 1, *a*) has not been reported from any post-Cretaceous rocks in the United States. It is, however, commonly present in both the Upper and Lower Cretaceous (Barremian according to Brenner, 1963; Coniacian–Maestrichtian according to unpublished U.S. Geological Survey data). Although Weyland and Krieger (1953) state that this form genus is known only from the Late Cretaceous, Couper (1958) reports it from the Wealden (Early Cretaceous), and Lantz (1958) from the Purbeckian (Late Jurassic).

Somewhat similar spores belonging to the genus *Cicatricosisporites* occur in both the Cretaceous and Tertiary. The species shown on figure 1, *b* is *Cicatricosisporites* cf. *C. subrotundus* Brenner 1963. The only

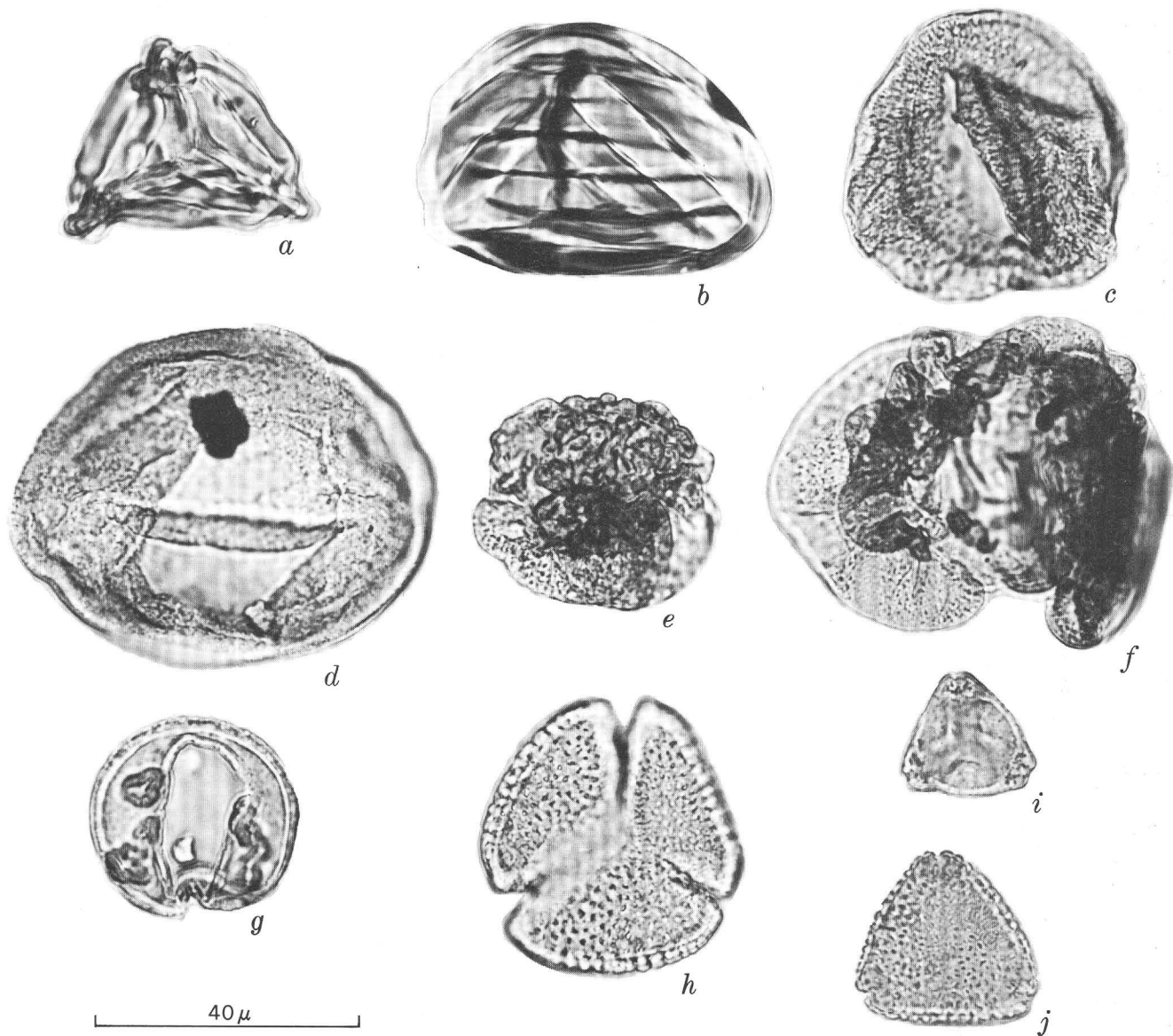


FIGURE 1.—Some of the more significant types of pollen and spores found in the Pond Bank deposit. Magnification $\times 1,000$. a, *Appendicisporites*; b, *Cicatricosisporites*; c, *Parvisaccites*; d, *Araucariacites*; e and f, *Rugubivesiculites*; g, *Granubivesiculites?*; h, Tricolporate pollen (*Rhoipites* sp.); i, *Plicapollis* sp., and j, *Proteacidites*.

previously recorded occurrence of this species is from the upper part of the Patapsco Formation (Albian) of Maryland.

The genus *Parvisaccites*, represented by figure 1, c, is a coniferous pollen type which is common in the Pond Bank deposit. This genus was originally described by Couper (1958) from the "Wealden and Aptian" of Britain. A similar form *Dacrydiumpollenites* was reported from the Tuscaloosa Formation (Groot and others, 1961). Leopold and Pakiser (1964) report *Parvisaccites* from the Gordo and McShan Formations (Cenomanian to Coniacian) in Alabama; Brenner (1963) found it in almost every polleniferous sample from the Potomac Group in Maryland; and I have seen it in the Magothy Formation (Coniacian) in Maryland, the

Ripley Formation (Campanian to Maestrichtian) in Kentucky and Tennessee, in the Clayton Formation (Paleocene) in Kentucky and Tennessee, but not above the Clayton. Thus the range of this pollen type in the eastern United States extends from the Lower Cretaceous into the Paleocene.

Araucariacites, represented by figure 1, d, is limited to the Cretaceous within the Mississippi embayment region. East of the Mississippi embayment, Brenner (1963) found this genus in the Arundel and Patuxent Formations (Barremian to Aptian) but in greater abundance in the Patapsco Formation (Albian according to Brenner). Leopold and Pakiser (1964) have found it in the Tuscaloosa Group (Cenomanian to Turonian) and in the McShan and Eutaw Formations of Alabama

(Turonian to Coniacian). I have found it in the Coffee Sand and in the Ripley and Owl Creek Formations but not above them. In the eastern United States this genus seems to be limited to the Cretaceous.

Figure 1, *e* and *f*, shows bisaccate pollen with rugulate crests of the *Podocarpus* type. The form genus is *Rugubivesiculites*. This genus has been reported from the following Cretaceous units in the United States: The Dakota Sandstone of Minnesota (Pierce, 1961); the Tuscaloosa and Magothy Formations of the Eastern United States (Groot and others, 1961); the Tuscaloosa Group and Eutaw and McShan Formations of Alabama (Leopold and Pakiser, 1964); the Frontier Formation of Wyoming;¹ and the Eagle Ford Shale of eastern Texas (Brown and Pierce, 1962). The genus occurs in samples from the type locality of the Magothy Formation of Maryland, and from the Ripley Formation of Tennessee. In Tennessee and Kentucky this form is present in the Upper Cretaceous, but it has not been found in the overlying Tertiary.

The distinctive monosulcate group with small vesicles, *Granabivesiculites?* (fig. 1, *g*), has been reported heretofore only by Pierce (1961) from the Dakota Sandstone (Cenomanian-Coniacian? according to Pierce) of Minnesota. Pierce erected three generic names for this group: *Granabivesiculites*, *Bacubivesiculites*, and *Clavabivesiculites*. The swellings or small vesicles at each side of the sulcus suggest affinity to the conifers with more fully developed bladders. This fossil type is rare in the Ripley Formation of Tennessee and Kentucky. In the Pond Bank material it is one of the common genera; at least three distinct species are recognizable.

The most common angiosperm pollen type in the Pond Bank material is represented by figure 1, *h* (*Rhoipites* sp.). It is a tricolporate pollen with a well-developed coarse reticulum. A form which is similar, if not identical, is common in the Magothy Formation at its type locality in Maryland. The same species occurs rarely in the Ripley Formation of the Mississippi embayment region. This form has not been observed above the Cretaceous.

The triporate pollen species with endoplicae (*Plicapollis* sp.) shown on figure 1, *i* has not been reported previously from the United States. It is present in preparations from the type locality of the Magothy Formation and in both Upper Cretaceous and lower Tertiary rocks of the Mississippi embayment region.

The triporate genus *Proteacidites* (fig. 1, *j*) is a numerically minor constituent of the Pond Bank assemblage. *Proteacidites* in the United States has been found in the Upper Cretaceous and Eocene rocks but not

in the Paleocene. It has not previously been reported from any Cretaceous localities in the Eastern United States, but I have found it in the Ripley Formation in Kentucky and in the Cusseta Sand of Alabama. The range of the genus *Proteacidites* is based on too few occurrences to ascribe a post-Santonian age to the Pond Bank pollen and spore flora with confidence.

The evolutionary stage in the diversification of angiosperm taxa provides a second line of evidence bearing on the age of the Pond Bank deposit. It is well known that rapid diversification of the pollen of angiosperms is characteristic of the Late Cretaceous. Among angiospermous pollen types the triporates are probably of the greatest stratigraphic significance (Groot and others, 1961; Pflug, 1953). The number and percentage of triporate pollen species present in a sample provide a clue to the approximate stratigraphic position of the sample in the Upper Cretaceous sequence. Unfortunately, palynological data for the Eastern United States are very limited, and no early Campanian or Santonian data are available.

The number of triporate species present in a sample ranges from zero in the Albian (Brenner, 1963) and Cenomanian (Pierce, 1961) to at least 50 in the Ripley Formation of late Campanian to early Maestrichtian age.

In the accompanying table, I have listed the number of triporate taxa found in Upper Cretaceous samples from the Eastern United States, and have shown the relation of triporates to the total pollen and spore assemblage, expressed as percentages. Both the number and percentage of triporates in a sample decrease with the age of the sample.

In the Pond Bank material, triporate pollen is rare, amounting to less than 0.5 percent of the total plant microfossils present. Only 6 species, including normal-pollen types of Pflug, were found in the entire assemblage. This paucity of triporate pollen certainly eliminates the Maestrichtian and late Campanian from consideration and suggests an age considerable older (see table).

AGE

Figure 2 charts the stratigraphic ranges, in the Eastern United States, of some of the genera and groups found in the Pond Bank material. The presence of angiosperm pollen indicates an age no older than Albian (late Early Cretaceous). No unequivocally angiosperm pollen has been reported from pre-Albian rocks anywhere in the world. The presence of the gymnosperm genera *Rugubivesiculites*, *Araucariacites*, and *Granabivesiculites*, and of the pteridophyte genus *Appendicisporites*, dates this deposit as older than Tertiary. The

¹ C. F. Upshaw, 1959, Palynology of the Frontier Formation, northwestern Wind River Basin, Wyoming: Missouri Univ. thesis.

presence of triporate pollen indicates an age no older than Turonian.

Reported occurrence of triporate species

[Formations arranged in order of increasing age from top to bottom]

Authority	Formation or deposit	Number of triporate taxa	Percentage of triporate taxa in assemblage
U.S. Geological Survey, unpublished data.	Ripley	50	26
Groot and others (1961).	Magothy	12	22
Leopold and Pakiser (1964).	McShan and Eutaw.	17	23
Do	Coker and Gordo	17	17.5
Groot and others (1961).	Tuscaloosa, Atlantic Coastal Plain.	8	20
Do	Raritan	4	12.5
Do	Tuscaloosa, Alabama.	1	4
Pierce (1961)	Dakota	0	0
Brenner (1963)	Patapsco	0	0
This report	Pond Bank deposit.	6	10

The paucity of triporate angiosperm pollen in both numbers and species contrasts sharply with the diversity and abundance of triporate angiosperm pollen in the Ripley Formation (late Campanian and early Maestrichtian). This indicates that the Pond Bank material is older than late Campanian. The extreme age limits of the Pond Bank material must then be early Turonian and middle Campanian.

The evidence from the number of triporate pollen taxa found suggests a probable Turonian to Coniacian age, which, in the absence of data from the Santonian, must remain under consideration. The evidence from the genus *Proteacidites* is contradictory. In the Eastern United States this genus is not known from below the Cusseta Sand (Campanian). I believe, however, that further work will reveal its presence in older Cretaceous strata in this region.

The evidence presented by the genus *Proteacidites*, indicating a Campanian or younger age, is contradicted by the abundance and variety of the *Granabivesiculites* group, which suggest a Cenomanian to Coniacian age. Although the *Granabivesiculites* group ranges from Cenomanian through Maestrichtian, its occurrence is very rare above the Coniacian.

The composition of the Pond Bank pollen and spore flora as a whole most closely resembles the flora seen in samples from the Magothy Formation and the Eutaw and McShan Formations.

The known ranges of the palynomorphs discussed, the early evolutionary stage represented by the triporate angiosperm assemblage, and the similarity of the assemblage as a whole to Eutaw and Magothy assemblages, rather than to younger or older assemblages, leads me to place the Pond Bank material in the interval represented by the late Turonian through early Campanian.

REFERENCES

Brenner, G. J., 1963, The spores and pollen of the Potomac Group of Maryland: Maryland Dept. Geology, Mines, and Water Resources Bull. 27, p. 1-215.
 Brown, C. W., and Pierce, R. L., 1962, Palynologic correlations in Cretaceous Eagle Ford Group, northwest Texas: Am. Assoc. Petroleum Geologists Bull. v. 46, no. 12, p. 2133-2147.
 Couper, R. A., 1958, British Mesozoic microspores and pollen grains: Palaeontographica, Abt. B., v. 103, p. 75-179.
 Groot, J. J., Penny, J. S., and Groot, C. R., 1961, Plant microfossils and age of the Raritan, Tuscaloosa, and Magothy Formations of the Eastern United States: Palaeontographica, Abt. B., v. 108, p. 121-140.

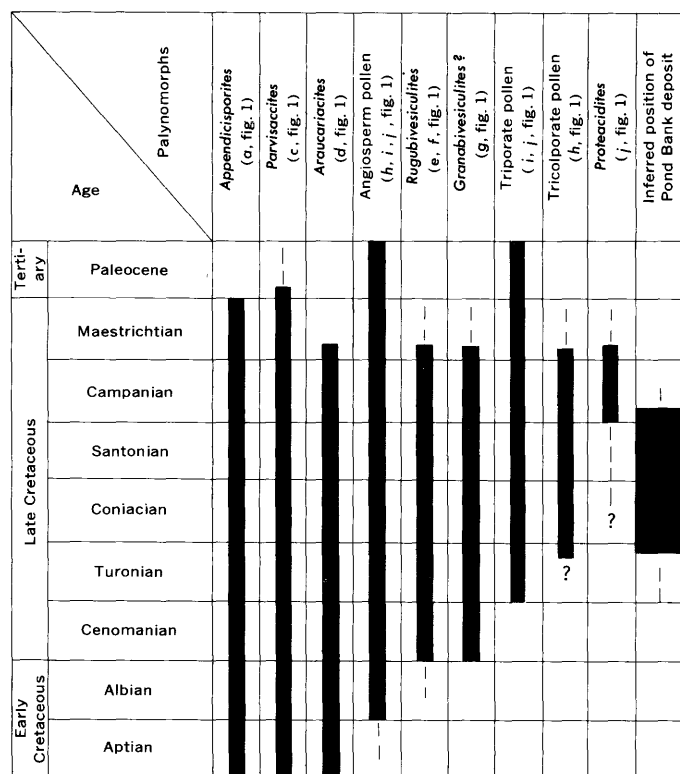


FIGURE 2.—Ranges in the Eastern United States of some Pond Bank palynomorphs. Dashed lines indicate possible but unproved age ranges.

- Lantz, Josette, 1958, Étude des spores et pollens d'un échantillon Purbeckien de l'Île d'Oleron : *Revue de Micropaleontologie*, v. 1, no. 1, p. 33-37.
- Leopold, E. B., and Pakiser, H. M., 1964, A preliminary report on the pollen and spores of the pre-Selma Upper Cretaceous strata of western Alabama : U.S. Geol. Survey Bull. 1160-E, p. 71-95.
- Pierce, R. L., 1961, Lower Upper Cretaceous plant microfossils from Minnesota : *Minnesota Geol. Survey Bull.* 42.
- Pflug, H. D., 1953, Zur Entstehung und Entwicklung des Angiospermiden Pollens in der Erdgeschichte : *Palaeontographica*, Abt. B., v. 95, p. 60-171.
- Weyland, Hermann, and Krieger, Wilhelm, 1953, Die Sporen und Pollen der Aachener Kreide und ihre Bedeutung für die Charakterisierung des mittleren Senons : *Palaeontographica*, Abt. B., v. 95, p. 6-29.



CLASSIFICATION OF THE SUPERFAMILY HEALDIACEA AND THE GENUS *PSEUDOPHANASYMMETRIA* SOHN AND BERDAN, 1952 (OSTRACODA)

By I. G. SOHN, Washington, D.C.

Abstract.—The shape of the carapace, the muscle-scar pattern, and the inferred nature of the soft parts of the fossil superfamily Healdiacea suggest that it does not belong to the suborders Platycopina and Metacopina but should be referred to the order Podocopida. On the basis of muscle-scar pattern the genus *Pseudophanasymmetria* is assigned to the superfamily Healdiacea. The diagnosis of this genus is emended to include dimorphism, and *Pseudophanasymmetria? afoveata* is considered a dimorphic form of *P. foveata*.

Living ostracodes are identified in part by the structure of the valves that completely enclose the soft parts, but mostly on detailed study of the appendages. Fossil ostracodes are classified solely on the morphology of the valves. With few exceptions, extinct genera and families are readily distinguished by study of the shell structures; however, the ordinal classification of fossil groups and its incorporation in the scheme for living forms is difficult. This paper discusses some criteria deduced from fossil ostracode shells that aid in the neontological classification of the Healdiacea.

PREVIOUS WORK AND CONCLUSIONS

The superfamily Healdiacea was established by Mandelstam (*in* Chernysheva, 1960, p. 337) in the Russian treatise on ostracoda to include the families Healdiidae Harlton, 1933, Darwinulidae Brady and Norman, 1889, and Scrobiculidae Posner, 1951. This superfamily was originally classified in the suborder Podocopina Sars, 1866, order Podocopida Müller, 1894. Dimorphism was excluded in the description of the superfamily, and the stratigraphic range was given as Silurian to Recent. Shaver (*in* Moore, 1961, p. Q359) assigned to the Healdiacea the families Healdiidae, Bairdiocyprididae Shaver, *in* Moore, 1961, ?Barychilinidae Ulrich, 1894, ?Cavellinidae Egorov, 1950, ?Krausellidae Berdan *in* Moore, 1961, and Pachydomellidae Berdan and Sohn *in* Moore, 1961. The American "Treatise on Invertebrate Paleontology" (Moore, 1961) classified this super-

family in the suborder Metacopina Sylvester-Bradley *in* Moore, 1961, order Podocopida Müller, 1894. Dimorphism was not mentioned in the description of the superfamily. Moderate sexual dimorphism was, however, inferred for most of the genera in the family Healdiidae. The stratigraphic range was given as Devonian to Lower Cretaceous.

The Late Cretaceous (Maestrichtian) genus *Pseudophanasymmetria* Sohn and Berdan, 1952 (type species *Phanassymmetria foveata* van Veen, 1936) was originally assigned to the Bairdiidae? (Sohn and Berdan, 1952, p. 10). Later (Moore, 1961, p. Q208), the genus was referred to the Bairdiacea, family uncertain, and Coryell (1963, p. 68, 1120) referred to this genus as "Uncertain, probably Macrocyprididae."

Current studies on the relationship of post-Paleozoic ostracodes with their Paleozoic ancestors indicate that *Pseudophanasymmetria* might more properly be referred to the Healdiacea, and that the superfamily Healdiacea should not be referred to the suborders Metacopina or Platycopina.

Gründel (1964) described the Early Jurassic family Pseudohealdiidae for healdiids with a reduced number of individual scars in the adductor muscle-scar complex. According to his diagnosis, members of Pseudohealdiidae have seven or fewer relatively large oval scars that may be surrounded by additional smaller scars. Working with Early Jurassic specimens, he traced the reduction in the number of individual scars from aggregate numerous scars in *Ogmoconcha* through seven scars of what he called a cytherellid shape in *Pseudohealdia* (*Ledahia*) Gründel, 1964, to five scars of a darwinulid shape in *Pseudohealdia* (*Pseudohealdia*) Gründel, 1964, (fig. 1) and concluded that Healdiacea properly belongs in the Platycopina. Van Morkhoven (1962, p. 104) suggested a similar classification for the Healdiacea. Triebel had earlier (1950, p. 114–118) referred the family Healdiidae to the suborder Platycopina.

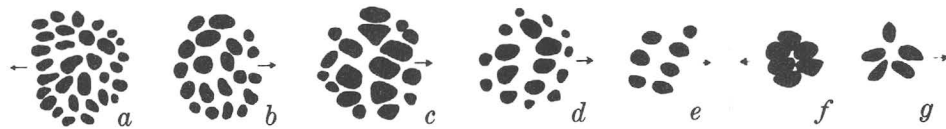


FIGURE 1.—Muscle-scar pattern of several representatives of Healdiacea. Illustrated is a morphologic transitional series from healdiid through cytherellid to darwinulid muscle scar (not to scale). *a*, *Healdia* sp. (after Triebel, 1941, pl. 5, fig. 50), Pennsylvanian; *b*, *Ogmoconcha contractula* Triebel (after Triebel, 1941, pl. 14, fig. 160), Lias; *c*, *Ogmoconcha* sp. Lias; *d*, *Ogmoconchella aspinata* (Drexler, 1958), Lias; *e*, *Pseudohealdia* (*Ledahia*) *septenaria* h, sp. Lias; *f*, *Pseudohealdia* (*Pseudohealdia*) *pseudohealdiae* n. sp., Lias; *g*, *Pseudohealdia* (*Pseudohealdia*) *nasuta* (Drexler, 1958) (after Drexler, 1958, pl. 25, fig. 11), Lias. From Gründel, 1964, p. 465, fig. 6.

Gründel (1964) illustrated a transitional series of adductor muscle scars from typical healdiid through cytherellid to darwinulid, all based on specimens from the Liassic. This does not demonstrate a phylogenetic sequence; it merely suggests a group of pre-Liassic ancestors. This sequence is pertinent to the present discussion because of the similarity of the muscle-scar pattern of *Pseudohealdia* (*Ledahia*) (fig. 1, *e*) to the muscle-scar pattern of *Pseudophanasymmetria* (fig. 2, *b*), suggesting the probable superfamily classification of the latter genus.

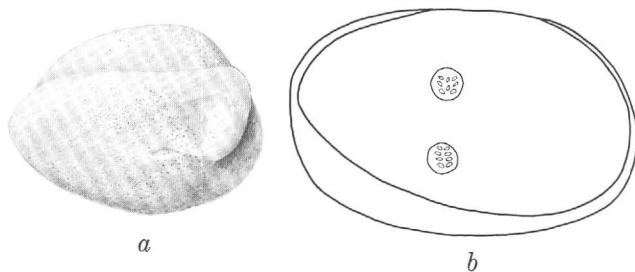


FIGURE 2.—*Pseudophanasymmetria foveata* (van Veen, 1936). *a*, complete carapace, dorsal view, approximately $\times 70$. Maestrichtian, South Limburg, the Netherlands, paratype, USNM 108231. *b*, complete carapace of *Pseudophanasymmetria*? *afoveata* (van Veen, 1936), lateral view of right side, camera-lucida drawing from radiograph, approximately $\times 113$. The specimen was tilted when posed for radiograph so that the muscle-scar patterns of both valves are shown. The upper pattern is probably of the right valve, the lower of the left valve. Mestrichtian, South Limburg, the Netherlands, paratype, USNM 108232. From Sohn and Berdan, 1952, text figs. 3, 5.

The removal of the Healdiacea from the suborder Metacopina is reasonable, but classifying the Healdiacea in the Platycopina (Platycopida Sars of Sohn, 1961, p. 109) raises several objections. The muscle-scar pattern of the Healdiacea consists of an adductor complex (central muscle scars of van Morkhoven, 1962, p. 47) and one or more accessory scars (frontal scars of van Morkhoven, 1962, p. 48). Frontal scars have not been recorded in the Platycopina. The Platycopina are of approximately equal height at the ends in lateral outline, presumably to accommodate the well-developed terminal

end with its platy furca in the posterior and the stubby biramous second antenna in the anterior portion. Healdiids usually have unequal ends with a lower posterior portion. This suggests a rudimentary styliiform furca, like that of the Podocopida, or longer frontal appendages. I indicated the importance of the type of furca and frontal appendages (second antenna) in the ordinal classification of living Ostracoda (Sohn, 1961, p. 109), but did not emphasize the fact that these terminal appendages are probably some of the more phylogenetically stable features of the group. The Healdiacea usually have spines or vertical ridges near the posterior; the Platycopina do not have such structures. The Platycopina may have marginal rims (*Cytherelloidea*); the Healdiacea do not. The overlap of the Platycopina is right valve over left; that of the Healdiacea is left valve over right.

Hartmann's suggestion (1963, p. 23 and following) that the Platycopina, in which he includes the Metacopina, are ancestral to the modern Podocopida, and that divergence must have occurred during or before the Ordovician, may be partly correct. *Sansabella* Roundy, 1926 (Palaeocopida, Kloedenellocopina *vide* Moore, 1961, p. Q187) and an undescribed marine Middle Triassic genus (Sohn, 1963, p. C58) have an aggregate muscle-scar pattern of the healdiid type (fig. 1, *b*) that resembles the muscle scar of the Devonian species of *Quasillites* (Moore, 1961, p. Q379, text fig. 298, fig. 2). *Quasillites* Coryell and Malkin, 1936 (Quasillitacea, Metacopina *vide* Moore, 1961, p. Q374) has a tripartite hinge and a ventrally truncated posterior, both characteristic of the Podocopida.

The Healdiacea may be considered as an independent lineage, starting in or before the Devonian and extending to at least the Late Cretaceous. For the reasons enumerated above, the Healdiacea should be considered as distinct from the Platycopida.

On the basis of these considerations the classification below is suggested for the Healdiacea and the genus *Pseudophanasymmetria*.

**SUGGESTED CLASSIFICATION FOR THE HEALDIACEA
AND THE GENUS PSEUDOPHANASYMMETRIA**

Order Podocopida Sars, 1865

The reference of the order Podocopida to Müller, 1894, stems from the fact that both the Russian treatise (Chernysheva, 1960) and the American treatise (Moore, 1961) followed Pokorný (1953, p. 221, 231) in classifying the suborders Podocopa Sars, 1865, and Platycopa Sars, 1865, in the order Podocopida. I have discussed this classification (Sohn, 1961, p. 109) and pointed out that because of the marked differences in the structure of the appendages and body of the two groups, they should both be given ordinal status.

The reason that Müller, 1894, is credited with the combined taxon is that he used the Tribe Podocopa to include Sars' two suborders (Müller, 1894, p. 202). Although Sars (1865) is usually listed under the year 1866, I follow Sars (1922, p. 2, 1928, p. VIII) who recorded the publication as 1865. The fact that this publication is included in the Zoological Record for the year 1865 is additional evidence that the paper was published in 1865.

Suborder unknown

As stated above, the superfamily Healdiacea has been classified in the suborder Podocopina (Mandelstam, *in* Chernysheva, 1960), in the suborder Metacopina (Shaver, *in* Moore, 1961), and also in the suborder Platycopina (van Morkhoven, 1962, and Gründel, 1964). The reasons for removing this superfamily from the Metacopina and the Platycopina were previously discussed. The muscle-scar pattern of the Healdiacea differs radically from the patterns known in the other superfamilies in the suborder Podocopina, except possibly that of Darwinulacea. Darwinulidae was in fact included in the Healdiacea (Mandelstam, *in* Chernysheva, 1960, p. 337). Pending additional information it is considered best to leave the subordinal classification of the superfamily in doubt.

**Superfamily Healdiacea Harlton, 1933, emend.
Gründel, 1964**

The original definition of the Healdiacea should be modified to include dimorphic forms and to exclude the families Darwinulidae and Scrobiculidae. Swain (*in* Moore, 1961, p. Q253) established the superfamily Darwinulacea for this fresh- and brackish-water family. The family Scrobiculidae was questionably assigned to the superfamily Kirkbyacea by Moore (1961, p. Q168), although Sohn (*in* Moore, 1961, note under Placideidae) disagreed with that assignment. This family differs from the Healdiacea in that the genera referred to it

are reticulate or punctate and have equal ends in lateral outline.

Family unknown

Pseudophanasymmetria does not fit into Gründel's family Pseudohealdiidae because of the 8 muscle scars in the adductor muscle-scar pattern, the greater asymmetry of the valves, and the simple hinge. The genus does not belong to the Krausellidae (Healdiacea?, Metacopina *vide* Moore, 1961, p. Q371) because the posterior end of neither valve is produced as a spine. It is excluded from the Macrocyprididae (Bairdiacea, Podocopina, Podocopida) by the presence of a straight dorsal margin, absence of duplicature, and different muscle-scar pattern. The description of a new family for this genus is deferred until more information becomes available.

Genus *Pseudophanasymmetria* Sohn and Berdan, 1952

Pseudophanasymmetria Sohn and Berdan, 1952, Wash. Acad. Sci. Jour., v. 42, p. 10; Moore, R. C., 1961, Treatise on invertebrate paleontology, p. Q208; Coryell, 1963, Bibliographic index and classification of Mesozoic Ostracoda, p. 68, 153, 1120.

Phanassymetria van Veen, 1936, Natuurhist. Maandblad, Jaarg. 25, no. 11-12, p. 177.

not *Phanassymetria* Roth, 1929, Jour. Paleontology, v. 3, p. 358.

Type species.—By monotypy *Phanassymetria foveata* van Veen, 1936, Upper Cretaceous, The Netherlands.

Diagnosis.—Markedly asymmetrical, minute ostracodes with shells not penetrated by conspicuous large pores. Larger valve overlaps smaller on all margins. Hinge straight, simple, bar-and-groove type. Both dorsal and lateral outlines subovate. Shell surface either smooth or punctate, dimorphism is shown by short curved dorsoposterior ridge subparallel to posterior margin of larger valve extending to approximately the midheight of the valve in one form and absence of this ridge in a second form. Inner lamella not observed, probably absent.

Discussion.—The above diagnosis differs from the original in the recognition of dimorphism. In the original paper Sohn and Berdan referred *Phanassymetria afoveata* van Veen, 1936, to *Pseudophanasymmetria* questionably because of the absence of the curved ridge on the larger valve (fig. 2, *a*). Both species are from the same collection, and it is now apparent that the difference between them is due to a type of dimorphism common to many groups of ostracodes. Van Veen discussed the presence of a minute dorsoposterior spine that is not visible on her illustrations nor on the para-

types available for study. Such spines are common in the Healdiacea.

Stratigraphic range.—Known only from the Maestrichtian of the Netherlands.

***Pseudophanasymmetria foveata* (van Veen, 1936)**

Figure 2, a

Phanassymmetria foveata van Veen, 1936, *Natuurhist. Maandblad*, Jahrg. 25, nos. 11–12, p. 177–178, pl. 10, figs. 16–22.

Phanassymmetria afoveata van Veen, 1936, *idem.*, p. 178, pl. 10, figs. 23–30.

Pseudophanasymmetria foveata (van Veen, 1936). Sohn and Berdan, 1952, *Wash. Acad. Sci., Jour.*, v. 42, p. 10, figs. 2, 4, 5; Moore, 1961, p. Q210, text v. 42, p. 11, figs. 3, 6; Coryell, 1963, *Bibliographic index and classification of Mesozoic Ostracoda*, p. 153, pl. 1, figs. 5–7 (fig. 7 is of *P? afoveata*).

Pseudophanasymmetria? afoveata (van Veen, 1936). Sohn and Berdan, 1952, *Wash. Acad. Sci., Jour.*, v. 42, p. 11, figs. 3, 6; Coryell, 1963, *Bibliographic index and classification of Mesozoic Ostracoda*, p. 153, pl. 1, fig. 7.

Discussion.—Sohn and Berdan (1952, p. 11) speculated that the extreme small size of the specimens, less than 0.5 mm in greatest length, might indicate that these individuals were young growth stages. The suggestion that dimorphism is indicated by the posterodorsal ridge invalidates that speculation, because dimorphism in ostracodes is considered to develop at or close to the adult stage.

Age and geographic distribution.—Known only from the Maestrichtian of the Netherlands.

REFERENCES

- Chernysheva, N. E., ed., 1960, *Osnovy paleontologii; spravochnik dlya paleontologov i geologov SSSR*; v. 8, Arthropoda. Trilobitomorpha and Crustacea: 515 p., 18 pls., 1,318 text figs.
- Coryell, H. N., 1963, *Bibliographic index and classification of the Mesozoic Ostracoda*: Dayton, Ohio, Univ. Dayton Press, 1,175 p., in 2 vols. [40 p. addendum, 9 p. errata (p. 49–57)], 28 pls.
- Drexler, Edith, 1958, *Foraminiferen und Ostracoden aus dem Lias α von Siebeldingen/Pfalz*: *Geol. Jahrb.*, v. 75, p. 475–554, pls. 20–27, 25 figs.
- Gründel, Joachim, 1964, *Zur Gattung Healdia (Ostracoda) und zu einigen verwandten Formen aus dem unteren Jura*: *Staat. Geol. Komm. Deutsch. Demokrat. Republik, Geologie*, Jahrg. 13, Heft 4, Berlin, p. 456–477, 1 pl., 7 text figs.
- Hartmann, Gert, 1963, *Zur Phylogenie und Systematik der Ostracoden*: *Zeitschrift zool. Syst. Evolutionsforschung*, v. 1, nos. 1–2, 154 p., 32 text figs. 2 tables.
- Moore, R. C., ed., 1961, *Treatise on invertebrate paleontology*, pt. Q, Arthropoda, 3. Ostracoda: *Geol. Soc. America and Univ. Kansas Press*, 442 p., 334 figs.
- Morkhoven, F.P.C.M. van, 1962, *Post-Paleozoic Ostracoda, their morphology, taxonomy and economic use*. Elsevier Publishing Co., v. 1, 204 p. illus.
- Müller, G. W., 1894, *Ostracoda; Fauna und flora des Golfes von Neapel*: *Zool. Station zu Neapel Mon.* 21, 404 p., 40 pls.
- Pokorný, Vladimír, 1953, *A contribution to the taxonomy of the Paleozoic ostracods: Czechoslovakia, Ústr. úst. geol., Sborník*, v. 20, Paleont. p. 213–232.
- Sars, G. O., 1865, *Oversigt af Norges marine Ostracoder*: *Norske Vidensk.-acad., Förh.* 1865, 130 p.
- 1922–1928, *An account of the Crustacea of Norway*: v. 9, Ostracoda, p. XII, 1–277, 119 pls.
- Sohn, I. G., 1961, *Revision of some Paleozoic ostracode genera. Aechminella, Amphissites, Kirkbyella and related genera*: *U.S. Geol. Survey Prof. Paper 330-B*, p. 106–160, pls. 7–12 [1962].
- 1963, *Middle Triassic Marine ostracodes in Israel*: *U.S. Geol. Survey Prof. Paper 475-C*, p. C58–C59, 1 text fig.
- Sohn, I. G., and Berdan, J. M., 1952, *Stratigraphic range of the ostracode genus Phanassymmetria Roth*: *Washington Acad. Sci. Jour.*, v. 42, p. 7–12, 6 text figs.
- Triebel, Erich, 1941, *Zur Morphologie und Ökologie der fossilen Ostracoden*: *Senckenbergiana*, v. 23, p. 294–400, 15 pls.
- 1950, *Die taxonomische Stellung des Ostracoden-Gattung Oqmoconcha und der Lectotypus von O. amalthei*: *Senckenbergiana*, v. 31, p. 113–120, 2 pls.



STRATIGRAPHIC DISTRIBUTION OF THE LATE CAMBRIAN MOLLUSK *MATTHEVIA* WALCOTT, 1885

By ELLIS L. YOCHELSON, J. F. McALLISTER, and ANTHONY RESO,¹
Washington, D.C., Menlo Park, Calif., Houston, Tex.

Work done partly in cooperation with the California Division of Mines and Geology

Abstract.—Specimens of *Matthevia*, a genus that has defied precise classification, are widespread in the Western United States. Characteristically they are silicified and may be identified on the outcrop by the presence of two narrow deep cavities in a solid subpyramidal mass. The genus seems to be confined to rocks of Late Cambrian Trempealeau age. In the Funeral Mountains of the Death Valley region, California, and in the Pahrnagat Range of southern Nevada, extensive fieldwork has demonstrated the stratigraphic utility of *Matthevia* in correlating sections of complexly faulted rocks. Except for this fossil, the rock sequences studied are poorly fossiliferous and otherwise difficult to correlate.

The enigmatic fossil *Matthevia* Walcott, 1885, was first described from the Late Cambrian Hoyt Limestone Member of the Theresa Dolomite near Saratoga Springs, N.Y. Specimens consist of a massive subpyramidal moderately narrow calcareous piece, in which are two elongate cavities, separated by a wide internal septum. Most specimens are more than 2 centimeters long. Although Walcott recognized the morphologic peculiarities of this genus, he thought that it had a single-piece shell, and as a matter of convenience he placed it under the "pteropod" gastropods. The type lot was refigured twice more by Walcott, but no additional descriptive work was done. The Hoyt Limestone Member is now conventionally placed in the Trempealeau Stage of the Upper Cambrian and dated by the occurrence of other fossils, particularly trilobites, in the fauna.

In recent years, new occurrences of *Matthevia* have been found outside the type area. Indeed, the genus is now known from such widespread areas in the Western United States that it is assuming the status of a useful guide fossil to the Trempealeau. The rocks

from which it has been collected are mainly unfossiliferous, and without the occurrence of this fossil their sequence would constitute something of a problem in precise age determination and correlation.

All the western specimens are silicified (fig. 1), and they are relatively easy to recognize in the field as they commonly etch out in partial relief from the limestone or dolomite matrix; many are rusty brown when weathered. The majority of the specimens are worn; the occurrence of the two cavities in the fossil provides shell areas particularly susceptible to erosion. A collection will thus provide specimens of several different shapes and sizes. Some specimens may be worn so that only one cavity is preserved; others are worn to a saddle shape, and at one locality a few of the specimens have been so strongly modified that they superficially resemble amphineuran plates like *Priscochiton* Billings. Nevertheless, the effects of this prefossilization modification are immediately obvious and the specimens may be readily identified in the field. In every collection at least one specimen shows a deep narrow cavity within the mass of silica, and commonly there are specimens which show the two characteristic cavities. Although there is a danger of confusing incomplete specimens with small chert nodules, the regular external form of *Matthevia* can be recognized, with a little experience, in even severely worn specimens.

In spite of the extensive wear of many specimens, there are some specimens on which growth lines and relatively delicate details are preserved, indicating that the specimens are virtually complete. The large bulk of specimens, and particularly the better preserved material, suggests an alternative zoological placement to that of the "pteropods." There appear to be subpyramidal masses of two slightly different shapes, though

¹ Staff Research Geologist, Tenneco Oil Co., Box 2511, Houston, Tex.

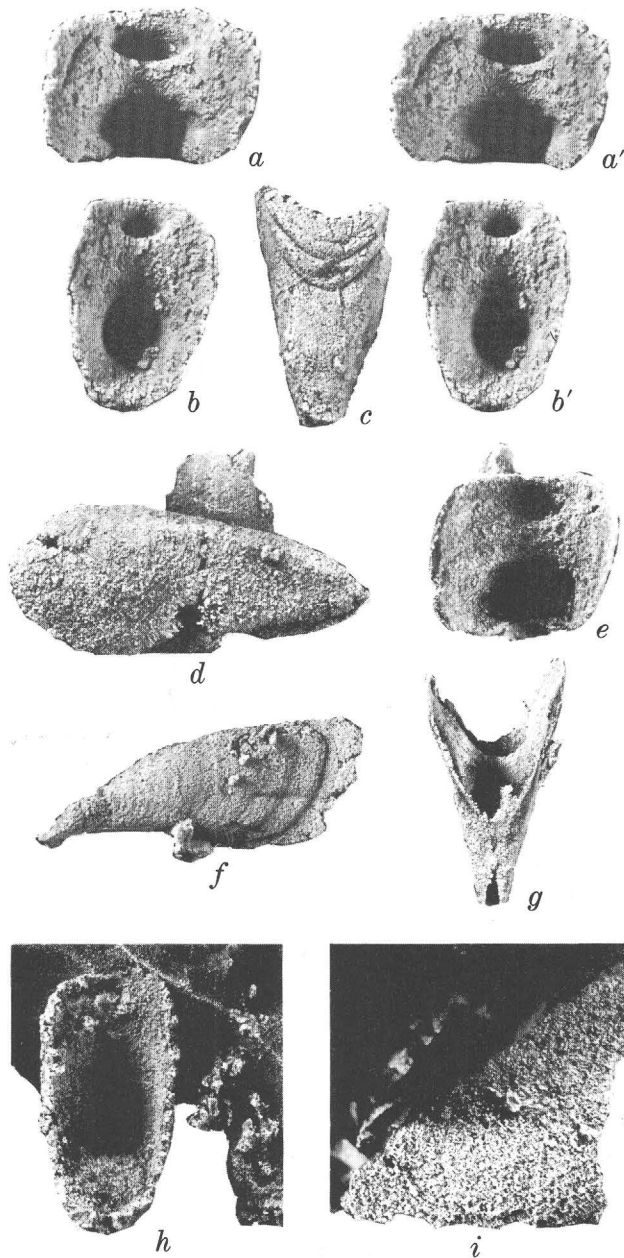


FIGURE 1.—Representative specimens of *Matthevia*: *a-a'*; stereo pair of wide form in end view ($\times 1\frac{1}{2}$), from USGS locality 1734-CO, USNM No. 145312; *b-b'*; stereo pair of narrow form in end view ($\times 1\frac{1}{2}$), from USGS locality 1734-CO, USNM No. 145313; *c*, dorsal view of specimen with well-preserved growth lines ($\times 1\frac{1}{2}$), from USGS locality 3368-CO, USNM No. 145314; *d, e*, side and end views of specimen ($\times 1\frac{1}{2}$) from USGS locality D-1057-CO, USNM No. 145315; *f*, side view of specimen with well-preserved growth lines ($\times 2$), from USGS locality 2073-CO, USNM No. 145316; *g*, ventral view of specimen (natural size) showing the flattened lower surface and the two cavities, from USGS locality D-1057-CO, USNM No. 145317; *h, i*, end and side views of a specimen partially freed from matrix by weathering ($\times 2$), from USGS locality 3815-CO, USNM No. 145318.

these differences are not apparent when one confines examination to specimens partially exposed on the outcrop. It may be that these two parts are the anterior

and posterior of the same animal. The mode of preservation of both calcareous and silicified specimens and the presence of growth lines strongly suggest that *Matthevia* is a mollusk. The morphology of the hard part or parts is not typical of any of the known classes of mollusks, and the genus may be the sole representative of a class that has left no other traces. This matter is discussed in more detail elsewhere (Yochelson, report in preparation).

Regardless of its zoological position, specimens of the genus are of considerable interest as stratigraphic guides. In the Funeral Mountains of the Death Valley region, California (fig. 2), where detailed mapping has been done by McAllister, *Matthevia* occurrences have been instrumental in interpreting some parts of the complex structure. The genus has proved equally useful to Reso in mapping the Upper Cambrian of the Pahranaगत Range, Lincoln County, Nev. (fig. 2) and in correlating the thick sequence of virtually barren Upper Cambrian cherty dolomites within the range and with those in other areas. This genus has been reported and collected from the Upper Cambrian of Texas (Cloud and Barnes, 1948, p. 118). *Matthevia* has also

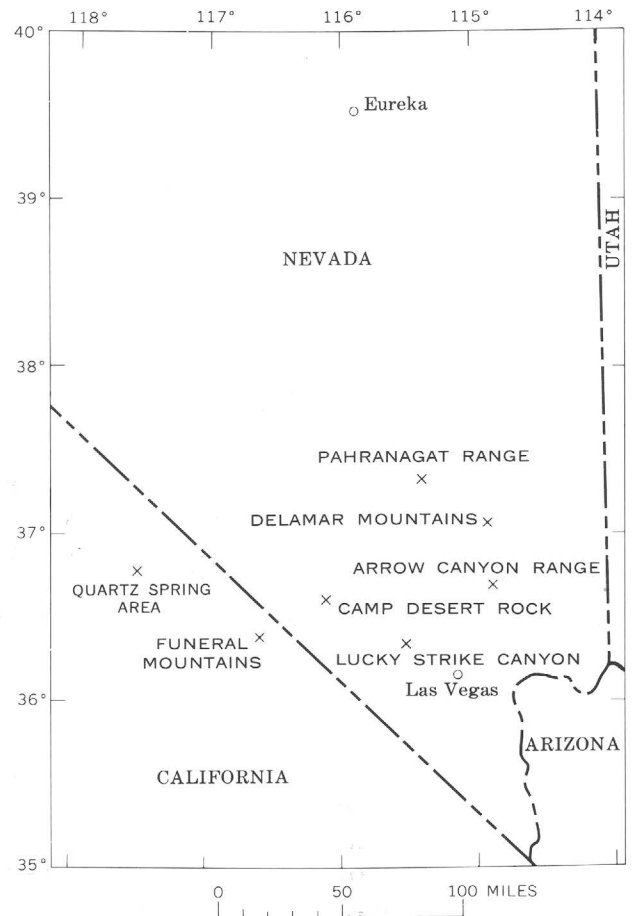


FIGURE 2.—Localities (X) where *Matthevia* or an associated fauna has been collected in Nevada and California.

been collected from the Stansbury Range in Utah; R. A. Robison noted its occurrence in the Notch Peak Limestone of the Paw Paw Mountains of that State (1964, oral communications). Though the occurrences in these last two States are interesting in themselves, more information is available about the far western localities.

OCCURRENCE OF MATTHEVIA IN NEVADA AND CALIFORNIA

In the Funeral Mountains, specimens of *Matthevia* occur in the Upper Cambrian Nopah Formation. Where the formation was measured in a continuously exposed section 1,720 feet thick (fig. 3, locality 1) north of Pyramid Peak, specimens were found only in the 280-foot dark-gray to medium-dark-gray dolomite unit designated n8 (fig. 4), somewhat above the middle of the formation. The measured section of the Nopah extends from the underlying Racetrack Dolomite in the Middle and Upper Cambrian to the base of the Pogonip Group in the Lower Ordovician. The Nopah Formation consists of alternating dark and light units of sporadically chert-bearing dolomite above a conspicuously clastic, fossiliferous unit (fig. 4, n1) at the base.

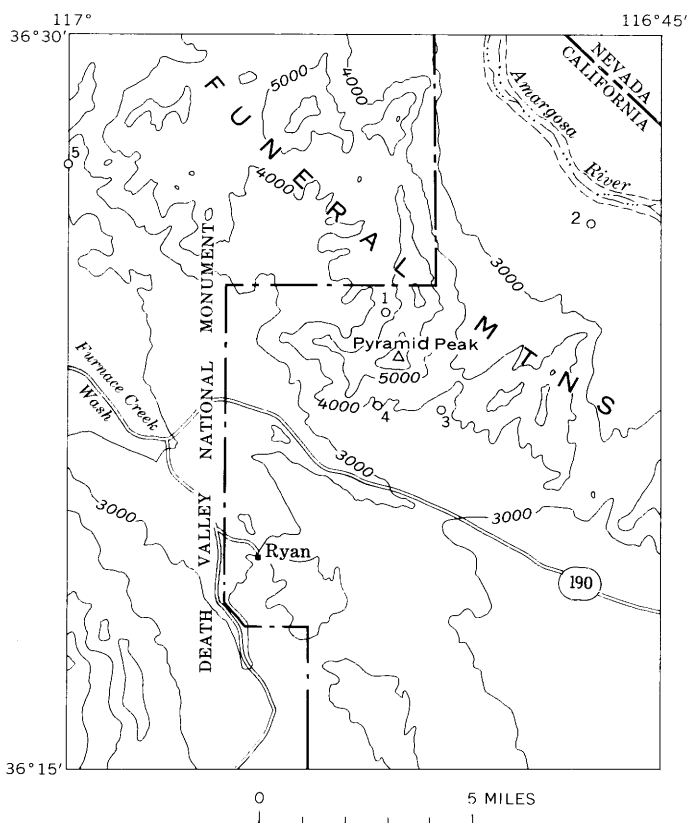


FIGURE 3.—Outline of the Ryan quadrangle, showing localities where *Matthevia* has been collected in the Funeral Mountains, Calif. 1, USGS localities 3814-CO, 3815-CO, 4399-CO, 4400-CO, 4401-CO; 2, 3818-CO, 4402-CO, 4403-CO, 4406-CO; 3, 4453-CO; 4, 4454-CO; and 5, 4455-CO.

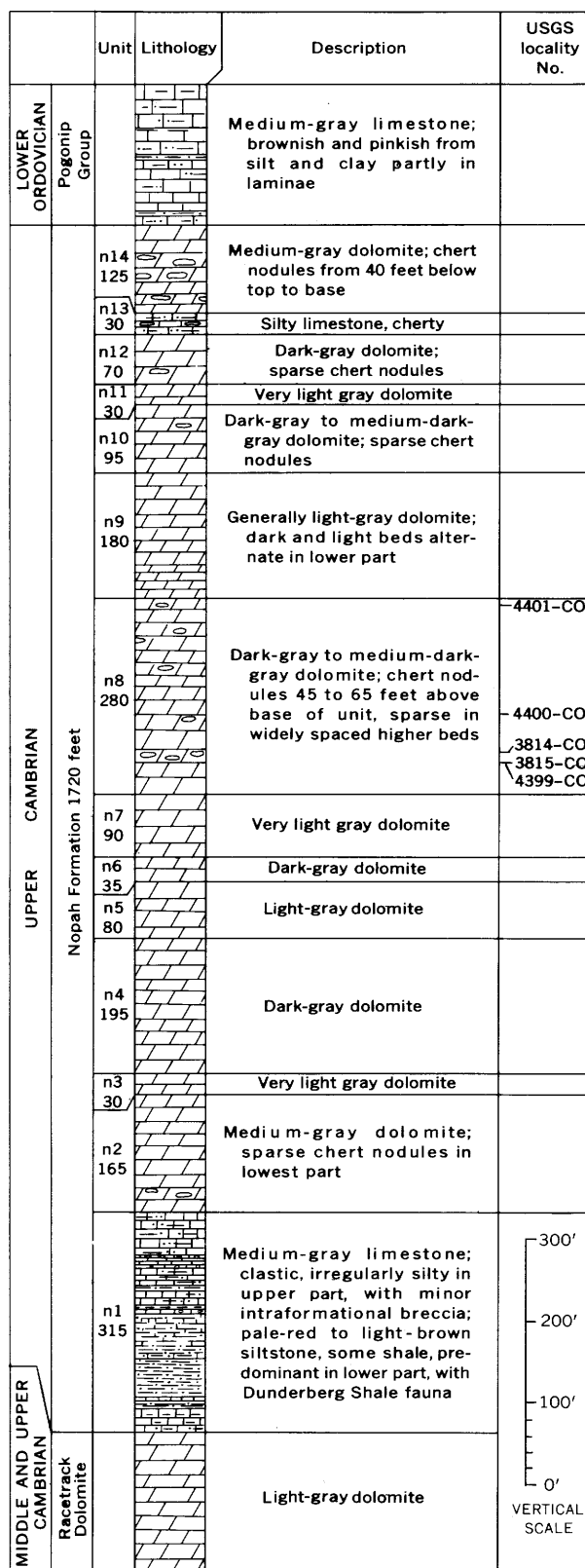


FIGURE 4.—Stratigraphic column of the Nopah Formation in the Funeral Mountains, Calif. Thickness of units (n1 to n14) in feet; distribution of collections containing *Matthevia* indicated by USGS locality numbers.

The sequence of gray dolomite units is interrupted near the top of the formation by a silty limestone unit (fig. 4, n13), lithologically like the Pogonip 125 feet higher. The dark dolomite units where they are isolated by faults or alluvium are difficult to distinguish from each other and from dark units in the underlying 3,700 feet of section. *Matthevia* at several of these places is a key to the stratigraphy and to a better resolution of structure.

The usefulness of *Matthevia* as a guide fossil of the Trempealeau Stage as far west as California is supported by a gastropod fauna associated with it in unit n-8 of the Nopah Formation in the Funeral Mountains and gastropods in a correlative part of the formation in the Quartz Spring area (fig. 2) about 60 miles west-northwest. At localities 1 and 2 (fig. 3) in the Funeral Mountains, the fauna includes *Strepsodiscus* sp., *Scaevogyra* sp., and *Matherella* n. sp., the last two suggesting equivalence to the Potosi and Eminence Dolomites in the Upper Cambrian of Missouri. The gastropod fauna in the Nopah of the Quartz Spring area, which also contains *Strepsodiscus* and *Matherella*, is placed very high in the Upper Cambrian by Josiah Bridge (*in* McAllister, 1952, p. 10) on the basis of his comparison with a fauna in the upper part of the Eminence Dolomite of Missouri and the Hoyt Limestone Member of the Theresa Dolomite of New York. Assignment of unit n8 to the Trempealeau Stage on this basis is in conformance also with the next faunas known below and above. About 800 feet lower in the Nopah, unit n1 contains Upper Cambrian trilobites and brachiopods (identified by A. R. Palmer, written communication, 1963) that occur in the Dunderberg Shale at Eureka, Nev. (Palmer, 1960, p. 56-57). About 710 feet above unit n8 and approximately 180 feet above the top of the Nopah, R. J. Ross, Jr., collected from the Pogonip north of Pyramid Peak a Lower Ordovician fauna that he assigns (written communication, 1963) to zone B of the Garden City Formation in Utah (Ross, 1951, p. 29).

The Pahrnatag Range Upper Cambrian sequence (Reso, 1963, p. 904-905) is generally similar to that of the Funeral Mountains. Beds of Franconian age containing *Billingsella* and beds containing Early Ordovician trilobites about 400 feet above the base of the Pogonip Group are stratigraphically separated by about 2,400 feet of virtually unfossiliferous rocks (fig. 5). Beds containing the Trempealeauan *Matthevia* about 800 feet above the beds with *Billingsella* therefore form an important mapping zone. Here again, the specimens of *Matthevia* are associated with algae and with small gastropods, tentatively identified as *Sinuopea*, another characteristic Late Cambrian form. Moreover, *Matthevia* provides the only current evidence for the

age of the base of the exposed section in the Arrow Canyon Range to the southeast (Langenheim and others, 1962) and for possible correlation of the Arrow Canyon section with sections in the Delamar Mountains (fig. 5). The discrete fault blocks and isolated outcrops in this part of the stratigraphic column emphasize the local importance of the key horizon.

COLLECTION LOCALITIES

The localities at which *Matthevia* has been found are listed below. The specimens listed by permanent locality numbers are cataloged and retained by the U.S. Geological Survey. Three other field occurrences in Nevada are reported by Reso, but specimens either were not collected or are not with the Geological Survey.

California

- 3814-CO-----Nopah Formation, 965-970 feet above base and 55-60 feet above base of unit n-8; 5,500 feet in straight line N. 18° W. from Pyramid Peak, Funeral Mountains, Ryan quadrangle, Inyo County, Calif. Coll. J. F. McAllister, 1962.
- 3815-CO-----Nopah Formation, 955 feet above base and 45 feet above base of unit n-8. Same locality as above. Coll. J. F. McAllister, 1962.
- 3818-CO-----Nopah Formation, isolated hill, 5.5 miles in straight line N. 56° E. from Pyramid Peak, Ryan quadrangle, Inyo County, Calif. Coll. J. F. McAllister, 1962.
- 4399-CO-----Nopah Formation, 950-955 feet above base and 40-45 feet above base of unit n-8; from main zone of *Matthevia*, about 5 feet thick, considered to be the same as 3815-CO; 5,200 feet in straight line N. 19° W. from Pyramid Peak, Funeral Mountains, Ryan quadrangle, Inyo County, Calif. Coll. J. F. McAllister, 1963.
- 4400-CO-----Nopah Formation, about 70 feet stratigraphically above 4399-CO. Same locality as above. Coll. J. F. McAllister, 1963.
- 4401-CO-----Nopah Formation, about 225 feet stratigraphically above 4399-CO. Same locality as 4399-CO. Coll. J. F. McAllister, 1963. (Doubtful occurrence—material poorly preserved.)
- 4402-CO-----Nopah Formation. Same general locality as 3818-CO. West side of hill up to low crest at south end. Coll. J. F. McAllister, 1963.
- 4403-CO-----Nopah Formation. Same general locality as 3818-CO. East side of hill, 125 to 175 feet from south end. Coll. J. F. McAllister, 1963.
- 4406-CO-----Nopah Formation. Same general locality as 3818-CO. West side of hill, about 430 feet from south end.
- 4453-CO-----Nopah Formation. East base of hill, 1.65 miles in straight line S. 39° E. from Pyramid Peak, Ryan quadrangle, Inyo County, Calif. Coll. J. F. McAllister, 1964.
- 4454-CO-----Nopah Formation. Crest near south end of spur, 1.35 miles in straight line S. 23° W. from Pyramid Peak, Ryan quadrangle, Inyo County, Calif. Coll. J. F. McAllister, 1964.
- 4455-CO-----Nopah Formation. Crest of spur, 3.07 miles due south from northwest corner of Ryan quadrangle, Inyo County, Calif. Coll. J. F. McAllister, 1964.

Nevada

- 3368-CO----- 1020-1030 feet above base of Desert Valley Formation of Reso (1963), W $\frac{1}{2}$, sec. 18, T. 7 S., R. 59 E. (unsurveyed), Pahrnatag Range, Lincoln County, Nev. Coll. Anthony Reso, 1958-60.

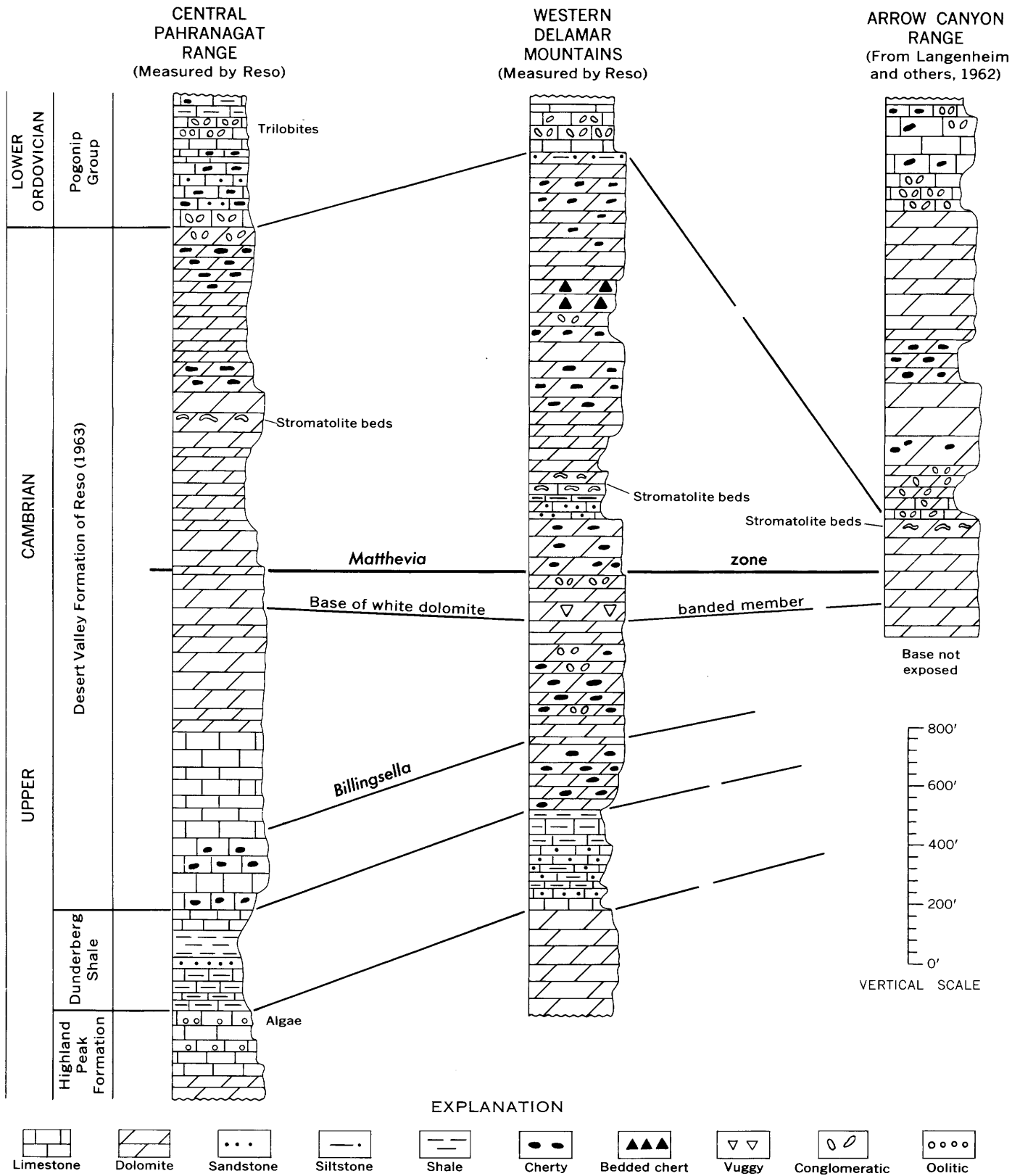


FIGURE 5.—Correlation of stratigraphic sections of the Desert Valley Formation of Reso (1963) in the Pahrnanagat Range, Delamar Mountains, and Arrow Canyon Range, Nev.

- Location----- 1144-1160 feet above base of Desert Valley Formation of Reso (1963), SW $\frac{1}{4}$ sec. 18, T. 7 S., R. 60 E. (unsurveyed), Pahranaagat Range, Lincoln County, Nev. Section measured by Anthony Reso, 1960. *Matthevia* specimens observed in rocks (some scraps in the private collection of Anthony Reso).
- Location----- 800-810 feet above the base of the Desert Valley Formation of Reso (1963), sec. 22, T. 10 S., R. 63 E. (unsurveyed), southwest part of Dalamar Mountains, Lincoln County, Nev. Section measured by Anthony Reso, 1960. *Matthevia* specimens observed in rocks (some scraps may be in Rice University collections).
- Location----- Approximately 175 feet below top of Desert Valley Formation of Reso (1963) (base not exposed), SW $\frac{1}{4}$ sec. 35, T. 14 S., R. 63 E.; NW $\frac{1}{4}$ sec. 2, T. 15 S., R. 63 E. (unsurveyed), Arrow Canyon Range, Clark County, Nev. Coll. Anthony Reso, 1960. One specimen sent to R. L. Langenheim, Jr., University of Illinois. Specimens may be found in the rocks halfway up the section between the white dolomite banded member in the Desert Valley Formation and the bench-forming limestone and dolomitic limestone of the lowest Pogonip Group.
- 4461-CO----- Nopah Formation, on small rise near center of Specter Range 15-minute quadrangle, along 3,640-foot contour, in area of beds overturned and dipping 50°: Nevada State coordinates (central zone) N. 686,500 feet, E. 665,000 feet, Camp Desert Rock quadrangle. Coll. E. N. Hinricks, 1964.
- D-1057-CO -- Nopah Formation, near head of Lucky Strike Canyon, along the ridge running east from the south end of hill 6,612, Charleston Peak quadrangle. Nevada State coordinates (east zone) N. 580,000 feet, E. 516,000 feet. Coll. R. J. Ross, Jr., 1961. [Ross (1964, p. C58) lists this as N. 570,000 feet, but this is a typographical error].
- Texas**
- 60-CO----- Wilberns Formation. Near top of hill over head of East Fork of Little Llano River, 4.4 miles S. 67° E. of school at Cherokee, San Saba County, Tex. Coll. Josiah Bridge, 1934.
- 1734-CO----- Dolomitic facies of San Saba Limestone Member near top of Wilberns Formation. Along west side of a pasture road, 1 mile west of the Blanco County line and 3,400 feet north of North Grape Creek, Gillespie County, Tex. Coll. L. H. Dixon and V. E. Barnes, 1947. (Additional material is at the Bureau of Economic Geology, in Austin, Tex., under Texas collection number 86-T-2-1F.)
- 1800-CO----- Dolomitic facies of San Saba Limestone Member, Wilberns Formation. Fall Creek section. About 3.9 miles NNE of town, between 3,000 and 3,100 feet NNE of the mouth of Fall Creek, just west of the second fence NE of Fall Creek and about 580 feet NE along it from small inlet on Colorado River, SE corner of San Saba County, Tex. Coll. P. E. Cloud, Jr., 1944. (Doubtful occurrence—material poorly preserved.)
- 3464-CO----- "*Hyolithes* bed", San Saba Limestone Member, Wilberns Formation. Everett Ranch road section. 5 miles NE of Lone Grove, Llano County, Tex. Coll. Josiah Bridge and W. H. Hass, 1938.
- Utah**
- 2073-CO----- Ajax Dolomite, from above the middle part, 50-75 feet of dark-gray dolomite that immediately underlies the Garden City Formation. Sec. 27, T. 1 S., R. 7 W., Timpie quadrangle, Tooele County, Utah. Coll. D. E. Arnold, 1955. (Additional material is at the Geology Department, University of Utah, Salt Lake City, Utah.)

REFERENCES

- Cloud, P. E., Jr., and Barnes, V. E., 1948, The Ellenberger group of central Texas: *Texas Univ. Pub.* 4621, 472 p., 44 pls.
- Langenheim, R. L., Jr., Carss, B. W., Kennerly, J. B., McCutcheon, V. A., and Waines, R. H., 1962, Paleozoic section in Arrow Canyon Range, Clark County, Nevada: *Am. Assoc. Petroleum Geologists Bull.*, v. 46, no. 5, p. 592-609.
- McAllister, J. F., 1952, Rocks and structure of the Quartz Spring area, northern Panamint Range, California: *California Div. Mines Spec. Rept.* 25, 38 p.
- Palmer, A. R., 1960, Trilobites of the Upper Cambrian Dunderberg Shale, Eureka district, Nevada: *U.S. Geol. Survey Prof. Paper* 334-C, p. 53-109.
- Reso, Anthony, 1963, Composite columnar section of exposed Paleozoic and Cenozoic rocks in the Pahranaagat Range, Lincoln County, Nevada: *Geol. Soc. America Bull.*, v. 74, p. 901-918, 2 pls.
- Ross, R. J., Jr., 1951, Stratigraphy of the Garden City formation in northeastern Utah, and its trilobite faunas: *Yale Univ., Peabody Mus. Nat. History Bull.* 6, 161 p.
- 1964, Middle and Lower Ordovician formations in southern Nevada and adjacent California: *U.S. Geol. Survey Bull.* 1180-C.
- Walcott, C. D., 1885, Note on some Paleozoic pteropods: *Am. Jour. Sci.*, v. 30, p. 17-21.



A CLASSIFICATION FOR QUARTZ-RICH IGNEOUS ROCKS BASED ON FELDSPAR RATIOS

By J. T. O'CONNOR, Denver, Colo.

Work done in cooperation with the U.S. Atomic Energy Commission

Abstract.—A classification for quartz-rich igneous rocks based on feldspar ratios is designed to relate chemically similar plutonic and volcanic rocks. The plutonic rocks are named modally, according to common geologic usage, and their normative mineralogy is calculated and used as the basis for a system to classify volcanic rock norms. The rocks to which this classification may be applied should have more than 10 percent quartz. The rock names are characterized as fields on a triangular diagram with percentage of Ab, Or, and An as the vertices of the triangle.

Many rock classification schemes have been applied to igneous rocks. However, few, if any, of these classifications take into account both the different methods of study of volcanic and plutonic rocks and the chemical similarities between igneous rocks of different crystallization history but common magmatic origin. Petrographic classifications generally fall into three types: modal, chemical, and modified chemical (for example, normative). Modal classifications are inadequate to describe aphanitic or glassy volcanic rocks. Chemical and modified chemical classifications are generally used to classify volcanic rocks.

Because of differences in chemical composition of normative minerals in volcanic rocks and modal minerals in plutonic rocks, chemically similar volcanic and plutonic rocks end up in different groupings in many classifications. An abundance of petrographic classifications, generally formulated without regard for the chemical variability of rock-forming minerals, has given rise to a proliferation of names for individual rock specimens. The following names were derived for the same rock specimen (a volcanic rock from the Nevada Test Site) from some of the commonly used rock classifications:

- rhyodacite (Williams and others, 1954)
- dellenite (Wahlstrom, 1955; Nockolds, 1954)
- rhyolite (Rittmann, 1952; Tuttle and Bowen, 1958)
- quartz latite (Johannsen, 1939; Petersen, 1961).

In this report the author will present a scheme which attempts to blend the presently used classifications into a simple system capable of adequately describing both volcanic and plutonic rocks. This system uses the modal mineralogy of plutonic rocks and the normative mineralogy of volcanic rocks, but allows direct comparison of the data gathered by these different methods.

PROPOSED CLASSIFICATIONS

The quartz-rich igneous rocks are those which have compositions such that their normative (or modal) mineralogy may be closely represented by points in the Qtz-Or-Ab-An tetrahedron with more than 10 percent quartz. Most petrographic classifications take advantage of this compositional grouping and classify the silicic igneous rocks by projecting their compositions on one or more faces of the tetrahedron. We, too, will utilize this grouping and the fact that above 10 percent quartz the variation in quartz content is a negligible factor in determining the rock type. After it is established that more than 10 percent quartz is present in the rock, the parameters used for classification are Or, Ab, and An. This amounts to a projection of compositional points from within part of the tetrahedron onto the feldspar face of the tetrahedron.

In order to establish an equivalence between the classification diagrams for volcanic rocks and plutonic rocks, it is first necessary to define one of the two divisions. Since modal data for plutonic rocks are abundant in the geologic literature and modal analysis is the most common method of defining these rocks, the plutonic classification is set up first (fig. 1). This classification is adapted from Nockolds (1954), Williams and others (1954), Tuttle and Bowen (1958), and other unpublished classifications. While figure 1 is similar in appearance to figure 3 and bears some resemblance to Hietanen's (1961) classification, it is a modal and not a normative classification. In this diagram, perthite

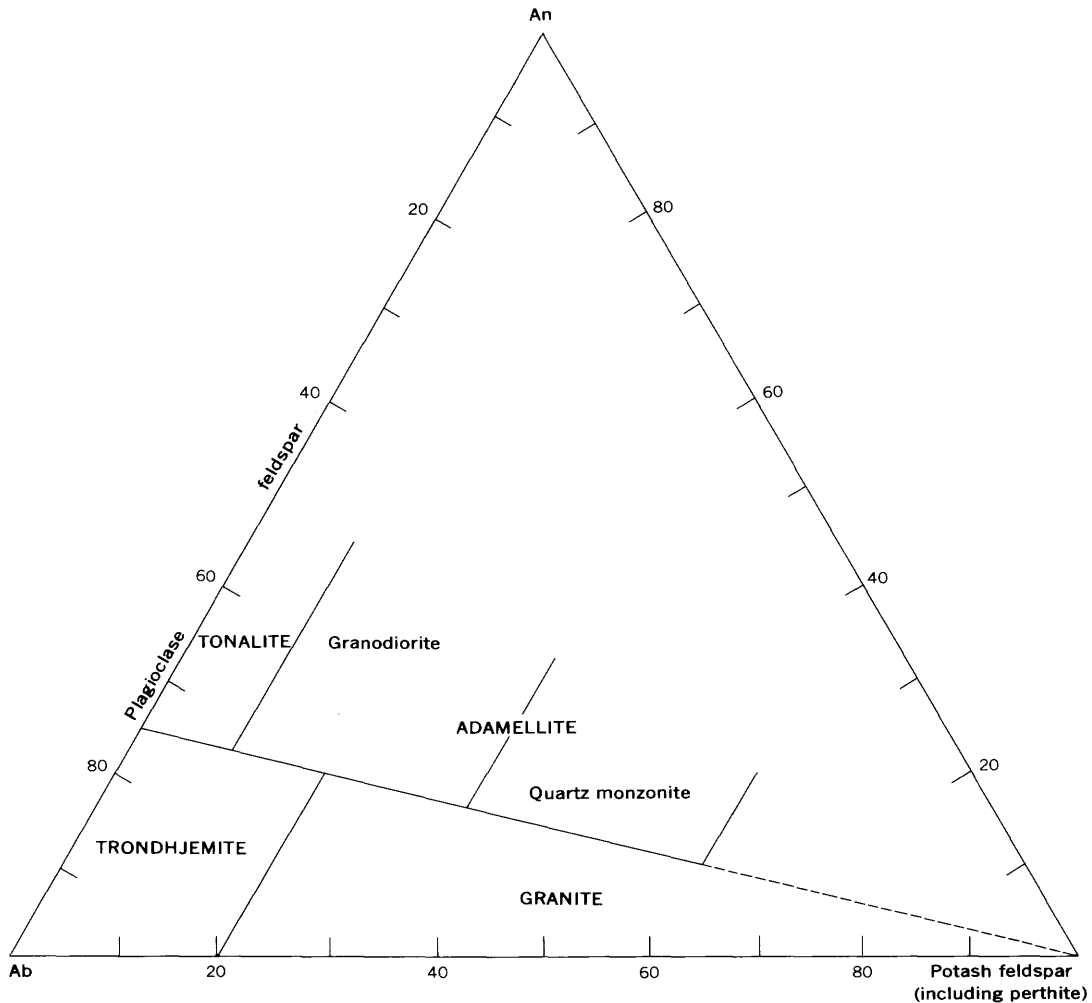


FIGURE 1.—Modal classification of silicic plutonic rocks. The potash feldspar-plagioclase feldspar ratio is determined from the mode. The albite-anorthite ratio is determined from the plagioclase feldspar. The term "adamellite" is used to maintain parallelism with the volcanic rock classification (fig. 3).

was plotted as potash feldspar unless broken into components in the mode. The Ab-An ratio was determined from the plagioclase feldspar.

The granite field of figure 1 comprises most of the lower part of the diagram along the Ab-potash feldspar join. In other classifications (for example, Nockolds, 1954) granite has been distinguished from quartz monzonite by the relative plagioclase content, no matter what the plagioclase composition. The presence or absence of plagioclase in a rock with the chemical composition of a granite is, however, the main difference between the subsolvus- and hypersolvus-granite of Tuttle and Bowen (1958). This criterion subdivides rocks formed from chemically identical magmas but with different crystallization histories, not rocks formed from chemically different magmas. This statement is not an attempt to abrogate the part played by chemical composition in forming the minerals of a particular rock; it merely points out that over the wide range of pressure-

temperature conditions under which granitic rocks may form, chemical identity does not imply, a priori, mineralogical identity. Plotted normative compositions of typical granite and "quartz monzonite" with plagioclase less calcic than An_{25} fall in the same area of the Ab-An-Or triangle (fig. 2).

The trondhjemite field is defined according to Goldschmidt (1916) and Hietanen (1943). The singular associations and widespread occurrence of trondhjemite (Goldschmidt, 1922; Turner and Verhoogen, 1951) are sufficient reason for perpetuating the preexisting name for this rock type, although mineralogically trondhjemite is an extension of the granite clan.

The rocks of the tonalite and adamellite groups of this classification are typically richer in lime than the rocks of the granite group (see Larsen, 1948). In the modal classification these rocks are restricted to fields with modal plagioclase more calcic than An_{25} . The adamellite field includes both granodiorite and quartz-

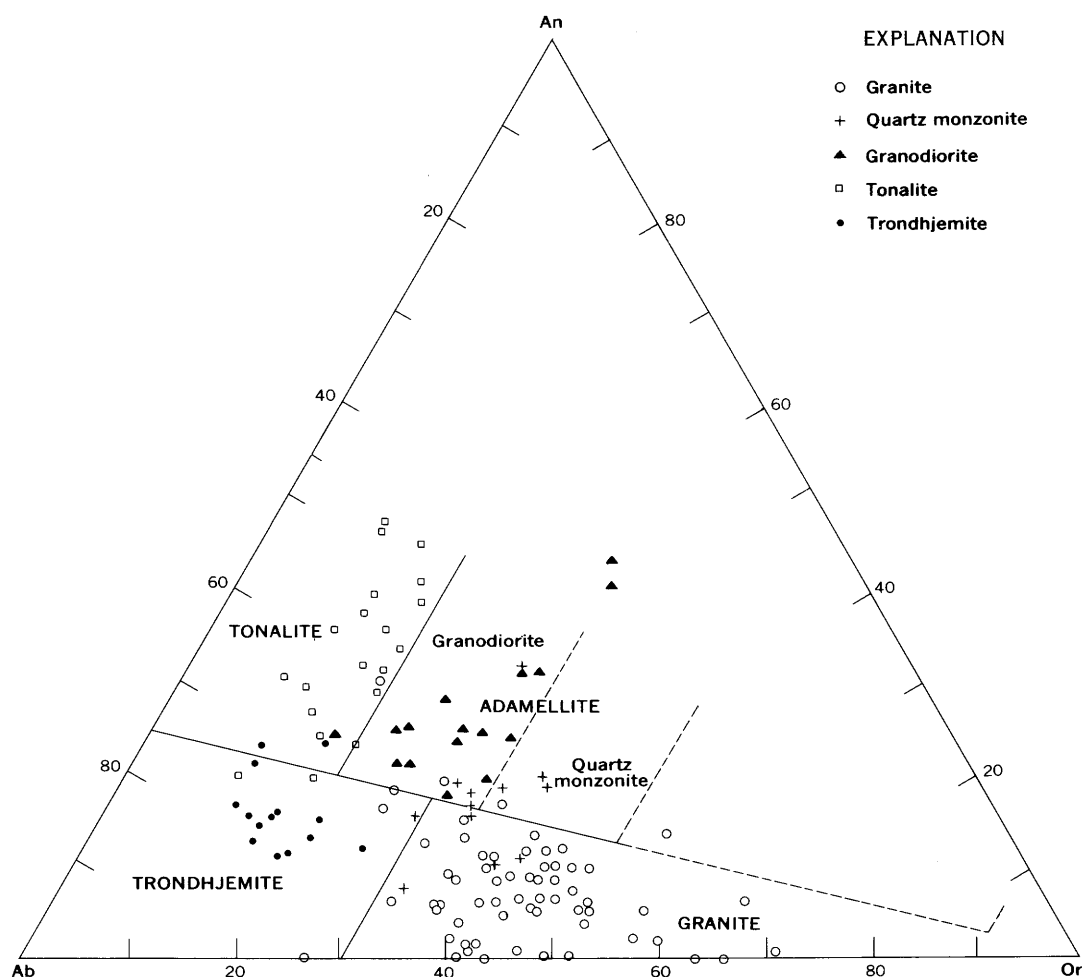


FIGURE 2.—Normative feldspar ratios from silicic plutonic rocks. One hundred and twenty-five partial molecular norms are plotted on the Ab-An-Or triangle. The field boundaries have been drawn to maintain the equivalence between the normative fields of this diagram and the modal fields of figure 1. The fields are labeled for the plutonic rock type to emphasize this correspondence; for the equivalent volcanic rock types see figure 3. The symbols represent the rock type as determined modally on figure 1.

monzonite. The name "adamellite" has been used in this sense to maintain parallelism with the dellinite field in the volcanic classification, which is explained below.

To define the normative volcanic fields, 125 plutonic rocks were selected which had been analyzed both modally and chemically. After classification of the rocks by plotting their modal analyses on figure 1, the normative mineralogy of the plutonic rocks was calculated and the molecular ratios of Or-Ab-An plotted on figure 2. Field boundaries were drawn so that the rocks defined by the modal feldspar ratios of figure 1 were similarly defined by the normative feldspar ratios of figure 2. By establishing these fields empirically the effect of variation in the composition of the modal feldspars from that of the normative feldspars and the effect of difference between molecular-percent ratios in

one diagram and volume-percent ratios in the other have been taken into account.

After determination of the boundaries of the normative fields which correspond to the fields from the modal classification the following rock names were applied to the volcanic rocks (fig. 3):

- rhyolite (calc-alkali rhyolite)-granite (calc-alkali granite) equivalents
- quartz keratophyre-trondhjemite equivalent
- dacite-tonalite equivalent
- dellenite-adamellite equivalent
- rhyodacite-granodiorite equivalent
- quartz latite-quartz monzonite equivalent

These are generally considered as volcanic-plutonic equivalent rocks. While mineral-name modifiers are best restricted to observed phenocryst minerals, some

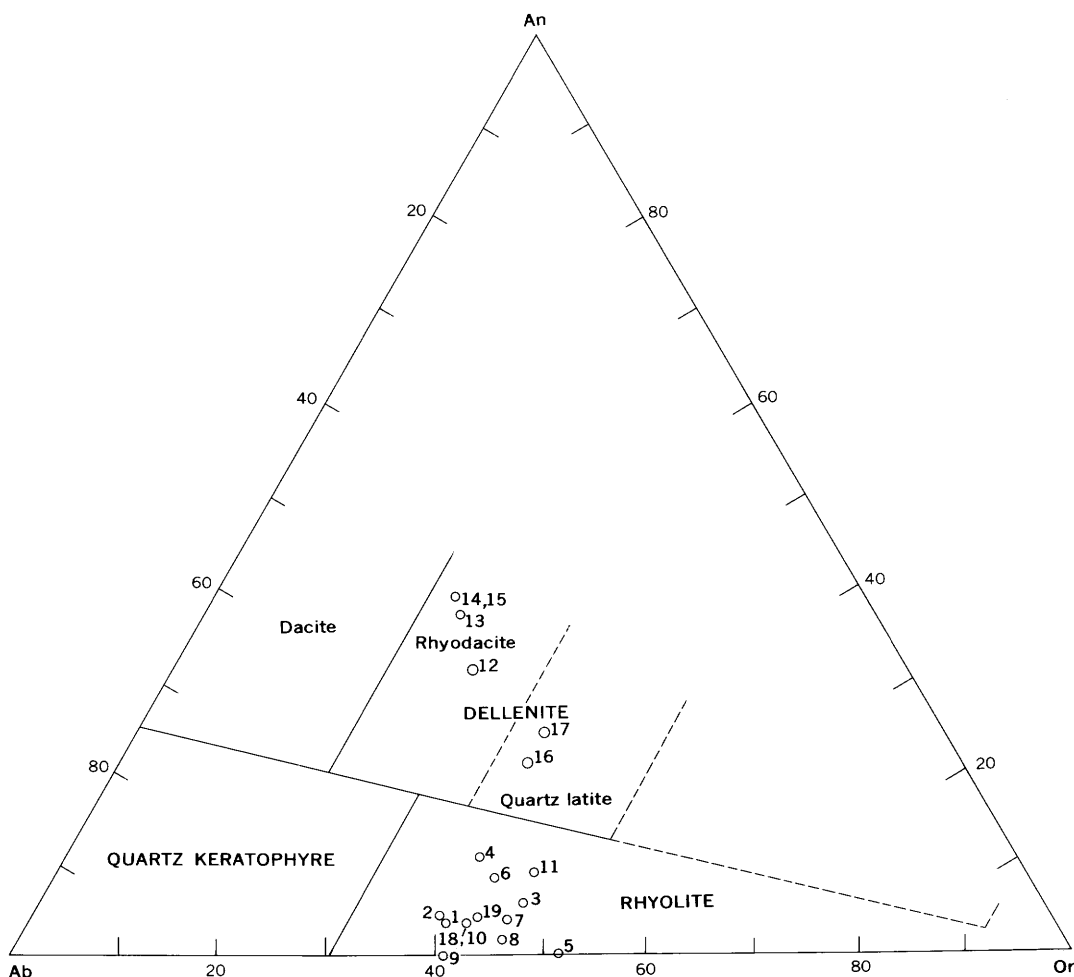


FIGURE 3.—Normative classification for silicic volcanic rocks. Normative Ab, An, and Or are plotted in molecular percent recalculated to 100 percent. The numbered points correspond to samples from the Nevada Test Site and vicinity. Chemical analyses of the samples are given in table 2. Samples 1, 3, and 6–11 are Piapi Canyon rhyolite ash-flow tuff; sample 2 is rhyolite lava flow of Fortymile Canyon; sample 4 is rhyolite lava flow of Calico Hills; sample 5 is rhyolite lava flow of Shoshone Mountain; samples 12–15 are dacite and rhyodacite (lava flows and breccias) of Wahmonie Flat; samples 16 and 17 are quartz-latite lava flow of Mount Salyer; sample 18 is rhyolite ash-flow tuff of the Thirsty Canyon; and sample 19 is rhyolite lava flow of Pillar Spring.

of the volcanic rock names are too firmly entrenched in geologic usage to be changed (for example, quartz latite). The phenocryst mineralogy should be useful in defining some units with similar normative mineralogy (for example, anorthoclase rhyolite versus sanidine-plagioclase rhyolite).

Many rocks with modal analyses which plot in the quartz-monzonite field have normative mineralogies which coincide with the potash-rich granodiorites (fig. 2). For this reason it is suggested here, as by other authors (Wahlstrom, 1955), that a general term, dellenite, is applicable to the volcanic equivalents of both granodiorite and quartz-monzonite. This general name "dellenite" does not abrogate the usefulness of the rock names "rhyodacite" and "quartz-latite" but indicates that the latter are less definitive.

CALCULATION OF THE MOLECULAR NORM

The use of this classification requires that the petrographer calculate the normative feldspar composition of the rock to be classified. The author has expressed this normative mineralogy in molecular percent because this simplifies most mineralogic applications in petrologic studies. The molecular percentage of a mineral in a rock may be calculated in several ways, with different results, depending upon the conventions used in establishing the chemical formula of the mineral. For general calculation of norms, the author uses Barth's (1962) modification of the Niggli system but, since the three feldspars used in this classification have the same number of cations in their conventional formulas, a simple method of direct calculation from a table is possible (table 1).

TABLE 1.—Guide for direct calculation of partial molecular norm
[Based on chemical analysis in weight percent; adapted from Wahlstrom (1955)]

1 percent of—		Is equivalent to (percent)—	
K ₂ O	In orthoclase	1.082	Al ₂ O ₃
		3.827	SiO ₂
		5.910	KAlSi ₃ O ₈
Na ₂ O	In albite	1.645	Al ₂ O ₃
		5.817	SiO ₂
		8.462	NaAlSi ₃ O ₈
	In acmite	2.318	FeO
		3.878	SiO ₂
CaO	In anorthite	7.197	NaFeSi ₂ O ₆
		1.818	Al ₂ O ₃
		2.143	SiO ₂
	In wollastonite	4.961	CaAl ₂ Si ₂ O ₈
		1.072	SiO ₂
TiO ₂	In sphene	2.072	CaSiO ₃
		0.702	CaO
		0.752	SiO ₂
P ₂ O ₅	In apatite	2.454	CaTiSiO ₅
		0.899	FeO
		1.899	FeTiO ₃
CO ₂	In calcite	0.948	CaO
		0.064	F
		1.705	Ca ₅ (PO ₄) ₃ F
K	In fluorite	1.274	CaO
		2.274	CaCO ₃
		1.476	CaO
		2.055	CaF ₂

The normative calcite, apatite, sphene, and fluorite are calculated first (for example, 0.20 percent CO₂ in

the analysis equals 0.20×1.274 percent=0.25 percent CaO and 0.20×2.274 percent=0.45 percent CaCO₃). Sphene is calculated only if insufficient FeO is present to produce ilmenite. The CaO for calcite, apatite, sphene, and fluorite is subtracted from the total CaO in the analysis, and the weight percentages of Ab, Or, and An are calculated respectively, from Na₂O, K₂O, and the residual CaO. If the calculated feldspars do not exhaust the alumina or silica in the analysis, the normative feldspars are divided by their respective molecular weights (Or=278.4, Ab=262.2, An=278.2) and recalculated to 100 mole percent. If alumina is not present in enough quantity to allow all the K₂O, Na₂O, and CaO to form feldspars, anorthite is reduced in quantity until the alumina deficiency is removed. If all the anorthite is used up without removing this deficiency, albite is reduced in quantity until the alumina deficiency is removed. If the chemical analysis does not contain sufficient silica to produce the feldspars and 10 percent quartz, the rock will not fit into the classification proposed here.

NEVADA TEST SITE VOLCANICS

As an example of the use of this system the chemical analyses and partial molecular norms for several representative specimens of the silicic volcanic rocks of the Nevada Test Site and vicinity are given in table 2. These norms are plotted by number on figure 3. It is immediately apparent by comparison with figure 2 that

TABLE 2.—Chemical analyses and partial molecular norms of silicic volcanic rocks from the Nevada Test Site and vicinity

Oxide or mineral	1	2	3	4	5	6	7	8	9	10	11	12	13	14	15	16	17	18	19
Chemical analyses																			
SiO ₂	69.0	73.6	70.5	68.5	74.3	71.4	69.02	67.12	76.03	69.85	65.73	63.3	59.7	58.1	60.5	67.2	68.1	66.0	68.9
TiO ₂	.35	.26	.25	.42	.22	.29	.41	.44	.15	.40	.40	.68	.78	.96	.82	.47	.47	.38	.34
Al ₂ O ₃	15.0	13.2	13.8	16.2	13.2	14.4	15.60	15.25	12.58	15.30	15.46	16.1	16.1	16.3	16.4	15.4	14.6	15.7	15.3
Fe ₂ O ₃	1.2	1.3	1.1	2.0	1.2	1.3	1.93	1.94	1.01	1.78	1.43	3.0	3.6	2.4	3.3	3.3	3.2	2.0	2.7
FeO	.61	1.1	.30	.30	1.30	.35	.18	.07	.09	.56	1.5	2.5	4.5	2.6	.04	.22	1.5	.65	.65
MnO	.10	.10	.06	.08	.04	.06	.08	.11	.10	.11	.09	1.0	.11	.14	.05	.04	.15	.13	.13
MgO	.34	.48	1.0	.50	.12	.48	.25	.41	.11	.29	.46	2.2	3.7	4.0	2.9	.65	.91	.97	.27
CaO	.94	1.1	1.8	2.4	.35	1.2	.94	2.02	.13	.76	1.39	4.6	6.3	6.8	5.4	2.7	2.8	.74	.46
Na ₂ O	4.2	3.7	3.6	3.6	2.8	3.8	4.36	4.27	4.3	4.82	3.88	3.0	2.8	2.8	2.8	2.8	2.5	4.8	5.0
K ₂ O	5.7	4.6	5.3	4.1	5.6	4.9	5.93	5.69	4.6	5.53	5.70	3.2	2.6	2.4	2.0	3.8	3.6	5.7	5.6
H ₂ O ⁺	2.8	.41	1.5	.84	.69	.23	.31	.51	.27	.15	3.61				2.9			2.0	.59
H ₂ O ⁻		.19		.23															
P ₂ O ₅	.12	.05	.10	.21	.04	.06	.07	.07	.01	.07	.07	.27	.29	.34	.29	.19	.20	.08	.04
CO ₂	.05	.15	.54	.05	.25	.06	.01	.94	.02		.01				.05			.05	
Cl							.02	.01	.02	.02	.04								
F							.05	.05	.03	.06									
Partial molecular norms																			
Or	38.6	38.3	45.6	38.0	52.5	42.2	45.2	45.7	41.2	41.8	45.3	28.3	23.9	22.6	19.0	37.5	37.6	42.2	41.3
Ab	57.9	57.7	48.5	50.6	47.5	50.0	50.5	52.1	58.6	55.3	46.8	40.4	39.1	39.8	40.7	41.7	21.2	54.0	55.9
An	3.4	3.9	5.9	11.4		7.8	4.3	2.3	.2	2.8	7.9	31.3	37.0	37.6	40.3	20.8	21.3	3.8	2.8

- Piapi Canyon rhyolite ashflow tuff.
- Rhyolite lava flow of Fortymile Canyon.
- Piapi Canyon rhyolite ashflow tuff.
- Rhyolite lava flow of Calico Hills.
- Rhyolite lava flow of Shoshone Mountain.

- Piapi Canyon rhyolite ashflow tuff.
- Dacite and rhyodacite of Wahmonie Flat.
- Quartz latite of Mount Salyer.
- Rhyolite ash-flow tuff of the Thirsty Canyon.
- Rhyolite lava flow of Pillar Spring.

the norms of the more silicic rocks of the Nevada Test Site fall in the same field as do the norms of granite. These rocks should properly be called rhyolite. They include the rocks of the Piapi Canyon Formation, the rhyolites of Fortymile Canyon, the rhyolites of Shoshone Mountain, the rhyolites of the Calico Hills, the rhyolite ash-flow tuffs of the Thirsty Canyon Tuff, and the rhyolite lava-flows of Pillar Spring. Intermediate silicic rocks such as the sequence at Wahmonie Flat and Mount Salyer have norms which fall in the dacite, rhyodacite, and quartz latite fields. Probably the majority of the rocks of the sequence at Wahmonie Flat and Mount Salyer belong in the rhyodacite category.

This report has offered a classification for those igneous rocks which have a chemical composition in the silicic (more than 10 percent quartz) portion of the Qtz-Or-Ab-An tetrahedron. Many of the rocks lying near the low-silica (less than 10 percent quartz) portion of this tetrahedron can be classified by a similar diagram. However, abundant iron with its variable oxidation states, and the presence of different modal and normative feldspathoids, makes direct comparison between plutonic and volcanic rocks of low silica content more difficult. This problem is left for further study.

REFERENCES

- Barth, T. F. W., 1962, *Theoretical petrology*: New York, John Wiley and Sons, Inc.
- Goldschmidt, V. M., 1916, *Geologisch-Petrographische Studien im Hoehgebirge des südlichen Norwegens*: Kristiania Vidensk.-selsk. Skr., Math.-Naturv. Kl. 2, 140 p.
- 1922, *Stammestypen der Eruptivgesteine*: Novske Vidensk.-akad. Skr., Math.-Naturv. Kl. 10, p. 6.
- Hietanen, Anna, 1943, *Über das Grundgebirge des Kalantigebietes im suwestlichen Finnland*: Comm.: Geol. Finland, Bull. 130.
- 1961, A proposal for clarifying the use of plutonic calc-alkalic rock names: U.S. Geol. Survey Prof. Paper 424-D, p. D340-D342.
- Johannsen, Albert, 1939, *A descriptive petrography of the igneous rocks*, v. 1: Chicago, Univ. of Chicago Press.
- Larsen, E. S., 1948, *Batholith of Southern California*: Geol. Soc. America Bull., v. 29, p. 66.
- Neuman, A. E., 1917, *Die Grundlehre des Blausteinaordnung*: Heidelberg Zeit. f. Min. u. Pet., v. 1, no. 1, p. 32-87.
- Nockolds, S. R., 1954, *Average chemical compositions of some igneous rocks*: Geol. Soc. America Bull., v. 65, p. 1007-1032.
- Petersen, D. W., 1961, *Descriptive modal classification of igneous rocks*: GeoTimes, v. 5, no. 6, p. 30-36.
- Rittmann, Alfred, 1952, *Nomenclature of volcanic rocks*: Bulletin volcanologique, ser. II, v. XII, p. 75-102.
- Turner, F. J., and Verhoogen, John, 1951, *Igneous and metamorphic petrology*: New York, McGraw-Hill Book Co., Inc.
- Tuttle, O. F., and Bowen, N. L., 1958, *Origin of granite in the light of experimental studies in the system NaAlSi₃O₈-KAlSi₃O₈-SiO₂-H₂O*: Geol. Soc. America Mem. 74.
- Wahlstrom, E. E., 1955, *Petrographic mineralogy*: New York, John Wiley and Sons, Inc.
- Williams, Howell, Turner, F. J., and Gilbert, C. M., 1954, *Petrography*: San Francisco, W. H. Freeman and Co.



GOLD FLAT MEMBER OF THE THIRSTY CANYON TUFF— A PANTELLERITE ASH-FLOW SHEET IN SOUTHERN NEVADA

By DONALD C. NOBLE, Denver, Colo.

Work done in cooperation with the U.S. Atomic Energy Commission

Abstract.—Silicic glass from the Gold Flat Member is chemically very similar to pantellerite glasses from the island of Pantelleria. The analysis shows very high percentages of Na, Fe, Zr, Cl, and F and very low percentages of Al, Ca, and Mg. The minor elements B, Be, Nb, Pb, Sn, Th, the rare alkalis, and the rare earths are 5 to 30 times more abundant than in typical granitic rocks.

Remarkably diverse suites of volcanic rock were erupted from a number of centers in southern Nye County, Nev., during the late Miocene and Pliocene (Noble and others, 1965). Alkalic and peralkalic rocks were erupted from two of the centers, the Black Mountain center (Christiansen and Noble, 1965) of middle Pliocene age, and an unnamed older center located 20 miles east of Black Mountain. The purpose of this preliminary note is to document an unusual silicic rock of extreme composition which was erupted from the Black Mountain volcano.

GEOLOGY

The Gold Flat Member crops out over an area of approximately 300 square miles centered on Black Mountain (fig. 1). The member is the fourth in the sequence of five ash-flow units of the Thirsty Canyon Tuff (Noble and others, 1964) which were erupted from the Black Mountain volcano. It is a compound cooling unit (Smith, 1960) made up of at least a dozen individual ash flows. The source of the member is now represented by an ovoid collapse caldera $3\frac{1}{2}$ miles in maximum diameter centered 1 mile west of Black Mountain. The original volume of the unit was between 2 and 5 cubic miles, only a fraction of which is now preserved.

The other members of the Thirsty Canyon Tuff are of comenditic, trachytic soda rhyolitic, and trachytic composition. Trachyte, trachytic soda-rhyolite, and trachyandesite lavas that were erupted from the Black

Mountain volcano interfinger with the Thirsty Canyon Tuff near Black Mountain.

PETROGRAPHY AND MINERALOGY

The Gold Flat Member varies from densely welded to partially welded. Eutaxitic structure is readily seen at most outcrops. Although the groundmass of most rocks is devitrified to a fine-grained intergrowth composed mainly of alkali feldspar and cristobalite and (or) quartz, a thin basal vitrophyre is present at most outcrops.

Phenocrysts, most of which are fractured portions of original euhedra, compose from 10 to 25 percent of the rock. Alkali feldspar makes up 80 to 90 percent of the phenocrysts, quartz 4 to 12 percent, sodic plagioclase 1 to 4 percent, and olivine, clinopyroxene, amphibole, and iron ore 0.5 to 2 percent each. Biotite, zircon, apatite, and chevkinite are present in trace amounts. Only preliminary optical, X-ray, and analytical work has been done on the phenocrysts. Complexly twinned euhedra of lime anorthoclase rimmed by a thin shell of soda-rich sanidine 1 to 2 centimeters in length make up about 20 percent of the alkali feldspar. The remainder consists of soda-rich sanidine crystals with a maximum diameter of about 5 millimeters. The olivine phenocrysts range in composition from Fe_0 to $Fe_{0.25}$, and variations in refractive index and pleochroism also suggest a range in the composition of the pyroxene phenocrysts. The amphibole is an iron-rich barkevikite with an iron to magnesium ratio of 15 to 1.

Lithic fragments 0.1 to 2 cm in diameter, consisting of fine-grained aggregates of alkali feldspar with very small amounts of clinopyroxene, and occasional cobble-sized inclusions of medium-grained porphyritic to non-porphyritic igneous rocks of various compositions, make up an additional 5 to 20 percent of the rock.

CHEMISTRY

An analysis of nonhydrated glass separated from marekanite ("apache tears") (Ross and Smith, 1955) from the basal vitrophyre of the cooling unit is given in table 1, column 1. The glass is dark greenish brown, refractive index 1.509, and contains numerous subequant anhedral microlites less than 10 microns in diameter. Such glass, because it has escaped the extensive ground-water leaching that most hydrated natural glasses have

undergone, accurately represents the liquid phase of the pantellerite magma. The sodium, iron, zirconium, and halogen content of the glass are extremely high for a silicic rock, and the aluminum, magnesium, and calcium content are abnormally low. The molecular ratio of alkalis to alumina is 1.8, whereas typical calc-alkalic rhyolites have a ratio of less than 1 and comendites a ratio only slightly greater than 1. The analysis is very similar to those of hyalopantellerites (table 1, columns

TABLE 1.—Chemical analyses of pantellerites and pantellerite glass separates

[ND, not determined]

Constituent	Analyses						
	1	2	3	4	5	6	7
SiO ₂	69.25	69.81	69.59	70.1	69.0	69.5	67.1
Al ₂ O ₃	9.10	8.59	11.27	8.7	10.5	11.5	10.4
Fe ₂ O ₃	3.70	2.28	1.87	2.2	3.0	4.0	4.2
FeO.....	2.61	5.76	4.18	5.5	2.1	1.2	1.5
MgO.....	.011	.10	.23	.11	.1	.3	.36
CaO.....	.06	.42	.44	.47	.4	.5	.39
Na ₂ O.....	7.00	6.46	6.28	6.8	7.1	5.2	4.8
K ₂ O.....	4.29	4.49	4.60	4.7	4.6	4.8	4.7
Rare alkalis.....	.16	ND	ND	ND	.15	.13	ND
H ₂ O ⁺14	.14	.13	.12	.1	.6	2.6
H ₂ O ⁻01	.05	.02	.01	-----	.3	.46
TiO ₂25	.45	.47	.46	.25	.3	.28
ZrO ₂78	.25	.12	.24	.6	.6	ND
P ₂ O ₅01	.13	.10	.04	.05	.07	.07
MnO.....	.19	.28	.28	.32	.17	.16	.18
CO ₂00	ND	ND	ND	.00	.05	<.05
SO ₃08	.06	.06	ND	.06	ND	ND
Cl.....	.78	.79	.38	.63	.65	.2	.51
F.....	1.30	ND	ND	ND	1.05	.5	.88
Other.....	.62	ND	ND	ND	.6	.5	ND
Less O.....	100.35	100.06	99.99	(100.4)	(100)	(100)	-----
	.72	.18	.09	.12	.6	.3	-----
Total.....	99.63	99.88	99.90	(100.3)	(100)	(100)	-----

1. Nonhydrated glass separate (D100126) from the Gold Flat Member of the Thirsty Canyon Tuff. Main analysis by D. F. Powers, using the methods described by Peck (1964); MgO determined by Joseph Haffty and Harriet Neiman using quantitative emission spectrographic methods (accuracy ± 15 percent); Na₂O and K₂O are averages of 2 gravimetric determinations (7.05, 7.07; 4.38, 4.41) by D. F. Powers and V. C. Smith corrected for rare alkali oxides; SO₃ by V. C. Smith; ZrO₂ determined by quantitative emission spectrographic methods (accuracy ± 10 percent) by P. R. Barnett; Cl and F values are averages of 2 determinations (0.78, 0.78; 1.28, 1.33) by V. C. Smith using the methods of Peck and Tomasi (1959) and Peck and Smith (1964). Aluminum oxide value represents gravimetric determination of 10.50 corrected for ZrO₂ and for Be, Nb, Th, and rare-earth oxides, which are included under "other". Concentrations of rare-earth elements not determined spectrographically are inferred using ratios calculated from the G-1 data of Haskin and Gehl (1963).
2. Hyalopantellerite P.R.C. No. 2000 from Pantelleria (Zies, 1960).
3. Hyalopantellerite P.R.C. No. 2007 from Pantelleria (Zies, 1960).
4. Average of 4 pantellerite glass separates from Pantelleria (Carmichael, 1962, p. 100, Nos. 1G, 2G, 3G, 4G).
5. Whole-rock composition of tuff of the Gold Flat Member based on composition of nonhydrated glass (analysis 1) and the inferred composition of the phenocrysts and lithic material in the tuff.
6. Average chemical composition of densely welded devitrified ash-flow tuff of the Gold Flat Member; weighted average of four rapid rock (Shapiro and Brannock, 1962) analyses. Main analyses by Paul Elmore, Sam Botts, Gillison Chloe, Lowell Artis, and H. Smith; halogens by V. C. Smith; zirconia by quantitative emission spectrography, P. R. Barnett, analyst. Spectrophotometric alumina determinations corrected for zirconium interference using data provided by Leonard Shapiro (written communication, 1964).
7. Vitrophyric ash-flow tuff (D110872W) from the Gold Flat Member; rapid rock analysis by Paul Elmore, Sam Botts, Gillison Chloe, Lowell Artis, and H. Smith.

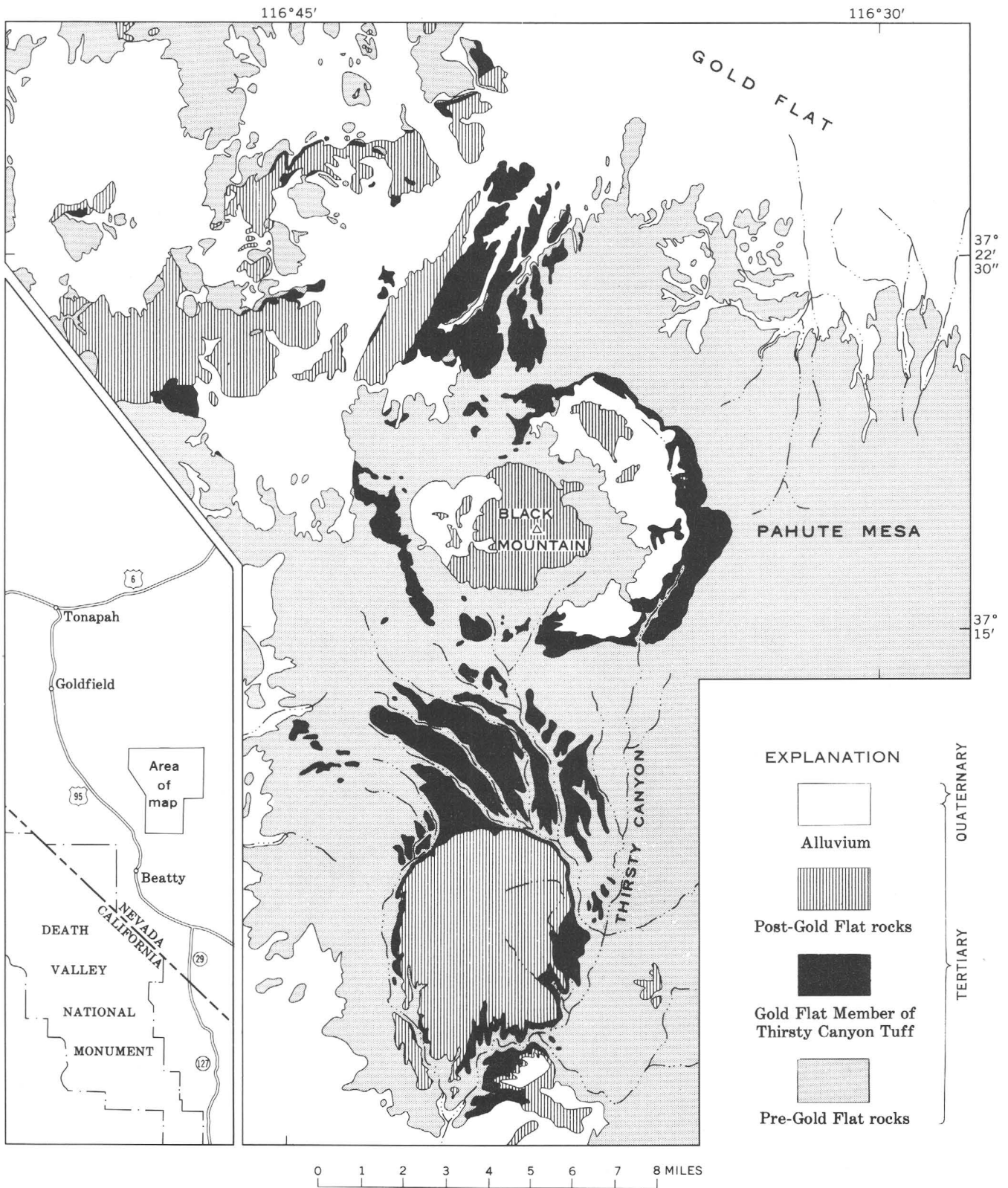


FIGURE 1.—Map showing the distribution of the Gold Flat Member of the Thirsty Canyon Tuff. Generalized from mapping done in 1962-64 by D. C. Noble, R. L. Christiansen, C. L. Rogers, and others. Faults in pre-Gold Flat rocks are not shown.

2 and 3) and pantellerite glasses (table 1, column 4) from the type area, the island of Pantelleria in the Mediterranean (Washington, 1913, 1914).¹

With the marked exception of sodium and the halogens, the whole-rock composition of the Gold Flat Member (table 1, column 5) calculated from (1) the glass analysis and (2) the inferred composition of the phenocrysts and lithic material in the tuff agrees well with the whole-rock analyses of densely welded, devitrified tuff from the Gold Flat Member (table 1, column 6).

More than a quarter of the sodium originally present in the Gold Flat Member has been lost from the devitrified rocks of the unit. As a result of the very high original alkali to alumina ratio of the rock, even with all the ferrous iron assigned to normative arfvedsonite and the remainder of the ferric iron assigned to acmite, more than 2 percent Na₂O is available beyond that required to form feldspar. The exact phase or phases that this excess soda entered into on cooling of the Gold Flat Member are not definitely known. However, it seems most probable that they were very soluble and thus readily removed by ground water. In addition, some sodium was probably leached by ground water from "stuffed" cristobalite formed by devitrification of the originally glassy groundmass at relatively high temperature (Noble, 1965). An even greater amount of sodium has been leached by ground water from densely welded vitrophyric tuffs (table 1, column 7).

Halogens, particularly chlorine, were lost from the tuffs on devitrification. A part of the halogens probably crystallized as soluble metal halides during devitrification and were subsequently removed by ground water. Fluorine and chlorine contents of an analyzed

vitrophyre (table 1, column 7) are similar to those of analysis 5 in table 1, and several hydrated glass separates have a halogen content almost as great as the nonhydrated glass. These data show that the chlorine and fluorine analyses of the nonhydrated glass are representative of the original halogen content of the groundmass of the member as a whole.

The results of quantitative spectrographic analysis of the glass from the Gold Flat Member are given in table 2, column 1. In addition, semiquantitative spectrographic analysis (Myers and others, 1961) of this glass gives the following values (in weight percent): Th 0.02, U <0.05, Ce 0.15, Nd 0.07, Sm 0.015, and the remainder of the rare earths below the limits of detection as given by Myers and others (1961, table 2). The

TABLE 2.—Quantitative spectrographic analyses of glasses and rocks of the Thirsty Canyon Tuff

[Analyses 1, 2, and 3, except for rare alkalis, by P. R. Barnett. Analysis 4 and all rare-alkali determinations by Joseph Hafity and Harriet Neiman. The analyses were made using the methods of Bastron and others (1960), slightly modified, and the method of Annell (1964). These methods have an overall accuracy of ±15 percent, except that they are less accurate near the limits of detection where only one digit is reported. All data are in weight percent]

Element	Analysis			
	1	2	3	4
B-----	0.01	0.008	0.009	0.003
Ba-----	.0005	.02	.019	<.0005
Be-----	.006	¹ .004	.0030	.0006
Co-----	<.0002	<.0002	<.0002	<.0002
Cr-----	<.0001	<.0001	.0001	<.0001
Cu-----	² .0017	.0003	.0003	<.0001
Ga-----	.0042	.0042	.0040	.0030
Hf-----	<.01	-----	-----	-----
La-----	.061	.047	.042	.011
Mo-----	.0006	.0004	.0005	.0005
Nb-----	.064	.030	.045	.007
Ni-----	<.0002	<.0002	<.0002	<.0002
Pb-----	.022	.015	.015	.004
Sc-----	<.0005	<.0004	<.0005	<.0002
Sn-----	.0050	.0034	.0037	.0006
Sr-----	.0002	.007	.015	.0002
V-----	<.0005	.0008	.003	<.0005
Y-----	.045	.030	.029	.0073
Yb-----	.0054	.0032	.0033	.0006
Li-----	.026	.018	-----	.0078
Cs-----	.0010	.0007	-----	<.0005
Rb-----	.095	.084	-----	.039

1. Nonhydrated glass separate (D100126) from the Gold Flat Member of the Thirsty Canyon Tuff.
2. Densely welded devitrified tuff (D111273W) of the Gold Flat Member.
3. Densely welded devitrified tuff (D111141W) of the Gold Flat Member.
4. Nonhydrated glass separate (D100437) from the Spearhead Member of the Thirsty Canyon Tuff.

¹ Corroborated by a determination of 38 ppm Be by neutron-activation techniques (Vaughn and others, this chapter, p. B151).

² Probably reflects contamination.

¹ The term "pantellerite" should be applied only to rocks which have approximately the same chemical composition as the type pantellerites (and in particular the hyalopantellerites) from Pantelleria, or to similar although more mafic silicic rocks such as the obsidian described by Lacroix (1930, analysis D). Comendites have the same chemical characteristics as pantellerites, but are less mafic and less peralkaline. Soda rhyolite is a more general term, which, in addition to comendite, includes metaluminous and subaluminous soda-rich rhyolites and sodic rhyolites with high alumina and low normative quartz content which are transitional to trachyte. Because the abnormally high iron and titanium content of pantellerites is highly atypical of rocks which are generally termed rhyolite, the specific term "pantellerite" should be used when it is warranted, instead of the more general term "soda rhyolite."

Groundmass chemistry is critical in the interpretation of peralkaline rocks. The phenocrysts included in a whole-rock analysis of a porphyritic rock will tend to obscure the true degree of differentiation that the magma has undergone. Thus a pantelleritic liquid may be so diluted by sanidine and quartz phenocrysts as to make the whole-rock analysis that of a comendite. Moreover, because of the vagaries of crystal accumulation and separation, whole-rock analyses will not, in general, represent a previously existing magmatic liquid.

concentration of Be, Nb, Pb, Sn, Th, the rare earths, and the rare alkalis are abnormally high, being as much as 10 times greater than in a typical comendite glass from the Spearhead Member of the Thirsty Canyon Tuff (table 2, column 4), which in turn is several times richer in most of these elements than the crustal average for granitic rocks (Taylor, 1964).

Analytical data on other alkalic and peralkalic glasses and rocks from southern Nye County show that the concentration of most of the minor elements discussed above varies systematically with the concentration of zirconium. This suggests that the Pantellerian pantellerites, which contain less than half the zirconium of the Gold Flat Member, also contain appreciably less Be, Nb, and rare earths than the Gold Flat.

GENESIS

The normative quartz-albite-orthoclase proportions of analyzed pantellerites are very similar to minima of the "pantellerite" systems studied experimentally by Carmichael and MacKenzie (1963), strongly suggesting that crystal-liquid equilibria are involved in the generation of natural pantelleritic liquids. The normative quartz-feldspar proportions of the glass from the Gold Flat Member are compatible with this interpretation. The available analyses of comenditic and pantelleritic glasses show a strong positive correlation between both alkali/alumina and $\text{Na}_2\text{O}/\text{K}_2\text{O}$ ratios and total iron. This relation, readily explainable by crystal fractionation, is difficult if not impossible to understand if the high sodium and total alkali contents of pantellerite liquids are explained by volatile transfer of alkalis.

The high iron, titanium, zirconium, and halogen content of pantellerites and their very low magnesium content suggest that they represent very late stage residual liquids. Moreover, the abnormally high concentration of rare earths, niobium, and other minor elements in the glass from the Gold Flat Member, analogous to that in the late-crystallizing fractions of alkaline intrusive bodies, as well as the high gallium to aluminum and rubidium to potassium ratios, can best be explained by extreme fractional crystallization. The concentration of these minor elements in the liquid portion of the pantellerite magma, shown by the whole-rock spectrographic analyses (table 2, columns 2, 3), is consistent with such an origin.

Carmichael and MacKenzie (1963) believe that pantellerite liquids form by the separation of sodium-rich alkali feldspar (Ab_{60} to Ab_{70}), sodic plagioclase, and pyroxene phenocrysts from melts of trachytic composition. To develop a high Na_2O to K_2O ratio as well as a high alkali to alumina ratio in a residual liquid by the separation of feldspar, the feldspar must be more

potassic than the liquid from which it crystallizes. Although trachyte lavas and tuffs were erupted from the Black Mountain volcano both before and after the emplacement of the Gold Flat Member, the ratio of Na_2O to K_2O in these rocks never exceeds unity. A melt with the extremely high Na_2O to K_2O ratio of the glass from the Gold Flat Member obviously cannot form by removal of sanidine with a Na_2O to K_2O ratio greater than 1.1 from a liquid containing subequal amounts of these oxides.

Mafic and low-silica intermediate alkalic rocks in general have much higher Na_2O to K_2O ratios than do alkalic trachytes. The Gold Flat Member, and possibly most pantellerites, are thus tentatively believed to have been generated by the direct fractionation of liquids of alkali basalt, mugearite, or "mugearite-trachyte" composition without the existence of magma of trachytic composition as an intermediate phase.

OTHER PANTELLERITE OCCURRENCES

Although a few comendites have previously been recognized in the western hemisphere, only two rocks that might accurately be termed pantellerites have been described. The groundmass composition computed from the whole-rock chemical analyses and the modal data given by Walker (1961) from a study in Oregon are, however, somewhat richer in aluminum and poorer in sodium than the Pantelleria glasses. The rock from Texas described by Lord (1900) is likewise high in alumina content. The obsidian artifact from Chichen Itza, Mexico, analyzed by Washington (1923) contains much less iron and titanium than do the Pantelleria glasses, and should be termed a comendite.

The Gold Flat Member is also one of the few pantellerite ash-flow tuffs known. Others occur on the island of Pantelleria and on the Eolian islands, both in the Mediterranean (Borsi and others, 1963), and published descriptions strongly suggest that similar rocks are present in at least several areas in east Africa.

REFERENCES

- Annell, Charles, 1964, A spectrographic method for the determination of cesium, rubidium, and lithium in tektites, in *Geological Survey Research 1964*: U.S. Geol. Survey Prof. Paper 501-B, p. B148-B151.
- Bastron, Harry, Barnett, P. R., and Murata, K. J. 1960, Method for the quantitative spectrochemical analysis of rocks, minerals, ores, and other materials by a powder d-c arc technique: U.S. Geol. Survey Bull. 1084-G, p. 165-182.
- Borsi, S., Marinelli, G., Mazzocini, F., Mittempergher, M., and Tedesco, C., 1963, Reconnaissance of some ignimbrites at Pantelleria and Eolian Islands: *Bull. Volcanol.*, v. 25, p. 359-363.
- Carmichael, I. S. E., 1962, Pantelleritic liquids and their phenocrysts: *Mineralog. Mag.*, v. 33, p. 86-113.

- Carmichael, I. S. E., and MacKenzie, W. S., 1963, Feldspar-liquid equilibria in pantellerites—an experimental study: *Am. Jour. Sci.*, v. 261, p. 382-396.
- Christiansen, R. L., and Noble, D. C., 1965, Black Mountain volcanism of southern Nevada [abs.]: *Geol. Soc. America Spec. Paper*. [In press]
- Haskin, Larry, and Gehl, M. A., 1963, The rare-earth contents of standard rocks G-1 and W-1 and their comparison with other rare-earth distribution patterns: *Jour. Geophys. Research*, v. 68, p. 2037-2043.
- Lacroix, A., 1930, Les roches hyperalcalines du massif du Fantalé et du col de Balla (Abyssinie), p. 89-102, in Teilhard de Chardin, P., Lamare, P., Dreyfuss, M., Lacroix, A., and Basse E., *Études géologiques en Éthiopie, Somalie, et Arabie Méridionale*: *Soc. géol. France Mem.* 14, 155 p.
- Lord, E. C. E., 1900, Report on igneous rocks from the vicinity of San Carlos and Chispa, Texas, in Vaughn, T. W., Rio Grande coal fields of Texas: *U.S. Geol. Survey Bull.* 164, p. 88-95.
- Myers, A. T., Havens, R. G., and Dunton, P. J., 1961, A spectrochemical method for the semiquantitative analysis of rocks, minerals, and ores: *U.S. Geol. Survey Bull.* 1084-I, p. 207-229.
- Noble, D. C., 1965, Ground-water leaching of sodium from quickly cooled volcanic rocks [abs.]: *Am. Mineralogist*. [In press]
- Noble, D. C., Anderson, R. E., Ekren, E. B., and O'Connor, J. T., 1964, Thirsty Canyon Tuff of Nye and Esmeralda Counties, Nevada: Art. 126 in *U.S. Geol. Survey Prof. Paper* 475-D, p. D24-D27.
- Noble, D. C., Kistler, R. W., Christiansen, R. L., Lipman, P. W., and Poole, F. G., 1965, Close association in space and time of alkalic, calc-alkalic, and calcic volcanism in southern Nevada [abs.]: *Geol. Soc. America Spec. Paper*. [In press]
- Peck, L. C., 1964, Systematic analysis of silicates: *U.S. Geol. Survey Bull.* 1170, 89 p.
- Peck, L. C., and Smith, V. C., 1964, Spectrophotometric determination of fluorine in silicate rocks: *Talanta*, v. 11, p. 1343-1347.
- Peck, L. C., and Tomasi, E. J., 1959, Determination of chlorine in silicate rocks: *Anal. Chem.*, v. 31, p. 2024-2026.
- Ross, C. S., and Smith, R. L., 1955, Water and other volatiles in volcanic glasses: *Am. Mineralogist*, v. 40, p. 1071-1089.
- Shapiro, Leonard, and Brannock, W. W., 1962, Rapid analysis of silicate, carbonate, and phosphate rocks: *U.S. Geol. Survey Bull.* 1144-A, p. A1-A56.
- Smith, R. L., 1960, Zones and zonal variations in welded ash flows: *U.S. Geol. Survey Prof. Paper* 354-F, p. 149-159.
- Taylor, S. R., 1964, Abundance of chemical elements in the continental crust—a new table: *Geochim. et Cosmochim. Acta*, v. 28, p. 1273-1285.
- Vaughn, W. W., Cramer, W. G., and Sharp, W. N., 1965, Gamma activation device for low-level beryllium analysis, in *Geological Survey Research 1965*: *U.S. Geol. Survey Prof. Paper* 525-B, p. B151-B154.
- Walker, G. W., 1961, Soda rhyolite (pantellerite?) from Lake County, Oregon: Art. 200 in *U.S. Geol. Survey Prof. Paper* 424-C, p. C142-C145.
- Washington, H. S., 1913, The volcanoes and rocks of Pantelleria, pts. 1 and 2: *Jour. Geology*, v. 21, p. 653-670; 683-713.
- 1914, The volcanoes and rocks of Pantelleria, pt. 3: *Jour. Geology*, v. 22, p. 16-27.
- 1923, Obsidian from Copan [Honduras] and Chichen Itza [Yucatan]: *Jour. Washington Acad. Sci.*, v. 11, p. 481-487.
- Zies, E. G., 1960, Chemical analysis of two pantellerites: *Jour. Petrology*, v. 1, p. 304-308.



PRECIPITATION AND RECYCLING OF PHOSPHATE IN THE FLORIDA LAND-PEBBLE PHOSPHATE DEPOSITS

By Z. S. ALTSCHULER, Washington, D.C.

Abstract.—Precipitated apatite and layered claylike apatite occur in the weathered and crudely reworked residuum of the Hawthorn Formation and are sources of some pellets and pebbles reworked into the overlying Bone Valley Formation. The occurrence of both types of apatite demonstrates that the phosphate pellets are not principally of fecal origin. The residual zone underlying the Bone Valley is characterized by rapid alternations of quiet-water sedimentation and turbulent reworking. The immaturity of first-cycle clastics derived from this littoral environment suggests that the well-rounded pellets that occur in the Hawthorn and Bone Valley Formations are the products of more extensive reworking.

Many marine phosphate deposits are composed of nodular or pelletal apatite which, by virtue of internal structure or texture or the petrography of its setting, can be ascribed to primary or early diagenetic origins. However, the phosphate pellets of the Hawthorn and Bone Valley Formations, in the land-pebble district of central Florida, are petrologically ambiguous. They are distinguished by derivative textures, and show little evidence of primary deposition. They lack (1) the spherulitic structure of the concretionary phosphates in the Cretaceous shales of Montana (Pecora and others, 1962) and Wyoming (McConnell, 1935), (2) the agglomerate or accretionary textures shown by the oolitic phosphate like that in the Phosphoria Formation (McKelvey and others, 1953) and the Karatau deposits in Kazakhstan (Bushinsky, 1964); and (3) the filled protozoan tests of the North African phosphorites (Cayeux, 1939).

PETROGRAPHY OF THE PELLETS

The pellets in the Bone Valley Formation are largely detrital. The Bone Valley is a Pliocene transgressive deposit of graded-bedded marine and estuarine clayey and pebbly sands. Its phosphate was concentrated and reworked from the underlying Hawthorn Formation as phosphatized and residually enriched weathering debris. The weathering and marine reworking of the Hawthorn

pellets are manifest in their Bone Valley occurrence in better rounding, in lighter colors (indicative of leaching and oxidation), and in a lower content of carbonate impurity and higher contents of phosphate and fluorine (Cathcart and McGreavy, 1950).

In the Hawthorn Formation, which is an extensive body of sparsely phosphatic Miocene limestones, dolomites, and marls, the pellets occur as lustrous ellipsoids and ovules of sand to granule size. These are crystalline aggregates of carbonate-fluorapatite (Altschuler and others, 1952) so fine grained as to be optically isotropic, or only faintly birefringent, and microgranular in texture. They are generally dark and structureless. Fine-grained inclusions of quartz and calcite and rhombs of dolomite are common, and phosphate pseudomorphs of rhombs are also present. Many pellets contain fine debris of protozoan tests and finely divided organic matter and iron oxides. The organic matter may be rudely clustered and aligned, and the internal clusters may rarely display flow texture, as in fecal pellets. However, these pellets in the land-pebble field are totally lacking in the surface markings and shaping that would make fecal-extrusion origin a certainty. Other pellets are clearly detrital fragments of bone or replaced fossiliferous limestone. Still others are featureless, difficult to classify, and possibly syngenetic.

The presence of a small percentage of rounded refractured grains offers proof that some Hawthorn pellets have been transported. Transport is even more widely inferred from additional evidence: Quartz inclusions in pellets are commonly finer than the quartz deposited with the pellets, the pellets are generally highly rounded and polished, and many pellets have bleached outer rims.

Thus the ovoidal pellets of the land-pebble district pose a problem, for whether they originate principally as fecal pellets as suggested by Bushinsky (1964) for all phosphate pellets, as replacements of nonphosphatic pellets, or as detrital fragments of syngenetic or re-

placement materials, they clearly demand a preexisting parent material or an earlier environment. This problem was recognized in other deposits by Cayeux (1939), who postulated that the pellets require two spatially separate environments—an area of precipitation in which pellets were formed by agitation, and an area of accumulation to which pellets were transported by bottom currents. Many beds in the Phosphoria Formation contain irregular phosphate pellets embedded in a cement or matrix of texturally similar phosphate, and many of the Phosphoria oolites contain cores of pelletal phosphate (Lowell, 1952; Cressman and Swanson, 1964). Similar direct progressions from precipitated to accretionary and reworked phases are seen in the Karatau phosphorites (Bushinsky, 1964; fig. 3). But layered precursors of clastic phosphate in the land-pebble phosphates are obscure.

In 1949, Altschuler and Boudreau reported observations of primary deposits of phosphate intimately associated with their clastic derivatives in the Bone Valley Formation, but the report was classified until 1956. After 1956 the authors have been engaged in other phases of the work. The current expansion of interest in the phosphates, and in their exploitation, recreates a forum and a stimulus to present anew our unpublished data and explanations on primary phosphate, along with more recent facts and suggestions.

PRE-BONE VALLEY WEATHERING AND CONCENTRATION

Preceding the deposition of the Bone Valley Formation the Hawthorn was subaerially weathered and its surface was marked by irregularities, karst features, and river channels (Cathcart, 1963). Its uppermost zone characteristically became enriched in the less soluble constituents, and it has therefore been referred to as a zone of residual enrichment. It is marked not merely by static leaching, however, but also by penecontemporaneous slump and brecciation, by crude lensing and bedding explainable by colluvial and fluvial processes, by recementation of carbonates, and by phosphatization (Altschuler and others, 1964a, b). The concurrent operation of these processes is clearly implied in the subaerial weathering and development of karst features on phosphatic limestones.

There is also evidence of contemporaneous marine incursion and reworking in the form of extensive burrowing, and in the many clastic fragments of littoral fossils, with molds and casts showing detailed preservation of small structures and surface ornamentation. This indicates nearby derivation and short transport.

PRIMARY PRECIPITATION AND RECYCLING OF APATITE

In addition to the mechanical concentration of apatite during weathering, chemical concentration, or precipitation, of apatite occurred during the marine incursions in the zone of residual concentration. It is manifest in thin (1–5 mm), discontinuous seams of brown hard aphanitic apatite. These deposits encrust surfaces of clay and dolomite, and coat and impregnate the inner linings of animal burrows. In many places the precipitated apatite infiltrates and incorporates sand and silt from the underlying substrate, or simply includes detritus rolled in during growth. Some of the crusts contain scattered protozoan-test fragments like those in the pellets of the Hawthorn and Bone Valley Formations. Fragments representing all stages of phosphate encrustation and incorporation occur as disoriented slump breccia in filled borings and as angular clastic pebbles reworked into adjoining or overlying lentils. Furthermore, small, angular or subrounded brown flakes and granules derived from this precipitated apatite occur among the other apatite pellets in overlying sands of the lowermost Bone Valley Formation. They may be distinguished from the more “normal” older Hawthorn detritus by their flatter shapes and greater angularity. They nevertheless indicate a pattern of derivation which becomes obscured through more extensive transport and reworking, but which may be of considerable importance in the generation of rounded pellets.

Striking additional examples of the reworking of precipitated phosphate are seen in the coarse black and brown pebbles and cobbles of phosphatized limestone and dolomite which have been transgressively reworked into the graded-bedded lower unit of the Bone Valley Formation. These pebbles are commonly flat or plate-like fragments with outer zones of black or brown organic-rich apatite, and cores of only partly replaced carbonates. Figure 1 illustrates a pebble showing two successions of recycling. Phosphate precipitation began in a quiet organic-rich environment colonized by boring organisms, and deposited a layer of black apatite that was devoid of coarse detritus. Precipitation was followed by high-energy erosion that tore off a slab of coherent precipitate and adjoining substrate. The fragment, probably somewhat eroded, was then redeposited in obverse position in a second quiescent lagoon or pan, where again apatite was precipitated from water of high biologic activity, coating the other side of the fragment and filling the old borings with a new generation of apatite of different color. The second surface was also bored prior to incorporation of the pebble in the Bone Valley gravels.

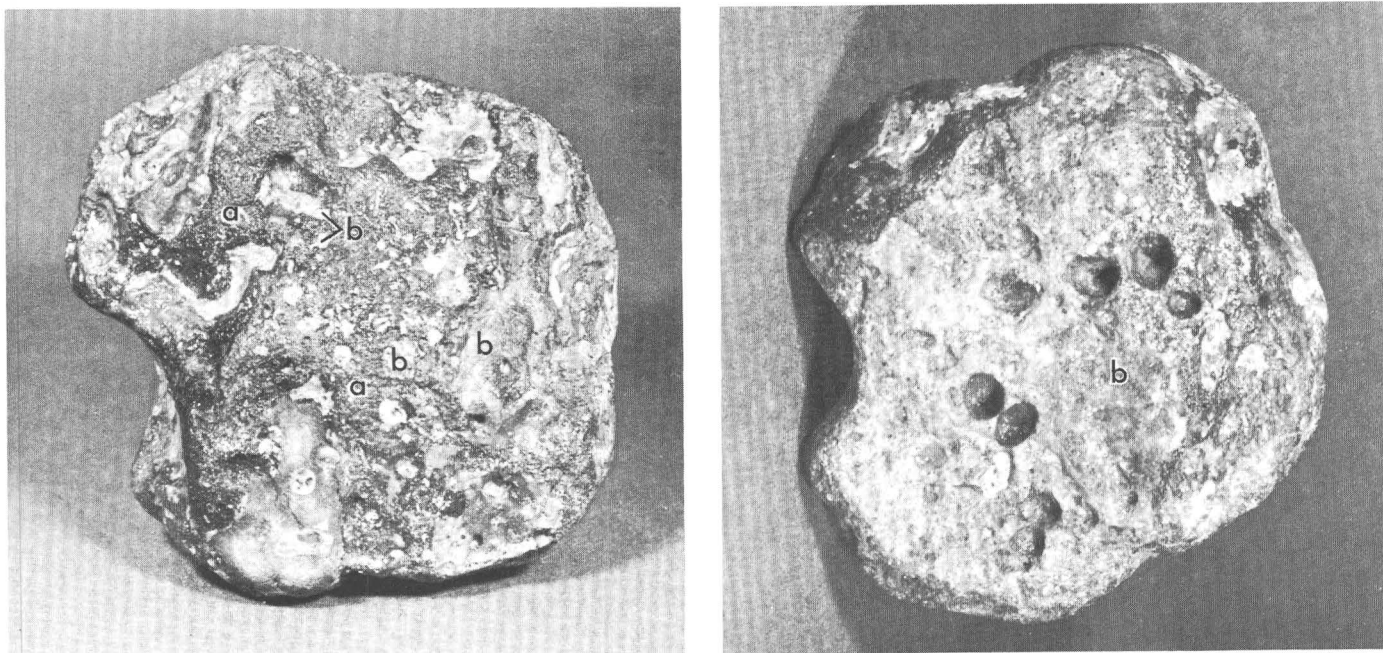


FIGURE 1.—Cobble of phosphatized limestone (natural size), Bone Valley Formation, Agricola, Fla., exemplifying two cycles of precipitation and reworking. *Left*, Black coating of precipitated apatite (a), showing borings filled with second generation of brown apatite (b). *Right*, Obverse of cobble, showing second coating of apatite (b) and later borings.

Another important variety of parent material, found in the Homeland, Fla., area, consists of cements and clayey members of graded sets in the lower Bone Valley. It is a mixture of very fine grained apatite and clay, and was described by Altschuler and Boudreau (1949) as follows:

The layering consists of a cycle of units ranging from 3 mm. to 1 cm. in thickness. The complete cycle may be broken down into the following four phases in order of superposition:

- (4) Medium- to fine-grained sand of quartz and detrital phosphate with a phosphatic cement
- (3) Coarse-grained sand of quartz and detrital phosphate with a phosphatic cement or matrix
- (2) Pebbles of claylike phosphate
- (1) Bedded claylike phosphate

Not all of the units are present in every cycle.

In much of this layering the units are not sharply defined, but grade into one another. This is particularly true where the layers of claylike phosphate are absent, and the succession becomes merely one of alternating fine- and coarse-grained material.

Some of the claylike phosphate layers show shrinkage cracks [or borings] which are filled with material of different appearance. The material filling the shrinkage cracks is detrital at some horizons (see pl. 9 [fig. 2 of this paper]) but in many samples it is a form of differently colored precipitated phosphate. Thus, the filled cracks do not necessarily represent a period of subaerial exposure. The cracking may be due to post-depositional shrinkage and the filling may be the result of wave or current action or of circulating ground-water solutions.

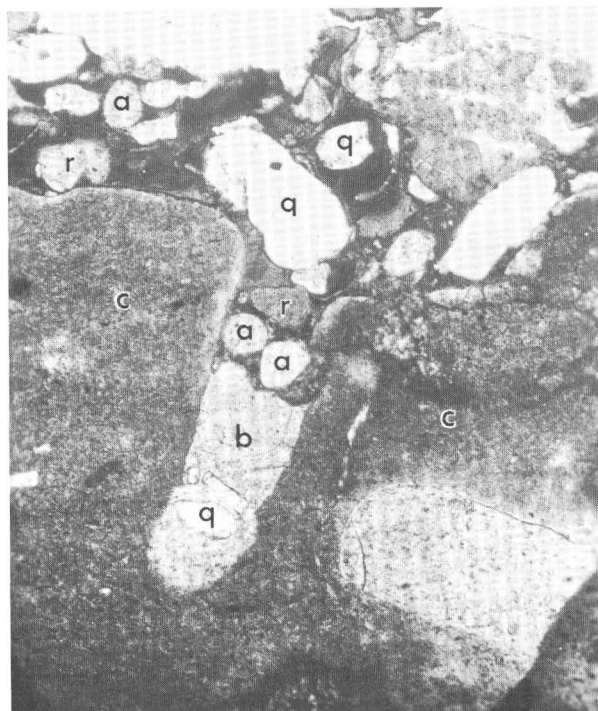


FIGURE 2.—Phosphatic clay from graded beds in the Bone Valley Formation, Homeland, Fla. Phosphatic clay (c) composed of apatite, millisite, and kaolinite, showing burrow or mudcrack filled with detrital quartz (q), apatite (a), bleached phosphatic clay (b), and reworked phosphatic clay (r). $\times 46$, crossed nicols. (From Altschuler and Boudreau, 1949.)

The bedding cycle outlined above may have originated in several ways. However, whatever interpretation is finally adopted must account for several salient features: the gradation from coarse- to fine-grained material, the probable derivation of the pebble layers by erosion of the claylike layers, and the possibility of occasional subaerial exposure due to very slight changes in sea level. This combination of features can be explained in a general manner by assuming an area of shallow-water phosphate deposition subjected to wave and current action of fluctuating competence. Recurrent and possibly seasonal changes associated with climatic variation could easily cause an alternation of periods in which currents were of greater and lesser competence. A possible interpretation is illustrated diagrammatically below:

<i>Possible interpretation</i>	<i>Lithology</i>
Submergence or greater wave activity.	Pebbles of claylike phosphate.
<i>Possible emergence</i>	
Quiescence-----	Claylike bedded phosphate.
(Wave activity diminishing upward)	Medium- to fine-grained sand of quartz and detrital phosphate, phosphatic cement.
Submergence or greater wave activity.	Coarse-grained sand of quartz and detrital phosphate, phosphatic cement.
	Pebbles of claylike phosphate and coarse quartz.
<i>Possible emergence</i>	
Quiescence-----	Claylike bedded phosphate.

Claylike phosphate is also found as irregular layers of white, chalky, aphanitic and lightweight apatite interspersed with true clay in the residual zone. It is commonly impure even if devoid of quartz or clastic apatite, being admixed with clay and occasionally with carbonates. Many white pebbles of obviously first-cycle nature, both in the residual zone as angular fragments and in the Bone Valley as rounded fragments, must derive from such material. This white claylike apatite may be widespread parent material in the land-pebble field, but it is not unequivocally a precipitated material. Its dominantly white color, despite occurrence in green or gray matrix, suggests that it is material that was bleached or weathered prior to deposition.

Similar materials occur in the "hardrock" phosphate deposits of northern Florida as a fine phosphatized limestone powder interstitial to the secondarily phosphatized limestone boulders (Sellards, 1913). Unequivocally supergene deposits of white apatite also occur in the Bone Valley Formation (Altschuler and Boudreau, 1949) and in the coastal plain of New Jersey (J. P. Owens, 1963, oral communication) under zones of leaching. The hydraulic operations by which the hard-rock phosphates were mined in the past used to create artificial lacustrine deposits of "white soft-rock" phos-

phates. It appears that natural deposits of weathered fine material, composed of phosphatized clay-size limestone and of clay, were common at some stages of the subaerial exposure and reworking of the Hawthorn Formation, and that similar materials were also washed into nearshore lagoons and basins during normal stages of clay accumulation. Such materials, even though of replacement origin, are nevertheless primary depositional precursors of first-cycle white phosphate pebbles.

The quantitative importance of the precipitated apatite crusts and of the claylike phosphate is difficult to assess without amassing quantitative petrographic data. The apatite pebbles of the Bone Valley Formation are largely made up of replaced Hawthorn limestone, although many of these pebbles are also veneered with precipitated apatite. The pellets in the Bone Valley may have been largely reworked as Hawthorn pellets, because many pellets also contain the veneers of later apatite. However, precipitated apatite is clearly the source of some first-cycle pellets in the Bone Valley Formation and may be an important source of original Hawthorn pellets. Bedded claylike white phosphate is relatively rare in the land-pebble district. Its importance as a source material should be evaluated from the occurrence of first-cycle pellets and pebbles deposited as white or light-colored detritus, in the midst of darker matrix.

GENETIC IMPLICATIONS

The occurrence of both precipitated and claylike deposits of apatite in the residual, or transitional, zone of the Hawthorn Formation establishes parent materials for a variety of pellet and pebble types in the Bone Valley Formation. However, the precipitated apatite does not necessarily reflect "normal" marine precipitation but rather a form of chemical recycling in which shallow marine apatite is derived from highly phosphatic waters enriched by weathering of low-grade phosphorites on the adjoining landmass. It is of interest to note that this process, as well as the accumulation of detrital flour as layers of claylike apatite, took place in a littoral environment in shallow quiescent basins. Both types of deposit were also characteristically reworked in turbulent transport by shortlived events, possibly single storms or tidal events.

In the residual zone these characteristics of cyclicality, and of rapid alternation of chemical and clastic facies, found expression in rudimentary bedding, in poor sorting, poor rounding, and in chaotically oriented soft fragments of apatite, attapulgite, montmorillonite, and dolomite, above their bleached and burrowed parent

layers. In these circumstances the moderately well rounded nature of most of the Hawthorn pellets suggests a history of extensive reworking, and possibly distant transport, rather than a derivation as syngenetic or fecal material from the immediate environment.

REFERENCES

- Altschuler, Z. S., and Boudreau, C. E., 1949, A mineralogical and chemical study of the leached zone of the Bone Valley Formation—A progress report: U.S. Geol. Survey Trace Elements Inv. 102, 67 p.
- Altschuler, Z. S., Cisney, E. A., and Barlow, I. H., 1952, X-ray evidence of the nature of carbonate-apatite [abs.]: Geol. Soc. America Bull., v. 63, p. 1230-1231.
- Altschuler, Z. S., Cathcart, J. B., and Young, E. J., 1964a, Geology and geochemistry of the Bone Valley Formation and its phosphate deposits, west-central Florida; Geol. Soc. America Guidebook [field trip No. 6], Ann. Mtg., Miami Beach, Fla., 68 p.
- 1964b, Geology and geochemistry of the Bone Valley Formation and its phosphate deposits, west-central Florida: Geol. Soc. America Roadlog [field trip No. 6], Ann. Mtg., Miami Beach, Fla., 11 p.
- Bushinsky, G. I., 1964, On shallow water origin of phosphorite sediments, *in* van Straaten, L.M.J.U., ed., Delta and shallow marine deposits: Amsterdam, Elsevier Publishing Co., p. 62-70.
- Cathcart, J. B., 1963, Economic geology of the Plant City quadrangle, Florida: U.S. Geol. Survey Bull. 1142-D, p. D1-D56.
- Cathcart, J. B., and McGreavy, L. J., 1959, Results of geologic exploration by core drilling, 1953, land-pebble phosphate district, Florida: U.S. Geol. Survey Bull. 1046-K, p. 221-298.
- Cayeux, Lucien, 1939, Les phosphates de chaux sédimentaires de France (France Métropolitaine et d'Outre-Mer), v. 3: Paris, Imprimerie Nationale.
- Cressman, E. R., and Swanson, R. W., 1964, Stratigraphy and petrology of the Permian rocks of southwestern Montana: U.S. Geol. Survey Prof. Paper 313-C, p. 275-569.
- Lowell, W. R., 1952, Phosphate rocks in the Deer Creek-Wells Canyon area, Idaho: U.S. Geol. Survey Bull. 982-A, p. 1-52.
- McConnell, Duncan, 1935, Spherulitic concretions of dahllite from Ishawooa, Wyoming: Am. Mineralogist, v. 20, p. 693-698.
- McKelvey, V. E., Swanson, R. W., and Sheldon, R. P., 1953, The Permian phosphorite deposits of western United States: Internat. Geol. Cong., 19th, Algiers 1952, Comptes rendus, sec. 11, p. 45-65.
- Mansfield, G. R., 1927, Geography, geology and mineral resources of part of southeastern Idaho: U.S. Geol. Survey Prof. Paper 152, 453 p.
- Pecora, W. T., Hearn, B. C., Jr., Milton, Charles, 1962, Origin of spherulitic phosphate nodules in basal Colorado Shale, Bearpaw Mountains, Montana: Art. 12 *in* U.S. Geol. Survey Prof. Paper 450-B, p. B30-B35.
- Sellards, E. H., 1913, Origin of the hardrock phosphate deposits of Florida: Florida Geol. Survey Fifth Ann. Rept., p. 27-80.



DISTRIBUTION OF TANTALUM IN SOME IGNEOUS ROCKS AND COEXISTING MINERALS OF THE SOUTHERN CALIFORNIA BATHOLITH

By DAVID GOTTFRIED and JOSEPH I. DINNIN,
Washington, D.C.

Abstract.—Neutron-activation and chemical analyses of tantalum have been made on 8 comagmatic igneous rocks, 7 pairs of coexisting biotite and hornblende, and 11 samples of the accessory minerals sphene, ilmenite, and magnetite. The results help fill a marked gap in the published geochemical literature. Tantalum content is lowest in the gabbroic rocks, 0.13 to 0.24 ppm, increases to a maximum in the tonalities, 0.45 ppm, and remains relatively constant in the granodiorite and quartz monzonites, 0.38 to 0.45 ppm. Biotite and hornblende, which account for about 80 percent of the tantalum in a tonalite and quartz monzonite, are progressively enriched in tantalum in the more siliceous rocks, but concomitantly decrease in abundance. The distribution coefficient, Ta in biotite/Ta in hornblende, ranges from about 2 in tonalites to 1 in granodiorite and 0.5 in the quartz monzonites. Sphene has the greatest tantalum content, 36 to 100 ppm, of any mineral in the batholith; ilmenite contains 6 to 10 ppm, and magnetite 0.3 to 1.8 ppm. From the limited data available the average tantalum content of the batholith is estimated to be 0.4 ppm.

Since the comprehensive study of Rankama (1944), our knowledge of the geochemistry of tantalum in igneous rocks has increased very little. The chief difficulty has been the lack of suitable analytical methods for the analysis of tantalum in the very low parts-per-million range. Consequently, systematic studies on the distribution of tantalum in igneous rocks and minerals of batholithic complexes of the calc-alkalic magma type are still virtually nonexistent. Recently, however, neutron-activation analysis has been applied to the determination of the tantalum content of a limited number of igneous rocks by Morris and Olya (1960), Atkins and Smales (1960), Butler and Thompson (1962), and Butler and Smith (1962). The precision of this method is such that quantitative analyses can now be made to within ± 10 percent on rocks and minerals containing only a few tenths of a part per million of tantalum. Analyses for tantalum by this technique have been uti-

lized in this report and were particularly valuable for evaluating the results obtained by a chemical method developed specifically for the determination of tantalum in the parts-per-million range in rocks and minerals. The neutron-activation analyses reported here were made by J. Thompson of the Imperial College of Science and Technology, University of London, to whom we are extremely grateful.

The chemical method used for the determination of tantalum (Dinnin, report in preparation) is based upon the selective extraction from fluoride solution of a tantalum-triphenylmethane complex. Tantalum is separated with niobium from the bulk of the rock-forming elements by extraction with methylisobutylketone from a mixture of dilute hydrofluoric and hydrochloric acids. The earth acids are stripped with dilute hydrogen peroxide solution, and the tantalum fluoride-crystal violet complex is selectively extracted from dilute hydrofluoric acid with benzene. The absorbance of the extracted solution is compared at 600 millimicrons with standards similarly extracted. A few tenths of a part per million of tantalum can be determined on a 1-gram sample with an uncertainty of 0.1 part per million.

TANTALUM IN ROCKS

The igneous rocks of the Southern California batholith provide us with an excellent opportunity to follow the behavior of tantalum through the various stages of differentiation of a calc-alkalic magma. Detailed field and laboratory studies of the igneous rocks by Larsen (1948) and Miller (1937) and of minerals by Larsen and Draisin (1950) make it possible to relate analyses for tantalum to the geologic occurrence, mineralogy, and chemical composition of some of the rocks and minerals of the batholith. The additional rocks and minerals used in this study are from the same rock

units described by them. Neutron-activation analyses for tantalum on eight selected rocks ranging in composition from olivine norite to a highly siliceous quartz monzonite are listed in table 1. Figure 1 shows the

TABLE 1.—Results of neutron-activation analyses of tantalum in igneous rocks from the Southern California batholith

[All determinations by J. Thompson, University of London]

Sample No.	Rock type	Position $\frac{1}{2}\text{SiO}_2 + \text{K}_2\text{O}$ —CaO—FeO —MgO	Tantalum (ppm)
SLRM 354	San Marcos Gabbro (olivine norite).	-16.0	0.13
SLRM 299	San Marcos Gabbro (hornblende gabbro).	-11.6	.20
LTS-1	San Marcos Gabbro (hornblende norite).	-7.5	.24
BL60-2	Lakeview Mountain Tonalite.	+8.6	.45
BL60-1	Bonsall Tonalite	+9.5	.44
S-2	Woodson Mountain Granodiorite.	+23.2	.38
EL38-167	Quartz monzonite of Rubidoux Mountain, coarse phase.	+25.5	.45
EL38-265	Quartz monzonite of Rubidoux Mountain, fine phase.	+27.7	.38

relation of the tantalum content of the rocks to their chemical composition, on a variation diagram of the type proposed by Larsen (1938). These data clearly show that tantalum is indeed an extremely rare element, inasmuch as none of these rocks contains more than half a part per million tantalum. Tantalum content is lowest in the gabbroic rocks and appears to increase systematically from 0.13 ppm in the lime-rich silica-poor olivine norite to 0.24 ppm in the more siliceous hornblende norite. This progressive increase continues up to the tonalites, which contain about 0.45 ppm tantalum. The granodiorite contains 0.38 ppm tantalum, and the quartz monzonites 0.38 and 0.45 ppm tantalum. Thus, tantalum shows approximately a twofold increase in absolute enrichment in the early stages of differentia-

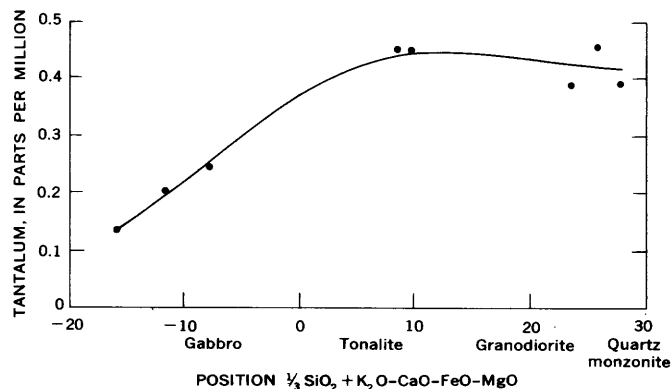


FIGURE 1.—Tantalum in igneous rocks of the Southern California batholith, plotted against the composition of the rocks.

tion, reaching a maximum in the tonalites, and then either remains relatively constant or decreases slightly in the later differentiates (fig. 1). Obviously, more extensive data are required to define the trend more precisely.

TANTALUM IN COEXISTING BIOTITE AND HORNBLENDE

Data on the manner in which tantalum is distributed among the various minerals of these rocks are of great importance for understanding the pattern of the variation of tantalum in the suite as a whole. Studies by Rankama (1944, 1948) and Fleischer and others (1952) on tantalum and niobium have clearly shown that there is a strong geochemical affinity between these elements and titanium. The ionic radii of these elements are 0.69 Å for Nb^{+5} , 0.68 Å for Ta^{+5} and 0.68 Å for Ti^{+4} (Arhens, 1952). An excellent discussion of the crystal chemistry and mineralogy of these elements has been published by Kuzmenko (1961). On the basis of this information, selected suites of the titanium-bearing minerals biotite, hornblende, sphene, ilmenite, and magnetite—from a wide range of rock types from the Southern California batholith—were analyzed for tantalum.

Analyses for tantalum in the hornblendes and biotites are listed in table 2, which also compares the analyses by neutron activation with those determined by the chemical procedure. Except for the wide discrepancy on one sample (EL 38-167, hornblende) the agreement between the completely independent methods is excellent. Plots of the tantalum content of these minerals against the chemical composition of their host rocks (fig. 2) yield smooth, well-fitting variation curves. These curves show that biotite and hornblende are progressively enriched in tantalum in the more siliceous rocks. However, it is significant that in the tonalites, biotite contains about twice as much tantalum as the coexisting hornblende; whereas, in the granodiorite, the tantalum content is the same in each mineral, and in the quartz monzonites, biotite contains about half as much tantalum as the hornblende.

Figure 3 shows the partitioning of tantalum between seven pairs of coexisting biotite and hornblende. The points fall on a smooth curve on this distribution diagram, and it appears likely that these coexisting minerals crystallized under equilibrium conditions. Mueller (1963) has examined the chemical data on five pairs of coexisting biotite and hornblende published by Larsen and Draisin (1950) and points out the possibility that a rather high degree of equilibrium was attained by these minerals with respect to iron and magnesium. The variation of the distribution coefficient, tantalum in

TABLE 2.—Tantalum in hornblende and biotite from igneous rocks of the Southern California batholith

Sample No.	Mineral	Parent rock	Position $\frac{1}{2}\text{SiO}_2 + \text{K}_2\text{O} - \text{CaO} - \text{FeO} - \text{MgO}$	Tantalum (ppm)		Distribution coefficient ¹
				Chemical	Neutron activation	Ta in biotite Ta in hornblende
LTS-1	Hornblende	San Marcos Gabbro (hornblende norite).	-7.5		0.17	
BL60-6	Hornblende	Green Valley Tonalite	+1.5	0.7		2.3
	Biotite			1.6		
BL60-2	Hornblende	Lakeview Mountain Tonalite	+8.6	.8	.88	2.1
	Biotite			1.7	1.64	
BL60-1	Hornblende	Bonsall Tonalite	+9.5	.9		1.7
	Biotite			1.5		
Ra135	Hornblende	Woodson Mountain Granodiorite	+21.2	2		1
	Biotite			2		
S-2	Biotite	Woodson Mountain Granodiorite	+23.2		1.62	
EL38-167	Hornblende	Quartz monzonite, coarse phase of Rubidoux Mountain.	+25.5	18	8.8	.4
	Biotite			6.6	6.4	
LTS-2	Hornblende	Quartz monzonite, coarse phase of Rubidoux Mountain.	+26.1	10		
	Biotite			4.8		
E138-265	Hornblende	Quartz monzonite, fine phase of Rubidoux Mountain.	+27.7	12		.5
	Biotite			6		

¹ Calculated from chemical analyses.

biotite/tantalum in hornblende, with changes in bulk chemical composition of the host rock is shown in figure 4. The coefficient ranges quite widely but systematically, from 2.3 in the most mafic tonalite to about 0.5 in the quartz monzonites. As pointed out by Neumann and others (1954) and Kretz (1961), distribution coefficients of coexisting mineral pairs can be expected to vary with composition and temperature of crystallization of the minerals. In the Southern California batholith, the composition of the magma, and hence of these minerals, has changed substantially during the course of differentiation, and crystallization may have taken place over a considerable temperature range. Thus the variations in the distribution coefficient obtained are quite expectable.

TANTALUM IN OTHER ACCESSORY MINERALS

Analyses for tantalum in titanium-bearing accessory minerals are listed in table 3. Listed in order of decreasing average tantalum content, the minerals are

TABLE 3.—Results of chemical determinations of tantalum in sphene, magnetite, and ilmenite from igneous rocks of the Southern California batholith.

Sample No.	Mineral	Parent rock	Tantalum (ppm)
G-3	Sphene	Tonalite	36
BL60-2	Sphene	Tonalite	75
S-13	Sphene	Granodiorite	80
S-9	Sphene	Granodiorite	100
LTS-1	Magnetite	Norite	0.3
S-8	Magnetite	Granodiorite	.3
S-14	Magnetite	Granodiorite	.9
	Ilmenite		10.0
S-15	Magnetite	Granodiorite	1.8
EL38-167	Magnetite	Quartz monzonite, coarse phase.	.5
	Ilmenite		6.0

sphene, ilmenite, and magnetite. Sphene, which occurs mainly in the tonalites and granodiorites, contains from 36 to 100 ppm tantalum and tends to be higher in the granodiorites. Magnetite contains from 0.3 to 1.8 ppm tantalum, the maximum Ta concentration occurring in the magnetite from a highly siliceous granodiorite. Two samples of ilmenite contain 6 and 10 ppm tantalum, indicating a twelvefold tantalum enrichment over that of magnetite from the same rocks.

TANTALUM BUDGET IN THE ROCK

The quantitative distribution of tantalum in a tonalite and a quartz monzonite is shown in table 4. The data indicate that the minerals considered in this paper account for nearly all the tantalum in the containing rocks. In each rock, biotite and hornblende account for more than 80 percent of the tantalum in the bulk rock. Most of the remaining tantalum is tied up in sphene, magnetite, and ilmenite. In the tonalite, biotite is by far the most important host mineral for tantalum; whereas in the quartz monzonite, hornblende contributes as much tantalum to the whole rock as does biotite. The data show that although the tantalum content of hornblende and biotite is greater in the quartz monzonite, these minerals are less abundant in such rocks than in the tonalites. In their study of the distribution of tantalum in granites containing biotite, ilmenite, and rutile, Znamenskii and others (1957) found that 50 to 73 percent of the tantalum in the rocks is present in biotite. However, in allanite- and sphene-bearing granitic rocks which contain about 0.3 percent sphene, at least 60 percent of the tantalum in the rocks is concentrated in sphene (Znamenskii and others, 1962; Znamenskii and Popolitov, 1964).

DISCUSSION

The data presented here show rather clearly the mineralogic control on the variation of tantalum in the igneous rocks of the Southern California batholith. The tantalum content of the rocks increases rather abruptly from the most mafic gabbro, which contains 0.13 ppm, to the tonalites, which contain 0.45 ppm. At that stage the tantalum content reaches a maximum, and

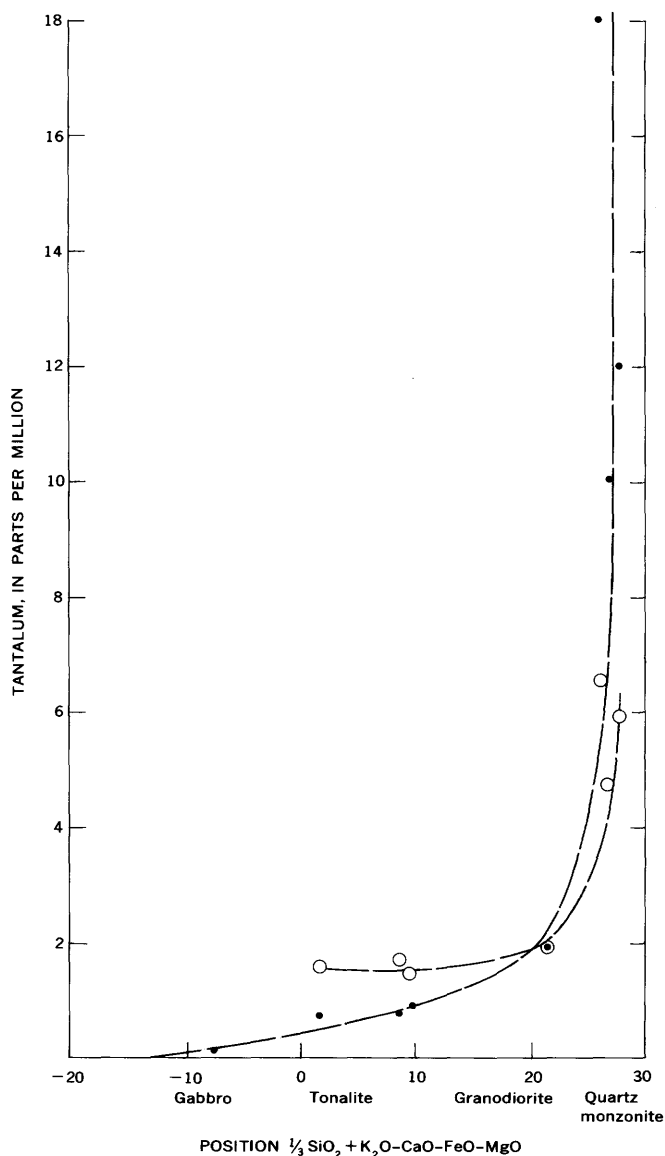


FIGURE 2.—Tantalum in biotite (circles) and hornblende (dots) plotted against composition of parent rock.

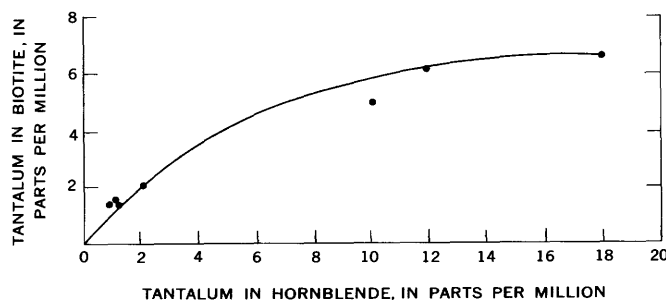


FIGURE 3.—Distribution of tantalum between biotite and hornblende.

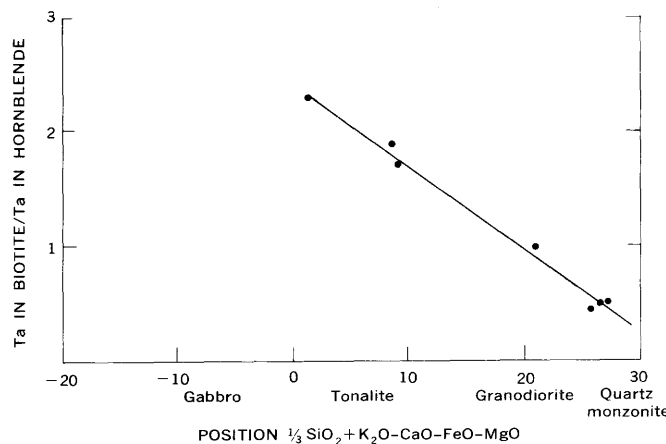


FIGURE 4.—Distribution coefficient, Ta in biotite/Ta in hornblende, plotted against composition of parent rock.

TABLE 4.—Contribution of tantalum-bearing minerals to the total tantalum budget in a tonalite and a quartz monzonite

Mineral	Tonalite BL60-2			Quartz monzonite EL38-167		
	Abundance (weight percent)	Ta (ppm)	Weight percent of mineral $\times \frac{\text{Ta(ppm)}}{10}$	Abundance (weight percent)	Ta (ppm)	Weight percent of mineral $\times \frac{\text{Ta(ppm)}}{100}$
Biotite.....	18	1.7	0.31	3	6.6	0.20
Hornblende.....	7	.8	.06	1	18.0	.18
Sphene.....	.06	75	.05			
Magnetite.....				.5	.5	.00
Ilmenite.....				≈ .1	6.0	≈ .01
Total tantalum by sum of minerals (ppm).....			.42			.39
Total tantalum measured on bulk rock (ppm).....			.45			.45

biotite first appears in the rocks as one of the major mineral constituents. From this point on, the amount of tantalum in the rocks depends chiefly upon the amount of biotite and hornblende present and upon the tantalum content of these minerals. Biotite and hornblende are present in progressively smaller amounts in the granodiorites and quartz monzonites, whereas concomitantly the tantalum content progressively increases in these minerals in the more siliceous rocks. Because of this inverse relation the amount of tantalum in the rocks ranging from tonalite to quartz monzonite remains relatively constant.

Chemical analyses of biotites and hornblendes from rocks of the Southern California batholith ranging in composition from gabbro to quartz monzonite (Larsen and Draisin, 1950) show that these minerals vary widely in composition. These variations indicate that the rocks have crystallized over a wide range of physicochemical conditions. The increase of tantalum in the minerals, which are similar to the minerals chemically analyzed, corresponds closely to Fe^{+2} content and the Fe^{+2}/Mg ratio, whereas no systematic relations exist between tantalum and titanium. Inasmuch as a coupled substitution is required for the substitution of tantalum for titanium, the amount of tantalum in these minerals may be controlled to a large extent by variations of the other chemical constituents in the minerals. The role of the minor constituents may be equally as important. Lithium, for example, is highly concentrated in mica and according to Kuzmenko (1963) plays an important role in the crystal chemistry of tantalum. Thus it appears that the variation of tantalum in these minerals is governed by the interaction of crystal-chemical and petrologic factors.

Considerably more data are required to make a reasonable estimate of the average tantalum content of the batholith. The available data, however, indicate that the tantalum content is on the order of 0.4 ppm. According to Rankama (1944) the average tantalum content of igneous rocks is 2.1 ppm. The average niobium content of the batholith is believed to be approximately 5 ppm (Gottfried and others, 1961). Thus, for the batholith as a whole the Nb/Ta ratio is 12.5. This ratio agrees reasonably well with the Nb/Ta ratio of 11.4 given by Rankama for igneous rocks.

REFERENCES

- Ahrens, L. H., 1952, The use of ionization potentials. I. Ionic radii of the elements: *Geochim. et Cosmochim. Acta*, v. 2, p. 155-169.
- Atkins, D. H. F., and Smales, A. A., 1960, The determination of tantalum and tungsten in rocks and meteorites by neutron activation analysis: *Anal. Chem. Acta*, v. 22, p. 462-478.
- Butler, J. R., and Smith, A. Z., 1962, Zirconium, niobium and certain other trace elements in some alkali igneous rocks: *Geochim. et Cosmochim. Acta*, v. 26, p. 945-953.
- Butler, J. R., and Thompson, A. J., 1962, Ta in the granite G-1: *Geochim. et Cosmochim. Acta*, v. 26, p. 516-517.
- Fleischer, Michael, Murata, K. J., Fletcher, J. D., and Narten, P. F., 1952, Geochemical association of niobium (columbium) and titanium and its geological and economic significance: U.S. Geol. Survey Circ. 225.
- Gottfried, David, Jenkins, Lillie, and Grimaldi, F. S., 1961, Distribution of niobium in three contrasting comagmatic series of igneous rocks: Art. 108 in U.S. Geol. Survey Prof. Paper 424-B, p. B256-B258.
- Kretz, Ralph, 1961, Some applications of thermodynamics to coexisting minerals of variable composition; Examples—orthopyroxene-linopyroxene and orthopyroxene-garnet: *Jour. Geology*, v. 69, no. 4, p. 361-387.
- Kuzmenko, M. V., 1961, The geochemistry of tantalum and niobium: *Internat. Geology Rev.*, v. 3, no. 1, p. 9-25.
- 1963, The role of micas in the process of tantalum concentration: *Doklady Akademii Nauk SSSR*, v. 140, no. 6, p. 1114-1116, Translation of O Roli Slyudv Protsesse Kontsentratsii tantala, *Doklady Akademii Nauk SSSR*, v. 140, no. 6, 1961, p. 1411-1414.
- Larsen, E. S., Jr., 1938, Some new variation diagrams for groups of igneous rocks: *Jour. Geology*, v. 46, p. 505-520.
- 1948, Batholith and associated rocks of Corona, Elsinore, and San Luis Rey quadrangles, southern California: *Geol. Soc. America Mem.* 29, 182 p.
- Larsen, E. S. Jr., and Draisin, W. M., 1950, Composition of the minerals in the rocks of the southern California batholith: *Internat. Geol. Cong.*, 18th, Great Britain, Rept., pt. 2, p. 66-79.
- Miller, F. S., 1937, Petrology of the San Marcos gabbro, southern California: *Geol. Soc. America Bull.*, v. 48, p. 1397-1426.
- Morris, D. F. C., and Olya, A., 1960, The determination of tantalum in rocks by neutron-activation analysis: *Talanta*, v. 4, p. 194-200.
- Mueller, R. F., 1963, Interaction of chemistry and mechanics in magmatism: *Jour. Geology*, v. 71, no. 6, p. 759-772.
- Neumann, Henrich, Mead, Judson, and Vitaliano, C. J., 1954, Trace element variation during fractional crystallization as calculated from the distribution law: *Geochim. et Cosmochim. Acta*, v. 6, p. 90-99.
- Rankama, Kalervo, 1944, The geochemistry of tantalum: *Comm. Geol. Finlande Bull.* 133, p. 1-78.
- 1948, On the geochemistry of niobium: *Acad. Sci. Fennicae Annales*, ser. A, III. Geol.-geog., no. 13, p. 1-57.
- Znamenskii, E. B., and Popolitov, E. I., 1964, Dependence of the geochemical behavior of niobium and tantalum on the paragenesis of titanium and titanium-containing minerals in granitic rocks: *Akad. Nauk SSSR, Sibirsk Otdel*, p. 57-62 [In Russian].
- Znamenskii, E. B., Konusov, V. V., Krinberg, I. A., Popolitov, E. I., Flerova, K. V., and Tsykhanski, V. D., 1962, Distribution of titanium, niobium and tantalum in sphene-containing granitoids: *Geochemistry*, no. 9, p. 800-806.
- Znamenskii, E. B., Rodionova, L. M., and Kakhana, M. M., 1957, Distribution of niobium and tantalum in granites: *Geochemistry*, no. 3, p. 267-270.



METALLIC COPPER IN STONY METEORITES

By MICHAEL B. DUKE and ROBIN BRETT,
Washington, D.C.

Abstract.—Electronmicroprobe analyses of meteoritic metallic copper indicate an iron content of 1.1 to 4.5 percent. Phase equilibrium considerations suggest that these values are too high. On the basis of electronmicroprobe analyses of copper-iron boundaries and of iron coated with small thicknesses of copper, we conclude that analyzed values of iron in meteoritic copper are unreasonably high because of fluorescence effects.

Copper in most of the stony meteorites occurs as small (1–20 micron) grains associated with troilite and nickel-iron (Ramdohr, 1963). In the Norton County, Kans., enstatite achondrite, copper grains almost as much as 1 mm in diameter occur. Electronmicroprobe analyses of this copper indicated an iron content of about 4.2 weight percent (Keil and Fredriksson, 1963). However, phase relations in the system Cu-Fe-S are inconsistent with reported microprobe determinations of iron in meteoritic copper. R. A. Yund (written communication, 1964) has shown that the assemblage Cu-Fe-troilite is stable only below $475^{\circ}\pm 25^{\circ}\text{C}$, being represented above that temperature by the assemblage bornite-Fe-troilite. It is doubtful that bornite was ever present with iron and troilite in meteorites at elevated temperatures, because the small amount of copper present could be contained in solid solution in troilite. The solubility of copper in troilite is about 2 weight percent at 600°C (Gehlen and Kullerud, 1962). At 475°C or less, copper with a low iron content would exsolve from the troilite, forming the observed Cu-Fe-troilite assemblage. Copper formed at 475°C in equilibrium with iron contains less than 0.2 weight percent iron in solid solution (Tammann and Oelsen, 1930), much less than the microprobe analyses show. This discrepancy suggested the present study.

The iron content of copper in the Miller, Bath, and Penokee chondrites (see accompanying table) was determined by using the microprobe constructed in a U.S. Geological Survey laboratory. Natural, copper-free troilite was used as a standard, and the data were corrected for background, counter deadtime, and fluo-

rescence. The apparent iron content ranged from 1.1 to 4.5 percent and varied within single copper grains, suggesting that analytical uncertainties were involved. The analyzed copper grains ranged from 10 to 20μ in diameter, which is larger than the spot size of the electron beam (2μ). The principal uncertainty appeared to lie in the possibility that $\text{CuK}\alpha$ radiation from the analyzed copper grain excited $\text{FeK}\alpha$ radiation in the surrounding iron-rich minerals.

Iron content of metallic copper in chondrites

<i>Meteorite</i>	<i>Number of grains analyzed</i>	<i>Number of separate analyses</i>	<i>Range of apparent Fe content</i>
Miller-----	1	2	1.1–1.6
Bath-----	1	3	1.5–1.6
Penokee-----	2	6	2.5–4.5

In order to assess the magnitude of $\text{FeK}\alpha$ radiation arising outside the analyzed copper grain, 4 pure iron fragments were polished and coated with metallic copper ranging from 0.8 to 3.5μ in thickness. The specimens were analyzed using both an Applied Research Laboratory microprobe and the USGS probe at excitation potentials shown in figure 1. For the thinnest layer the $\text{FeK}\alpha$ radiation is produced by direct penetration of the electron beam and by secondary (fluorescence) excitation due to the X-ray continuum and the characteristic $\text{CuK}\alpha$ radiation. For greater thicknesses the electron beam is entirely absorbed by the copper layer, and the $\text{FeK}\alpha$ radiation arises only from fluorescent excitation, primarily by $\text{CuK}\alpha$. The intensity of $\text{FeK}\alpha$ apparently decreases exponentially with the thickness of the copper layer, but is equivalent to 3 percent or more of iron for iron covered by 3.5μ of copper.

The data show the importance of both the excitation potential and the X-ray takeoff angle on the fluorescence effect. The ARL probe may be used at lower excitation potentials than the USGS probe. The lower the potential, the smaller the beam penetration and hence the smaller the fluorescence effect. For a given excitation potential, the USGS probe, which has an X-ray takeoff

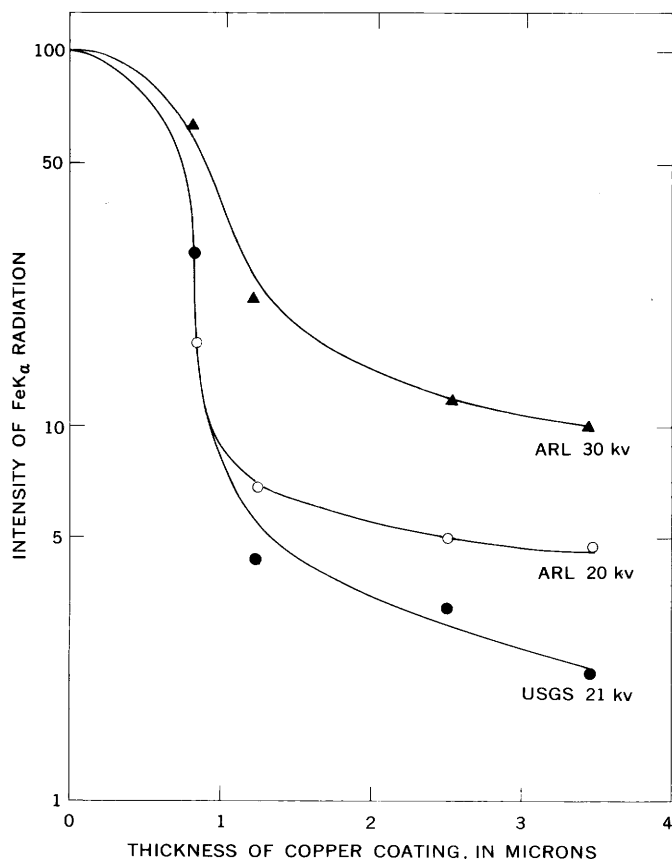


FIGURE 1.—Intensity of $\text{FeK}\alpha$ (normalized against the intensity for pure iron and corrected for background) plotted against the thickness of the copper layer covering the metallic iron. *ARL*, Applied Research Laboratory determination; *USGS*, U.S. Geological Survey determination.

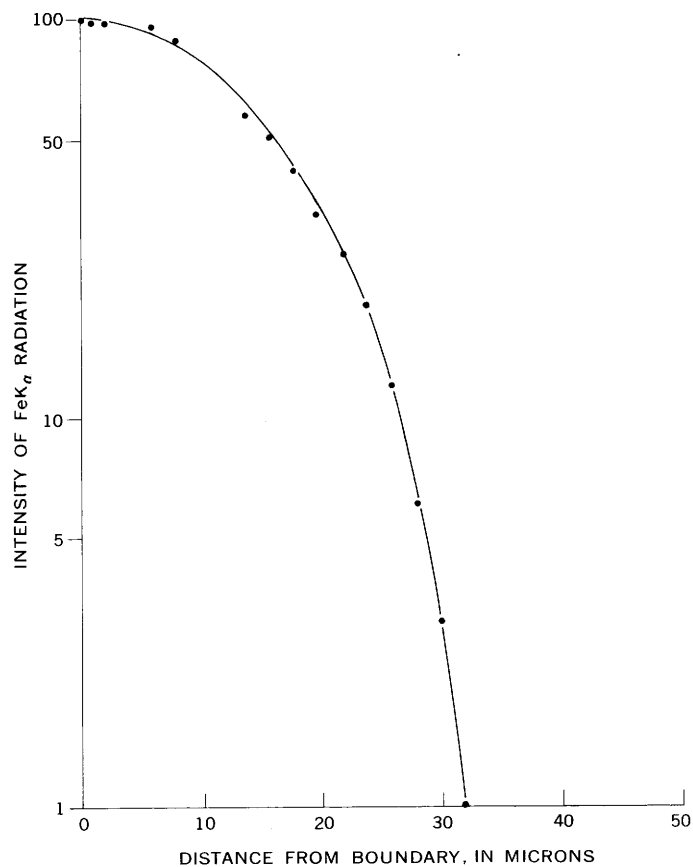


FIGURE 2.—Intensity of $\text{FeK}\alpha$ (normalized against the intensity for pure iron and corrected for background) plotted against the distance from the vertical iron-copper boundary.

angle of about 6° , gives a much smaller fluorescence effect than does the *ARL* electronmicroprobe which has a takeoff angle of 52.5° . This difference is due to the much longer path through which X-rays are absorbed in the *USGS* probe.

A pure copper–pure iron vertical boundary was also examined by means of an *ARL* microprobe at an excitation potential of 25 kilovolts. The intensity of $\text{FeK}\alpha$ radiation arising from points within the copper was determined at measured distances from this boundary. The intensity of $\text{CuK}\alpha$ radiation remained constant over the distance measured. The results shown in figure 2 indicate that there is an observable fluorescence effect at distances of as much as 30μ from the boundary. For points within 20μ of the boundary, the effect is extremely pronounced.

On the basis of the phase-equilibria data and our experiments with copper-iron boundaries we suspect that

the analyzed values of iron in copper are unreasonably high, owing to fluorescence effects. It is necessary, therefore, to analyze large grains or to separate the copper from the matrix in order to determine the true iron content. Although the reported size of copper grains in the Norton County achondrite is apparently large enough to greatly reduce the fluorescence effect, the thicknesses of the grains analyzed by Keil and Fredriksson are unknown. We were unable to examine the copper analyzed by them because the largest copper grain in their sample was destroyed by mild repolishing (Prof. P. Ramdohr, oral communication, 1964). Our search of Norton County achondrite fragments rich in metal and sulfides disclosed no copper grains large enough for electronmicroprobe analysis (the copper is present as thin plates, in some cases enclosing sulfide grains), and we have been unable to repeat their analyses.

We are grateful to Prof. Lincoln LaPaz, University of New Mexico, and to E. P. Henderson, U.S. National Museum, for supplying samples. We also thank James Munford, National Aeronautics and Space Administration, Greenbelt, Md., who coated the iron specimens and measured the thicknesses of the Cu layers; L. S. Walter, NASA, Greenbelt, Md., who assisted with the ARL microprobe; and Isidore Adler, NASA, Greenbelt, Md., formerly of the U.S. Geological Survey, who advised on electronmicroprobe analytical techniques. The work was in part financed by a Carnegie Institution of Washington postdoctoral fellowship granted to Brett.

REFERENCES

- Gehlen, K. V., and Kullerud, Gunnar, 1962, Pyrrhotite-pyrite-chalcopyrite assemblages: Carnegie Inst. Washington, Yearbook 61, p. 154-155.
- Keil, Klaus, and Fredriksson, Kurt, 1963, Electron microprobe analysis of some rare minerals in the Norton County achondrite: *Geochim. et Cosmochim. Acta*, v. 27, p. 939-948.
- Ramdohr, Paul, 1963, The opaque minerals in stony meteorites: *Jour. Geophys. Research*, v. 68, p. 2011-2036.
- Tammann, G., and Oelsen, W., 1930, Die Abhängigkeit der Konzentration gesättigter Mischkristalle von der Temperatur: *Z. anorg. Chem.*, v. 186, p. 257-288.



K-Ar AND Rb-Sr AGES OF BIOTITE FROM THE MIDDLE JURASSIC PART OF THE CARMEL FORMATION, UTAH

By RICHARD F. MARVIN, JAMES C. WRIGHT,
and FRANK G. WALTHALL, Denver, Colo.,
Beltsville, Md., Washington, D.C.

Abstract.—K-Ar and Rb-Sr dating of biotite occurring in the Carmel Formation gave ages ranging from 165 to 140 m.y. and 163 to 85 m.y., respectively. No simple relation between chemical or physical factors and the variation in ages was discerned. However, the data strongly suggest that the variation in isotopic age is a result of alteration caused by the base-exchange action of ground water on the biotite.

In southwestern Utah, the Carmel Formation at the type locality, Mount Carmel (fig. 1), contains limestone with marine mollusks which date the lower part of the formation as Middle Jurassic (Bajocian). In this area the limestone overlies bentonite which consists chiefly of illite, kaolinite, and mixed-layer chlorite-illite-montmorillonite in variable proportions with minor amounts of biotite, sanidine, quartz, apatite, hornblende, and zircon (Schultz and Wright, 1962). The present study was undertaken in the hope that

biotite from bentonite layers in the Carmel Formation would give a definitive isotopic age for the Bajocian strata in Utah. However, variable K-Ar and Rb-Sr ages preclude a unique age assignment, and the variations in the measured ages, rather than a definitive isotopic age for the Bajocian, are the main topic of this paper.

Bentonite layers, averaging only an inch in thickness, occur at many places in the Carmel Formation. In southwestern Utah, the bentonite is at or near the base of the Carmel Formation, usually resting directly on the Navajo Sandstone of Triassic(?) and Jurassic age (Wright and Dickey, 1962). A Bajocian age for the limy lower unit of the Carmel Formation in southwestern Utah is shown by an association of molluscan species that includes the pelecypods *Thracia weedi* Stanton, *Trigonia elegantissima* Meek, and *Vaugonia conradi* (Meek and Hayden) (Imlay, 1964, p. C3-C4). In central Utah this unit of the Carmel contains, in addition, the pelecypods *Myophorella yellowstonensis* Imlay, *Myophorella montanaensis* Meek, *Gervillia montanaensis* Meek, and *Goniomya montanaensis* Meek, and an ammonite genus similar to *Zemistephanus*. In the Twin Creek Limestone of Wyoming and northern Utah this assemblage as a whole, as well as some of the individual species, is restricted to Member C, which is considered late Bajocian because it contains ammonites resembling *Zemistephanus* and *Chondroceras*, and because it immediately overlies Member B, which contains an ammonite assemblage indicative of early late Bajocian age (R. W. Imlay, written communication, September 1964).

In the southwesternmost corner of Utah (between Gunlock and Cedar City), a red siltstone within the

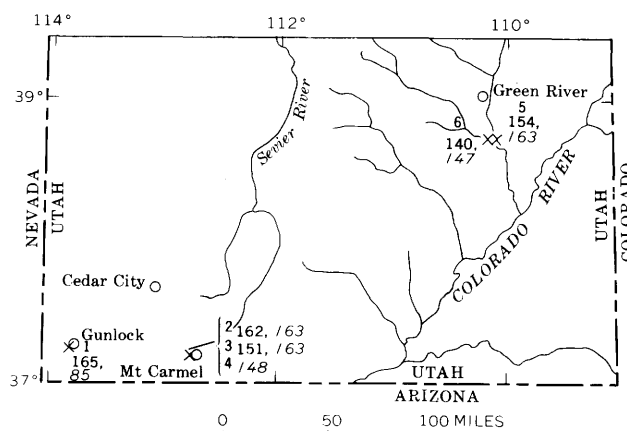


FIGURE 1.—Sketch map of southern Utah, showing locations (X) and sample numbers (1 to 6) of analyzed biotite concentrate. Ages are in millions of years: K-Ar age in roman (as, 165), Rb-Sr in italic (as, 85).

lower part of the Carmel Formation underlies the biotite-bearing bentonite. No fossils have been found in the red siltstone, but because of its similarity in lithology and stratigraphic position to Member A (Gypsum Spring Member) of the Twin Creek Limestone, it is considered of Bajocian age.

The bentonite layers of east-central Utah which occur near the top of the Carmel Formation are younger and possibly were formed during the Bathonian. These lie above the limestones containing marine mollusks used to date the Carmel Formation, and hence a somewhat younger age might be expected.

Schultz and Wright (1962) investigated the bentonites of southwestern Utah and found that they range in composition from dominantly montmorillonite to kaolinite and illite. The nonclay minerals are rare crystals of sanidine, biotite, apatite, hornblende, zircon, and, rarely, quartz. Only the sporadic presence of a few microcline crystals indicates that any part of the bentonite beds is nonvolcanic in origin.

The bentonite layers occurring in east-central Utah were not included in the mineralogic investigation by Schultz and Wright (1962), but they are mineralogically the same as the layers in southwestern Utah and are closely related to them in geologic time and stratigraphic occurrence.

The location and a brief description of the bentonite samples used in this investigation are given in table 1. Approximate locations are shown on figure 1. Descriptions of the biotite samples are given in table 2; analytical data and computed ages are given in tables 3 and 4. Potassium analyses were made by flame photometry using lithium as an internal standard; argon, rubidium, and strontium were determined by isotope-dilution techniques. The overall analytical error for the K-Ar determinations is approximately ± 5 percent of the calculated age. The estimated errors given for the Rb-Sr age determinations (table 4) include a probable error assigned on the basis of the enrichment in radiogenic strontium.

The biotite concentrated from the six bentonite samples ranges from dark green to dark yellow brown. Apatite is present as microscopic inclusions. A subordinate part of the biotite in all concentrates has been oxidized to opaque black iron-rich oxybiotite which is common in volcanic rocks. The biotite in sample 1 has been partly altered to vermiculite; this is evident both under the petrographic microscope and in X-ray powder diffraction photographs. Samples 3 and 6 are contaminated with kaolin flakes carried into the magnetic concentrate by attached minute grains of hydrous iron oxide. The low potassium content of some of the biotite samples (table 3) is caused by chemical altera-

TABLE 1.—Description and location of bentonite samples from the Carmel Formation

Sample No.	Field No.	Description	Locality
Southwestern Utah			
1-----	PP 7	Base of green bentonite outcrop, underlying limestone in Carmel Formation.	Near Gunlock, sec. 32, T. 40 S., R. 47 W., Washington County.
2-----	PP 4	Base of purple bentonite outcrop, underlying limestone in Carmel Formation.	Mount Carmel Junction, sec. 30, T. 41 S., R. 7 W., Kane County.
3-----	PP 4 R	Reddish-purple bentonite layer near sample 2.	Mount Carmel Junction.
4-----	MC 7	Purple bentonite layer 3.5 feet above sample 2.	Mount Carmel Junction.
East-central Utah			
5-----	C 78	Reddish bentonite layer 12 feet above highest limestone bed in Carmel Formation.	Red Wash Box Canyon, NE $\frac{1}{4}$ sec. 3, T. 24 S., R. 17 E., Grand County.
6-----	C 79	Reddish bentonite layer at the highest limestone bed in Carmel Formation.	Bobbin Butte, sec. 11, T. 24 S., R. 16 E., Emery County.

TABLE 2.—Grain size and mineral composition of analyzed biotite concentrates from the Carmel Formation

Sample No.	Grain size (mm)	Mineralogy, from X-ray diffraction data	Estimated mineral percentages, by volume
1-----	0.1-0.8	Dominantly biotite plus minor amounts of oxybiotite and vermiculite.	97 mica. 3 white clay.
2-----	0.1-0.6	Dominantly biotite plus minor amount of oxybiotite. No vermiculite.	95 mica. 5 impurities.
3-----	0.08-0.2	-----	85 mica. 15 reddish clay.
4-----	0.03-0.2	-----	-----
5-----	0.03-0.2	Predominantly biotite plus a small amount of oxybiotite. No vermiculite.	95 mica. 5 reddish clay and iron oxide.
6-----	0.03-0.2	Dominantly biotite plus minor amounts of oxybiotite, kaolin, and non-crystalline hydrous (?) iron oxide. No vermiculite.	80 mica. 20 clay and iron oxide.

tion and by dilution with clay minerals and hydrous iron oxides which could not be separated.

Potassium-argon age determinations (table 3) were made on 5 of the 6 samples; sample 4 was too small for argon determination. The K-Ar ages range from 140 to 165 million years. Six Rb-Sr age determinations

(table 4) also are variable, ranging from 85 to 163 million years. The maximum ages approach the value of 166 million years, which Kulp (1961) gives as the time boundary between the Bajocian and Bathonian.

The range in ages is attributed to chemical alteration of the biotite; however, the data fail to reveal a simple relation. For example, sample 1 with a low potassium content of 3.96 percent gives a K-Ar age of 165 million years (table 3), the highest value found. The rubidium content of the sample is 484 parts per million (table 5), the highest in the group, and the ratio K/Rb of 82 is the lowest of the group. The abnormally low ratio of K/Rb might be explained as the result of

TABLE 3.—K-Ar age determinations of biotite from the Carmel Formation

[K determinations by P. Elmore and F. G. Walthall; Ar determinations by R. F. Marvin and H. H. Thomas]

Sample No.	K (percent)	K ⁴⁰ (ppm)	Radiogenic Ar ⁴⁰ (ppm) ¹	Ar ⁴⁰ /K ⁴⁰	Age (m.y.)
Southwestern Utah					
1-----	3.96	4.83	0.0489	0.0101	165
2-----	7.12	8.69	.0860	.00990	162
3-----	6.61	8.06	.0739	.00917	151
4-----	6.13	-----	-----	-----	-----
East-central Utah					
5-----	6.12	7.47	0.0700	0.00937	154
6-----	4.29	5.24	.0440	.00851	140

Decay constants: $K^{40}\lambda_s = 0.585 \times 10^{-10} \text{ yr}^{-1}$,
 $\lambda_\beta = 4.72 \times 10^{-10} \text{ yr}^{-1}$.

Abundance: $K^{40} = 1.22 \times 10^{-4} \text{ g/g K}$.

¹ The percentage of radiogenic argon to total argon was greater than 87 in all analyses. Analytical error is approximately ± 5 percent of the calculated age.

TABLE 4.—Rb-Sr age determinations of biotite from the Carmel Formation

[Analysts: F. G. Walthall and C. E. Hedge]

Sample No.	Rb ⁸⁷ (ppm)	Normal Sr (ppm)	Radiogenic Sr ⁸⁷ (ppm)	Radiogenic Sr ⁸⁷ / Total Sr ⁸⁷	Sr ⁸⁷ / Rb ⁸⁷	Age (m.y.)
Southwestern Utah						
1-----	137	110	0.172	0.02	0.00125	85 ± 50
2-----	108	11.6	0.259	0.25	0.00240	163 ± 10
3-----	97.4	30.5	0.243	0.10	0.00249	163 ± 15
4-----	96.2	28.7	0.221	0.10	0.00230	
	93.1	20.2	0.203	0.13	0.00218	148 ± 15
East-central Utah						
5-----	106	21.9	0.254	0.14	0.00239	163 ± 10
	107	20.4	0.255	0.15	0.00239	
6-----	65.4	35.4	0.149	0.06	0.00228	147 ± 15
	66.6	38.0	0.142	0.05	0.00213	
	67.6	36.5	0.141	0.05	0.00208	

Decay constant: $Rb^{87} \lambda_\beta = 1.47 \times 10^{-11} \text{ yr}^{-1}$.
 Abundance: $Rb^{87} = 0.283 \text{ g/g Rb}$.

TABLE 5.—K-Rb ratios and comparative K-Ar and Rb-Sr ages of analyzed biotites

Sample	K (percent)	Rb (ppm)	K/Rb	Age (m.y.)	
				K-Ar	Rb-Sr
1-----	3.96	484	82	165	85
2-----	7.12	381	187	162	163
3-----	6.61	¹ 342	193	151	163
4-----	6.13	329	186	-----	148
5-----	6.12	¹ 376	163	154	163
6-----	4.29	¹ 235	182	140	147

¹ Average, see table 4.

differential leaching with greater relative loss of potassium than of rubidium, but the relatively large amount of strontium in the sample is not compatible with this explanation. Sample 1 contains 110 ppm of normal strontium (table 4) compared to 12–38 ppm in the other 5 samples. The large amounts of rubidium and strontium in sample 1 suggest the possible introduction of these elements from ground water. The computed age of 85 million years has no real significance.

Three Rb-Sr determinations give similar ages of 163 m.y. (table 5), which fall between the two K-Ar ages of 162 and 165 m.y. The remaining ages, excluding sample 1, range from 140 to 154 m.y., averaging 148 m.y. Again, two Rb-Sr ages are similar, 147 and 148 m.y., whereas the K-Ar ages give the extremes. The grouping of the ages suggested the possibility of a second event at approximately 150 m.y. ago, but the variability of the K-Ar ages and the unreasonably low Rb-Sr age of 85 m.y., computed for sample 1, argue more strongly for alteration of the biotite by ground water. This conclusion is supported by the partial vermiculite structure of the biotite in sample 1 and the alteration of enclosing tuff to various clay minerals. Also, there is no evidence for deep burial of the Jurassic sedimentary rocks or of a thermal event in the sample localities that would account for the lower ages.

There is an apparent correlation between the K Ar age and size range of the analyzed samples. The finer grained mica gives lower ages. Although the lower ages for the finer grained biotite might suggest loss of argon through diffusion, an equally reasonable explanation might be the greater ease of attack by ground water.

Samples 3 and 6 have a large percentage of clay contaminant; the effect of the contaminant on Rb-Sr ages could not be ascertained. Sample 3 gives a Rb-Sr age compatible with samples 2 and 5; sample 6 gives a lower age but agrees with the age of sample 4.

We conclude that the best minimum age for these bentonite layers is 163 m.y. Ground-water alteration of the biotite is the principal cause of the variability of the K-Ar and Rb-Sr ages. The chemical processes of al-

teration may have been very complex. The K-Ar and Rb-Sr isotopic systems have not been altered to the same degree, but even more difficult to comprehend is that neither system gives consistent results. Kulp and Engels (1963), in discussing the causes for discordance in K-Ar and Rb-Sr ages of micas, point out that base exchange in micas may result through the action of ground water. They conclude that very large amounts of potassium may be removed from biotite by base exchange without affecting the K-Ar age; however, addition of rubidium from ground waters would be expected to be accompanied by removal of Sr^{87} , so that "the Rb-Sr age will be lowered relative to the unchanged K-Ar age" (Kulp and Engels, 1963, p. 234).

In the samples from the Carmel Formation, sample 1 follows the Kulp-Engels suggestion, with the Rb-Sr age being less than the K-Ar age; sample 2 gives virtually concordant results; samples 3, 5, and 6 are reversed with the K-Ar age less than the Rb-Sr, suggesting perhaps a thermal effect. However, this seems unlikely, considering the proximity of samples 2 and 3 and samples 5 and 6. Thus, a definitive conclusion cannot be drawn

from the available data, except that ground-water alteration which may have acted over a long period of time in a variable manner appears to be the most satisfactory explanation. Our study further emphasizes that caution is required in dating biotite from altered tuffs. Biotite-sanidine pairs afford a useful combination but, unfortunately, sufficient sanidine for analysis was not available in the samples from the Carmel Formation.

REFERENCES

- Imlay, R. W., 1964, Marine Jurassic pelecypods, central and southern Utah: U.S. Geol. Survey Prof. Paper 483-C, p. C1-C42.
- Kulp, J. L., 1961, Geologic time scale: *Science*, v. 133, no. 3459, p. 1105-1114.
- Kulp, J. L., and Engels, Joan, 1963, Discordances in K-Ar and Rb-Sr isotopic ages, in *Radioactive dating*: Internat. Atomic Energy Agency, Vienna, p. 219-238.
- Schultz, L. G., and Wright, J. C., 1962, Bentonite beds of unusual composition in the Carmel Formation, southwest Utah: Art. 198 in U.S. Geol. Survey Prof. Paper 450-E, p. E67-E72.
- Wright, J. C., and Dickey, D. D., 1962, Relations of the Navajo and Carmel Formations in southwestern Utah and adjoining Arizona: Art. 197 in U.S. Geol. Survey Prof. Paper 450-E, p. E63-E67.



POTASSIUM-ARGON AGES OF SOME PLUTONIC ROCKS, TENAKEE AREA, CHICHAGOF ISLAND, SOUTHEASTERN ALASKA

By MARVIN A. LANPHERE, ROBERT A. LONEY, and DAVID A. BREW,
Menlo Park, Calif.

Abstract.—Potassium-argon age measurements are compatible with the interpretation that a Chichagof Island granitic complex composed predominantly of syenite is early Paleozoic in age. Discordance between apparent ages of hornblende and biotite probably reflects the metamorphic effects of a nearby tonalitic batholith of Mesozoic age. An age of 406 m.y. obtained on hornblende from syenite is considered a minimum for the Paleozoic intrusive complex. These results are similar to potassium-argon and lead-alpha ages reported for intrusive rocks about 230 miles farther south in the Bokan Mountain area of Prince of Wales Island.

In a recent investigation, Lanphere and others (1964) reported potassium-argon and lead-alpha age measurements that indicated an early Paleozoic, probably Ordovician, age for granitic rocks of the Bokan Mountain area of Prince of Wales Island, southeastern Alaska (fig. 1). In the present study, potassium-argon ages that we interpret to represent an early Paleozoic age were obtained for comagmatic granitic rocks in the Tenakee area of Chichagof Island, approximately 230 miles northwest of the Bokan Mountain area.

A reconnaissance geologic map of Chichagof Island has been published by Loney, Berg, and others (1963), and more detailed reports are in preparation. Loney, Condon, and Dutro (1963) studied the stratigraphy of the middle Paleozoic rocks in an area located a few miles north of Tenakee Inlet (fig. 1). The eastern third of the Tenakee area is underlain by Silurian argillite and graywacke, Silurian (?) and Devonian (?) limestone, and Devonian limestone and interbedded conglomerate. The age assignments of some of these units are based on more recent work. The western two-thirds of the area is underlain largely by intrusive rocks of Paleozoic and probable or inferred Mesozoic age.

A large tonalitic batholith which occupies the southwestern part of the Tenakee area is Mesozoic, probably Cretaceous, on the basis of a lead-alpha age of 110 ± 20

million years (T. W. Stern, written communication, 1963) for zircon from tonalite on the south shore of Tenakee Inlet and west of the area covered by figure 1. Smaller areas of granitic rocks in the vicinity of Tenakee Inlet (fig. 1) are inferred to be of Mesozoic age. Ages measured on the Gypsum Creek Quartz Monzonite located about 10 miles north of Tenakee Inlet provide additional evidence of Mesozoic plutonism on eastern Chichagof Island. A potassium-argon age of 103 ± 5 m.y. for biotite (R. F. Marvin, written communication, 1964) and a lead-alpha age of 150 ± 20 m.y. for coexisting zircon (T. W. Stern, written communication, 1963) differ by more than analytical uncertainty, but these ages indicate a probable Cretaceous age of the Gypsum Creek Quartz Monzonite.

The igneous complex extending from Point Hayes northward past the town of Tenakee lies just west of the Devonian limestone-conglomerate sequence. Hornblende syenite and biotite syenite are the predominant rock types in the complex; hornblende- and biotite-bearing monzonite, granodiorite, granite, trondhjemite, syenodiorite, and nepheline- and sodalite-bearing syenite are less abundant rock types (Loney, Berg, and others, 1963). The presence of abundant clasts of syenite and of related rock types in the limestone-conglomerate sequence suggests that they were derived from the adjacent plutonic complex and that the plutonic rocks are pre-Devonian. Unfortunately, the field relations between the units are not clear because of poor exposures. The Paleozoic age assignment for this complex of intrusive rocks is based on data presented in this paper.

A belt of hornfels, schist, and marble lies between the syenite-rich complex and the tonalitic batholith to the west. Smaller areas of these metamorphic rocks occur northeast of the syenite-rich complex and as iso-

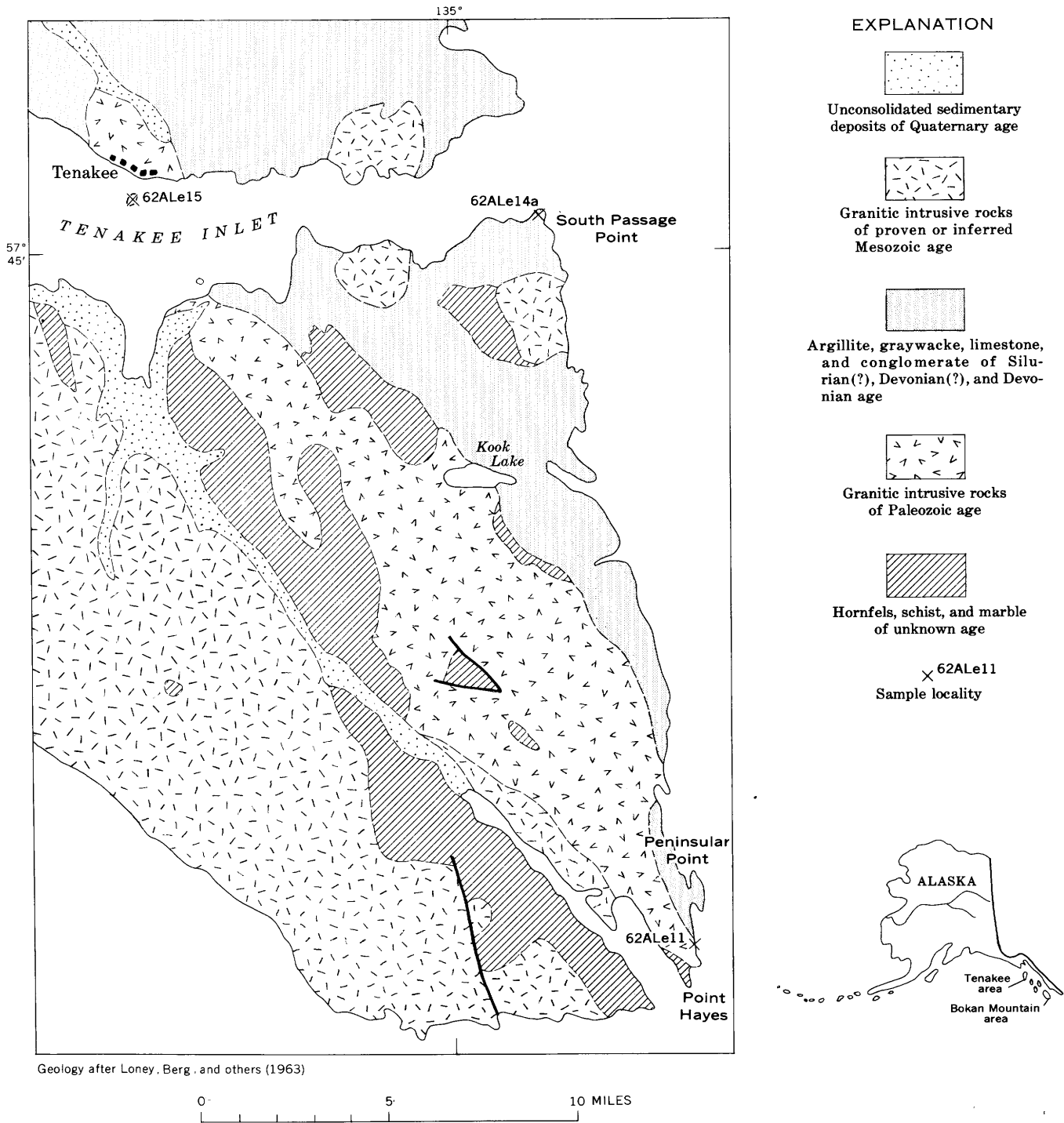


FIGURE 1.—Generalized geologic map of the Tenakee area, southeastern Alaska, showing location of dated samples.

lated masses within the complex. Loney, Berg, and others (1963) considered these metamorphic rocks to be metamorphosed Devonian sedimentary rocks, but the distribution of these metamorphic rocks suggests that they may have been metamorphosed by the syenitic complex and thus be pre-Devonian in age. However, no fossils have been found in the metamorphic rocks, and

the relation of the metamorphic rocks to the igneous complex is poorly shown in the field. Thus, the age assignment of the rocks from which the metamorphic rocks were derived is largely speculative.

Potassium-argon ages were determined for hornblende from 2 samples of syenite, for biotite from 1 sample of syenite, and for hornblende from a quartz

Potassium-argon ages for plutonic rocks, Tenakee area, Chichagof Island, southeastern Alaska

[Argon analysis and one potassium analysis for sample 62ALe15 made by M. A. Lanphere and T. Y. Wen at the California Institute of Technology. All other analyses made in the U.S. Geological Survey laboratories, Menlo Park, Calif. Potassium analyses by H. C. Whitehead and L. B. Schlocker; argon analyses by M. A. Lanphere]

Sample No. (fig. 1)	Rock	Mineral	K ₂ O, in analyses (percent)	Average K ₂ O (percent)	Ar ⁴⁰ _{rad.} (10 ⁻¹⁰ moles/g)	Ar ⁴⁰ _{rad.} Ar ⁴⁰ _{total}	Apparent age (millions of years)
62ALe11	Syenite	Biotite	6.84; 6.84; 6.83	6.84	12.41	0.78	119 ± 5
	do	Hornblende	2.30; 2.29; 2.30	2.30	8.987	.91	247 ± 10
62ALe14a	Boulder of quartz diorite	Hornblende	0.254; 0.259; 0.262	.258	1.131	.53	275 ± 11
62ALe15	Syenite	Hornblende	1.67; 1.63; 1.65; 1.66	1.65	11.15	.87	406 ± 16

Decay constants for K⁴⁰: $\lambda_e = 0.585 \times 10^{-10} \text{ year}^{-1}$

$\lambda_\beta = 4.72 \times 10^{-10} \text{ year}^{-1}$

Atomic abundance of K⁴⁰ = 1.19×10^{-4}

diorite clast in the Devonian conglomerate unit. Samples 62ALe11 and 62ALe15 (see fig. 1 for sample localities) are coarse-grained hornblende syenite which consists primarily of orthoclase microperthite, highly altered calcic oligoclase, and dark-green hornblende. The orthoclase microperthite is 3 or 4 times as abundant as the calcic oligoclase. Biotite is an accessory mineral in sample 62ALe15, where it occurs as cores in a small fraction of hornblende grains. Biotite in sample 62ALe11 occurs both as large discrete grains and as aggregates of very fine grains that crosscut hornblende grains, apparently in an alteration relation. Accessory minerals in both samples include white mica, quartz, apatite, zircon, and opaque iron minerals. Epidote is an accessory mineral in sample 62ALe11.

Sample 62ALe14a, from South Passage Point, is a well-rounded boulder of quartz diorite approximately 2 feet by 18 inches in size. The quartz diorite consists primarily of quartz, potassium feldspar, plagioclase, and pale-green hornblende. Plagioclase is about three times as abundant as potassium feldspar. The rock is altered so that some hornblende grains are partly chloritized, potassium feldspar is extensively altered to clay minerals(?), plagioclase is partly saussuritized, and epidote is scattered through the clast.

For the potassium-argon analyses (see accompanying table) the estimated uncertainty in determining the concentration of K⁴⁰ and radiogenic Ar⁴⁰ is approximately 2 percent for each isotope. The plus-or-minus value assigned each age is the estimated standard deviation of analytical precision, exclusive of any systematic error introduced by an uncertainty in the value of the decay constant for electron capture of K⁴⁰. The argon analyses were made using standard isotope dilution techniques. Potassium was determined with a flame photometer using a lithium internal standard. Replicate analyses generally agree within approximately 1 percent.

In discussing the results presented in this paper we assume that the potassium-argon ages are minimum

ages because there is no available evidence which indicates that hornblende or biotite in normal plutonic rocks incorporate significant amounts of radiogenic argon during crystallization.

The 406 ± 16 m.y. age for hornblende from sample 62ALe15 suggests an early Paleozoic age for the syenitic complex. The stratigraphic significance and regional implications of this result are discussed later in this paper.

The analyses of sample 62ALe11 reflect the contact metamorphic effects of the nearby tonalitic batholith. The 119-m.y. potassium argon age for sample 62ALe11-biotite indicates that the biotite was formed or recrystallized during the period of Mesozoic plutonism; this date agrees well with the lead-alpha and potassium-argon ages mentioned previously. We were unable to obtain a pure hornblende concentrate, free of fine-grained, intergrown biotite, from sample 62ALe11. An X-ray diffraction trace of the hornblende concentrate which was used for the isotopic analysis showed that the concentrate actually is a hornblende-biotite mixture. The high potassium content (see table) also suggests that the hornblende concentrate contains an appreciable amount of biotite. The 247-m.y. age measured on the hornblende-biotite mixture is a minimum age for the hornblende component, and this result confirms the Paleozoic age assigned to the syenitic complex on the basis of the age of 62ALe15. It is clear that 62ALe11 hornblende retained a significant "memory" of a Paleozoic age, though the extent of this memory cannot be calculated because the X-ray data are not precise enough to make a correction for the biotite impurity.

The clasts in the conglomerates of the eastern part of the area must be Devonian or older in age because Devonian fossils are found in limestone which intertongues with the conglomerates (Loney, Berg, and others, 1963). But the 275-m.y. date for hornblende from the quartz diorite boulder (sample 62ALe14a) in the conglomerate is at least 70 m.y. younger than the 345-m.y. date accepted for the end of the Devonian Period

(Kulp, 1961). The alteration of the boulder suggests the possibility that it may have been affected by emplacement of the granodiorite pluton located approximately 1½ miles south of South Passage Point (fig. 1), but the reason for the apparent loss of radiogenic argon from the hornblende of sample 62ALe14a is not definitely known. Clasts of syenite collected at Peninsular Point were not suitable for analysis because the hornblende has been completely replaced by chlorite.

The 406-m.y. age for hornblende (sample 62ALe15) suggests a Silurian age for the syenitic complex of the Tenakee area, based on current estimates of the geologic time scale (Kulp, 1961). However, we consider a Silurian assignment a minimum because, as stated previously, we assume that the potassium-argon ages are minimum values. We suggest a probable Ordovician age for the syenitic complex, based on the agreement, within analytical uncertainty, between the potassium-argon ages of sample 62ALe15 hornblende and the 431 ± 21 -m.y. and 446 ± 22 -m.y. ages of hornblende from the quartz monzonite and quartz diorite units of the Bokan Mountain area of Prince of Wales Island (Lanphere and others, 1964). In the Bokan Mountain area, which

is about 230 miles south of the Tenakee area, the metamorphic effects attributable to Mesozoic plutonism are minor, and the potassium-argon ages of hornblende from the older intrusive units were interpreted to indicate emplacement during the Ordovician period (Lanphere and others, 1964). Although the composition of plutonic rocks is quite different in the widely separated Tenakee and Bokan Mountain areas, the similar potassium-argon ages obtained in the two areas suggest that southeastern Alaska was the locus of important early Paleozoic granitic emplacement.

REFERENCES

- Kulp, J. L., 1961, Geologic time scale: *Science*, v. 133, p. 1105-1114.
- Lanphere, M. A., MacKevett, E. M., Jr., and Stern, T. W., 1964, Potassium-argon and lead-alpha ages of plutonic rocks, Bokan Mountain area, Alaska: *Science*, v. 145, p. 705-707.
- Loney, R. A., Berg, H. C., Pomeroy, J. S., and Brew, D. A., 1963, Reconnaissance geologic map of Chichagof Island and northwestern Baranof Island, Alaska: U.S. Geol. Survey Misc. Geol. Inv. Map I-388.
- Loney, R. A., Condon, W. H., and Dutro, J. T., Jr., 1963, Geology of the Freshwater Bay area, Chichagof Island, Alaska: U.S. Geol. Survey Bull. 1108-C, 54 p.



A LARGE TRANSITIONAL ROCK GLACIER IN THE JOHNSON RIVER AREA, ALASKA RANGE

By HELEN L. FOSTER and G. WILLIAM HOLMES,
Washington, D.C., Beltsville, Md.

Abstract.—The rock glacier in the Johnson River area is notable because of its well-developed mesorelief features, because it is one of the few reported in Alaska which descends below tree limit, and because it is visibly moving forward. The rock glacier, approximately 1 mile long, is an end member of an unbroken series of ice-related features and merges upvalley with an ice-cored moraine 2 miles long, which merges with an ice glacier in the cirque.

A long narrow train of bouldery debris fills a tributary valley in the drainage basin of the Johnson River in east-central Alaska (fig. 1); the lower third of the train is a rock glacier. As defined by Capps (1910), a rock glacier is an accumulation of rock debris in a tongue-shaped, fan-shaped, or spatulate form, resembling a small glacier. It has characteristic longitudinal ridges and transverse crescentic furrows and ridges on its upper surface, and, when active, terminates in a steep bare slope.

The rock glacier is one of several in the Johnson River area, but rock glaciers are not as abundant here as Wahrhaftig and Cox (1959) found them to be in the central Alaska Range. Although rock glaciers are not commonly reported in literature on Alaskan geology, they are known to occur in the Brooks and Wrangell Ranges and in the Chugach, Talkeetna, and Mentasta Mountains.

The rock glacier described in this paper merges upvalley with a long ice-cored ablation moraine whose surface form indicates that the moraine is slowly moving down the valley. The ablation moraine extends upvalley for nearly 2 miles to an area where it is transitional with a small active cirque glacier. Most rock glaciers in the Alaska Range heretofore described do not merge with ice-cored ablation moraines or with glaciers, but head in empty cirques or extend outward from valley sides (Wahrhaftig and Cox, 1959, p. 409). Hence, the rock glacier described in this paper is a fea-

ture transitional between a moving ice-cored moraine and a rock glacier at present unrelated to glacial ice.

FORM

Moraine.—The dimensions, form, slope, and mesorelief features of the moraine and rock glacier are shown on figure 2. The upper end of the moraine is unmarked by a terminal ridge, but lies along a zone where rocky debris becomes so concentrated as to obscure the glacier ice. The most prominent features of the moraine are longitudinal ridges which extend for about 2 miles from the ice glacier to the rock glacier. The ridge on the south side is covered by the toe of a talus fan near the ice margin; it is joined downvalley by two smaller ridges which also originate from talus fans. These ridges are apparently stable, are covered by tundra vegetation, and appear to contain more small interstitial debris than the main body of the moraine. A fosse as much as 25 feet deep lies between the marginal ridges and the valley wall except where talus fans encroach on the edges. The north side of the moraine is bounded by an unstable ridge of unweathered boulders about 18 feet wide and 25 feet high. A deep fosse separates this ridge from the valley wall. In the fosse, a small stream flows to a point near the lower boundary of the moraine, where the stream has been diverted through the valley side to the north. To the south of this ridge is a second, lower ridge, covered with weathered and lichen-covered boulders. Down the center of the moraine is a broad bouldery ridge or elongated lobe, approximately 75 feet wide and 25 to 40 feet high. Between these ridges are hummocks and lobes as much as 25 feet high, composed mostly of unweathered boulders arranged in an apparently random fashion. A few thaw pits occur in the moraine; the largest (fig. 1) is located at about 4,500 feet above sea level near the lower end of the moraine. This pit is



FIGURE 1.—Oblique aerial view, to the south, of the lower rock glacier, ice-cored moraine, and cirque glacier in the Johnson River area. A, diverted stream; B, moving front of the rock glacier. A large thaw pit is indicated by arrow. Photograph by U.S. Army Air Force, 1941.

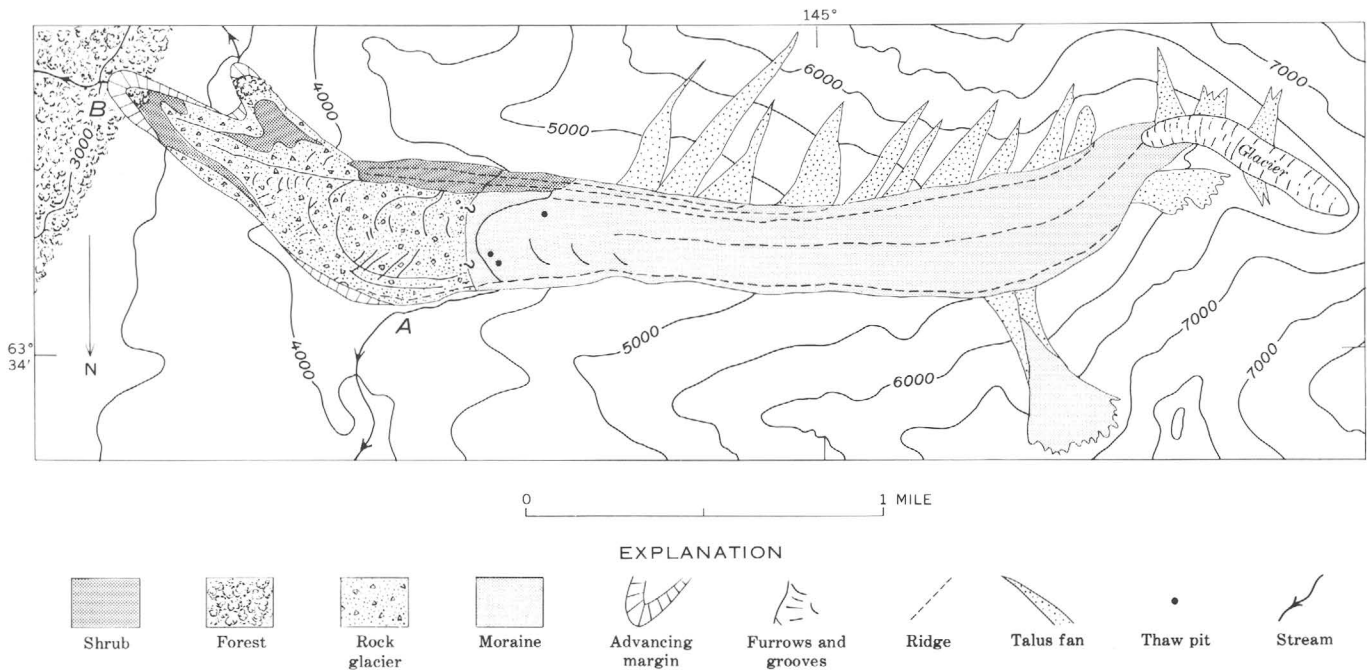


FIGURE 2.—Sketch map of the rock glacier, moraine, and ice glacier in the Johnson River area. Map is oriented with south at top, for comparison with figure 1. A, diverted stream; B, moving front of rock glacier.



FIGURE 3.—Northern terminus of the bilobate rock glacier (B, figs. 1 and 2), with scattered spruce trees on its upper surface. Boulders and smaller fragments as well as vegetation frequently can be seen sliding down the active face. The lower boundary of the rapidly moving surface layer is dashed.

about 50 feet deep and contains banded glacial ice exposed in the walls, underlying bouldery ablation moraine.

Rock glacier.—The boundary between the ablation moraine and the rock glacier is difficult to place without drill holes or excavations. It probably lies in the area between the lowest thaw pits and the uppermost concentration of concentric furrows and ridges (Wahrhaftig, written communication, 1962). This area is about 4,300 feet above sea level. A gravity survey might be used to determine this boundary.

The gross slope of the rock glacier is nearly the same as that of the moraine, with a slight increase in gradient near the lower end of the rock glacier. The north side of the rock glacier is oversteepened, with slope angles of as much as 45° , whereas the south flank is gently inclined. Oversteepening of the north flank is probably caused by spreading of the rock glacier at a slight bend in its course. Boulders roll down the north flank and over the adjacent tundra. Widening of the rock glacier in this area is also indicated by the diversion of a lateral stream (A, figs. 1 and 2) into the next valley. The two marginal fosses of the moraine continue along the sides of the rock glacier. The terminus is asymmetrically bilobate; the northern lobe reaches the lower elevation and is apparently more active. The moving face (fig. 3) of the northern terminal lobe is at a 33° angle of repose, and is about 150 feet high.

A two-layer structure in the rock glacier can be seen at the moving front (fig. 3). The upper layer, 15 to 25 feet thick, is composed of unstratified, poorly sorted,

blocky debris. The lower layer is composed of somewhat sorted, finer debris. The textural difference is the result of a crude sorting process as the upper layer is disturbed and slides over the lower layer. The larger blocks cascade to the foot of the slope, leaving finer debris on the slope at the angle of repose.

Diagnostic mesorelief features abound on the rock glacier. These include transverse crescentic furrows and ridges 25 to 800 feet long, bowed downslope, and typically with relief of 5 to 10 feet. Many of the furrows are covered with boulders which are nearly free of lichens; the absence of lichens may be due to persistent snow drifts and to recent movement of the surface. In places, lichen-covered boulders have rolled into the furrows, suggesting surface movement. Longitudinal trenches, also characteristic, are common. Most of them are about 5 feet deep (although some are as deep as 25 feet), V shaped in profile, and floored by lichen-free boulders. Radial trenches, resembling extension fractures of a glacier, intersect both the longitudinal ridges and the crescentic furrows. Steps occur in the terminal area. The treads are typically 100 feet wide, and the risers are roughly 20 feet high. Boulders on the treads of the steps are mostly lichen covered, but those on the risers are fresh, indicating recent movement.

COMPOSITION

The rock glacier and ice-cored moraine are composed of various mixtures of rock, ice, and water. The rock component consists of material ranging from boulders to silt- and clay-size particles, and resembles till. However, because a significant source of material is talus, a bulk analysis would probably show that the material is coarser than the local till.

From exposures at the snout, on the flanks, and in steps and lobes it is apparent that boulders are concentrated on the surface. This may be due to a sifting out and downward migration of fine material by movement of the surface layer, to downward migration of fine material, or to contribution of large fragments from talus fans. Surface boulders are typically large—commonly 3 feet in diameter. Nearly all the boulders are angular or subangular, and none of those seen are faceted or striated.

Boulder counts made in the rock glacier show granite to be predominant (47 to 88 percent), with minor amounts of fine-grained mafic rocks (7 to 19 percent), diorite (2 to 28 percent), and felsite (1 to 9 percent). This lithology bears out the conclusion of Wahrhaftig and Cox (1959, p. 415) that rock glaciers in the Alaska Range are derived mostly from rocks which break up into large blocks, such as granite, rather than rocks which weather into small slabs, such as schist.

The ice content of the ablation-moraine section may be 80 percent or more, even near the lower end of the section. At 4,500 feet elevation a large thaw pit revealed slightly dirty glacial ice overlain by only about 5 feet of rock debris.

The ice content of a rock glacier may also be high. Wahrhaftig (written communication, 1962) reports that tunnels in rock glaciers in the San Juan Mountains of Colorado and in the Sierra Nevada of California show that below a thick layer of debris these rock glaciers are almost pure ice. As the Alaska Range rock glaciers are in the permafrost zone and at high elevations, their ice content must be comparable to those in the mountains in Colorado and California. This ice may have been inherited from the ablation moraine or, less likely, may have formed as massive ice bodies in permafrost. Minimum potential ice content could be inferred from calculations of the porosity of rock glacier debris if such data were available. In the absence of these data, porosity values for till may serve as a guide. Published values for 6 Connecticut till samples range from 11.5 to 21 percent (Meinzer, 1923, p. 11) and for 3 till samples (boulder clay) from England, from 23.4 to 25.5 percent (Manger, 1963, p. E42). We calculated approximate porosity values for about 30 till samples from New Hampshire, based on specific gravity of the till samples (Goldthwait, 1948, p. 10-11) and specific gravity of rocks similar to those in the State (Birch and others, 1942, p. 14, 20-25); these values range from 12 to 28 percent. Therefore, on the assumption that permafrost occurs in the rock glacier and that adequate moisture was available, the minimum ice content is probably one-tenth to one-fourth of the volume of the rock glacier.

Water is present in liquid form, during the warm season, above the permafrost table and in the glacier ice beneath the moraine. It may fill thaw depressions in the ablation moraine, but very little was observed flowing from the snout of the rock glacier or in lateral channels, and none of that was milky. The small amount of rock flour in the streams may be explained by: (a) a small quantity of ice within or below the debris of the rock glacier, (b) little grinding of rocks within the rock glacier or glacier, (c) filtration of rock flour by the debris downvalley, or (d) a very conservative regime characterized by low accumulation and low ablation. The first suggestion is not consistent with Wahrhaftig's report of ice in the rock glaciers in the Sierra Nevada and the San Juan Mountains, and the second seems unlikely because we saw much fine-grained material in the moving front and in thaw pits. The clarity of the streams probably results from low ablation, which may be due to the protecting cover of debris,

together with some filtering action by the large mass of material.

SOURCE OF DEBRIS

Debris in rock glaciers originates from talus, from moraines, or from a combination of these sources (Kesseli, 1941, p. 203-204). The rock glacier here described is composite in origin, being composed of talus, of morainal material, and of debris from a small tributary rock glacier. The ice-cored ablation moraine appears to be the chief source of the debris. This is suggested by the physical relation with the moraine and by relic patterns and forms on the rock glacier similar to morainal topography (fig. 1). Talus now plays a small role in contributing rock material to the debris train, although renewed talus formation is evident on the south wall of the valley, where there is a series of long, unweathered, visibly active talus fans beneath the steep granitic face of the canyon. Negligible debris is now being contributed by the three easternmost fans, but the fans upvalley are encroaching on the old, weathered lateral ridge of the moraine. The amount of debris from the tributary rock glacier is minor.

VEGETATION

The most common form of vegetation on the rock glacier and moraine is lichen, which covers most boulders, except those in furrows and trenches, those on the risers of steps, and those on the moving margins. Grass, moss, blueberry, and other low plants are abundant on the upper surface of the terminal area, as well as along the margins up to an elevation of about 4,500 feet. Shrubs (alder, birch, and juniper) grow up to an elevation of about 3,400 feet on the northern lobe and a little higher on the southern. Spruce and aspen occur up to the tree limit, about 3,100 feet above sea level and about 240 feet from the northern snout. The forest trees are scattered, but none appear tilted except at the edge of the moving front. However, the thin, peat-enriched soil and turf are disrupted in the terminal zone, apparently from irregular shear stress parallel to the surface. The largest tree near the lower edge of the northern lobe is approximately 125 years old, as determined by a tree-ring count. The oldest tree, located on the southern lobe, is about 150 years old.

MOVEMENT

The dynamic character of the rock glacier is shown in several ways. In June 1960, boulders and smaller fragments were observed sliding and bouncing down the advancing face at intervals of 1 or 2 minutes. One fragment struck a member of the field party, which is a

warning to future investigators working in this area. Abundant evidence of the movement of material was seen. Uprooted green aspen and spruce trees were lying on the face of the rock glacier, and large living trees around the foot of the rock glacier were gashed and mutilated as a result of blows from cascading blocks. Small earth flows occurred on the talus slope, probably as a result of the thawing of seasonal frost. The north side of the rock glacier, about half a mile from the snout, has spread laterally, as was indicated by the exposure of unweathered and lichen-free debris on the flank and by the encroachment of boulders over the tundra vegetation.

Other evidence for movement is provided by (1) the crescentic ridges, which Wahrhaftig and Cox (1959, p. 434) suggest are surface expressions of thrusting along closely spaced shear surfaces in the rock glacier, and by (2) the recent formation of steps and trenches.

The maximum rate of movement of the upper surface near the snout can be estimated from the distribution and age of the trees growing there. The maximum possible distance of travel of a tree growing on the surface is from the tree limit (at the upper edge of the forest on the northern snout) to the edge of the moving face, a distance of about 240 feet; the oldest tree found near the edge was about 125 years old. Thus, the most rapid downvalley movement possible of the upper surface by this calculation is about 1.9 feet per year. This agrees with the measured upper-surface velocities on the Clear Creek rock glacier in the Healy (1:250,000) quadrangle, in the Alaska Range, where the rate ranged from 1.3 to 2.5 feet per year (Wahrhaftig and Cox, 1959, p.

396). It is apparent, however, that movement of the upper surface of the snout is not rapid enough to prevent continual establishment of forest growth up to the local tree limit, even as the surface slides downvalley.

Wahrhaftig and Cox (1959, p. 396) have developed a formula which states that the ratio of the thickness of the upper layer of debris to the total thickness of the rock glacier at its snout is proportional to the ratio of the velocity of the toe of the rock glacier to the velocity of its upper surface. Using this relation, the toe of this rock glacier is computed to be advancing at a maximum rate of about 0.019 to 0.031 foot per year. However, limited observations indicate that the computed figure may be a minimum one for this particular rock glacier.

REFERENCES

- Birch, Francis, Shairer, J. F., and Spicer, H. C., eds., 1942, Handbook of physical constants: Geol. Soc. America Spec. Paper 36, 325 p.
- Capps, S. R., 1910, Rock glaciers in Alaska: Jour. Geology, v. 18, p. 359-375.
- Goldthwait, Lawrence, 1948, Glacial till in New Hampshire: New Hampshire State Plan. and Devel. Comm. Mineral Resources Survey, pt. 10, p. 3-11.
- Kesseli, J. E., 1941, Rock streams in the Sierra Nevada, California: Geog. Rev., v. 31, p. 203-227.
- Manger, G. E., 1963, Porosity and bulk density of sedimentary rocks: U.S. Geol. Survey Bull. 1144-E, 55 p.
- Meinzer, O. E., 1923, The occurrence of ground water in the United States: U.S. Geol. Survey Water-Supply Paper 489, 321 p.
- Wahrhaftig, Clyde, and Cox, Allan, 1959, Rock glaciers in the Alaska Range: Geol. Soc. America Bull., v. 70, p. 383-436.



DISSECTED GRAVELS OF THE RÍO COPIAPÓ VALLEY AND ADJACENT COASTAL AREA, CHILE

By KENNETH SEGERSTROM, Denver, Colo.

Work done in cooperation with the Instituto de Investigaciones Geológicas de Chile under the auspices of the Agency for International Development, U.S. Department of State

Abstract.—Cenozoic history of the area is largely shown by the sediments and landforms of upland-gravel, stream-terrace, and marine-terrace deposits. Upland gravel was probably deposited in late Tertiary time before the present course of the Río Copiapó was established. Fluvial-terrace gravel represents a major episode of river aggradation during an interruption of a long Pleistocene cycle of valley deepening. Surfaces of marine-terrace deposits at altitudes of 95 to 140 m and 175–235 m above sea level may represent interglacial or interstadial episodes, or both. Local faulting has vertically displaced a high marine terrace at least 40 m.

Much of the Cenozoic history of the valley of the Río Copiapó, one of the few through-going rivers of extremely arid northern Chile, and of the adjacent coastal area, must be interpreted through study of dissected gravel deposits. These deposits are here described and related to the sequence of events that produced and modified the present river valley and coastal terrace.

DRAINAGE AND RELIEF

The Río Copiapó (fig. 1) is the major (and only perennial) stream in the area. The channel of the Río Copiapó falls a little more than 1,200 meters in a distance of 156 kilometers. The mean discharge of the stream near its mouth is about 200 liters per second, but along much of its upper and middle courses the flow is perhaps 3 to 5 times that much. The present discharge of the river bears no relation to its natural regimen because large quantities of water are withdrawn for irrigation. Tributaries of the Río Copiapó are all without perennial surface flow in the area of figure 1.

The terrain is generally rugged; steep slopes are common, particularly near the valleys of the river and of some of its tributaries. Some interfluvies 1,500 to 2,500 m above sea level, or as much as 460 m higher than the

river nearby, are parts of a less-rugged matureland. Fluvial terraces which are a few meters to 100 m or more above the river extend along the sides of major valleys, and a broad marine terrace is present along the coast.

UPLAND GRAVEL

Upland gravel occurs as remnants of a broad rolling plain that formerly covered extensive areas on both sides of the Río Copiapó valley from about 16 km south-east of Elisa de Bordo to Pabellón (fig. 1). The plain is considered to be a southerly extension of the pampa of northern Chile, because it follows the same alignment as that feature and is at the same altitude, 1,000 to 1,300 m above sea level. The plain is interrupted by hills and ridges of resistant rock (Segerstrom, 1963b).

West of Elisa de Bordo an east-facing escarpment which attains a height of 460 m above the river (fig. 2, left) exposes a section of horizontally bedded gravel, 60 to 100 m thick, that overlies southeast-dipping conglomerate and volcanic rocks of the Cerrillos Formation (Cretaceous) with great angular discordance (fig. 3). The gravel deposit is a mixture of boulders, cobbles, and pebbles of volcanic, plutonic, and sedimentary rocks, in a matrix of sand, silt, and clay. The deposit is ill sorted, thick bedded, and, so far as is known, unfossiliferous. The proportion of granite cobbles is disproportionately high in relation to the limited occurrence of plutonic rock in the vicinity, which suggests that part of the gravel material was transported from distant outcrops in the high Cordillera. Therefore, the deposit and landform presumably were very extensive.

The upland gravel is important in the physiographic history of the region; like the deeply weathered bedrock that underlies it, the upland gravel is a relic

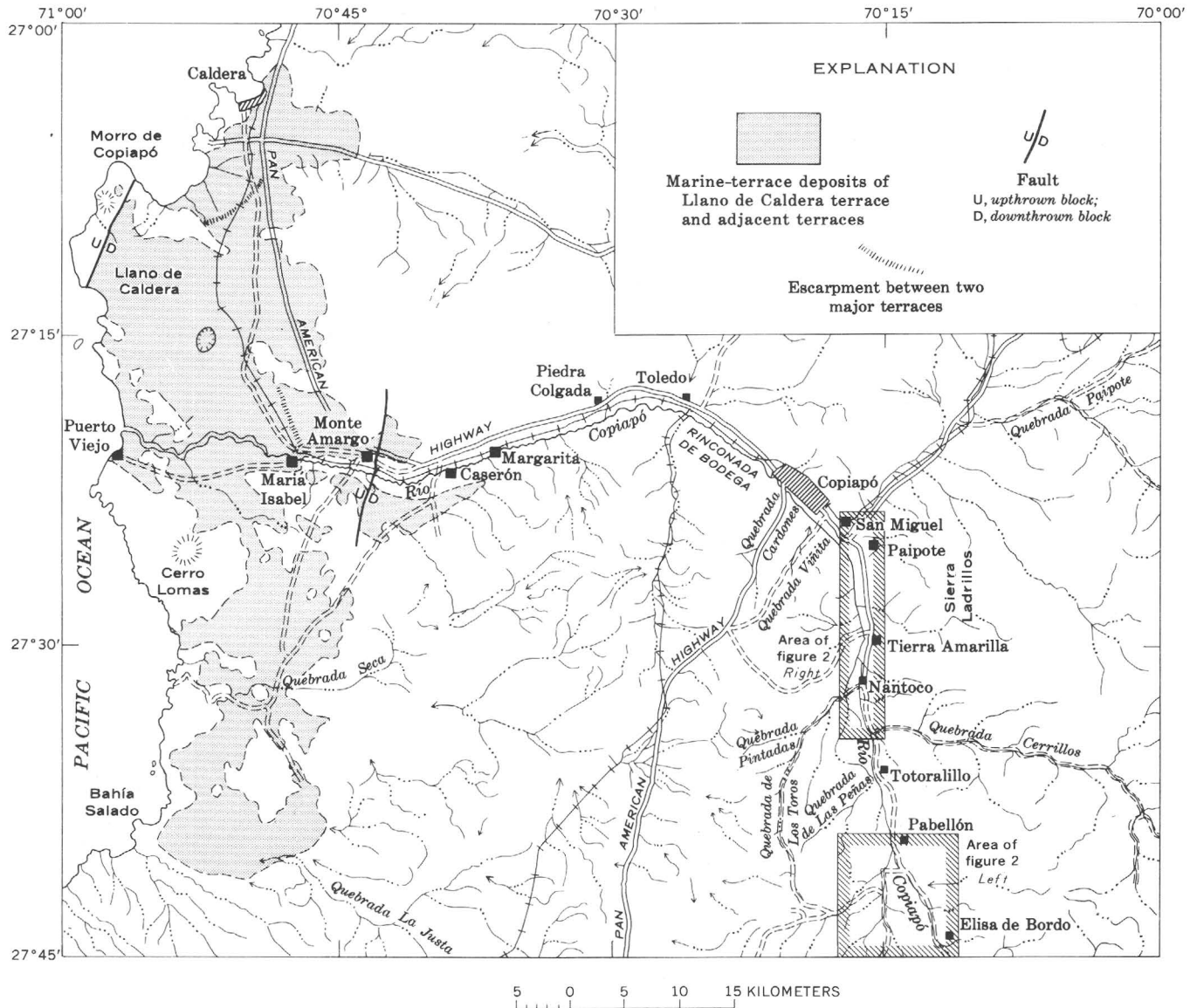


FIGURE 1.—Index map of part of the Río Copiapó watershed, and adjacent areas, showing locations of figure 2 left and right, and distribution of marine-terrace gravel. Base map from World Aeronautical Chart 1317, Point Morro.

of a mature land that antedates the formation of the Río Copiapó valley and dates back to Tertiary time (Segerstrom, 1963b, p. 517). At least locally the river was superposed on the gravel cover at the east side of a broad ancestral valley that extended from the south along to the present Quebrada Sacramento.

STREAM-TERRACE DEPOSITS

Stream-terrace deposits, or “fringing gravels,” which are fill deposits along the Río Copiapó and its tributaries, are much younger than the upland or “mantling” gravels (Willis, 1929, p. 95). The most extensive fluvial terrace along the Río Copiapó flanks the east side

of the valley for about 16 km, from Nantoco to San Miguel (fig. 2, right). The terrace, which descends relatively steeply from Sierra Ladrillos toward the Río Copiapó, consists chiefly of material derived from the east rather than from farther up the main valley (to the south). The deposit has been deeply dissected, and the underlying bedrock is exposed in large areas between the terrace segments. The segments typically stand about 70 m above the adjacent valley floor at the lower brink of the terrace and 150 m at the upper limit. However, at some places where the terrace escarpment has been cut back unusually far from the river, the brink is as much as 100 m or more above

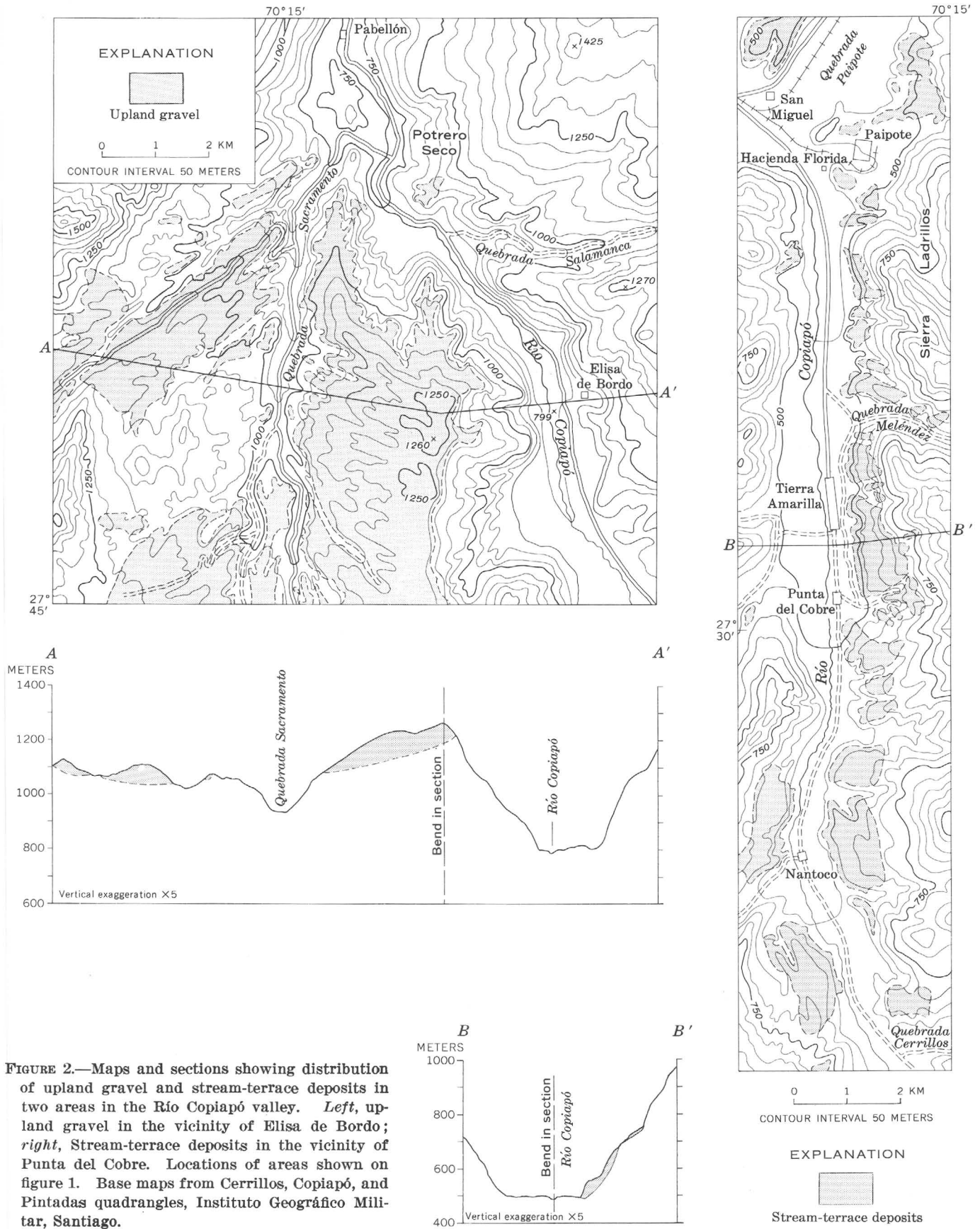


FIGURE 2.—Maps and sections showing distribution of upland gravel and stream-terrace deposits in two areas in the Río Copiapó valley. *Left*, upland gravel in the vicinity of Elisa de Bordo; *right*, Stream-terrace deposits in the vicinity of Punta del Cobre. Locations of areas shown on figure 1. Base maps from Cerrillos, Copiapó, and Pintadas quadrangles, Instituto Geográfico Militar, Santiago.

the valley floor, and the apices of some coalescing fans that are major components of the terrace deposit stand 225 to 250 m above the valley.

Two well-preserved terrace remnants remain on the west side of the river near Nantoco (fig. 2, *right*). The more southerly remnant has an abrupt eastern escarpment 107 to 115 m high that drops directly to the river. On the opposite side of the river, the brink of a terrace north of the mouth of Quebrada Cerrillos is 93 m above the river.

Small remnants of fluvatile-gravel terraces with escarpments approximately 20 m high occur along the northern flank of the valley between San Miguel, at the mouth of Quebrada Paipote, where the Río Copiapó swings westward, and a point about halfway between Toledo and Piedra Colgada. Similar remnants on the southern flank extend up Quebrada Viñita, Quebrada Cardones, and along Rinconada de Bodega. An isolated terrace of about the same height occurs far downstream, to the north of Margarita. Locations are shown on figure 1, but because of space limitations the fluvatile terraces are not shown on this figure.

The character of the bedding and sorting in the stream-terrace deposits is highly variable. At some places, bedding is excellent; at most places it is ill defined. Some of the thickest deposits contain boulders as much as 2 m in diameter set in a matrix so clay rich as to be virtually impervious. In some lenses of gravel-to silt-size material, sorting is excellent. All gradations of sorting between the two extremes are exhibited. No plant remains or other fossils have been found in the stream-terrace deposits, despite intensive search.

Multiple terraces are present on the lower reaches of Quebrada de las Peñas, a tributary of the Río Copiapó west of Totoralillo (fig. 1). About 1 to 2 km upstream from the west edge of the Río Copiapó valley, five terraces in the fill deposits of the quebrada rise steplike above the channel (fig. 4). The highest of these terraces is about 20 m above the present watercourse, and the lowest one 4 to 5 m. Such a valley-in-valley cross profile, where more than one terrace is present on both sides of the stream channel, is fortuitous and highly localized. The present channel of the quebrada is being widened by the undercutting and caving of its gravel banks during the infrequent storms that produce runoff, and this is probably how most of the intermediate terraces have been destroyed. The most persistent terrace is the highest, at the 20-m level.

The terrace levels at 70 to 115 m along the main valley represent a major episode of river aggradation—an interruption of a long Pleistocene valley-deepening cycle. The 20-m level is evidence of a later degradational episode. The lower levels along the Quebrada de las Peñas

represent minor degradational episodes in a Recent cycle of large-scale aggradation whose existence is shown by a thick fill of clastic deposits over bedrock in the main valley bottom. The bottom fill has been modified by later smaller scale trenching.



FIGURE 3.—View westward from Elisa de Bordo, showing horizontal deposits of upland gravel that unconformably overlie tilted beds of the Cerrillos Formation.

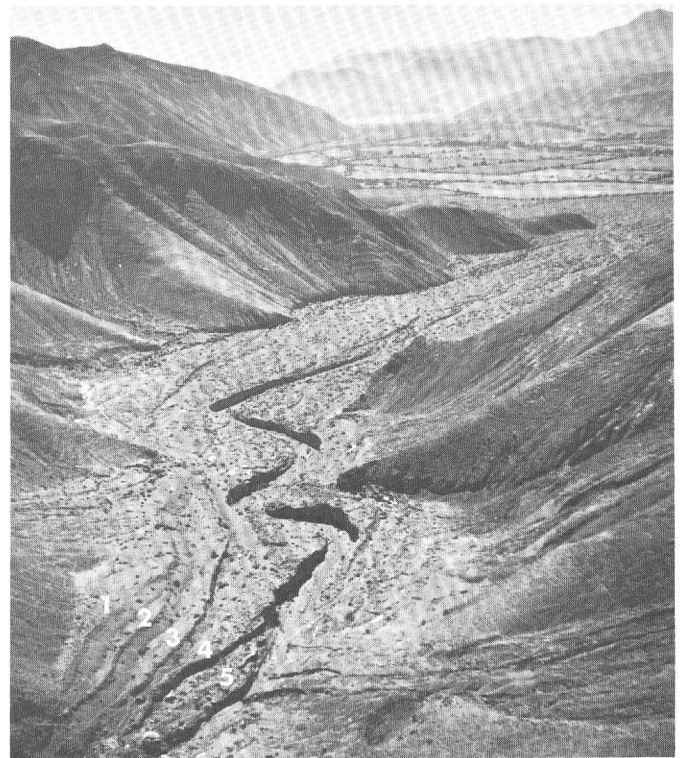


FIGURE 4.—View northeastward down Quebrada de las Peñas toward the Río Copiapó valley, showing five stream terraces in foreground (numbered consecutively from oldest to youngest).

MARINE-TERRACE DEPOSITS

From Margarita to the sea (fig. 1) the Río Copiapó valley traverses an area that was a marine embayment during Pleistocene time. Several marine terraces are preserved, the main one of which is called the Llano de Caldera terrace.

At the latitude of the Río Copiapó, the Llano de Caldera terrace extends about 16 km eastward, rising from about 95 m above sea level at the brink of a seaward escarpment to 137 m at the foot of the escarpment north of María Isabel. The terrace extends 60 km southward from near Caldera to Bahía Salado. It is 8 to 16 km wide. Eolian deflation in a central undrained zone has produced a basin whose bottom is 83 m above sea level (shown with depression contour on fig. 1).

Along the north side of the river valley a higher terrace extends about 8 km eastward, rising from about 175 m at the brink of the scarp north of María Isabel to 230 m at the brink of an east-facing escarpment. A north-northeast-striking fault which crosses the valley (fig. 1) has dropped the eastern block 40 to 50 m with respect to the western block. From the foot of the fault scarp the downfaulted terrace extends as much as 11 km farther up the valley, on the south side of the river, to an altitude of 180 m, where the terrace level becomes practically that of the present floor of the Río Copiapó valley.

On very narrow elevated beaches at the eastern edge of the former embayment, shells have been found as high as 268 m above sea level.

Along the present coast, an escarpment about 10 km south of Caldera (fig. 1) marks the boundary between

the Llano de Caldera terrace and a lower zone of terrace levels 15 m to 60 m above sea level. Elsewhere, this zone is very narrow and because of scale limitations is not shown on figure 1.

Marine beds that underlie the Llano de Caldera and higher terrace surfaces to the east are sandy and gravelly; they contain abundant mollusks and some sharks' teeth, most of which are morphologically undistinguishable from the remains that litter modern beaches (Segerstrom, 1963a). Specimens of the mollusk *Isognomon* collected near Quebrada Seca at about 100 m above sea level are larger than the average of modern forms; they may represent a warm-water species (José Corvalán, oral communication, June 1962). Hence, at least the uppermost Llano de Caldera terrace sediments were probably deposited during an interglacial or interstadial period.

There is abundant evidence of Quaternary crustal movements along the Chilean coast (Segerstrom, 1964, p. 167-168); in northern Chile the amount of general crustal uplift probably exceeds that of eustatic fall of sea level. The faults near Monte Amargo and the Morro de Copiapó are local evidence that at least part of this uplift is differential.

REFERENCES

- Segerstrom, Kenneth, 1963a, High marine terraces in the Caldera region of northern Chile [abs.]: Geol. Soc. America Spec. Paper 73, p. 237-238.
- 1963b, Matureland of northern Chile and its relationship to ore deposits: Geol. Soc. America Bull., v. 74, p. 513-518.
- 1964, Quaternary geology of Chile; brief outline: Geol. Soc. America Bull., v. 75, p. 157-170.
- Willis, Bailey, 1929, Earthquake conditions in Chile: Washington, Carnegie Institution Pub. 382, 178 p.



EARTH CRACKS—A CAUSE OF GULLYING

By WILLIAM KAM, Phoenix, Ariz.

Work done in cooperation with the Arizona State Land Department and the Maricopa County Municipal Water Conservation District

Abstract.—The development of earth cracks accompanying land-surface subsidence that results from differential compaction of heterogeneous unconsolidated sediments favors gullyng. Where newly formed earth cracks transect drainageways, lower base levels established at the points of transection favor more rapid erosion and the formation of gullies upstream from the cracks. At other places, new gullies form upslope from earth cracks where no drainageways had existed before. Where the material beneath the cracks does not absorb the water transmitted by these gullies, diversion of the gully streams along the cracks may lead to changes in drainage pattern.

Gullyng and changes in drainage patterns have occurred at several localities in southern Arizona (fig. 1)

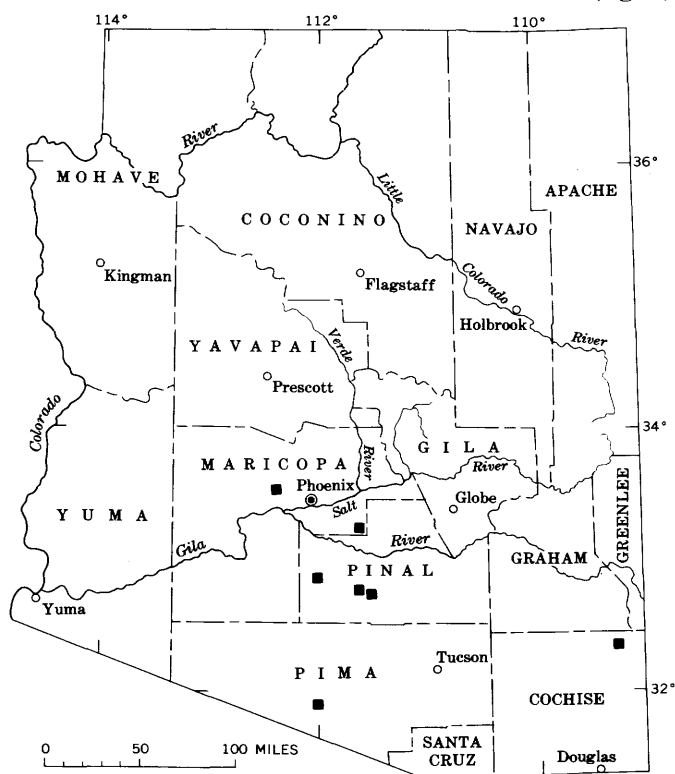


FIGURE 1.—Map of Arizona showing some areas (squares) where earth cracks have developed in alluvial deposits.

following the formation of earth cracks. According to Robinson and Peterson (1962, p. 7) these cracks accompany land subsidence which is a result of the differential compaction of heterogeneous unconsolidated alluvial deposits. Thus, land subsidence and the accompanying formation of cracks in the surface can be added to the suggested causes of gullyng, which include changes in climate, tectonic uplift, destruction of vegetative cover by fire or overgrazing, cutting of ruts along wagon trails, or a combination of these and any other factors that upset the regimens of streams.

Compaction by plastic deformation is part of a continuous complex process in the lithification of detrital sedimentary rocks (Pettijohn, 1949, p. 477). Compaction involves the elimination or reduction of pore spaces, accomplished by the partial squeezing out of interstitial fluid and the closer packing, reorientation, crushing, and deformation of grains. However, sedimentary materials vary greatly in their compressibility. Coarse-grained material, such as sand, is deposited with relatively low porosity and undergoes very little change in volume thereafter. Fine-grained materials deposited in quiet water generally have high initial porosity and are susceptible to great changes in volume with loading.

In the Basin and Range physiographic province the basins are underlain to a considerable depth by unconsolidated and semiconsolidated sediments derived from the bordering mountains. These sediments, ranging in particle size from clay to boulders, are distributed as lenses of different thickness and areal extent. Under natural conditions, the sediments having the higher porosities are compressed more under equal loads of overburden. The amount and distribution of land-surface subsidence are related, therefore, to the thickness and areal extent of the more compressible materials. In places where the subsidence rates differ appreciably within short horizontal distances, the resulting buildup of tensile stresses in the earth materials commonly leads to the formation of ruptures extending

downward from the land surface. Earth cracks thus produced may trend at any angle to the existing drainageways, and also may appear within playas.

Wherever a newly formed crack transects a drainageway it produces a lower local base level for the up-gradient segment of the drainageway. Gullying is likely to occur in this upstream segment if the crack is sufficiently wide and deep, and if it penetrates sufficiently permeable material, so as to transmit downward all the overland runoff from an appreciable area. The rate at which gullies form and the size and depth that they attain probably are governed principally by the relative rates at which water enters the crack and is absorbed by its walls or bottom, and by the length of time required for the crack to become so filled with sediment that gullying upstream from that point is arrested. Figure 2 shows a typical crack along which gullying is in progress.

A long earth crack in western Pinal County transects several drainageways (fig. 3). Upstream from their points of transection some of the drainageways have become deeply entrenched, but downgradient from the same points they have remained shallow. The presence of trees and shrubs now growing in the earth crack shows that it has served as an effective drain for several years; the approximate age of the crack probably could be determined from shrub- and tree-ring analyses. The longer an earth crack serves as an effective drain by permitting the infiltration of water which flows into it, the more likely the upstream drainageway segments emptying into it are to become entrenched, and the less likely the former pattern of drainage is to become reestablished.

According to Pashley (1961, p. 96), runoff entering a crack ordinarily does not flow laterally along it but moves downward to flow into unsaturated permeable

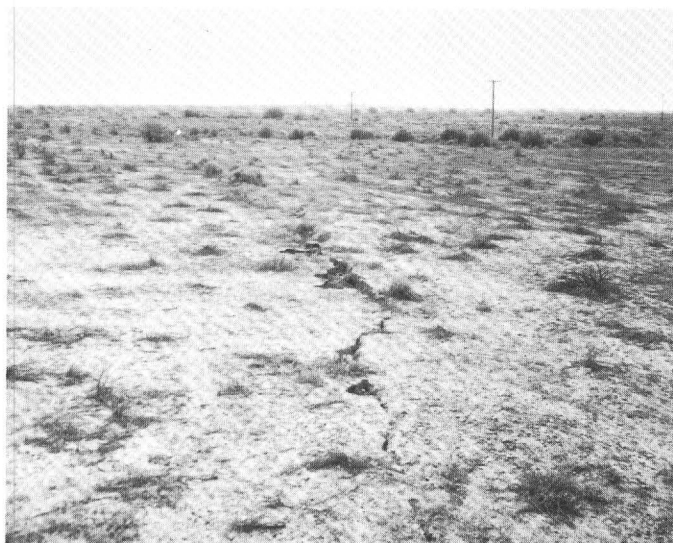


FIGURE 2.—*Left*, Earth crack 13 miles northwest of Phoenix in sec. 2, T. 2 N., R. 1 W., Maricopa County, Ariz. *Right*, Gully developing normal to the same fissure.

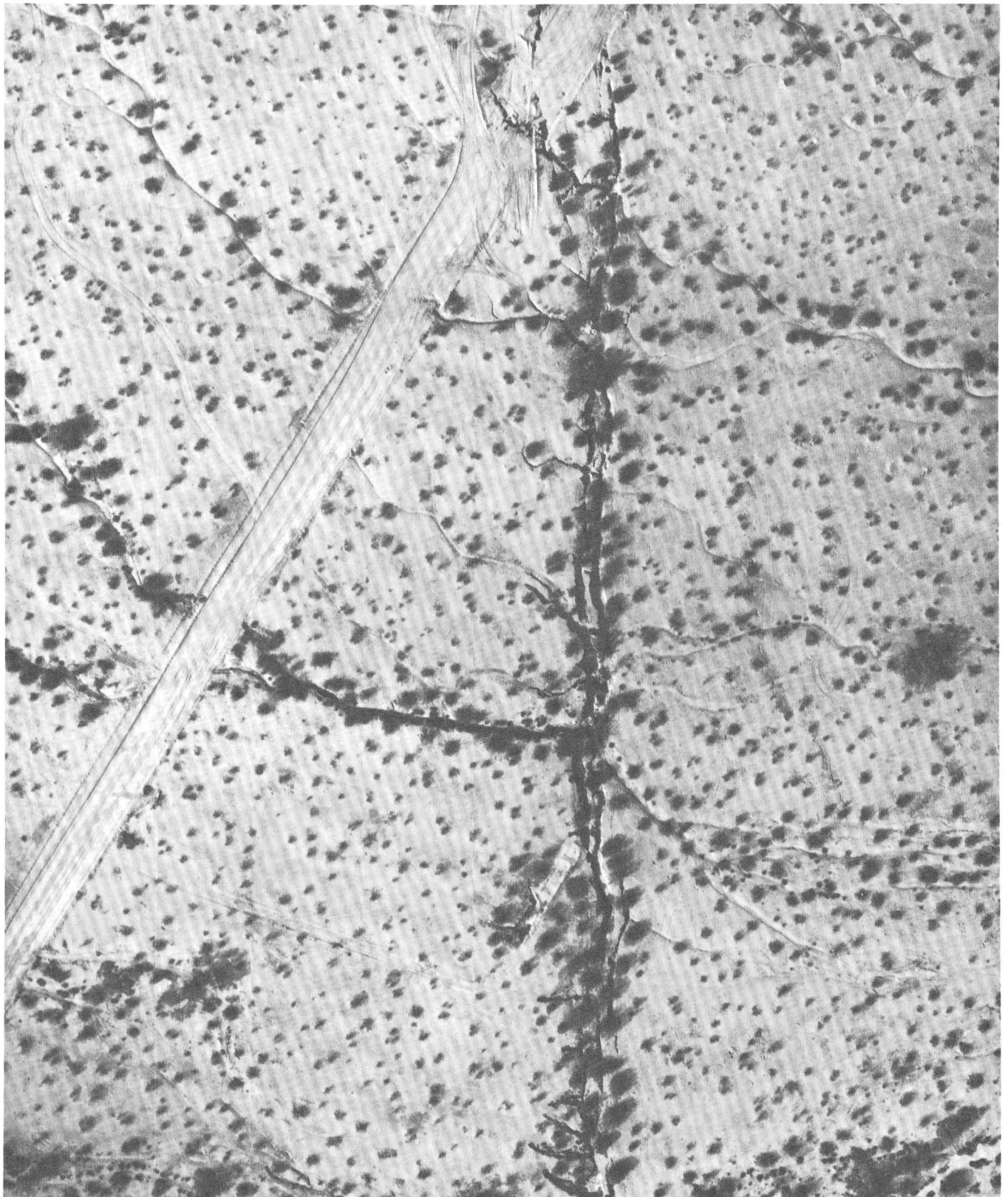


FIGURE 3.—Aerial photograph of earth cracks about 40 miles south of Phoenix in sec. 19, T. 6 S., R. 3 E., showing terminated and incised drainages.

materials above the main zone of saturation or into the main zone of saturation itself. However, where all the water cannot be transmitted downward, lateral flow in the crack is initiated; where the gradient along the crack is favorable, part of the gully may grow along the crack and a change in the pattern of surface drainage may be established.

Compaction by plastic deformation, land-surface subsidence, and the formation of earth cracks apparently are related geologic processes in the Basin and Range physiographic province. Where artesian aquifers underlie the basins, the effect of ground-water withdrawal from them and the subsequent changes in head undoubtedly accelerate the rates of compaction

by reducing buoyant forces in the aquifers. However, prior to pumping, the same effect probably manifested itself in long, extremely dry climatic periods, during which pressure losses in the artesian aquifers and gravity drainage from the water-table aquifers occurred naturally.

REFERENCES

- Pashley, E. F. Jr., 1961, Subsidence cracks in alluvium near Casa Grande, Arizona: *Arizona Geol. Soc. Digest*, v. 4, p. 95-101.
- Pettijohn, F. J., 1949. *Sedimentary rocks*: New York, Harper and Bros., 526 p.
- Robinson, G. M., and Peterson, D. E., 1962, Notes on earth fissures in southern Arizona: *U.S. Geol. Survey Circ.* 466, 7 p.



GLACIAL DEPOSITS OF NEBRASKAN AND KANSAN AGE IN NORTHERN KENTUCKY

By M. M. LEIGHTON and L. L. RAY,
Urbana, Ill., Washington, D.C.

Abstract.—Confirmatory evidence that the glacial drift of pre-Illinoian age on the uplands of northern Kentucky represents two distinct ages has recently been found. Two tills that are deeply weathered and widely separated in time of deposition have been well exposed in a roadcut some 15 miles southwest of downtown Cincinnati, Ohio, in Boone County, Ky. On the basis of their topographic position and their relation to the regional distribution of younger glacial deposits, their profiles of weathering, and their relation to the geomorphic development of the region, the older till is assigned a Nebraskan age and the overlying till a Kansan age.

Glacial drift on the uplands of northern Kentucky has been given several age designations. Although Wright (1890) described it as lying beyond the moraines now known to mark the boundary of the ice of Wisconsin age (fig. 1), he concluded that the moraines and the deposits beyond were of the same age. T. C. Chamberlin (*in* Wright, 1890, p. 15) disagreed with this age designation, stating, "I entertain the view that the drift sheets of the interior which terminate in attenuated borders—and I hold that there are more than one of these—are more ancient than the drift which terminates in the recognized ridged moraines." By the turn of the century Leverett (1899, 1902) and others had concluded that the drift of northern Kentucky was of Illinoian age, an interpretation followed on the "Glacial Map of North America" (Flint and others, 1946). Later studies (Durrell, 1956) showed that the boundary of the drift of Illinoian age was not coincident with the outer margin of the drift on the uplands of northern Kentucky, but was more restricted (fig. 1), and that no drift of Illinoian age occurs on these uplands. Therefore, the drift on the uplands must be of pre-Illinoian age. On the "Glacial Map of the United States East of the Rocky Mountains" (Flint and others, 1959) it is shown as Kansan in age. It has been sus-

pected (Durrell, 1961) that the drift of Kansan age on the uplands of northern Kentucky may represent more than a single drift, but confirmatory evidence has been lacking. A new cut along Pleasant Valley Road in Boone County, Ky. (fig. 1), provides the confirmatory evidence. Interpretations made here suggest the framework for revisions of older interpretations, as suggested by Rich (1956).

GLACIAL DEPOSITS ALONG PLEASANT VALLEY ROAD

The gently rolling upland crossed by Pleasant Valley Road has been dissected by a network of small creek valleys. There is no indication from surface features that the upland has been glaciated. Deeply weathered glacial drift is exposed in numerous shallow roadcuts; however, two distinct tills, marked by advanced profiles of weathering, crop out in an especially deep roadcut 1.8 miles northwest of the junction of Pleasant Valley Road with U.S. Highway 42 (see fig. 1 and U.S. Geological Survey 7½-minute topographic quadrangle, Union, Ky.). This roadcut, about 300 feet long and up to 25 feet deep, is at the long grade where Pleasant Valley Road descends from the uplands to cross a small unnamed creek valley (fig. 2). Here, especially well exposed on the northeast side of the road (figs. 2 and 3), an upper till overlies a lower till. The interpretation that the lower till is of Nebraskan age and the overlying till is of Kansan age rests on the relation of these two tills to the regional distribution of younger tills, on the topographic position of the Pleasant Valley roadcut, and on the relation of the advanced profiles of weathering to the geomorphic development of the region, which they reflect and confirm.

The following three sections made at this roadcut indicate the character of the two tills:

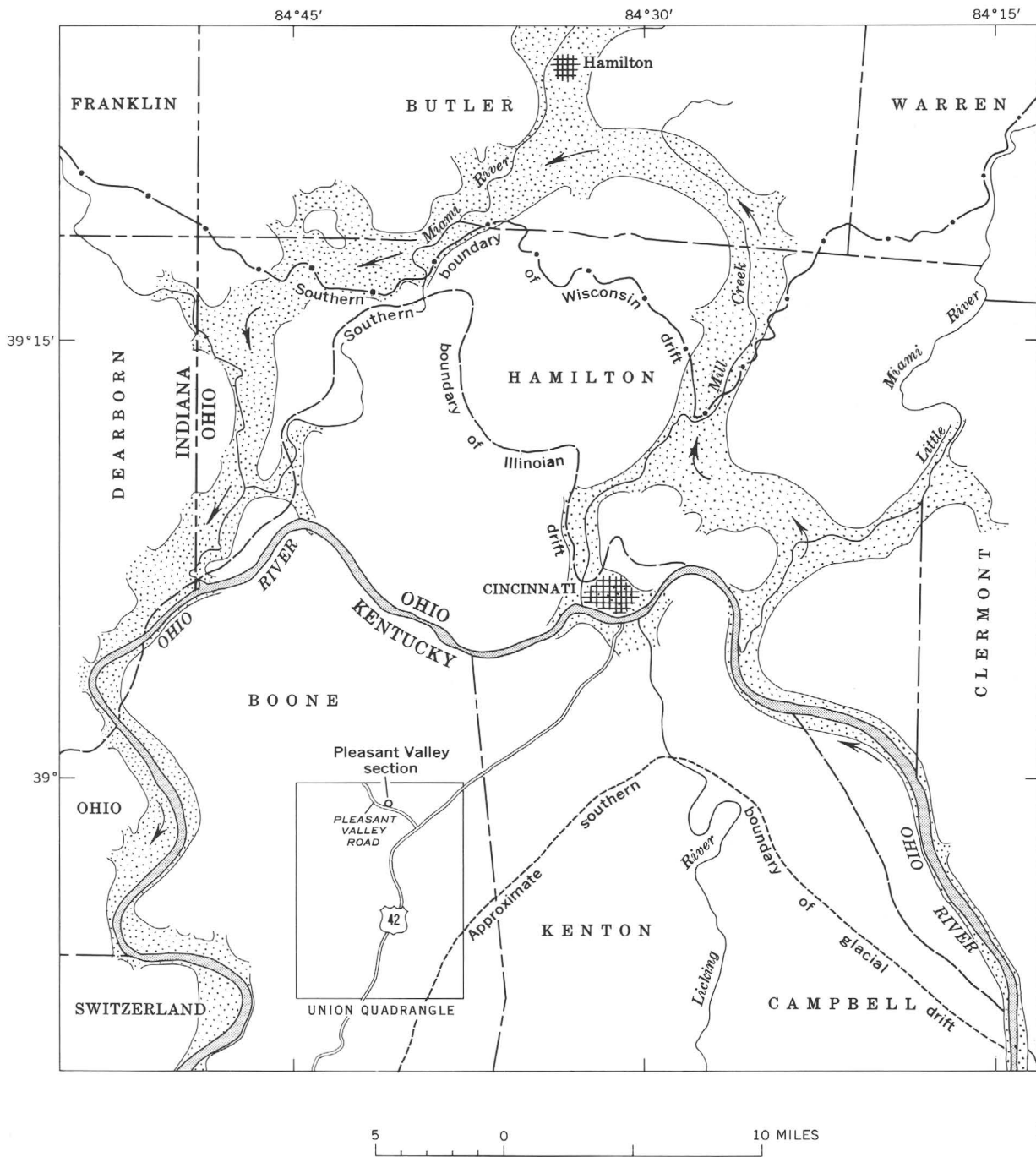


FIGURE 1.—The Cincinnati region, Ohio, Kentucky, and Indiana, showing location of Pleasant Valley Road section and its relation to glacial boundaries and to the ancient (stippled and with arrows) and present valley of the Ohio River. Modified from published reports, mainly Flint and others (1959), Goldthwait and others (1961), and Durrell (1961). Symbols for cities indicate only the downtown or central sections.



FIGURE 2.—Cut along Pleasant Valley Road, high above incised valley. Arrow is at top of gumbotil developed on Nebraskan drift. Slumping of outcrop is controlled by gumbotil.

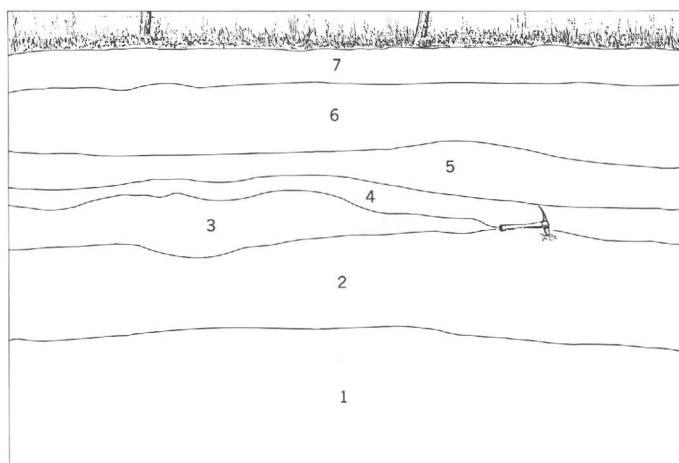


FIGURE 3.—Above, Photograph of section 1 in cut along Pleasant Valley Road. Pick is at top of gumbotil of Nebraskan age. Below, Sketch showing units in profiles of weathering in drift of Nebraskan and Kansan age in the cut. See stratigraphic section 1.

Section 1. Near southeastern end of roadcut (fig. 3)

	Thickness (feet)
Wisconsin (loess) :	
7. Loess, leached; with thin soil at top-----	3
Kansan (altered drift) :	
6. Silttil (second-cycle profile) ¹ brown, leached; thin gray soil at top; a few small resistant pebbles scattered throughout silty matrix-----	2-3
5. Gumbotil (horizon 2 of primary profile), dark-gray, clayey, tenacious; pebbles small and resistant--	2
4. Till (horizon 3), leached; pebbles larger and less altered than those in gumbotil of unit 5-----	1
Nebraskan (altered drift) :	
3. Black soil remnants (horizon 1)-----	1
2. Gumbotil (horizon 2), gray, tenacious, leached; pebbles small and resistant-----	3
1. Till (horizon 3), leached; pebbles larger than those in gumbotil of unit 2 of this section-----	3

¹ For discussion of primary and secondary cycles and of horizons of the profile of weathering, see Leighton and MacClintock (1930, 1962).

Section 2. West of section 1, about midway along length of roadcut as shown on figure 2

	Thickness (feet)
Wisconsin (loess) :	
7. Loess, leached; thin soil at top-----	2
Kansan (altered drift) :	
6. Silttil (second-cycle profile) in erosional remnants of truncated profile; contains scattered, small, resistant pebbles; noncalcareous-----	2
5. Till (horizon 3), much weathered; contains FeMnO concentrate; pebbles larger in lower part than in upper part-----	3
Nebraskan (partly altered drift) :	
4. Gumbotil (horizon 2), brownish-gray; in erosional remnant; shrinkage cracks conspicuous when dry-----	3
3. Till (horizon 3), leached; pebbles larger than those in gumbotil of unit 4-----	2
2. Till (horizon 5), calcareous, unoxidized; matrix compact-----	4
Covered by slumped material-----	3
1. Till (horizon 5), calcareous, unoxidized; crops out in deeper part of cut a few feet to west-----	3

Section 3. Near western end of roadcut, just downslope from slumped area shown on figure 2

	Thickness (feet)
Gravel of former roadbed-----	2
Kansan (altered drift) :	
7. Silttil (second-cycle profile)-----	2
6. Gumbotil (horizon 2 of primary profile)-----	4
5. Till (horizon 3), leached and oxidized-----	1
4. Till (horizon 4), calcareous and oxidized-----	2-3
Nebraskan (partly altered drift) :	
3. Till (horizon 4), leached; truncated profile; concentration of ferric oxides (ferreto zone)-----	2
2. Till (horizon 5), calcareous and unoxidized; minute woody fragments in matrix-----	3
1. Silt, sand, and clay of proglacial origin, calcareous; rests on limestone bedrock-----	8

Data from other exposures along Pleasant Valley Road reinforce conclusions drawn from these sections.

As of 1964 in a roadcut 0.9 mile to the southeast, there is exposed 5 feet of deeply weathered till. At a lower altitude, some 200 feet down the road, 4 feet of calcareous till containing limestone pebbles overlies non-calcareous gumbotil of which only 1 foot is exposed. Thus, two distinct old tills are recorded—one, assigned Kansan age, overlying one assigned Nebraskan age.

Half a mile farther southeast along Pleasant Valley Road, on the upland at an altitude of 860 feet, 3 feet of gumbotil crops out in a roadcut (fig. 4) beneath 4 feet of

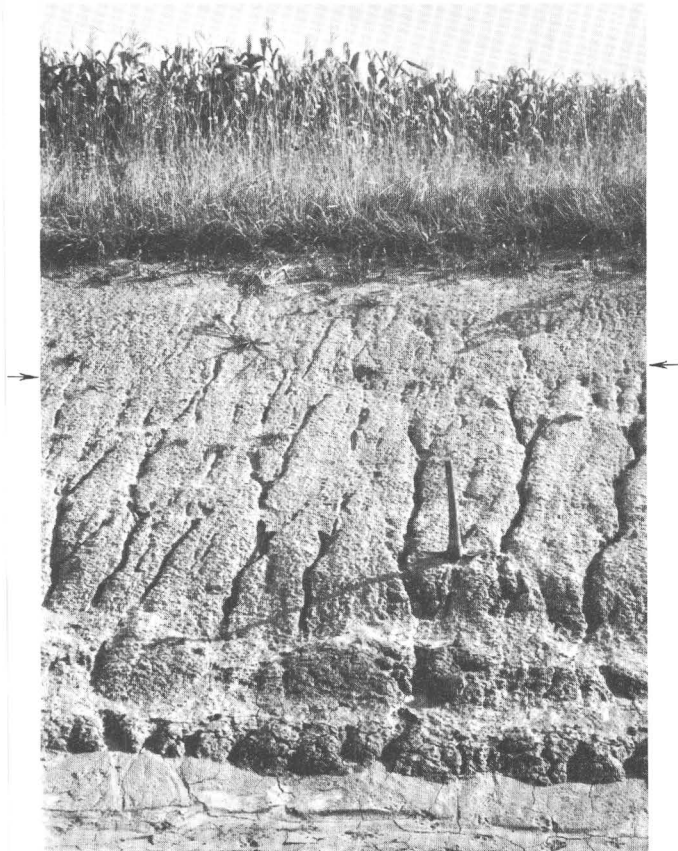


FIGURE 4.—Exposure on Pleasant Valley Road, 1.4 mile southeast of area shown on figures 2 and 3. Pick marks top of Kansan gumbotil (3 feet exposed), which is overlain by 4 feet of second-cycle silttil. At the surface is a 2-foot mantle of Wisconsin loess with a well-drained profile of weathering. Marginal arrows mark top of silttil and base of Wisconsin loess.

silttil and 2 feet of surficial loess. This gumbotil is the upper till of the uplands to the northwest, and it is identified as Kansan till because its advanced weathering far exceeds that of drift of Illinoian age.

PROFILES OF WEATHERING AND THE RELATED GEOMORPHOLOGY

Profiles of weathering in the upland tills reflect the character of the drainage conditions and thus of the

landscape. Where conditions of drainage were poor, gumbotil developed; where conditions of drainage were good, silttil developed. Where gumbotil was developed in the primary cycle of weathering and drainage conditions improved, secondary silttil developed (Leighton and MacClintock, 1930, 1962). Thus, changes in conditions of drainage, which are related to the glacial and geomorphic history of the Cincinnati region, are in turn reflected in the character of the profiles of weathering of the upland drifts.

The first glacier to invade the Cincinnati area, the Nebraskan, moved across an extensive upland of low relief into the area that today is northern Kentucky (fig. 1). Conspicuous remnants of the preglacial upland, locally at elevations of 800 to 900 feet, are widely recognized in southeastern Indiana, northern Kentucky, and southwestern Ohio, where they have been referred to the Lexington peneplain (Fenneman, 1916, 1938). In the Cincinnati area the upland appears to have been drained by northward-flowing streams which occupied broad, shallow valleys 50 to 100 feet below gently undulating interflaves.

Preglacial drainage was disrupted by the ice invasion of Nebraskan age, which dammed and ponded the northward-flowing streams. Proglacial outwash and other sediments deposited in these ponded valleys in front of the advancing ice were overridden at some places (see section 3). Ponded streams were forced into new channelways, some of which, augmented by the voluminous glacial melt waters, became permanently established. Thus, by the close of Nebraskan time the Ohio River appears to have been established upon the upland surface of the Cincinnati area. Its course differed in part from that of today, however, for it followed the well-known ancient channelway northward around Cincinnati to Hamilton, Ohio, and thence southwestward to join what is now the present Ohio valley west of Cincinnati (fig. 1).

Drainage was poorly organized, especially in the glaciated areas, after establishment of the Ohio River across the upland. During Aftonian time, the master stream, the Ohio, entrenched its valley below the drift-covered upland surface. Bedrock benches indicative of this stage of landscape dissection have been noted (Brand, 1934; Durrell, 1961), but without the interpretation here given. Short tributary streams sharply entrenched in bedrock eroded headward from the deepened major valley into the margin of the poorly drained upland, thereby improving drainage conditions. Far from the master stream, however, glacial drift on the upland remained little eroded and poorly drained; it became deeply weathered in place, as is indicated by the presence of gumbotil.

Following Aftonian weathering and erosion the Kansan ice advanced across the drift-mantled uplands of northern Kentucky, south and southwest of Cincinnati. This advance appears to have been slightly less extensive than that of the earlier Nebraskan. Effacement of the glacial surface features by deep weathering and erosion during Yarmouth and later time was so complete that virtually no surface features referable to either of these glaciations remain.

During Yarmouth, the longest of the interglacial times, the Ohio River in the Cincinnati area appears to have cut its bedrock valley to its greatest depth, the so-called "Deep Stage" (Rich, 1956). It was one of the major rivers of the continent and a striking example of early glacial diversion of pre-Pleistocene drainage. Valleys tributary to the major streams were accordingly deepened again and extended farther headward into the drift-covered upland where weathering of the drift was continuing in place. The presence of gumbotil in the profile of weathering, as in sections 1 and 3, indicates that the area crossed by the Pleasant Valley Road remained poorly drained throughout most of Yarmouth time. The silttil, which resulted from a second cycle of weathering imposed on the primary cycle, records the headward extension of valleys into this area, which in turn created better drainage and led to eluviation of much of the clay from the gumbotil. The sharply incised valley shown in figure 2 and the topographic position of the silttil in the same figure disclose the striking relationship between silttil and topography. Gumbotil of Nebraskan and that of Kansan age could not have been formed after the present valley had been cut. Development of the silttil on drift of Kansan age required the improved drainage conditions. The topographic unconformity here is thus intermediate in age.

During the third glacial invasion of the area, the Illinoian, which came late in the Pleistocene, the entrenched river channel around Cincinnati was in large part ice blocked so that it was not then a through drainageway (fig. 1). It was at this time that a new channel was developed beyond the ice margin from the present mouth of the Little Miami River to the mouth of the Miami River (Durrell, 1961). The resulting gorgelike river channel in this area separated the drift-covered uplands of Kentucky from those of Ohio.

No ice of Illinoian age moved on to the uplands of northern Kentucky. It did, however, occupy a part of the upland north of Cincinnati (Goldthwait and others, 1961), and marginal lobes extended into and down

the deeply entrenched valleys (Durrell, 1956, 1961). At several places along the Ohio, both above and below Cincinnati, ice assigned an Illinoian age pushed across the entrenched Ohio valley and deposited small masses of till along the valley wall in Kentucky (fig. 1). Leverett (1929) noted that some of this till occurs at, and perhaps well below, present river level.

Weathering and erosion of the drift in northern Kentucky continued during both the Illinoian ice invasion and the succeeding Sangamon time, for lack of a mantle of loess in this area left the older till exposed at the surface. When drainage conditions on the uplands improved, however, as a result of the deepening and extension of the drainage net, profiles of weathering on the glacial deposits were modified. Conditions were no longer favorable for the formation of gumbotil, and second-cycle silttil developed on the exposed gumbotils. Today, drift deposits generally have second-cycle silttil where good drainage conditions have been long established.

Although the last glaciation, the Wisconsin, fell short of reaching northern Kentucky, its extensive outwash valley trains choked the major glacial drainageways in the Cincinnati area. These were source areas for the thin veneer of loess that mantles the glaciated areas in this part of northern Kentucky. The loess ranges from 6 or more feet in thickness nearest the source areas to less than 2 feet near the outer boundary of the upland drift. It is thoroughly leached and silty and exhibits a profile of weathering indicative of good drainage. Where the loess overlies silttil it may merge with it so imperceptibly that, where the loess is thin, the two may be difficult to separate in the field except on the basis of the weathered chert, quartz, and quartzite pebbles scattered through the silttil. Where the loess is thicker, its demarcation from the silttil can be more readily determined. Weathering of the underlying drifts has been impeded since deposition of the blanket of loess.

REFERENCES

- Brand, L. S., 1934, Some notes on the Pleistocene history of the Cincinnati region: *Ohio Jour. Sci.*, v. 34, p. 67-85.
- Durrell, R. H., 1956, Illinoian boundary in southwestern Ohio and northern Kentucky [abs.]: *Geol. Soc. America Bull.*, v. 67, p. 1751.
- 1961, The Pleistocene geology of the Cincinnati area, in *Guidebook for field trips, Cincinnati meeting: Geol. Soc. America Guidebook Ser.*, 1961, p. 47-57.
- Fenneman, N. M., 1916, *Geology of Cincinnati and vicinity: Ohio Geol. Survey Bull.* 19, 207 p.
- 1938, *Physiography of eastern United States: New York, McGraw-Hill*, 714 p.

- Flint, R. F., and others, 1946, *Glacial map of North America*: Geol. Soc. America Spec. Paper 60.
- 1959, *Glacial map of the United States east of the Rocky Mountains*: New York, Geol. Soc. America.
- Goldthwait, R. P., White, G. W., and Forsyth, J. L., 1961, *Glacial map of Ohio*: U.S. Geol. Survey Misc. Geol. Inv. Map I-316.
- Leighton, M. M., and MacClintock, Paul, 1930, *Weathered zones of drift sheets of Illinois*: Jour. Geology, v. 38, p. 28-53.
- 1962, *The weathered mantle of glacial tills beneath original surfaces in north-central United States*: Jour. Geology, v. 70, p. 267-293.
- Leverett, Frank, 1899, *The Illinois glacial lobe*: U.S. Geol. Survey Mon. 38, 817 p.
- 1902, *Glacial formations and drainage features of the Erie and Ohio basins*: U.S. Geol. Survey Mon. 41, 802 p.
- 1929, *The Pleistocene of northern Kentucky*: Kentucky Geol. Survey, ser. VI, v. 31, p. 1-71.
- Rich, J. L., 1956, *Pre-Illinoian age of upland till in southeastern Indiana, southwestern Ohio, and adjacent parts of Kentucky* [abs.]: Geol. Soc. America Bull., v. 67, p. 1756.
- Wright, G. F., 1890, *The glacial boundary in western Pennsylvania, Ohio, Kentucky, Indiana, and Illinois*: U.S. Geol. Survey Bull. 58, 112 p.



AGE AND ORIGIN OF THE PUGET SOUND TROUGH IN WESTERN WASHINGTON

By DWIGHT R. CRANDELL, DONAL R. MULLINEAUX,
and HOWARD H. WALDRON, Denver, Colo.

Abstract.—Radiocarbon dates from nonglacial deposits indicate nonglacial aggradation in the Puget Sound lowland from more than 35,000 years ago to 15,000 years ago. Subsequent ponding of lowland drainage by the Puget glacier lobe during the Vashon Stade of the Fraser Glaciation and deposition of outwash sediments from the Puget lobe resulted in further aggradation. Aggradation was followed by advance of the lobe and ice scour of the Puget Sound trough to a maximum depth of about 930 feet below present sea level.

The deep troughs and intervening plateaus of the Puget Sound lowland are the dominant physiographic features of the area, and their formation, which was chiefly in Pleistocene sediments, has been discussed repeatedly. Most recent authors have favored a hypothesis under which the troughs were fluvially eroded into a preexisting plain, then modified by glacial scour during the last glaciation. However, recent detailed study of the Pleistocene geology of Seattle and reconnaissance study of the central part of the lowland suggest that the Puget Sound trough was actually formed by ice scour rather than simply modified by it. This paper, which presents the evidence and interpretations that lead to this conclusion, concerns the trough occupied by the main body of Puget Sound. However, some of the discussion probably bears on the age and origin of other deep troughs in the central part of the lowland.

The Puget Sound trough, which extends from Admiralty Inlet southward to Tacoma (fig. 1), is about 40 miles long and generally 3 to 5 miles wide. Throughout most of its length, its depth is 600 to 700 feet; a maximum depth of about 930 feet below sea level is reached at a point just north of Seattle (U.S. Coast and Geodetic Survey Chart 6401). Puget Sound is connected to the Strait of Juan de Fuca and the Pacific Ocean by Admiralty Inlet, which is only 100 to 200 feet deep at its northern end. The Puget Sound trough is the largest of many comparable troughs in the Puget Sound low-

land; most of these, such as Hood Canal and Saratoga Passage (fig. 1), are now occupied by sea water.

The last glaciation of the lowland occurred during the Vashon Stade (see accompanying table), when an ice sheet originating in the coastal mountains of southwestern British Columbia flowed southward into the Puget Sound lowland to form the Puget lobe. At its maximum extent this lobe terminated about 50 miles south of Seattle, and it probably attained a thickness of at least 4,000 feet over the Puget Sound trough at Seattle.

TABLE 1.—*Geologic-climate units of the later part of Pleistocene time in the Puget Sound lowland and their relation to stratigraphic units*

[After Crandell and others (1958) and Armstrong and others, report in preparation]

Geologic-climate unit		Stratigraphic units described in this paper
Fraser Glaciation	Sumas Stade	
	Everson Interstade	
	Vashon Stade	Vashon Drift Esperance Sand Member Lawton Clay Member
Olympia Interglaciation		Nonglacial deposits
Salmon Springs Glaciation		

STRATIGRAPHY AND CHRONOLOGY

Deposition of a conformable sequence of nonglacial and glacial sediments in the central part of the lowland preceded cutting of the Puget Sound trough; thus the age, origin, and original lateral extent of these sediments are critical to an understanding of the origin of the trough. According to Bretz (1913, p. 188-194, 199, 226-227) the sediments are chiefly alluvium formed by glacial streams that aggraded the lowland to a broad

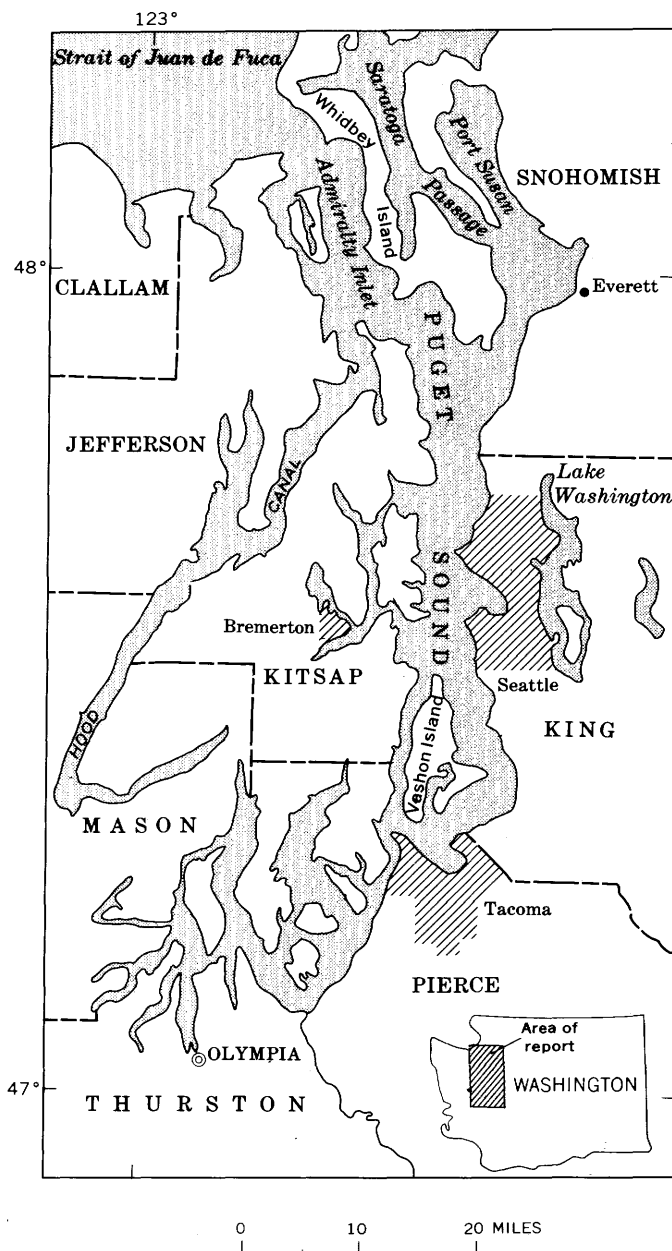


FIGURE 1.—Puget Sound and adjacent area in western Washington.

flat plain during a pre-Vashon glaciation; deposition ended as a result of about 1,000 feet of uplift, which also caused streams to erode deep valleys before the Vashon Stade. By a second interpretation (Willis, 1898, p. 119), the sediments are ice-marginal outwash deposited between adjacent ice tongues during repeated occupations of the lowland by the Puget lobe; the ice itself preserved preexisting troughs while outwash built up the adjacent uplands. A third interpretation, suggested by our current studies, is that the sediments represent virtually continuous nonglacial and glacial

aggradation just before and during an early part of the Vashon Stade.

A nonglacial deposit at the base of the sequence in the Seattle area, on the east side of the Puget Sound trough, consists of interbedded sand, silt, and clay which are of fluvial and lacustrine origin (Mullineaux and others, 1964). A correlative deposit occurs in the upland on the west side of the Puget Sound trough west and south of Seattle; south of the latitude of Seattle the deposit commonly includes beds of fluvial gravel. Radiocarbon dates from peat and wood in the non-

glacial deposits range from about 15,000 to 24,000 years before the present in the Seattle area (Mullineaux and others, 1964) and from about 28,000 to 35,000 years B.P. in the lowland south of Seattle (Dorn and others, 1962). The deposits probably were formed on the broad, locally ponded flood plains of rivers that drained northward toward Admiralty Inlet during the Olympia Interglaciation (Mullineaux and others, 1964). The flood plains were bounded by uplands that consisted chiefly of sediments formed during older glaciations and interglaciations. To what extent the uplands of the present coincide with those old uplands is not known. The flood-plain deposits now extend to a height of about 65 feet above present sea level on the east side of the trough at Seattle, and to a comparable altitude on the west side of the Puget Sound trough directly opposite (Sceva, 1957, pl. 1).

Deposition of the nonglacial fluvial sediments was brought to an end by the southward advance of the Puget glacier lobe, which blocked the northward drainage from the lowland and formed a proglacial lake. Silts and clays were deposited in this lake, conformably over the nonglacial sediments, to a height of 150 feet or more above present sea level. These silts and clays constitute the Lawton Clay Member of the Vashon Drift (Mullineaux and others, 1964). The Lawton Clay Member grades conformably upward into the Esperance Sand Member of the Vashon Drift, which is regarded as proglacial outwash and is the youngest widespread deposit formed before the glacier overrode the lowland.

The interpretation of these deposits is fundamental to an explanation of the history of the trough. The age, distribution, and conformable nature of the nonglacial deposits and Lawton Clay Member provide a lower limit for the age of the trough, while the origin and distribution of the Esperance Member may bear on its location and configuration.

Newcomb (1952, p. 20) recognized two major units within the Esperance and stated that "The earlier phase of the sand member appears to be a coarser continuation of the horizontal Admiralty clay, whereas the later outwash phase is undoubtedly the advance outwash of the Vashon glacier." In this paper the Esperance Sand Member is restricted to the "later outwash phase" of Newcomb, following the usage proposed by Mullineaux and others (1964).

The Esperance Sand Member is chiefly fine to medium sand that contains some thin beds of silt. Lenticular beds of coarse sand and granule- to pebble-gravel are common, and in some areas increase upward in abundance, thickness, and coarseness. The sediments display a variety of types of stratification. Most

commonly the lower part of the sand is massive or horizontally bedded, suggesting that the early part of the deposition occurred in quiet, ponded water. Current bedding and cut-and-fill stratification become more abundant toward the top, indicating later fluvial deposition. The direction of foresetting in the sand in the central part of the lowland indicates southward or southeastward transport of sediment.

The Esperance Sand Member is widely distributed in the uplands, both east and west of the Puget Sound trough, from Admiralty Inlet to Tacoma. The sand is widely distributed in the Seattle area between altitudes of about 150 and 400 feet. Many of the sea cliffs west of Everett expose as much as 150 feet of the sand. In Kitsap County, Sceva (1957, pl. 1) mapped the correlative of the sand along the east side of Hood Canal.

The Esperance Sand Member is an extensive and thick sedimentary deposit formed before the lowland was overridden by the Puget lobe. The sediment is believed to have come from the Puget lobe (1) because of the south and southeast dips of the foreset bedding of the deposit, and (2) because the only likely alternative sources, alpine glaciers in the Cascade Range during the Fraser Glaciation, were apparently of insignificant size during the advance of the Puget lobe (Vance, 1957). We postulate, therefore, that the Esperance was deposited by outwash streams, and that it probably was derived largely from the reworking of older unconsolidated glacial and nonglacial deposits in the lowland by the Puget lobe during its advance, even though part of the sand may represent alluvium introduced by streams draining the Cascade Range.

Following deposition of the Esperance Sand Member the Puget lobe overrode the Seattle area, terminating near the southern margin of the Puget Sound lowland about 50 miles from Seattle. Subsequent retreat of the glacier uncovered the Seattle area by about 13,500 B.P. (Rigg and Gould, 1957). Thus, using the youngest date (15,000 B.P.) for the nonglacial deposits as an older limit for the Vashon Drift, we conclude that the episode of deposition of the Lawton and Esperance Members and occupation of the Seattle area by the Puget lobe was limited, before and after, by dates of about 15,000 and 13,500 years, respectively. The short time between these limiting dates suggests that the Esperance was overridden by the glacier immediately after its deposition.

ORIGIN OF TROUGH

Three hypotheses for the origin of the Puget Sound trough and other similar troughs in the lowland have previously been suggested: (1) glacial scour into a pre-existing fill (LeConte, 1874); (2) preservation of pre-

glacial valleys during building up of intervening ridges (Willis, 1898); and (3) stream erosion into a preexisting fill (LeConte, 1874; Bretz, 1913). LeConte thought that glacial erosion was the more probable of the two hypotheses he suggested; he proposed that in either case the troughs had been cut when the region was higher above sea level than it is now. Willis assumed the existence of preglacial valleys and proposed that ice tongues in the valleys preserved them while glaciofluvial deposits built up the adjacent uplands to form broad plateaus. Bretz pointed out, however, that the plateaus are not cored with bedrock, and that some deposits can be correlated from one plateau to another. He favored fluvial erosion of the troughs in a preexisting fill, after regional uplift of about 1,000 feet during a pre-Vashon nonglacial episode.

The evidence now recognized along the Puget Sound trough and described above suggests that glacial scour is the only hypothesis consistent with facts now at hand. The stratigraphic sequence and age of the deposits at Seattle provide the most compelling evidence. These indicate that the site of the Puget Sound trough adjacent to Seattle had been aggraded to a surface several tens of feet above present sea level by the end of the Olympia Interglaciation, only about 15,000 years ago. Subsequently, with no evidence of an intervening erosional period, the fill was further raised to a level more than 150 feet above present sea level by the deposition of lacustrine silt and clay as the Puget lobe blocked the Strait of Juan de Fuca. Uninterrupted aggradation continued with the deposition of sand over the silt and clay until the glacier overrode the Seattle area. This evidence seems to prove that no deep trough existed when the glacier reached the area, yet the trough in virtually its present shape had been formed by the time the glacier retreated, less than 1,500 years later. Thus, the glacier must have eroded the trough. Although this interpretation depends chiefly on the stratigraphic sequence and age of the deposits, it is strongly supported by the alignment and shape of the Puget Sound trough and other troughs. First, the long axes of these troughs closely parallel the dominantly southward direction of movement of the Puget lobe during the Vashon Stade. Second, the floor of the Puget Sound trough lies hundreds of feet below the deepest part of Admiralty Inlet, which strongly suggests deepening by glacial scour. Finally, smaller basins with several hundred feet of closure indent the floor of the main trough, and their direction of elongation parallels the trend of the trough (see U.S. Coast and Geodetic Survey Charts 6445 and 6446).

Implicit in the proposal that glacial scour produced the trough is a rejection of the commonly held idea that

the Puget Sound region was elevated and subsequently depressed by as much as 1,000 feet in late Pleistocene time (Bretz, 1913; Newcomb, 1952; Sceva, 1957; Crandell and others, 1958). This hypothesis of regional uplift and subsidence rests wholly on the depth of the troughs and on the inference that they were subaerially eroded by streams or glaciers. We have found no independent evidence of late Pleistocene change in level of this amount in the Puget Sound lowland.

We do not know why or how the glacier eroded so deeply at one place in the broad lowland and not at another. Three alternative explanations may be noted: (1) If the Esperance Sand Member was spread in front of the Puget lobe as a continuous sheet, burying preexisting topography up to a present altitude of about 400 feet, the locations of the Puget Sound trough and other similar troughs might well be random. (2) If, however, the gross outline of the trough existed during Olympia time, the trough might have localized deposition of the Olympia sediments, the Lawton Clay Member, and the Esperance Sand Member. The difference in resistance to erosion between these loose, saturated sediments and the older, highly compacted deposits might then have favored deepest scour where the younger sediments were thickest. (3) Finally, a preexisting trough might have influenced ice scour if it were not completely filled with the Esperance Sand Member (J. H. Mackin, University of Texas, oral communication, 1964). By this last interpretation, a tongue of ice may have entered a shallow preexisting valley or trough in advance of the main body of the Puget lobe, preserving the trough as the later, upper parts of the Esperance were deposited beyond its margins. The preexisting trough then localized ice scour, resulting in erosion of the trough to its ultimate depth.

Although such a lobation of the Puget glacier may satisfactorily explain localization of the Puget Sound trough, it seemingly does not adequately account for the position of some deep depressions, such as the Lake Washington trough, that are closed at their northern ends. It may well be that some depressions were localized by preexisting topography, that others were scoured in wholly random positions, and that still others were localized by factors not yet understood.

The postulated eroding ability of the Puget lobe during the Vashon Stade was probably not unique, for the presence of an extensive erosional unconformity below the youngest pre-Vashon till in the central part of the lowland suggests the possibility that the glacier that deposited the till also deeply scoured the lowland.

REFERENCES

- Bretz, J. H., 1913, *Glaciation of the Puget Sound region*: Washington Geol. Survey Bull. 8, 244 p.

- Crandell, D. R., Mullineaux, D. R., and Waldron, H. H., 1958, Pleistocene sequence in southeastern part of the Puget Sound lowland, Washington: *Am. Jour. Sci.*, v. 256, p. 384-397.
- Dorn, T. F., Fairhall, A. W., Schell, W. R., and Takashima, Y., 1962, Radiocarbon dating at the University of Washington I: *Radiocarbon*, v. 4, p. 1-12.
- LeConte, Joseph, 1874, On the great lava-flood of the Northwest; and on the structure and age of the Cascade Mountains: *Am. Jour. Sci.*, v. 7, p. 259-367.
- Mullineaux, D. R., Waldron, H. H., and Rubin, Meyer, 1964, Stratigraphy and chronology of late interglacial and early Vashon glacial time in the Seattle area, Washington: U.S. Geol. Survey Bull. 1194-0.
- Newcomb, R. C., 1952, Ground-water resources of Snohomish County, Washington: U.S. Geol. Survey Water-Supply Paper 1135, 133 p.
- Rigg, G. B., and Gould, H. R., 1957, Age of Glacier Peak eruption and chronology of post-glacial peat deposits in Washington and surrounding areas: *Am. Jour. Sci.*, v. 255, no. 5, p. 341-363.
- Sceva, J. E., 1957, Geology and ground-water resources of Kitsap County, Washington: U.S. Geol. Survey Water-Supply Paper 1413, 178 p.
- Vance, J. A., 1957, The geology of the Sauk River area in the northern Cascades of Washington: Univ. Washington, Ph.D. thesis, available on microfilm from University Microfilms, Inc., Ann Arbor, Mich.
- Willis, Bailey, 1898, Drift phenomena of Puget Sound: *Geol. Soc. America Bull.*, v. 9, p. 111-162.



RATE OF ICE MOVEMENT AND ESTIMATED ICE THICKNESS IN PART OF THE TETON GLACIER, GRAND TETON NATIONAL PARK, WYOMING

By JOHN C. REED, JR., Denver, Colo.

Abstract.—Markers placed on the Teton Glacier near the snowline in August 1963 advanced as much as 37 feet in 13 months while the terminus of the glacier remained in the same position. Movement was nearly uniform in amount and direction across the glacier to within less than 100 feet of the edges; evidently the glacier moved mostly as a rigid mass, presumably by intense shear in a thin basal and marginal zone and by slippage over the bed. Computations based on changes in surface slope and elevation suggest that the glacier may be as thin as 50 feet at the line of markers.

The Teton Glacier lies at altitudes of between 10,200 and 11,400 feet, at the head of a spectacular cirque between the east ridge of the Grand Teton and Mount Owen (fig. 1). The glacier has been described by Fryxell (1935), and its retreat since 1929 has been discussed by Reed (1964). On August 16, 1963, metal stakes and marks on boulders were placed along a line

across the glacier (Reed, 1964, fig. 1 and table 2) just below the snowline. Figure 2 shows the outline of the glacier and the position of the line of markers. On September 21, 1964, these markers were resurveyed, and a new set of stakes was placed along the original line. Table 1 shows the direction and amount of movement of the 1963 markers; table 2 gives the position of the 1964 stakes. A large erratic boulder marked as point G, about 300 feet downglacier from the line of markers, was perched on a 5-foot ice pedestal when it was surveyed in 1963. In 1964 the boulder was found 105 feet S. 47° E. of its 1963 position. This amount of movement, which is far greater than that of any of the marks in the line of profile, is thought to be due to toppling and sliding from successive pedestals in the manner described by Fryxell (1933).

TABLE 1.—*Movement of markers on Teton Glacier from Aug. 17, 1963, to Sept. 21, 1964*

Point	Distance from mark on south wall in 1963 (feet)	Marker	Horizontal movement (feet)	Direction	Altitude above datum (feet) ¹		Remarks
					1963	1964	
0_-----	0	Red paint "X" on bedrock_--	0	-----	623. 6	623. 6	
1_-----	29	Iron pipe_-----	-----	-----	614. 2	-----	Marker lost.
2_-----	117	do_-----	32. 7	S. 38° E.	617. 8	612. 0	Ice surface.
3_-----	215	do_-----	35. 3	S. 42° E.	629. 6	617. 6	Do.
4_-----	310	Red paint on boulder_-----	² 32. 7	S. 50° E.	657. 7	653. 6	Top of boulder, 5 ft above ice surface in 1963.
5_-----	410	Iron pipe_-----	35. 2	S. 53° E.	645. 4	640. 4	Ice surface.
6_-----	510	do_-----	36. 2	S. 53° E.	639. 2	634. 7	Do.
7_-----	610	do_-----	36. 9	S. 55° E.	646. 8	640. 5	Do.
8_-----	710	do_-----	36. 7	S. 57° E.	649. 7	644. 4	Do.
9_-----	810	do_-----	37. 0	S. 56° E.	647. 4	638. 8	Do.
10_-----	910	do_-----	36. 6	S. 59° E.	650. 8	642. 8	Do.
F_-----	1,000	Red paint on boulder_-----	² 39. 8	S. 53° E.	661. 5	654. 3	Top of boulder, 2 ft above ice surface in 1963.
11_-----	1,010	Iron pipe_-----	31. 4	S. 58° E.	660. 0	651. 6	Ice surface.
12_-----	1,110	do_-----	26. 8	S. 55° E.	661. 8	655. 9	Do.

¹ Assumed datum. To convert to approximate altitude above sea level, add 9,780 ft.

² Part of movement may be due to sliding of boulder off ice pedestal.

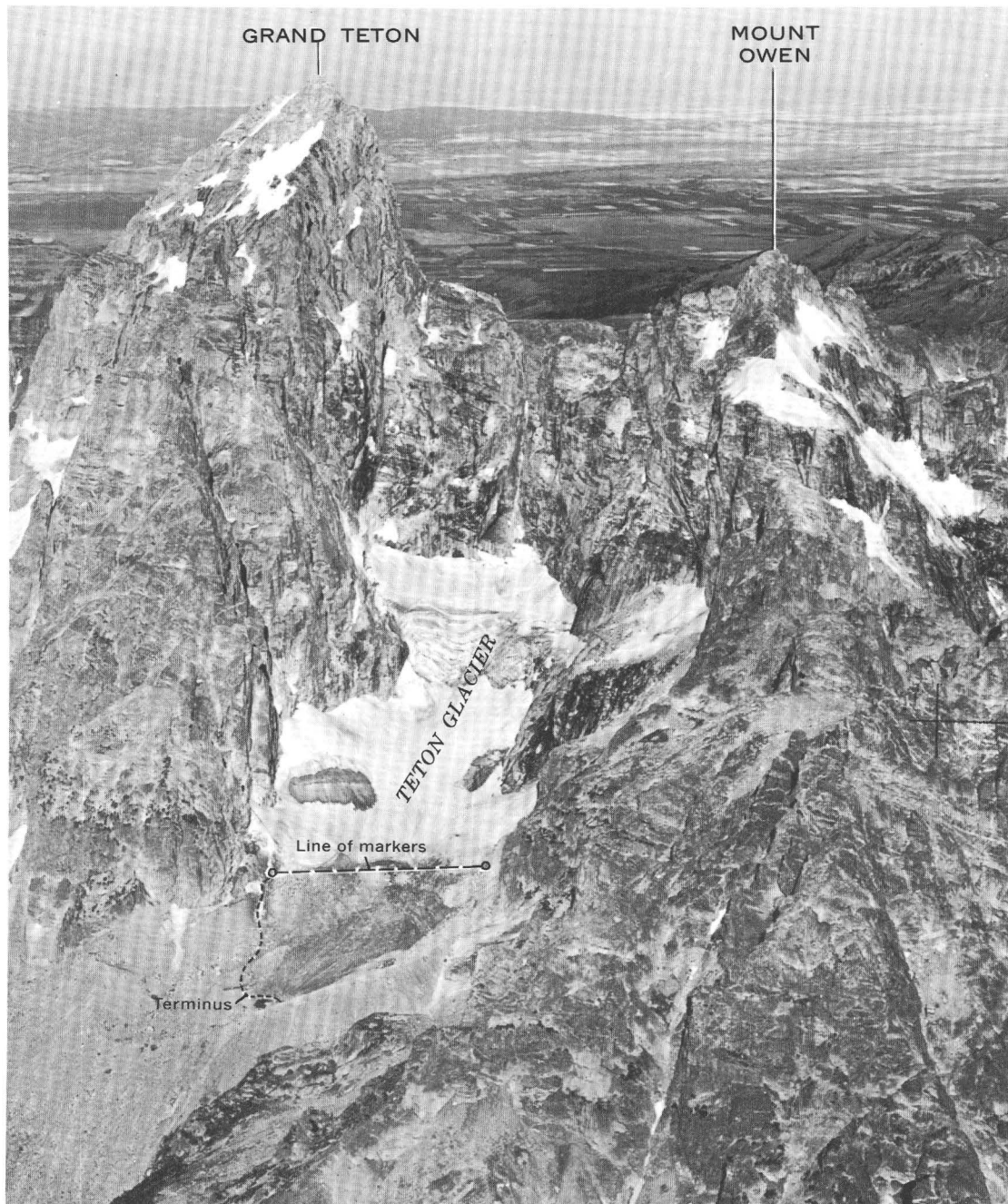


FIGURE 1.—Aerial photograph of Teton Glacier from the east, showing approximate position line of markers used for movement measurements, and terminus of glacier. Photograph by A. S. Post, University of Washington, August 19, 1963.

The metal stakes driven into the ice in 1963 had melted out of the ice and lay on the glacier surface in 1964, but the horizontal position of all but one of them could be recovered within a foot or two by taking the center of a small circle of painted rocks originally piled around them. Although toppling of the stakes prevented direct measurement of ablation and of the

amount of vertical movement, ablation must have exceeded 1.5 feet—the depth to which the stakes were originally driven. There was no indication that the stakes or the rocks piled around them affected the rate of ablation. So that their further movement can be determined in subsequent years, each of the 1963 stakes was redriven in its 1964 position.

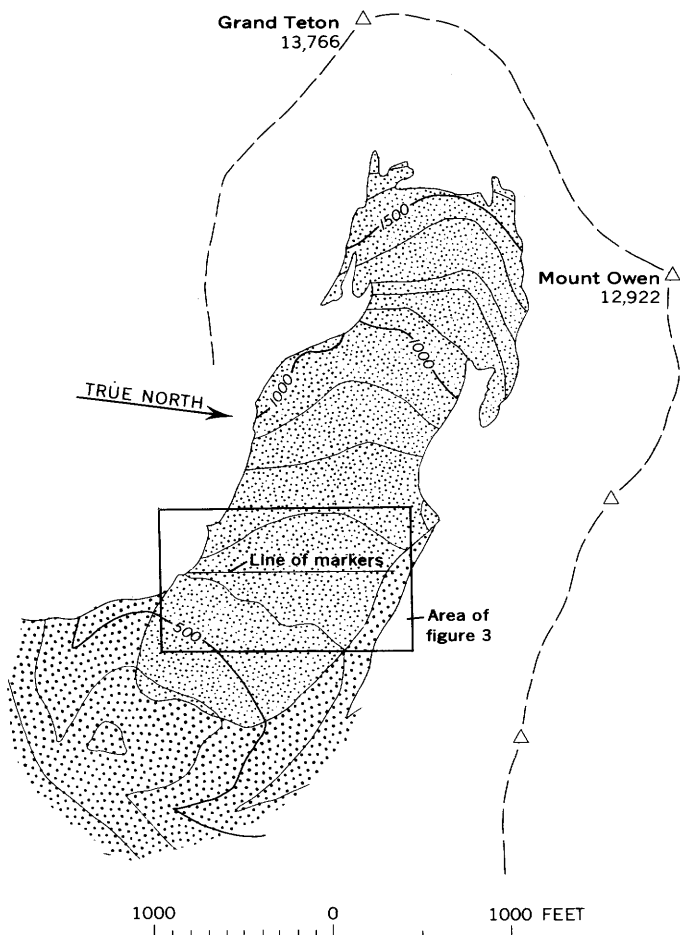


FIGURE 2.—Map of Teton Glacier showing line of markers and outline of figure 3. Lightly stippled area is ice, and heavily stippled area is moraine; debris-laden ice at lower end of glacier is not differentiated. Contour interval 100 feet, based on arbitrary datum approximately 9,780 feet above sea level. Contours and outline of glacier generalized from Reed (1964, fig. 1). Mountain peaks (triangles) and connecting ridges (dashed line) from U.S. Geological Survey topographic map of Grand Teton National Park. Altitude of peaks is in feet above mean sea level.

TABLE 2.—Location and altitude of markers on line across Teton Glacier on Sept. 21, 1964¹

Point	Distance from red paint mark on south wall (feet)	Altitude of ice surface above datum (feet)
1	17	619.5
2	87	619.3
3	185	623.7
4	310	649.0
5	410	643.7
6	510	636.4
7	610	645.1
8	710	645.6
9	810	644.0
10	910	648.8
11	1,010	656.8
12	1,110	659.2

¹ Point 1 has no marker. All other markers are iron pipes 2 ft long driven 1.5 ft into ice, with projecting ends painted orange and surrounded by orange-painted rocks.

Figure 3 shows graphically the changes in profile along the original line and the pattern of horizontal movements of the 1963 markers. The profiles show that the glacier in September 1964 was generally from 1 to 3 feet thinner along the original line of markers than about 13 months earlier, in August 1963. The terminus of the glacier remained in virtually the same position in 1964 as in 1963. A thickening of the upper part of the glacier noted in 1963 (Reed, 1964) has not yet affected the profile at the line of section, and at the present rate of horizontal movement would not be expected to do so for several decades. The change in altitude of the ice surface at the original markers between 1963 and 1964 represents the loss due to ablation and the descent due to downhill movement. For all markers the change in altitude exceeds the difference between the 1963 and 1964 profiles, which demonstrates a downward component of movement, but lack of ablation data prevents a determination of the inclination of the movement with respect to the ice surface.

Direction and amount of horizontal movement are surprisingly consistent across nearly the entire width of the glacier and are independent of the local slope of the ice surface. Points near the edges moved almost as rapidly as points near the center (table 1). The surface ice in this part of the glacier apparently moves as a nearly rigid mass, and differential movement is mostly confined to narrow zones at the sides (and presumably to a zone at the base).

The rate of horizontal movement is comparable to rates reported by Alden (1923), Gibson and Dyson (1939), and Johnson (1964) for the Grinnell Glacier in Glacier National Park, but it is unexpectedly rapid for such a small glacier in a region of much lower precipitation. The maximum movement measured by Waldrop (1964) in the Arapaho Glacier, Colorado, was only about 12 feet per year. Apparently the glacier is nearly in equilibrium (Reed, 1964). W. B. Myers (oral communication, 1964) has pointed out that such rapid movement therefore suggests that the ice must be relatively thin, in order to arrive at any reasonable mass budget for the glacier.

The thickness can be calculated by considering basal shear stress as a function of the cross-sectional geometry of the glacier. Meier (1960, p. 39), following Nye (1952, p. 85), stated the general relation in the form

$$\sigma = \frac{R}{d} \gamma Z \sin \alpha, \tag{1}$$

where σ is the shear stress at depth Z below the center line, γ is the specific weight of ice, R is the hydraulic radius of the section, d is the total depth, and α is the

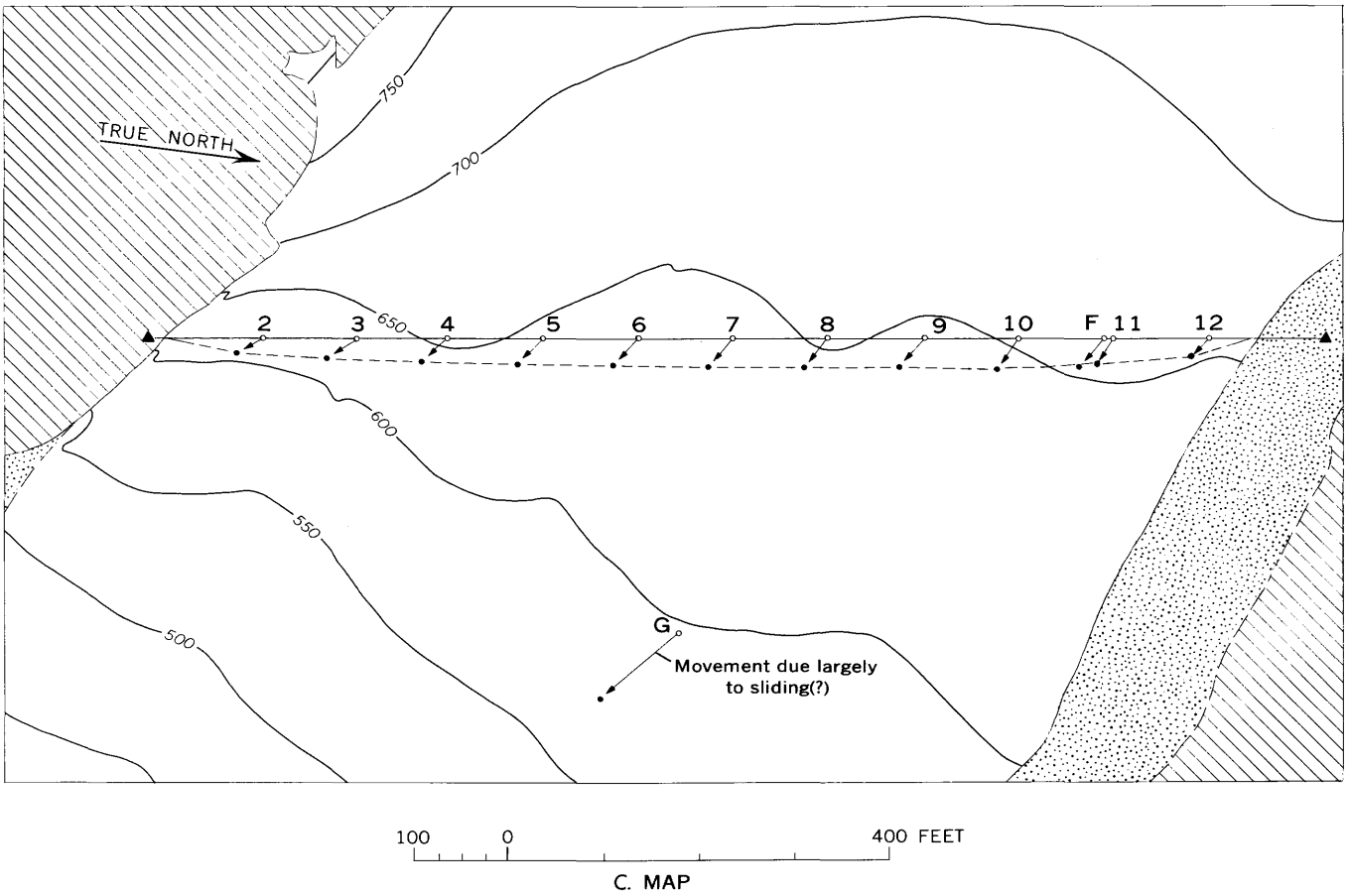
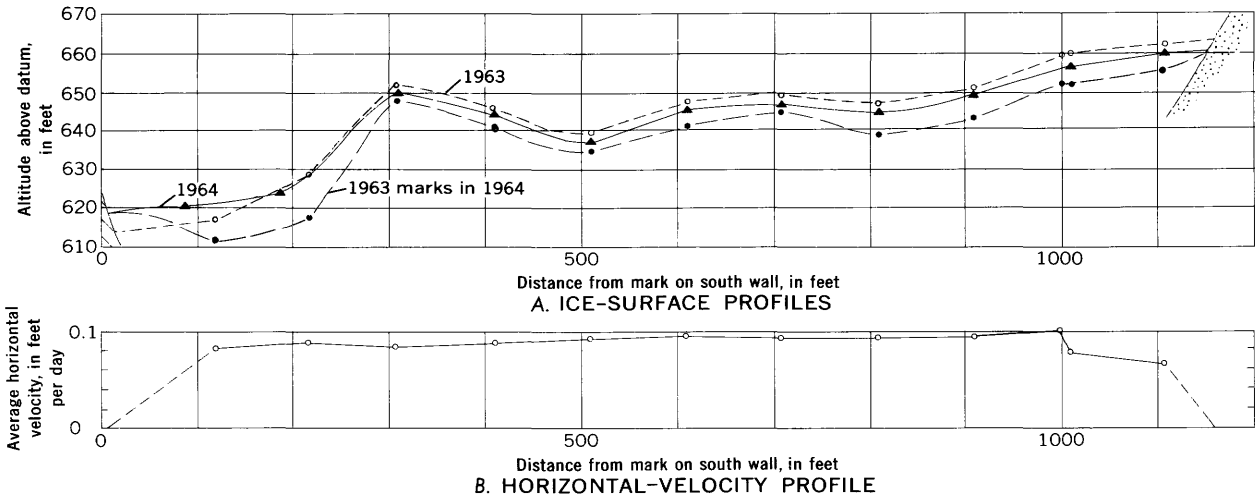


FIGURE 3.—A, Ice-surface profiles; B, Horizontal-velocity profile. Open circles represent markers placed in 1963; dots, the same markers in 1964; and triangles, the markers placed in 1964. C, Map (from Reed, 1963) showing amount of horizontal movement of markers placed in 1963. Contour interval 50 feet, based on arbitrary datum approximately 9,780 feet above sea level. Ruled areas are bedrock; stippled areas are moraine. Open circles show position of markers in 1963; dots show position of same markers in 1964. Triangles show position of fixed reference points marked by red-paint X's.

angle of surface slope in the direction of flow. The thickness is estimated from this formula by assuming that, for small changes in thickness, all factors other than thickness and slope are constant. Then, if shear stress at the base at time t_0 equals the stress at time t_1 , equation 1 gives

$$Z_1 = \frac{\Delta Z \sin \alpha_0}{\sin \alpha_1 - \sin \alpha_0}, \quad (2)$$

where Z_1 is the thickness at t_1 , α_0 and α_1 are the respective surface slopes, and ΔZ is the change in elevation of the ice surface during the interval from t_0 to t_1 .

Surface slope and change in elevation of the ice surface near the middle of the profile were estimated from contour maps of the glacier in 1954 and 1963 (Reed, 1964, fig. 1). These data and ice thicknesses calculated from equation 2 are given in table 3. The thicknesses, less than 50 feet, seem rather small, but they are surprisingly consistent in view of the uncertainties involved in the estimates of slope and change in surface elevation. Even if they are of only the correct order of magnitude, they support the inference that the central part of the Teton Glacier is very thin. This may explain the lack of internal plastic flow in the movement profile (fig. 3).

Direct measurements of surface slope and change in elevation along the profile in the future may allow more reliable estimates of ice thickness.

TABLE 3.—Changes in slope and ice thickness between 1954 and 1963, and estimated ice thickness

Point	ΔZ (decrease in thickness, in feet)	α_0 (1954 slope)	α_1 (1963 slope)	Z_1 (computed ice thickness in 1963, in feet)
6-----	8	7.8°	9.1°	49
8-----	6	7.1°	7.9°	46
9-----	11	7.1°	8.9°	44

REFERENCES

Alden, W. C., 1923, Rate of movement in glaciers of Glacier National Park: Science, new ser., v. 57, p. 268.
 Fryxell, F. M., 1933, The migration of superglacial boulders: Jour. Geology, v. 41, p. 737-747.
 ——— 1935, Glaciers of Grand Teton National Park, Wyoming: Jour. Geology, v. 43, p. 381-397.
 Gibson, G. R., and Dyson, J. L., 1939, Grinnell Glacier, Glacier National Park, Montana: Geol. Soc. America Bull., v. 50, p. 681-696.
 Johnson, Arthur, 1964, Glacier observations, Glacier National Park, 1963: U.S. Geol. Survey open-file report, 23 p.
 Nye, J. F., 1952, The mechanics of glacier flow: Jour. Glaciology, v. 2, p. 82-91.
 Meier, M. F., 1960, Mode of flow of the Saskatchewan Glacier, Alberta, Canada: U.S. Geol. Survey Prof. Paper 351, 70 p.
 Reed, J. C., Jr., 1963, Map of the lower portion of the Teton Glacier, Grand Teton National Park, Wyoming: U.S. Geol. Survey open-file report.
 ——— 1964, Recent retreat of the Teton Glacier, Grand Teton National Park, Wyoming, in Geological Survey Research 1964: U.S. Geol. Survey Prof. Paper 501-C, p. C147-C151.
 Waldrop, H. A., 1964, Arapaho Glacier, a sixty year record: Univ. Colorado Studies, Series in Geology, no. 3, 37 p.



USE OF MAGNETIC SUSCEPTIBILITY AND GRAIN DENSITY IN IDENTIFICATION OF BASALT FLOWS AT THE NEVADA TEST SITE

By K. A. SARGENT, Denver, Colo.

Work done in cooperation with the U.S. Atomic Energy Commission

Abstract.—Two lithologically similar groups of olivine basalt flows were distinguished by plotting magnetic susceptibility versus grain density. The identification was found to be more rapid than, and as accurate as, that based upon petrographic criteria alone.

Magnetic susceptibility and grain-density analyses proved to be useful criteria for identifying two basalt groups of very similar appearance and lithology. The groups studied occur in the Jackass Flats and Skull Mountain quadrangles of the Nevada Test Site, Nye County, Nev. Each group is about 250 feet thick and consists of seven or more flows of olivine basalt of Tertiary age. The older unit is the basalt of Skull Mountain; the younger is the basalt of Kiwi Mesa. Megascopic separation of these units is impossible in outliers and outcrops where recognizable overlying or underlying rocks are not exposed. Petrographic data provided useful criteria for identification, but magnetic susceptibility versus grain-density plots were found to be as accurate and more rapid.

PETROGRAPHY

The basalts are generally similar in texture and composition, except for the presence of local quartz xenocrysts in the basalt of Skull Mountain. The basalts are porphyritic, with intersertal and diabasic to trachytic groundmass textures. The phenocrysts are largely plagioclase (An_{53-56}), and diopsidic augite, with olivine (Fo_{88-92}) and hypersthene in subordinate amounts. Quartz xenocrysts occur in many flows of the basalts of Skull Mountain. The xenocrysts are corroded and embayed. Reaction rims of euhedral diopsidic augite and brown glass ($N < \text{balsam}$) are present around the quartz. Essential minerals in the groundmass are plagioclase (An_{48-53}) and diopsidic augite.

Varietal olivine is more fayalitic in the groundmass than in the phenocrysts. Accessory minerals are quartz, magnetite, ilmenite, hypersthene, and zircon. Interstitial glass ($1.52 < N < 1.53$) is colorless to dark brown and gray and locally contains abundant fine-grained magnetite. Secondary minerals include iddingsite and hematite as major constituents and uralite, sericite, chalcedony, and calcite as minor constituents.

Seventeen modal analyses based on 500 to 1,000 point counts are given in table 1. Figures in volume percent are reported to the nearest one-tenth percent.

Although their mineralogical characteristics overlap, the basalts of Skull Mountain generally contain less groundmass plagioclase, more phenocryst plagioclase, more groundmass pyroxene, and less opaque material than those of Kiwi Mesa.

A comparison (table 2) of the ratio of total plagioclase to total pyroxene plus olivine shows that basalts of Kiwi Mesa (with one exception) have a ratio of more than 2.5, while basalts of Skull Mountain have a ratio of less than 2.5. The exception is an aberrant basalt with nearly 40 percent of total olivine and pyroxene (KAS 5-23-3).

MAGNETIC SUSCEPTIBILITY AND GRAIN DENSITY

Table 3 lists the magnetic susceptibility and powdered grain density of 51 samples known to belong to the basalts of Skull Mountain and Kiwi Mesa.¹ Magnetic-susceptibility values are accurate to within 1 percent; grain-density values were determined by the method described by the American Petroleum Institute (1960) and are accurate to ± 0.02 grams per cubic centimeter. Samples were taken from the densest part of each flow,

¹ Magnetic susceptibility and powdered grain density determined at the physical properties laboratory, U.S. Geological Survey, Denver, Colo.

TABLE 1.—*Modal analyses, in volume percent, of basalts of Skull Mountain and Kiwi Mesa*

Thin section	Glass	Groundmass plagioclase	Plagioclase phenocrysts	Total olivine	Total quartz	Pyroxene phenocrysts	Groundmass pyroxene	Opaque minerals (magnetite, ilmenite, hematite)
Basalts of Skull Mountain								
KAS 5-23-2	28.8	39.5	2.5	3.9	0.5	0.0	19.3	5.5
KAS 5-23-1B	20.0	42.9	5.9	11.4	.2	.1	13.5	6.0
KAS 5-22-20	30.4	39.2	7.6	5.2	.8	.4	14.4	2.0
KAS 5-22-19	11.6	51.7	5.0	11.0	1.7	.3	14.7	4.0
KAS 5-22-18	9.4	47.8	5.8	10.0	.0	.6	18.0	8.4
KAS 5-22-17	8.1	47.8	8.6	10.9	.8	.1	18.3	5.4
KAS 5-14-2	6.4	47.8	12.4	13.0	.0	.0	12.8	7.6
KAS 5-14-1	25.0	40.0	3.6	.4	1.2	.0	26.2	3.6
Basalts of Kiwi Mesa								
KAS 5-23-3	3.0	50.4	0.8	20.0	0.0	0.0	19.6	6.2
Kiwi 7	5.2	62.4	2.0	10.6	.0	.0	10.4	9.4
Kiwi 6	10.6	60.0	3.8	3.4	.0	.0	10.2	12.0
Kiwi 5	7.2	65.0	3.6	6.2	.0	.8	10.0	7.2
Kiwi 4	13.2	53.4	4.6	.0	.0	.0	12.6	16.2
Kiwi 3	15.6	58.8	1.8	3.0	.0	.2	5.0	15.6
Kiwi 2B	12.8	60.6	1.2	9.0	.0	.4	11.8	4.2
Kiwi 2A	18.6	56.4	1.0	9.8	.0	.4	8.0	5.8
Kiwi 1	17.6	53.2	4.4	8.8	.0	1.0	8.6	6.4

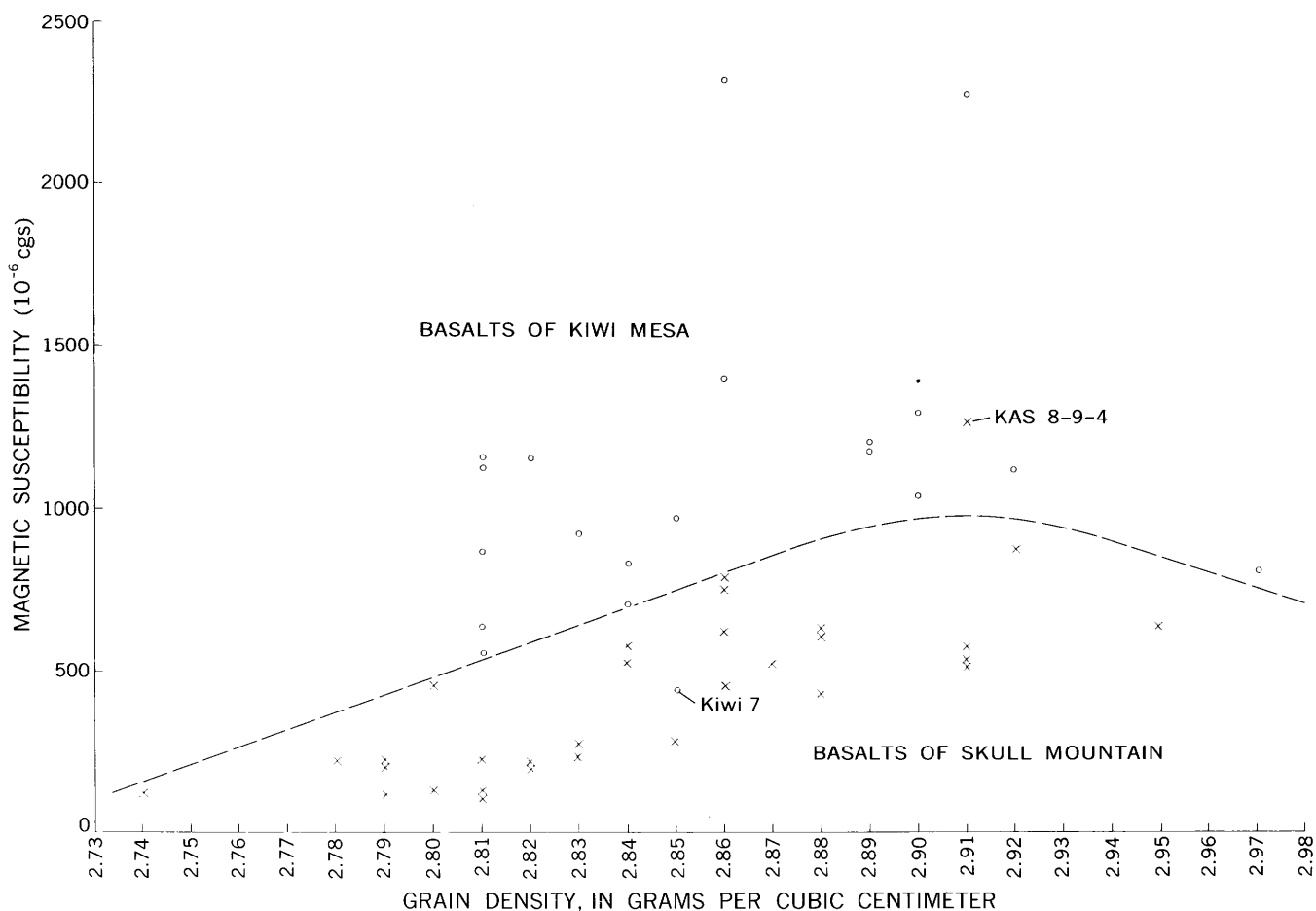


FIGURE 1.—Plot of magnetic susceptibility against grain density of basalts of Skull Mountain (x) and basalts of Kiwi Mesa (o). Dashed line separates most points of basalts of Skull Mountain from those of Kiwi Mesa.

TABLE 2.—Comparison of total plagioclase with total pyroxene plus olivine of basalts of Skull Mountain and Kiwi Mesa, based upon the measured modes

Sample	Total plagioclase	Total pyroxene plus olivine	Ratio of total plagioclase to total pyroxene plus olivine
Basalts of Skull Mountain			
KAS 5-23-2	42.0	23.2	1.81
KAS 5-23-1B	48.8	25.0	1.95
KAS 5-22-20	46.8	20.0	2.34
KAS 5-22-19	56.7	26.0	2.18
KAS 5-22-18	53.6	28.6	1.87
KAS 5-22-17	56.4	29.3	1.92
KAS 5-14-2	60.2	25.8	2.33
KAS 5-14-1	43.6	26.6	1.64
			2.01 Average
Basalts of Kiwi Mesa			
KAS 5-23-3	51.2	39.6	1.29
Kiwi 7	64.4	21.0	3.07
Kiwi 6	63.8	13.6	4.69
Kiwi 5	68.6	17.0	4.04
Kiwi 4	58.0	12.6	4.60
Kiwi 3	60.6	8.2	7.39
Kiwi 2B	61.8	21.2	2.92
Kiwi 2A	57.4	18.2	3.15
Kiwi 1	57.6	18.4	3.13
			3.83 Average

generally below the vesicular upper part and above the brecciated base.

A plot (fig. 1) of magnetic susceptibility versus grain density shows that basalts of Skull Mountain have generally lower magnetic susceptibility and occupy a different field than those of Kiwi Mesa. The disparity shown by samples Kiwi 7 and KAS 8-9-4 may be due to a gross analytical error beyond the normal statistical limit. However, the disparity may be real and may indicate a true overlap.

INTERPRETATION OF VARIATIONS IN PHYSICAL PROPERTIES

Werner (1945, p. 50) reports that the magnetic susceptibility of rocks is determined mainly by the magnetite content. He also notes two observations pertinent to this study: (1) susceptibility values show considerable scattering for similar volume percent of magnetite, and (2) the susceptibility decreases considerably faster than the magnetite content. Mooney and Bleifuss (1953) concur and further state that the scatter of susceptibility values probably results from variations in shape and orientation of magnetite grains. Koenigsberger (1938, p. 123) reports that magnetic susceptibility decreases with decreasing grain size; however, Mooney and Bleifuss (1953, p. 386) suggest an opposite trend.

TABLE 3.—Magnetic susceptibility and grain density of basalts of Skull Mountain and Kiwi Mesa

Sample	Magnetic susceptibility (10 ⁻⁶ egs)	Grain density (g/cm ³)
Basalts of Skull Mountain		
KAS 10-28-11	227.0	2.81
KAS 10-28-10	119.2	2.81
KAS 10-28-9	535.7	2.91
KAS 10-28-8	528.2	2.84
KAS 10-28-7	289.5	2.83
KAS 10-28-6	647.5	2.95
KAS 10-28-5	455.9	2.86
KAS 10-28-4	291.9	2.85
KAS 10-28-3B	760.0	2.86
KAS 10-28-3A	791.4	2.86
KAS 10-28-2	519.8	2.91
KAS 10-28-1B	444.6	2.88
KAS 10-28-1A	579.1	2.91
KAS 9-25-2	200.7	2.82
KAS 9-25-1	120.5	2.79
KAS 8-9-4	1267.2	2.91
KAS 8-9-2	626.8	2.86
KAS 8-9-1	580.5	2.84
KAS 8-6-1CB	143.8	2.74
KAS 8-6-1CA	235.6	2.78
KAS 8-6-1B	116.6	2.81
KAS 8-6-1A	208.9	2.79
KAS 5-23-2	224.7	2.82
KAS 5-23-1A and B	245.5	2.83
KAS 5-22-20	142.3	2.80
KAS 5-22-19	523.6	2.87
KAS 5-22-18	621.0	2.88
KAS 5-22-17	628.6	2.88
KAS 5-14-2	879.4	2.92
KAS 5-14-1	461.3	2.80
EM 6-61	227.0	2.79
Basalts of Kiwi Mesa		
KAS 10-27-4	1043.0	2.90
KAS 10-27-3	1124.3	2.92
KAS 10-27-2	1299.2	2.90
KAS 10-27-1	814.1	2.97
KAS 9-25-3	2272.6	2.91
KAS 9-24-7	1204.4	2.89
KAS 9-24-5	839.6	2.84
KAS 9-24-4	647.5	2.81
KAS 9-24-2	2333.7	2.86
KAS 5-23-3	1173.9	2.89
Kiwi 7	449.0	2.85
Kiwi 6	979.3	2.85
Kiwi 5	556.2	2.81
Kiwi 4	1398.3	2.86
Kiwi 3	1160.2	2.81
Kiwi 2B	1154.4	2.82
Kiwi 2A	1122.0	2.81
Kiwi 1	873.7	2.81
EM 8-61	700.2	2.84
EM 7-61	925.3	2.83

In the present study, the ratio of magnetite to other opaque minerals (hematite and ilmenite) is small and probably variable. The sample regression line shown

on figure 2 indicates that magnetic susceptibility increases with increasing average grain size of opaque minerals and supports the view of Koenigsberger (1938, p. 123). This plot (fig. 2) and plots of grain density versus percentage of opaque minerals plus olivine (fig. 3), and of grain density versus percentage of glass (fig. 4) split the basalts into two fields. There is one aberrant point in each plot; however, none of these aberrant points refer to the same sample in the separate graphs.

The basalts of Skull Mountain and Kiwi Mesa vary about equally in density. The Kiwi Mesa types, how-

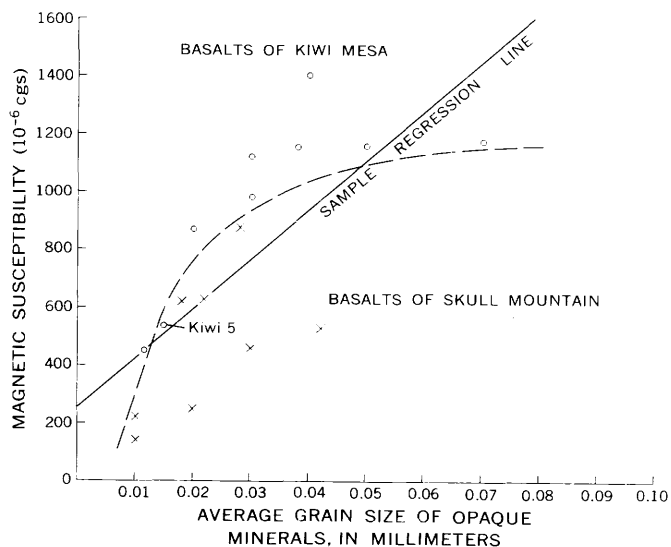


FIGURE 2.—Plot of magnetic susceptibility versus average grain size of opaque minerals. Solid line is sample regression line. Dashed line separates most points of basalts of Skull Mountain (x) from those of Kiwi Mesa (o).

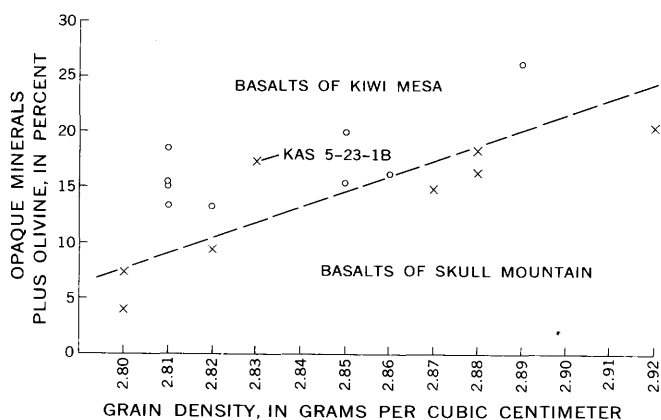


FIGURE 3.—Plot of grain density versus percentage of opaque minerals plus olivine. Dashed line separates most points of basalts of Skull Mountain (x) from those of Kiwi Mesa (o).

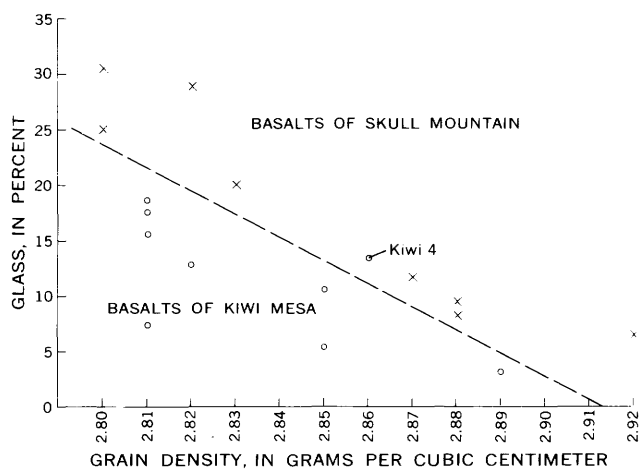


FIGURE 4.—Plot of grain density versus percentage of glass. Dashed line separates most points of basalts of Skull Mountain (x) from those of Kiwi Mesa (o).

ever, have a higher content of magnetic minerals as shown by generally higher magnetic susceptibility and by petrographic evidence. The basalts of Kiwi Mesa probably have more of their total iron in the form of magnetite, whereas the basalts of Skull Mountain either have less total iron or they have proportionately more of their iron tied up in less magnetic minerals such as pyroxene and olivine.²

These data indicate that magnetic susceptibility in these basalts varies directly with magnetic-mineral content and with magnetic-mineral grain size. The use of magnetic susceptibility and grain density in correlation has been found to be of particular value where the flow in question occurred in an isolated outcrop and determinative field evidence is lacking.

REFERENCES

- American Petroleum Institute, 1960, API recommended practice for core-analysis procedure: New York, American Petroleum Institute RP40, p. 16-17.
- Koenigsberger, J. G., 1938, Natural residual magnetism of eruptive rocks: *Terrestrial Magnetism and Atmospheric Electricity*, v. 43, p. 119-130, 299-320.
- Mooney, H. M., and Bleifuss, Rodney, 1953, Magnetic susceptibility measurements in Minnesota; pt. II, Analysis of field results: *Geophysics*, v. 18, no. 2, p. 383-393.
- Werner, Sture, 1945, Determinations of the magnetic susceptibility of ores and rocks from Swedish iron ore deposits: *Sver. Geol. Unders.*, v. 39, 79 p.

² Chemical data obtained after submittal of this paper suggest that although the basalts of Skull Mountain have approximately the same total iron content as do the basalts of Kiwi Mesa, the latter have over three times the Fe_2O_3 content. This suggests that the basalts of Kiwi Mesa have a higher magnetite content.



THE BEST VALUE OF POROSITY OF LAPILLI TUFF FROM THE NEVADA TEST SITE

By G. EDWARD MANGER, Washington, D.C.

Work done in cooperation with the U.S. Atomic Energy Commission

Abstract.—A study of the porosity of 10 selected specimens of lapilli tuff from the Nevada Test Site shows that (1) porosity based on water-displacement and mercury-displacement bulk volume differs by about 1 percent; (2) total and apparent porosity where based on the same bulk volume are virtually equal, but a seeming excess of total over apparent porosity arises because the densities of the powdered portions of the test specimens are not typical of the grain densities of the whole specimens; and (3) the volume of sealed-off pores, including sealed-off vesicles, does not exceed 0.1 percent porosity. Because of the wide range in porosity, tests on 234 specimens would be necessary to obtain a mean porosity with a standard error of only 0.25 percent.

For the evaluation of the effects of underground explosions on the physical properties of tuff at the Nevada Test Site in southern Nevada, questions arose whether the methods used for the porosity determinations yielded the best values, whether vesicles that may be present represent sealed-off pores, and whether the porosity of large volumes of tuff is adequately represented by tests on a limited number of specimens.

Experiments which were limited by field-laboratory conditions were performed on 10 specimens of lapilli tuff from subunit T of the bedded tuffs of the Paintbrush Tuff.¹ The specimens are parts of a core obtained at a depth of about 400 feet from an air-drilled hole which extended laterally about 25 feet from a tunnel to a chamber which later served as the site for a nuclear explosion. The core samples from which the test specimens were derived were irregularly spaced along the drill hole.

TECHNIQUE

Composition of test specimens

The test specimens consisted of well-consolidated white lapilli tuff. The surfaces of the shaped test specimens were very fine grained and smooth. According

¹ Formerly called subunit T of the Survey Butte Member of the Plapi Canyon Formation of the Oak Spring Group.

to F. A. McKeown and D. D. Dickey (U.S. Geol. Survey, written communication 1958), chalky white tuff with many lithic fragments is characteristic of subunit T. The lapilli tuff commonly contained dark rock fragments from less than 1 mm to 4 mm long, but fragments of such size were not present in the test specimens.

R. E. Wilcox and Theodore Botinelly (U.S. Geol. Survey, written communication, 1958) report that the average tuff from subunit T (their specimen B-222) consists of 1.8 percent phenocrysts, 4.5 percent xenoliths, and 87.9 percent shards and lapilli. The 87.9 percent shards and lapilli consists of 35 percent heulandite, 8 percent cristobalite, 11 percent montmorillonite, and 34 percent amorphous material and crystalline material too fine for X-ray identification. Vesicles are stated to constitute 5.8 percent of the specimen. Additional work by Botinelly (written communication, 1961) shows that much of the heulandite is close to clinoptilolite in composition but shows some variation in thermal and X-ray properties. The 1.2 percent of vesicles is near the minimum that has been reported for the Paintbrush Tuff. The actual test specimens were not examined microscopically. However, the laboratory measurements (see table) indicate that such mineralogical variation as was present resulted in a maximum of less than 9 percent variation about the mean of the measured grain-powder densities for all 10 samples.

The grains of the groundmass of the white lapilli tuff of subunit T are reported to fit closely together, and there is very little interstitial material (Wilcox and Botinelly, written communication, 1958). This close fit of the grains and the very small amount of interstitial material may explain the observed stability of the specimens in water.

The elements of porosity determinations

Total porosity is a measure of the total void volume of a rock and is the excess of bulk volume over grain volume, per unit of bulk volume. Experimentally, as

in this study, total porosity is usually determined as the excess of grain density over bulk density, per unit of grain density. Apparent porosity, often called effective or net porosity, is a measure of the apparent void volume of a rock and is determined as the excess of bulk volume over grain volume and occluded pore volume, per unit bulk volume. The excess of bulk volume over grain volume and occluded pore volume, or apparent void volume, is determined by the fluid capacity of the permeable pores of the rock.

Experimental procedure

Sequential tests were run on 10 specimens. Pieces of core were shaped to rounded multiplaned specimens from about 4 cm³ to 7 cm³ in volume, and were free of reentrant surfaces. The specimens were oven-dried at 105°C for 8 hours and cooled in a desiccator. A selected specimen was weighed to 1 milligram. This measurement and all others were made to 4 significant figures. Bulk volume was determined as the volume of mercury displaced by the specimen from a heavy-walled cylindrical glass bottle provided with a center-hole glass stopper. While the stopper was being pressed in place, the specimen was kept submerged in the mercury and moved by means of a needle inserted through the stopper hole in order to release possibly entrapped air bubbles. The volume of the displaced mercury was obtained from its weight by a correction for an ambient temperature of about 25°C. When removed from the glass bottle the specimen was brushed to remove the adhering mercury, redried in the oven for 2 hours at 105°C, cooled in the desiccator, and reweighed. The loss of weight given by the difference between the first and second dry weights represents attrition occurring during the determination of bulk volume by mercury displacement. This loss of weight was considered to be proportional to the loss of volume and permitted correction of the mercury-displacement bulk volume in terms of the subsequently determined water-displacement bulk volume. The specimen was then evacuated to less than 1 mm of mercury pressure in a glass desiccator, which pressure was held for half an hour, after which enough de-aerated water was admitted to cover the specimen. Bubbling ceased in about 15 minutes, and, after an additional 15 minutes, the vacuum desiccator was opened to the atmosphere for at least 2 hours. On removal of the water-saturated specimen from the vacuum desiccator, the "excess" water was eliminated by touching the specimen with thoroughly moist absorbent paper, and the specimen was weighed as quickly as possible, to 1 milligram. Pore volume was determined as the weight of water absorbed, corrected to 4°C from an average ambient temperature of about 25°C. Immediately after the saturated specimen was weighed

in air, its bulk volume was determined from the loss of weight by suspended immersion in previously boiled and cooled tapwater, with the loss of weight similarly corrected for the temperature of the immersing tapwater. The effect of dissolved solids on the specific gravity of the tapwater in which the samples were weighed was considered to be negligible, as a representative sample of tapwater at the Nevada Test Site showed only 389 parts per million total dissolved solids (Alfred Clebsch, Jr., U.S. Geol. Survey, oral communication, 1958). Subsequent to the determination of the loss of weight in water, the specimen was oven-dried at 105°C for 8 hours and cooled in a desiccator. A portion of the specimen was pulverized to yield about 2 grams of powder for the determination of grain density in a 50-ml pycnometer with a side arm and a glass-stopper thermometer. Distilled water served as the pycnometer liquid. In order to de-aerate the powder, the mixture of water and powder was boiled in the pycnometer about 10 minutes. Temperature corrections for the density of the distilled water were made to 0.1°C. For checking purposes, repeated sequential tests were made on several specimens.

Conditions which interfere with obtaining the best values of porosity

There are a number of conditions which interfere with obtaining the best values of porosity. It is well known that the observed bulk volumes are method-dependent and that bulk volumes obtained by water displacement and mercury displacement rarely are equal. An excess of total over apparent porosity results from the presence of occluded pores, but a spurious excess of total porosity results from the following interfering conditions: (1) significant adsorption of water by the grain powder during the pycnometric determination of its volume, (2) incomplete saturation of permeable pores during the determination of apparent pore volume, and (3) a density of the grain-powder portion of the specimen greater than the grain density of the whole specimen. According to the methods used in this study, the only known cause, other than measurement error, for a spurious and unreal deficiency of total porosity with respect to apparent porosity is that the density of the grain-powder portion of the specimen is less than the grain density of the whole specimen.

RESULTS

The bulk volume effect

The data obtained by the experiments are shown in the accompanying table. For all 10 specimens of lapilli tuff the means of total and apparent porosities based on water-displacement bulk densities or volumes exceed the means based on mercury-displacement bulk densities

or volumes by about 1 percent porosity. For specimen No. 13, however, the total porosity based on mercury-displacement bulk density is in excess. This is due to a larger mercury than water-displacement bulk volume. The abnormally high grain-powder densities of specimens Nos. 10 and 11 apparently are due to the chance inclusion in the tuff of a fragment or of fragments of lapilli tuff or xenoliths of unusually high density. If these 2 specimens are omitted the porosities which are based on water displacement bulk volumes are in excess by about 0.8 percent porosity. Thus a difference of about 1 percent porosity is due to differences in the water- and mercury-displacement bulk volumes.

Excess of total porosity due to occluded pores or to spuriously indicated occluded pores

The table shows that for all 10 specimens of lapilli tuff the mean excess of total over apparent porosity where based on water-displacement bulk density or volume is about 1 percent porosity. Similarly the mean excess of total over apparent porosity where based on mercury-displacement bulk volume is about 1 percent porosity. Although the mean total porosity is in excess, specimens Nos. 15, 2, 7, and 1 show unreal excesses of apparent porosity; these are specimens which in general show the lowest grain-powder densities. With the omission as before of the 2 specimens with the highest grain powder densities, the excess of total porosity for the remaining 8 specimens is reduced to 0.18 percent porosity. Thus the volume of occluded pores, or the spurious volume of occluded pores due to the mentioned interfering conditions, lies between 0.18 percent and 1 percent porosity.

The preceding relations suggest that the excess of total porosity over apparent porosity depends upon the grain-powder density. This dependence is illustrated in figure 1, where the excess total porosity is plotted as a function of the grain-powder density. The dependence of the excess of total porosity over apparent porosity on the grain-powder density is expressed numerically (Ezekiel and Fox, 1959, p. 130) by the coefficient of determination (r^2) where (r) is the coefficient of correlation. The coefficient of determination shows the extent to which the variance in one variable is determined by the variance in another variable. If the dependence is causal, the coefficient shows the extent to which the variance in one variable is caused by the variance in another variable. Because repeat determinations of grain-powder density indicate that measurement error is not significant, the deficiencies of total porosity as shown by 4 of the 10 specimens are caused by the density of the powder portion of the specimen being lower than the grain density of the whole specimen.

The 10 specimens in the table show a mean excess of total porosity based on water-displacement bulk density over apparent porosity based on water-displacement bulk volume of 0.96 percent and a coefficient of determination of 0.88. Thus it is indicated that 0.88 of the 0.96 percent average excess of total over apparent porosity, or 0.84 percent excess total porosity, is caused by the fact that the powder densities are not typical of the specimen. Then 0.96 percent porosity less 0.84 percent porosity, or 0.12 percent porosity, represents the maximum possible volume of occluded pores, or the maxi-

Total and apparent porosity of lapilli tuff of subunit T of the Paintbrush Tuff from the Nevada Test Site in southern Nevada

[Measurements by G. E. Manger and C. C. Hawley]

Specimen No.	Grain-powder density (g cm ⁻³)	Pore volume (ml) by water absorption	Bulk volume (ml) by displacement of—		Bulk density dry (g cm ⁻³) based on bulk volume		Porosity (percent)			
			Water	Mercury	Water	Mercury	Total, based on bulk density		Apparent, based on bulk volume	
							Water	Mercury	Water	Mercury ¹
15.....	2. 232	1. 802	4. 394	4. 333	1. 342	1. 361	39. 87	39. 02	41. 01	40. 18
2.....	2. 273	1. 511	4. 253	4. 170	1. 490	1. 519	34. 45	33. 17	35. 53	34. 24
7.....	2. 279	1. 570	4. 895	4. 826	1. 554	1. 576	31. 81	30. 85	32. 07	31. 10
13.....	2. 304	2. 343	6. 202	6. 235	1. 396	1. 388	39. 41	39. 76	37. 78	38. 11
8.....	2. 314	2. 401	5. 912	5. 819	1. 360	1. 382	41. 23	40. 28	40. 61	39. 66
1.....	2. 319	1. 994	5. 103	5. 025	1. 425	1. 447	38. 55	37. 60	39. 07	38. 13
3.....	2. 323	1. 509	4. 070	4. 011	1. 448	1. 470	37. 67	36. 72	37. 08	36. 15
4.....	2. 361	2. 685	6. 554	6. 436	1. 356	1. 381	42. 57	41. 51	40. 97	39. 89
10.....	2. 442	2. 803	6. 756	6. 615	1. 360	1. 389	44. 31	43. 12	41. 49	40. 24
11.....	2. 502	1. 449	4. 629	4. 493	1. 585	1. 633	36. 65	34. 73	31. 30	29. 22
Average.....	2. 335	-----	-----	-----	-----	-----	38. 65	37. 68	37. 69	36. 69
Average without specimens 10 and 11.....	2. 301	-----	-----	-----	-----	-----	38. 20	37. 36	38. 02	37. 18

¹ For the apparent porosity based on mercury-displacement bulk volume, the pore volume as indicated by the volume of absorbed water is decreased by the excess water-displacement over mercury-displacement bulk volume.

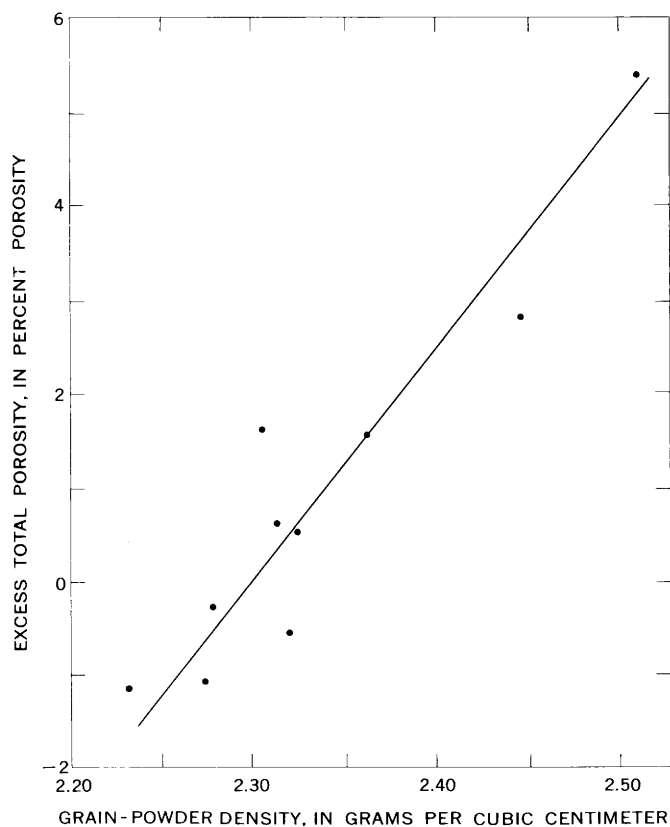


FIGURE 1.—Excess of total porosity of lapilli tuff based on grain-powder density over apparent density. Both total and apparent porosity are based on bulk volume as determined by water displacement.

imum possible spurious volume of occluded pores due to the previously mentioned interfering conditions. In contrast to the large coefficient of determination shown by the relation of the excesses of total porosity over apparent porosity to grain-powder density, the coefficient of determination for the total porosities with respect to grain-powder density is 0.07 and for apparent porosities with respect to grain-powder density, 0.06.

With the 2 extremely high excesses of total porosity of figure 1 omitted, the mean of the excesses and deficiencies of the remaining 8 specimens as previously stated is 0.18 percent porosity, and the coefficient of determination is 0.55. Accordingly, the maximum possible volume of occluded pores, including those represented by any vesicles which may be present, is 0.08 percent porosity.

Grain density

The mean value for the grain density of the specimens may be obtained from figure 1. After elimination of the 2 specimens with the highest grain-powder densities, the grain-powder densities of the remaining 8 specimens are equally distributed about zero median excess total porosity. This distribution suggests that the

excesses and deficiencies of total porosity are due to normal sampling error in the selection of portions of the specimens for the determination of grain-powder density, and that the mean grain density of the specimens is indicated at the point on the graph where the excess total porosity is zero. At zero excess total porosity the grain-powder density is 2.298 g cm^{-3} with a standard error of the estimate ($\bar{S}_{y \cdot x}$) of 0.011 g cm^{-3} , where $\bar{S}_{y \cdot x} = \frac{\sum z^2}{n-2}$, with z = the excess of the actual over the estimated grain-powder density, and n = the number of observations, which in the present case is 10. Because at zero excess total porosity the total and apparent porosities are equal, the mean grain density may also be derived by use of the relation that the grain density is equal to the bulk density divided by 1 minus the fractional apparent porosity. By this relation the same mean value of 2.298 g cm^{-3} is obtained for the grain density of the specimens, whether the relation is based on water-displacement bulk density and bulk volume or on mercury-displacement bulk density and bulk volume.

CONCLUSIONS

The smooth surfaces of the test specimens suggest that the best values of bulk volume, and therefore the best values of porosity, may be based on mercury-displacement bulk volume. The mean apparent porosity in the table of the 10 samples so based is 36.69 percent and the mean total porosity is 37.68 percent. In view of the fact that for 1 of the 10 specimens the mercury-displacement bulk volume exceeds the water-displacement bulk volume, a more conservative porosity may be based on an average of water- and mercury-displacement bulk volume; accordingly, the mean apparent porosity is 37.19 percent and the mean total porosity is 38.16 percent. Because in the present specimens of tuff the volume of occluded pores does not exceed 0.12 percent porosity, and may be zero, the mean apparent porosity of 37.19 percent is considered to be the better value.

Owing to the wide range in porosity of the 10 specimens of lapilli tuff as shown in the table, the standard error of the mean (S_{Mx}) is 1.21 percent, where $S_{Mx} = \frac{\bar{S}_x}{\sqrt{n}}$, with \bar{S}_x = standard deviation of the items in the universe, and n = the number of items in the sample, which in the present case is 10. To obtain a mean with a standard error of only 0.50 percent porosity would require tests on 59 specimens, and to obtain a mean with a standard error of 0.25 percent would require tests on 234 specimens.

The methods used in this study excluded the effects of one interfering condition which should be mentioned.

For specimens of tuffaceous sandstone obtained from near the present specimens of lapilli tuff, apparent porosity based on the volume of air evacuated from the test specimens exceeded apparent porosity based on the volume of absorbed water by 17 percent. Obviously, air should not be used as a measure of the pore volume of tuff from the Paintbrush Tuff.

The specimens which were used in the porosity tests did not exceed 7 milliliters in bulk volume. Limiting the bulk volume to this value may have helped in ob-

taining the indicated complete saturation of the evacuated specimens as a measure of pore volume. Boiling the mixture of grain powder and water evidently resulted in complete removal of entrapped or possibly adsorbed air in the pycnometric determination of grain-powder density.

REFERENCE

Ezekiel, Mordecai, and Fox, K. A., 1959, *Methods of correlation and regression analysis*, 3d ed.: New York, John Wiley and Sons, Inc., 548 p.



GAMMA ACTIVATION DEVICE FOR LOW-LEVEL BERYLLIUM ANALYSIS

By WILLIAM W. VAUGHN, WILLIAM G. CRAMER,
and WILLIAM N. SHARP, Denver, Colo.

Abstract.—An improved device using the photoneutron reaction Be^9 (gamma-neutron) Be^8 has been developed for the quantitative analysis of beryllium in crushed rock samples and solutions. The operating part is an annular-shaped chamber consisting, from center outward of a γ -source, sample holder, lead γ -shield, paraffin moderator, and a ring of low-voltage proportional counters. A remotely controlled pneumatic system is used to raise a 1-curie gamma source from storage below floor level to the center of the sensitive chamber for each analysis. A beryllium content of 1 ppm can be determined with a 400-g sample. Each analysis requires approximately 5 minutes.

Several instruments using the Be^9 (gamma-neutron) Be^8 reaction for low-level beryllium determinations have been reported (Brownell, 1959; Vaughn, 1960; Mezhiborskaya, 1962). The principal differences between the earlier instruments and the instrument described here are the use of B^{10} -lined low-voltage proportional counters for thermal neutron detection, a remotely operated pneumatic "rabbit" system for handling the radioactive source safely and reliably, and an annular-shaped sensitive chamber. Detection is made possible by the fact that beryllium in a gamma flux of 1.66 million electron volts (minimum energy) is randomly converted to Be^8 with the emission of a photoneutron. The photoneutrons, decreased in energy to thermal range, can be counted and the results converted to a value of beryllium by comparison with a standard calibration curve.

The equipment developed by the U.S. Geological Survey has been in use for approximately 4 years. A minimum amount of maintenance has been required, and the only equipment replaced has been the radioactive isotope (Sb^{124}), which has a useful life of about 4 months. Solid and liquid calibration standards have been carefully prepared. Each standard weighs 400 grams and is permanently sealed in aluminum containers identical with those used for sample analysis (see fig. 1). The analytical time depends somewhat on the

accuracy desired and is normally about 5 minutes for materials containing 1 to 100 parts per million of beryllium. Except for being crushed to $\frac{1}{4}$ -inch size, the solid samples are untreated and are not subjected to contamination by extensive preparation procedures. The liquids are usually laboratory solutions, but samples taken directly from natural waters and contained in a polyethylene bottle are easily accommodated. Most of the determinations made with the instrument have been made using solid sample material.

The Be analyzer has served a twofold purpose in our geologic program: (a) the arbitrary classification by beryllium content of a large number of untreated rock and alluvium samples, and (b) the detailed study of the distribution of beryllium in the parts per million range in a given geologic environment.

The reproducibility and accuracy of the quantitative determinations made with the beryllium analyzer compare favorably with results from wet chemical methods and emission spectrography. The large sample size, which assures a representative analysis, and the freedom from matrix effects, inherent in spectrographic methods, are unique advantages of this technique. Brief studies were made of interference from naturally occurring neutron absorbers, such as lithium and boron, and from density contrast in natural rock. Neither effect is considered serious in geologic studies.

MECHANICAL DESIGN

The mechanical design of the instrument (fig. 1) permits rapid and safe operation by inexperienced personnel. The important elements of the counting chamber are arranged coaxially for maximum sensitivity. The Sb^{124} gamma source (*A*) travels vertically in an aluminum tube (*B*) which extends from the storage position, 3 feet below floor level, to the center of the counting chamber. The coaxial sample cup (*C*), spun from 0.040-inch aluminum, has a hollow center post for entry

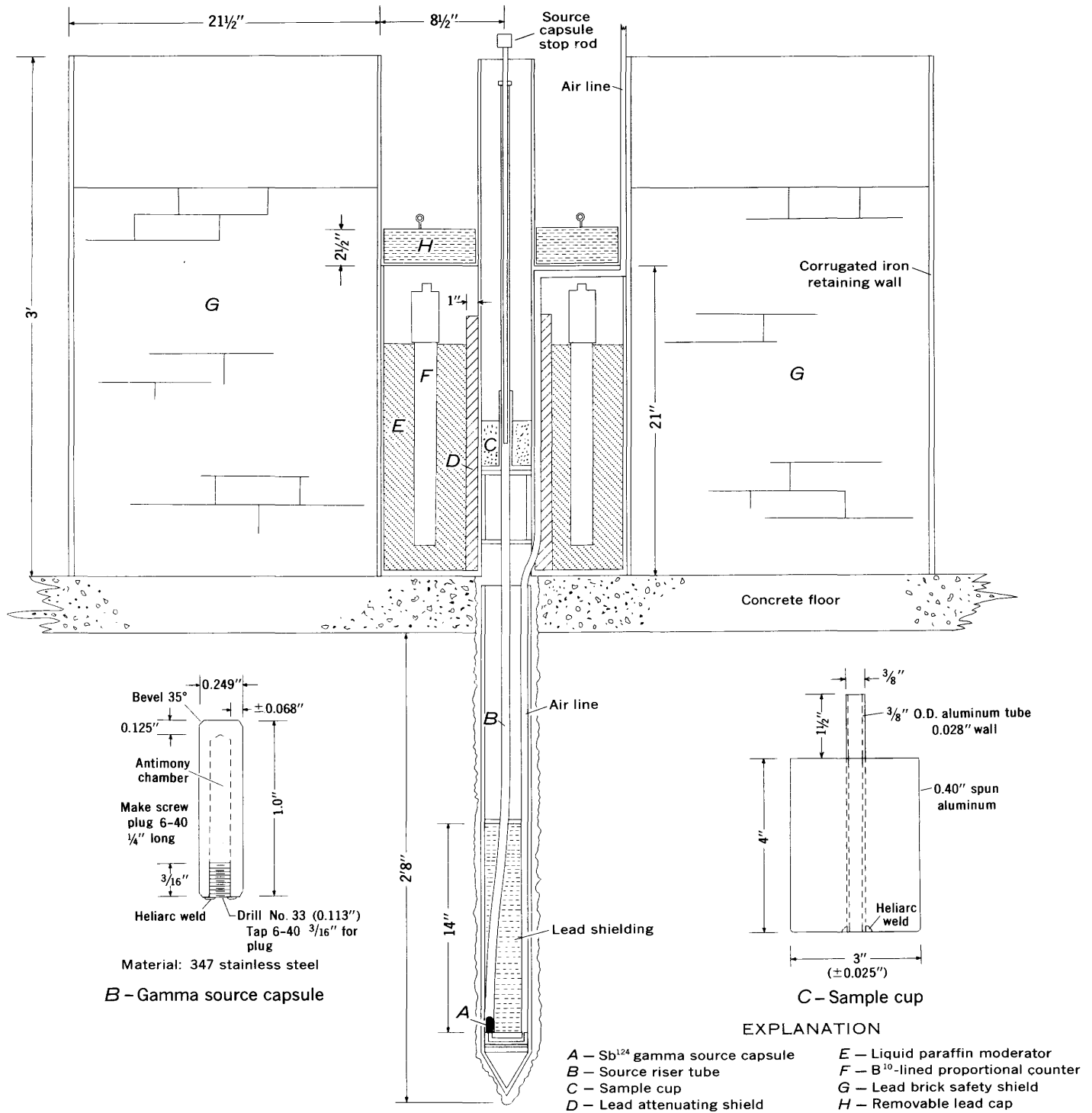


FIGURE 1.—Generalized diagram of gamma-activation device for low-level beryllium analysis.

of the source tube. A solenoid valve controls a 10-pound-per-square-inch pneumatic system to raise the gamma source from storage to operating position. The source is returned to storage by gravity. In this position the metallic source capsule completes an electric circuit which turns on a safety light. A 1-inch-thick

lead shield (D) attenuates the gamma-ray flux from the Sb¹²⁴ source but transmits the photoneutrons released from the beryllium with little loss of energy. The neutrons are thermalized by a liquid paraffin moderator (E) and detected by the B¹⁰-lined proportional counters (F). Five tons of lead (G) serve as an overall radia-

tion shield. A removable lead cap (*H*) covers the paraffin moderator and the proportional counters. A spring-loaded collet-type extractor fits over the center posts of the sample cup and facilitates changing samples (fig. 2).

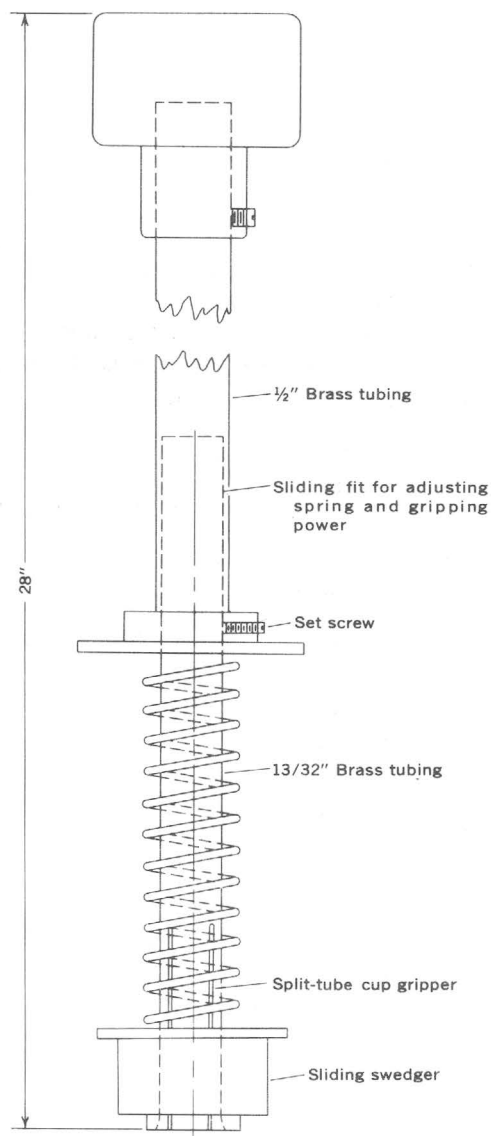


FIGURE 2.—Sample-cup extractor for use with gamma activation device.

CIRCUITRY

The six B^{10} -lined low-voltage proportional counters (fig. 3) are connected in parallel and have a common load resistor, R_1 . The signal developed at R_1 corresponds roughly in size and shape to the type of radiation triggering the counter tubes (see Vaughn and others, 1962, figs. 3 and 4). Thus, although the counter tubes are sensitive to gamma and neutron radiation, a

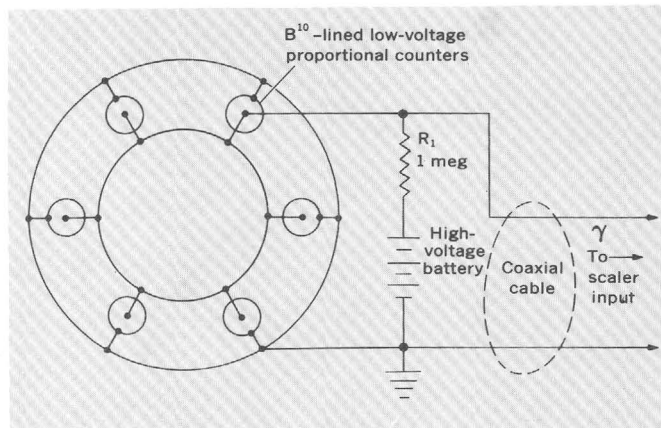


FIGURE 3.—Schematic diagram showing parallel connection and other details of the electrical circuit for proportional counters used in the gamma activation device.

favorable operational mode may be selected that will eliminate the unwanted gamma background and allow the neutrons from the beryllium to be detected efficiently. With a high-voltage setting of 667 volts on the counter tubes, thermal neutrons will produce pulses with approximately 4 millivolts amplitude at R_1 .

A conventional scaler with an input sensitivity variable down to 1 mv is adequate for this instrument technique. It is desirable to have a well-regulated power source, and the room temperature should be controlled to $\pm 5^\circ$ F. The only background interference is due to cosmic radiation and amounts to approximately 70 counts per minute.

CALIBRATION

Typical calibration curves for liquid and solid standards are shown in figure 4. Both curves are virtually linear; however, the solid standard gives a higher counting rate per unit value of beryllium, probably because of the greater absorption of neutrons in the liquid. Liquid samples are advantageous over solid material, however, because of their low density contrast and homogeneity.

Sb^{124} GAMMA SOURCE

The antimony source pellet is fabricated and thoroughly tested for physical defects before it is irradiated and becomes a radioisotope. Solid metallic antimony of commercial grade is sealed with a heliarc weld in a stainless steel (type 347) case (fig. 1). The case and weld are surfaced with an abrasive polishing compound to a satin finish and heated to 1000° F. After cooling, the weld is inspected visually with a microscope. In addition the capsule may be tested for leaks under vacuum by immersion in water. The capsule is then irradiated in a reactor to the specified 1-curie intensity.

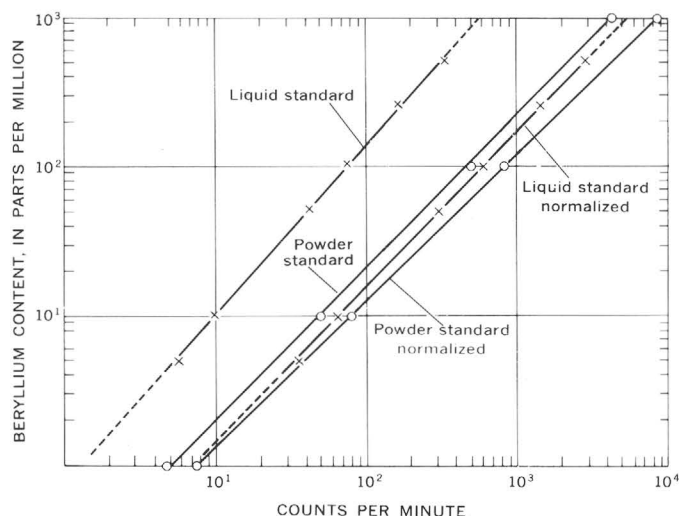


FIGURE 4.—Calibration curve for the gamma activation device.

The antimony before activation has a natural relative abundance of 57.25 percent of Sb^{121} and 42.75 percent of Sb^{123} . On activation the Sb^{121} becomes radioactive Sb^{122} , which decays rapidly to stable Te^{122} . The Sb^{123} becomes radioactive Sb^{124} and similarly by beta-gamma decay becomes stable Te^{124} ; however, there are two isomeric short-lived forms of Sb^{124} , one of which may by transition through gamma emission become Sb^{124} with a 60-day half life; the other may decay directly by beta emission to Te^{124} . The Sb^{124} with 60-day half life, which is the principal isomeric form, provides the gamma rays

for the photoneutron (γ -n) reaction with beryllium (Bradford, 1953).

The threshold for neutron yield from the beryllium atom is 1.63 Mev, and many of the gammas from Sb^{124} are above this threshold. Although it is possible to release neutrons from beryllium with other forms of atomic projectiles, antimony is particularly suitable as a gamma-emitting isotope because of its convenient half life, low cost, and availability.

The gamma activation or photoneutron method of detecting and analyzing for beryllium can be adapted to many special situations. Specifically the technique can be applied to borehole logging, to continuous sample or ore scanning, to specific small-size sample analysis [this last apparatus would use solid-state components and the $\text{Be}^9(\alpha\text{-n})\text{C}^{13}$ reaction]. Some of these applications already have been used by the Geological Survey, and work and development along these lines will continue.

REFERENCES

- Bradford, J. R., 1953, Chart of the isotopes: Cleveland, Ohio, Harshaw Scientific, Div. of the Harshaw Chemical Co.
- Brownell, G. M., 1959, A beryllium detector for field exploration: *Econ. Geology*, v. 54, no. 6, p. 1103-1114.
- Mezhiborskaya, Kh. B., 1962, Photoneutron method of determining beryllium: Translated from Russian Consultant's Bureau Plenum Press, New York, 30 p.
- Vaughn, W. W., Wilson, E. E., and Ohm, J. M., 1960, A field instrument for quantitative determination of beryllium by activation analysis: U.S. Geol. Survey Circ. 427, 9 p.



USE OF X-RAY FLUORESCENCE IN DETERMINATION OF SELECTED MAJOR CONSTITUENTS IN SILICATES

By HARRY J. ROSE, JR., FRANK CUTTITTA,
and RICHARD R. LARSON, Washington, D.C.

Abstract.—An X-ray fluorescence method is described for the quantitative determination of Al_2O_3 , total iron, CaO, K_2O , TiO_2 , and MnO in milligram amounts of silicates. Sample solutions are adsorbed on powdered chromatographic paper, the paper is dried and pelletized, and then exposed to the X-ray beam. Particle-size, absorption, and enhancement effects common to the analysis of powdered samples are eliminated, the method being generally applicable to elements with $Z > 12$. Furthermore, standards are easily prepared from solutions of pure metals or oxides to cover the anticipated analytical range. Working curves are linear, with detection limits being in the microgram and submicrogram level. Results for these elements are comparable to those obtained by analysts for diabase W-1 and granite G-1. The method can be used for the microanalysis of major constituents in very small amounts of geologic and extra-terrestrial materials such as rocks, minerals, impactites, tektites, and meteorites. A switching arrangement which greatly facilitates the use of a single electronic array for both the vacuum and controlled-atmosphere spectrometers is also presented.

The search for techniques that can increase analytical capabilities, especially in quantitative micro- to semi-microanalysis, is a continuing effort in U.S. Geological Survey laboratories. Analysis of geologic and extra-terrestrial materials such as impactites, chondrules, tektites, minerals, and phase separates of meteorites and rocks often requires microanalytical techniques because of limited sample size.

Semimicro determinations of the major constituents (SiO_2 , Al_2O_3 , total iron, K_2O , CaO, TiO_2 , and MnO) of tektites by X-ray fluorescence spectroscopy using 50-milligram samples have been reported by Rose and others (1964). This procedure has been used to analyze a wide variety of geologic materials, and the method has been found applicable to quantities as small as 25 mg.

However, this amount represents a practical lower limit for the $Li_2B_4O_7 \cdot La_2O_3$ fusion technique (Rose and others, 1962, 1963), particularly for the analysis of elements of low atomic number. Yet, in many instances, compositional data are needed where the total amount

of material being studied is much less than 25 mg, especially when rare mineral specimens or scarce extra-terrestrial materials are involved. A method has been developed in which solution techniques combined with X-ray fluorescence spectroscopy are applied to the quantitative determination of Al_2O_3 , total iron, K_2O , CaO, TiO_2 , and MnO in milligram amounts of silicates.

Many of the problems inherent in the X-ray fluorescence analysis of powdered samples (Claisse, 1956; Andermann, 1961; Rose and others, 1962), such as particle size, crystal structure, and matrix effects due to absorption and enhancement, are eliminated by the presentation to the X-ray beam of a homogeneous specimen in the form of sample solution adsorbed onto commercially available powdered chromatographic paper (powdered cellulose), dried at 80°C, and pelletized on a cellulose backing. Solution techniques also offer a means of separating or concentrating very low levels of elements of interest by precipitation with a carrier, by extraction, or by microelectrolytic methods.

Furthermore, in addition to using reference standards such as granite G-1, diabase W-1, and National Bureau of Standards standard samples, standards as needed are easily prepared from solutions of pure metals or oxides which may be combined in varying proportions to cover the anticipated analytical range. Experimental data show that calibration curves are linear, with determination and detection limits at the microgram and submicrogram levels, respectively. The oxide concentration present in the samples is obtained from the calibration curves relating X-ray intensity to chemical composition.

INSTRUMENTATION

Two single-channel X-ray spectrometers were used, one an air- or helium-path unit equipped with a platinum target X-ray tube, and the other a vacuum spectrometer having a dual-target (chromium and tungsten)

TABLE 1.—Operating conditions for X-ray fluorescence analysis

Element	Crystal ¹	λ	Wavelength (Å) ²	Target	Path	Counter
¹³ Al	Eddt	142.53	8.337	Cr	Vacuum	Proportional.
²⁶ Fe	LiF	57.47	1.936	Pt	Air	Scintillation.
²⁰ Ca	Eddt	44.85	3.358	Cr	Vacuum	Proportional.
¹⁹ K	Eddt	50.30	3.741	Cr	Vacuum	Do.
²² Ti	LiF	86.09	2.748	Pt	He	Do.
²⁵ Mn	LiF	62.93	2.102	Pt	Air	Scintillation.

¹ Abbreviations: Eddt, ethylene diamine ditartrate; LiF, lithium fluoride.
² $K_{\alpha 1}$ reflection used.

X-ray tube. The platinum target was used for the determination of Fe_2O_3 , MnO, and TiO_2 and the chromium target for CaO, K_2O , and Al_2O_3 . A switching arrangement, described below, was devised that greatly facilitated the use of a single electronic array for both spectrometers. A constant-potential source operating at 50 kilovolts and 40 milliamperes was used. A pulse-height analyzer was used with a 4.5-volt base level, a 12-v window, and a line pulse adjusted to 7.5 v. Counting times were selected by determining the interval required to attain reasonable statistics on the lowest standard for each element. The operating conditions, crystals used, and other pertinent data are given in table 1. Because fluorescent radiation of elements having atomic numbers $Z \leq 22$ is absorbed by air, the spectrometer sample chamber is flushed with helium for the determination of elements in the range $Z \leq 22$ but > 12 , where $Z=12$ is the cutoff for detection by this method. In order to allow the system to come to equilibrium between sample changes, it is advisable to flush the sample chamber for about 1 minute.

Only a single electronic console, which provides accessory power and electronic readout circuits, is necessary to operate the two spectrometers. Because the two spectrometers have identical electrical requirements, a relay-switching circuit was devised to provide an automatic and instantaneous switchover. Such an arrangement eliminates the time-consuming changing of cable connections that invariably contributes to the failure of one or more of the circuits.

As shown in figure 1, the switch consists of three four-pole, double-throw relays for the power and voltage circuits and a coaxial relay to handle the signal circuits. All the relays are actuated from a single toggle switch mounted on the front panel of the console. Connectors were mounted on the back panel of the console to accommodate all the cables from the spectrometers.

There is one precaution that should be observed. Although heavy-duty relays were selected, the high voltage to the detector tube should be turned off before switching from one spectrometer to the other, to prevent arcing at the contacts.

PROCEDURE

A 4- to 10-mg portion of the sample is weighed in a tared 15-milliliter platinum crucible to ± 0.01 mg. One ml of 5:2:3 HF:HNO₃:H₂O is added to the platinum crucible containing the accurately weighed silicate sample. The crucible is covered, placed on a steam bath, and allowed to simmer for several hours until the sample is decomposed. The resulting solution is evaporated to dryness on the steam bath three times; 1 ml of 1:1 HNO₃ is added to the residue remaining after each evaporation. The silica-free nitrates are dissolved in 1.0 ml of 1:4 HNO₃. Nitric acid is used as the solvent medium in preference to acids containing heavier atoms, for example H₂SO₄, HCl, HClO₄, and H₃PO₄, to minimize absorption of X-rays. This solution is absorbed onto 500 mg of powdered chromatographic paper, the resulting moist pulp being mixed thoroughly with a small Teflon stirring rod, and then dried overnight at 80°C. The dried paper is then mixed in a boron carbide mortar and the ground powder is pressed into a pellet 1 inch in diameter. For additional strength, the pellet

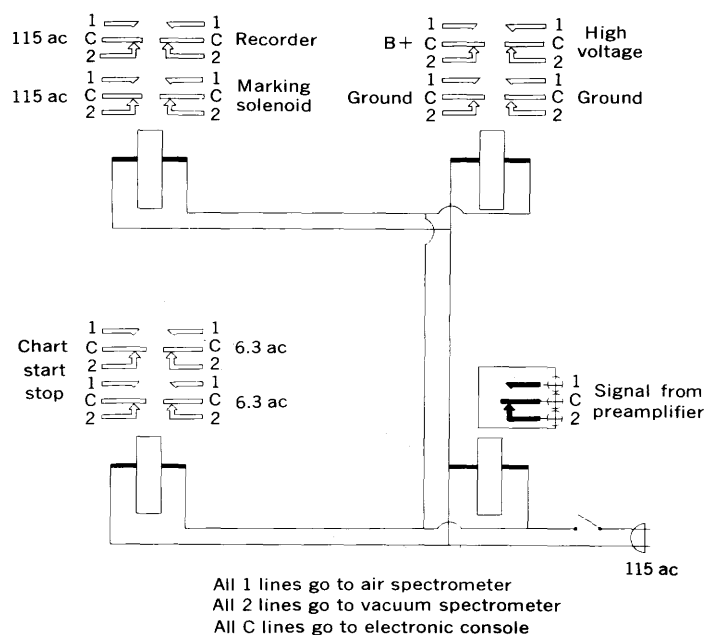


FIGURE 1.—Diagram of relay switching circuit.

is prepared as a double layer, with powdered chromatographic paper as a backing. The pellet is then exposed to the X-ray beam.

DISCUSSION AND RESULTS

Optimum ratio of solution to absorbent

Figure 2 presents data for titania, showing the increase in counting rate as the ratio of absorbent to solution is decreased (curve *A*). The sample weight was kept constant by absorbing 1 ml of a solution of GW-1 (1.54 mg/ml) on 100-, 200-, 300-, 400-, and 500-mg samples of powdered cellulose. Although the intensities are higher with smaller quantities of absorbent, the optimum ratio of solution to absorbent is 1 ml to 500 mg, a ratio that just provides complete absorption of the sample solution.

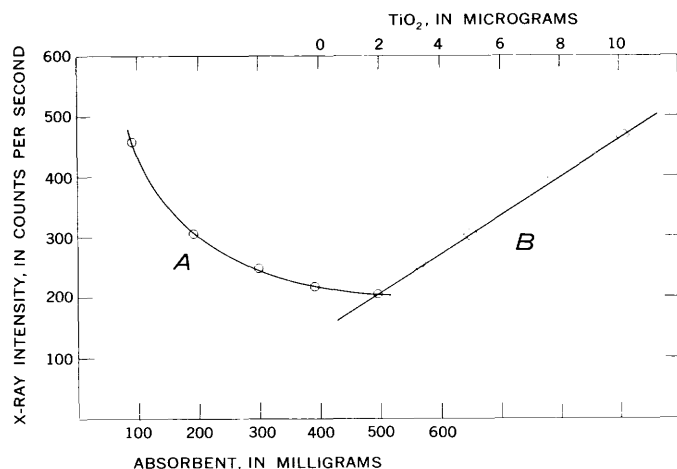


FIGURE 2.—Effect of varying amounts of absorbent and TiO_2 on measured X-ray intensities. Curve *A*, effect of varying amounts of absorbent on measured X-ray intensities for a constant sample weight of TiO_2 . Curve *B*, same data on the X-ray intensities for TiO_2 , as used for curve *A*, but calculated on the basis of 100 mg of absorbent.

Effect of variable sample weight

The effect of a variable sample weight on counting rates when using a constant amount (500 mg) of powdered cellulose absorbent is shown in figure 3. One-milliliter aliquots containing 1, 2, 3, and 4 mg of each of three reference standards (granite G-1, diabase W-1, and a 1:1 mixture of G-1 and W-1) were processed by the solution-pellet method, and the resultant X-ray counting rates were related to the titania content of the samples. The data show that even a fourfold change in sample weight has little or no effect upon the linearity of the concentration-intensity relation. This direct correlation is also implied in curve *B* (fig. 2), where the data shown in curve *A* were replotted to represent the counting rates associated with the titania content (in

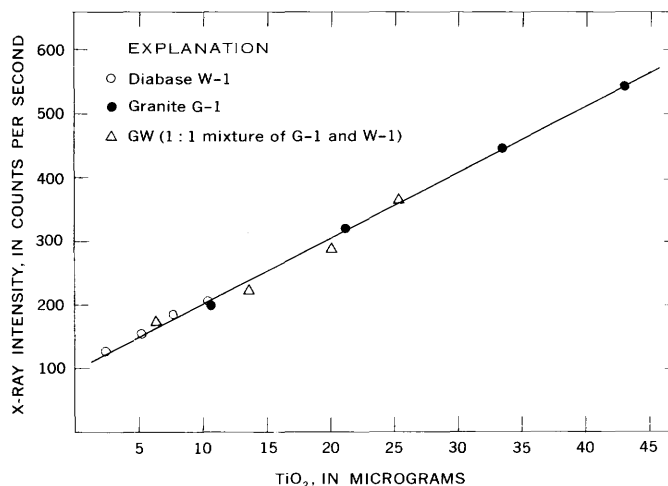


FIGURE 3.—X-ray intensity as a function of variable sample weight of TiO_2 for constant weight of absorbent (500 mg).

micrograms) per 100 mg of the sample-impregnated absorbent.

Effect of variable composition

Effects arising from the variability of composition of silicate samples might have been expected to significantly interfere with the accurate determination of oxide concentrations in an unknown sample. A suite of analyzed silicates (granite, diabase, tektites, and synthetic glasses) was processed using a constant amount (500 mg) of absorbent and sample weights ranging from 4 to 10 mg. These reference materials represent a variable silica content ranging from 45 to 87 percent. The data for titania are presented in figure 4. The linearity of the curve indicates that variations in composition of silicate samples have little or no effect upon the direct correlation of the oxide concentration with the X-ray fluorescence intensity.

The lack of compositional effects may be attributed to the fact that the sample submitted to the X-ray beam is virtually powdered cellulose, and as such, the role of the sample matrix on X-ray absorption or enhancement is reduced to a minimum. The experimental data and correlations shown for titania on figures 2 and 3 hold for all the other oxides (Al_2O_3 , total iron as Fe_2O_3 , CaO , K_2O , and MnO) studied, and their presentation here would only represent duplication of the data already shown above.

Pellet preparation

Because sample preparation is the largest single factor that affects the accuracy of any analytical procedure, caution must be exercised in presenting a uniform pelletized sample layer to the X-ray beam. The solution must be carefully added to the cellulose powder and,

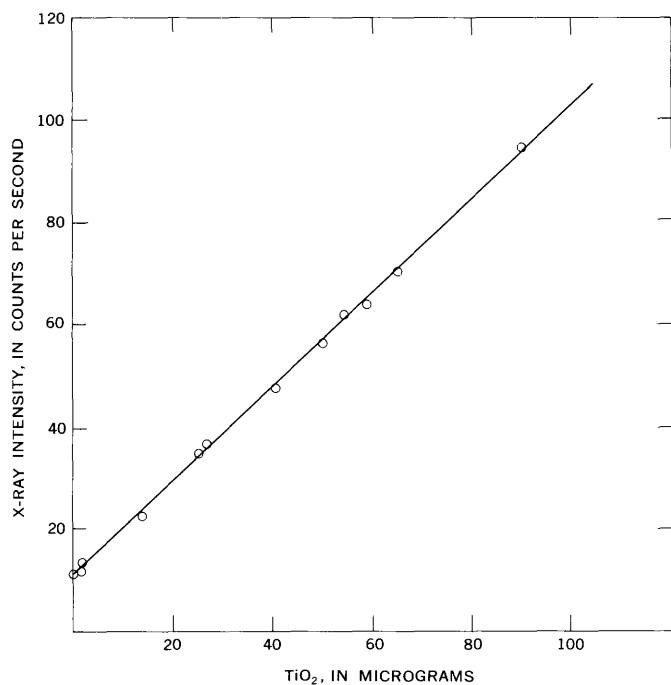


FIGURE 4.—X-ray intensity as a function of weight of TiO₂, in micrograms, for silicates for variable composition.

when dry, the powder must be thoroughly mixed. With the double-pellet technique, the sample layer must be spread uniformly on the powdered chromatographic paper backing before application of final pressure. Pressures in excess of 50,000 pounds per square inch are recommended to insure both high precision and maximum X-ray intensity. The pellets used in this study were prepared using a pressure of 70,000 pounds psi.

Comparison of analytical results

A comparison of the analytical results obtained by the proposed X-ray fluorescence-solution technique with

related chemical data is presented in table 2. The reported chemical results are averages of duplicate determinations by various previously described methods (Rose and others, 1964). The chemical determinations by these different techniques, were closely monitored by similar determinations on granite G-1, diabase W-1, and selected National Bureau of Standards certified samples.

The analytical data presented in table 2 show that X-ray fluorescence values determined for Al₂O₃, total iron as Fe₂O₃, CaO, K₂O, TiO₂, and MnO agree well with the reported chemical values for these oxides. The technique requires less than 10 mg of silicate sample and has limits of measurability of about 1 microgram for Fe₂O₃, CaO, K₂O, TiO₂ and MnO and about 50 μg for Al₂O₃. These limits of measurability can be lowered as indicated in figure 2 (curve A) by reducing the ratio of paper absorbent to sample. Sample preparation techniques are presently under investigation that should eventually permit the determination of silica by this method.

REFERENCES

- Andermann, George, 1961, Improvements in the X-ray emission analysis of cement raw mix: *Anal. Chemistry*, v. 33, p. 1689-1695.
- Claisse, Ferdinand, 1956, Accurate X-ray analysis without internal standard: *Quebec Dept. Mines, Prog. Rept. 327*, 16 p.
- Rose, H. J., Adler, Isidore, and Flanagan, F. J., 1962, Use of La₂O₃ as a heavy absorber in the X-ray fluorescence analysis of silicate rocks: *Art. 31 in Geol. Survey Prof. Paper 450-B*, p. B80-B82.
- 1963, X-ray fluorescence analysis of the light elements in rocks and minerals: *Applied Spectroscopy*, v. 17, no. 4, p. 81-85.
- Rose, H. J., Cuttitta, Frank, Carron, M. K., and Brown, Robena, 1964, Semimicro X-ray fluorescence analysis of tektites using 50-milligram samples: *Art. 157 in U.S. Geol. Survey Prof. Paper 475-D*, p. D171-D173.



THE PROBLEM OF AUTOMATIC PLATE READING AND COMPUTER INTERPRETATION FOR SPECTROCHEMICAL ANALYSIS

By A. W. HELZ, Washington, D.C.

Abstract.—The problem of completely automating spectrum-plate reading and interpretation is discussed. Spectrochemical analyses of geologic materials by such means would benefit from the use of more of the data recorded in the spectrum than is feasible by manual methods. Increased speed and accuracy could be expected to result.

Quantitative spectrochemical analysis is based upon the determination of the intensity of a spectral line either relative to some other spectral line or background, or to the same spectral line produced under known standardized conditions. Spectral-line intensities are measured with highest precision by the direct use of multiplier phototubes. Because of the necessity of integrating the intensities over an extended exposure time, the apparatus required for this increases in complexity as the number of lines to be observed increases.

For the analytical problem where the primary objective is the determination of many elements rather than the attainment of the highest precision on a few, the photographic plate is without peer because of its ability to record 10,000 lines simultaneously. In an analytical scheme in which many elements are sought, the spectrographer, for practical reasons, makes use of only a fraction of the information displayed on a photograph of a spectrum. There is just too much information to use effectively. For elements in concentrations above the limits just detectable, lines in addition to the most sensitive come into view. The relative intensities for the lines of any one element present at fixed concentration are not constant, but depend upon the excitation conditions, which in turn are dependent not only upon the energy input to the source but also on the kind and amounts of other elements present, their chemical combination, and physical state. The same statement also applies to the intensity of a line for any one element relative to the intensity of lines for every other element present in the source.

An analytical determination could be improved if more of the information in a spectrum were used than is practical now. One can conceive of a computer, with its facility for handling very large amounts of data extremely rapidly, that would base a decision on the concentration of any one element on all of the observable lines for that element, and include corrections for the concentrations of all other elements present, major and minor, and for perhaps arc conditions based on carbon lines, cyanogen bands, and other concomitant factors. Much of the information needed for such a computational problem is not as elusive as may seem at first; it may be found in spectra of analyzed standards. By using a sufficient variety of standards covering all pertinent combinations of concentrations of major and minor elements, the essential reference data are available. The critical features are the large amount of data to be handled and the high precision needed for transferring the information from the spectrum to a form suitable for computer handling.

If 60 elements are sought in the analysis the computer may have stored information on more than the minimum number of spectral lines, perhaps twice as many. This opportunity to handle a greater amount of data is the chief advantage sought. The data consist of (1) wavelengths (for identification), (2) the relation between line intensity and concentration for each line, (3) the relation between percent transmission of the developed photographic line and the intensity of the radiation that produce the image, and (4) corrections for background, emission source, spectral interferences, and matrix and interelement effects.

AVAILABLE APPARATUS

Computer development and precise and rapid data reading from photographs sufficient for handling the above problem have been demonstrated in numerous

other applications. Anderson and Moser (1958) describe the use of a computer for converting spectrographic-line transmittances to element concentrations with an improvement over manual methods in both speed and reliability. These authors start with manually selected lines and transmittancy measurements. A similar example of the use of a computer for completing spectrochemical calculations is given by Schalge and others (1964). A table is supplied by the computer giving information on not only the concentrations of the elements but also error estimates and initial data. Tunnicliff and Weaver (1964) extend the computer handling of manually collected data to include corrections for interferences from other elements and to choosing the "best" value to report for each element. Their program was used routinely for determining 15 elements, with gains in economy and accuracy.

There are a number of commercially available direct-reading spectrometers that include automatic data computation. Calibration curves and corrections for interelement interferences are electronically represented, and results are given directly in percentage composition.

Computer handling of data such as illustrated above starts with input data of specific spectral lines and with either the corresponding "blackness" on the photographic plate or the output of a photomultiplier tube. The initial problem of data collecting requires rapid highly precise instrumentation for either (1) measuring all the lines in a spectrum or (2) measuring a predetermined set of lines selected from the large number present. An example of method (1) above, recording all spectral lines with high accuracy, is given by Steinhaus and Engleman,¹ who described a comparator and digital computer programmed to find and measure spectral lines recorded on photographic plates. A precision densitometer and linear comparator supply the computer with a list of optical transmission values at equal intervals (1 or 5 microns) along the spectrum. More than 200 lines per minute are measured with a precision better than 0.1μ for sharp lines 25μ wide. Four line shapes are distinguished: symmetrical, shaded toward longer wavelength, shaded toward shorter wavelength, and wide lines.

The second method of data collecting, measuring a predetermined set of lines, would reduce the amount of data collected before involving the computer. This method is more exacting in that an instrument is required to measure transmittancies at numerous preselected spectral positions regardless of the actual pres-

ence of a line. High-speed counting and switching systems as well as other programming devices are available for accomplishing such a reading schedule.

A brief survey of the factors that indicate the size and complexity of the problem follows.

FACTORS AFFECTING AUTOMATIC PLATE READING AND COMPUTER INTERPRETATION

Choice of spectral lines

In a procedure for the quantitative spectrochemical analysis of rocks, ores, and minerals, Bastron and others (1960) list 154 spectral lines commonly employed, along with the useful concentration ranges. Not all useful lines are included and not all the lines listed are used in an analysis. Variations in excitation techniques and sample materials determine the choice. However, the list suffices to illustrate the problems involved. In total number of lines, the table is not much different from that ultimately required.

In table 1 the lines given in the above reference are arranged in order according to wavelength—as they would appear in a spectrum. (Potentially useful lines in the cyanogen region have been added.) The calculated spacing of the lines as obtained with a high dispersion grating spectrograph is also shown. The table was arranged specifically to illustrate several aspects of the problem.

Uneven distribution of spectral lines

The irregular spacing of the special lines imposes stringent but attainable requirements for the precise location and rapid response of the microphotometer for recording the lines. A constant-velocity traveling microscope is envisioned for recording percent transmission of the lines. If 5 minutes is taken as a reasonable time for scanning a 20-inch spectral length and a line width of 25μ is assumed, then the transmission of lines must be recorded at a rate greater than 68 readings per second in order to measure 2 lines just touching each other, or to record the transmission during the time for traversing 1 spectral line.

TABLE 1.—Analytical spectral lines arranged according to wavelength

[Boxheads explained at end of table, p. B163]

1	2	3	4	5	6
Be.....	2348. 61	300	9. 72	0. 25	Zr 2348. 59
As.....	2349. 84	85	9. 97	7. 18	Cu 2349. 85
Te.....	2385. 76	70	17. 15	5. 55	Cr 2385. 74
Se.....	2413. 52	-----	22. 70	16. 66	
B.....	2496. 78	240	39. 36	. 19	
B.....	2497. 73	480	39. 55	7. 25	Fe 2497. 80
P.....	2534. 01	22	46. 80	. 50	
Hg.....	2536. 52	1500	47. 30	3. 36	
P.....	2553. 28	38	50. 66	. 33	Fe 2553. 18
P.....	2554. 93	15	50. 99	8. 62	Fe 2555. 07

¹D. W. Steinhaus and Rolf Engleman, Jr., 1963, Automatic comparator for measurement of line spectra: Paper presented at annual meeting, Optical Society of America, October 1963.

TABLE 1.—Analytical spectral lines arranged according to wavelength—Continued

[Boxheads explained at end of table, p. B163]

1	2	3	4	5	6
Sb.....	2598.06	600	59.61	3.47	
Lu.....	2615.42	1200	63.08	7.16	Fe 2615.42
Ge.....	2651.18	1200	70.24	.26	
Al.....	2652.49	15	70.50	1.39	
Pt.....	2659.45	280	71.89	.19	
Al.....	2660.39	20	72.08	.55	Fe 2660.40
Pb.....	2663.17	300	72.63	2.56	
Au.....	2675.95	340	75.19	7.74	
Ta.....	2714.67	300	82.93	7.51	
Zr.....	2752.21	75	90.44	3.13	Mn 2752.32
Tl.....	2767.87	440	93.57	1.77	
Mg.....	2776.69	38	95.34	.70	
As.....	2780.20	140	96.04	.55	
Mg.....	2782.97	36	96.59	3.62	
Mn.....	2801.06	480	100.21	2.58	
Eu.....	2813.95	340	102.79	3.82	
Pb.....	2833.07	950	106.61	1.39	
Sn.....	2839.99	1400	108.00	2.43	Mn 2840.00
Mg.....	2852.13	6000	110.43	2.84	
Hf.....	2866.37	240	113.27	.81	V 2866.42
Th.....	2870.41	48	114.08	1.50	Cr 2870.44
Sb.....	2877.92	140	115.58	.74	Cr 2877.98
Si.....	2881.58	260	116.32	2.97	
W.....	2896.45	190	119.29	.31	
Bi.....	2897.98	400	119.60	1.74	Mn 2897.99
Eu.....	2906.68	320	121.34	.94	
Lu.....	2911.39	600	122.28	6.45	
Ga.....	2943.64	950	128.73	.11	Fe 2943.57
Ga.....	2944.18	150	128.84	1.00	
Mn.....	2949.20	240	129.84	3.18	
Ru.....	2965.16	60	133.02	1.09	
Yb.....	2970.56	280	134.11	10.02	Ti 2970.56
Fe.....	3020.64	280	144.13	.18	
Cr.....	3021.56	360	144.31	.86	
Fe.....	3025.84	38	145.17	.35	
Gd.....	3027.61	160	145.52	2.29	
Ge.....	3039.06	750	147.81	.06	
In.....	3039.36	800	147.87	2.29	Fe 3039.32
Ni.....	3050.82	280	150.16	.09	V 3050.88
In.....	3051.25	-----	150.25	2.67	
Ni.....	3064.62	40	152.92	.02	
Pt.....	3064.71	320	152.94	.60	
Bi.....	3067.72	3600	153.54	.51	
Mn.....	3070.27	22	154.05	2.38	
Al.....	3082.16	320	156.43	.32	V 3082.11
Fe.....	3083.74	24	156.75	3.56	
Ni.....	3101.55	240	160.31	.15	Ti 3101.53
V.....	3102.30	400	160.46	1.36	
Hf.....	3109.12	80	161.82	2.49	
Pr.....	3121.57	14	164.31	.25	Co 3121.57
Au.....	3122.78	160	164.56	1.53	V 3122.89
Be.....	3130.42	480	166.09	.12	
Be.....	3131.07	320	166.21	.04	Zr 3131.11
Tm.....	3131.26	700	166.25	.69	Cr 3131.21
Hf.....	3134.72	95	166.94	.04	
Nd.....	3134.90	13	166.98	3.47	V 3134.93
Ti.....	3152.25	20	170.45	1.32	
Ca.....	3158.87	20	171.77	.91	
Nb.....	3163.40	140	172.68	1.02	
Ti.....	3168.52	130	173.70	.37	

TABLE 1.—Analytical spectral lines arranged according to wavelength—Continued

[Boxheads explained at end of table, p. B163]

1	2	3	4	5	6
Mo.....	3170.35	1100	174.07	.93	Fe 3170.35
Sn.....	3175.02	550	175.00	.09	
Fe.....	3175.45	7	175.09	1.59	
V.....	3183.41	420	176.68	.18	
V.....	3183.98	700	176.86	.22	
V.....	3185.40	500	177.08	1.71	
Mo.....	3193.97	950	178.79	.21	V 3193.92
Nb.....	3194.98	120	179.00	.12	
Y.....	3195.62	300	179.12	1.22	
Ce.....	3201.71	90	180.34	3.65	Ti 3201.57
Tb.....	3219.95	130	183.99	.16	Fe 3219.81
Er.....	3220.73	85	184.15	.01	Ce 3220.87
Ir.....	3220.78	500	184.16	1.79	
Tl.....	3229.75	120	185.95	.17	Fe 3229.87
Er.....	3230.58	220	186.12	.40	Sm 3230.54
Li.....	3232.61	17	186.52	1.94	Ti 3232.79
V.....	3242.28	800	188.46	.08	
Pd.....	3242.70	1200	188.54	.48	
La.....	3245.12	70	189.02	.07	
Pr.....	3245.46	12	189.09	.42	
Cu.....	3247.54	5000	189.51	1.37	Mn 3247.54
Sm.....	3254.38	70	190.88	1.33	Fe 3254.36
Cd.....	3261.06	32	192.21	.11	
Ti.....	3261.60	100	192.32	.14	
Os.....	3262.29	320	192.46	1.56	Fe 3262.28
U.....	3270.12	18	194.02	.59	
Zr.....	3273.05	160	194.61	.18	V 3273.03
Cu.....	3273.96	2500	194.79	1.35	
Ag.....	3280.68	5500	196.14	1.21	Mn 3280.76
Fe.....	3286.76	28	197.35	.52	
Yb.....	3289.37	2600	197.87	.74	Fe 3289.44
Tb.....	3293.07	160	198.61	1.70	Fe 3293.14
Os.....	3301.56	800	200.31	.15	
Na.....	3302.32	30	200.46	.06	
Zn.....	3302.59	90	200.52	.08	Na 3302.32
Na.....	3302.99	15	200.60	1.63	Zn 3302.94
Ta.....	3311.16	140	202.23	1.75	
Dy.....	3319.88	90	203.98	.90	Eu 3319.89
Tb.....	3324.40	400	204.88	.70	Fe 3324.54
Y.....	3327.88	600	205.58	.07	Sm 3327.90
Nd.....	3328.27	24	205.65	.34	Cr 3328.35
Mg.....	3329.93	-----	205.99	.29	V 329.85
Gd.....	3331.39	140	206.28	1.22	
La.....	3337.49	200	207.50	1.50	
Zn.....	3345.02	140	209.00	.49	Ti 3344.93
Cs.....	3347.44	-----	209.49	.61	
Gd.....	3350.48	550	210.10	.08	Eu 3350.43
Rb.....	3350.89	-----	210.18	.57	
Sc.....	3353.73	900	210.75	3.81	
Ti.....	3372.80	480	214.56	2.02	
Ag.....	3382.89	2800	216.58	1.82	Nd 3382.81
Zr.....	3391.98	900	218.40	.97	Fe 3392.01
Rh.....	3396.85	480	219.37	.43	Fe 3396.98
Ho.....	3398.98	900	219.80	1.12	Er 3398.94
Pd.....	3404.58	2600	220.92	.64	Fe 3404.34
Dy.....	3407.80	480	221.56	.17	Er 3407.79
Sm.....	3408.67	70	221.73	1.22	Er 3408.68
Ni.....	3414.76	750	222.95	4.03	
Rh.....	3434.89	700	226.98	.37	
Ru.....	3436.74	650	227.35	2.48	

TABLE 1.—Analytical spectral lines arranged according to wavelength—Continued

1	2	3	4	5	6
Co-----	3449.17	260	229.83	.87	
Co-----	3453.50	1300	230.70	1.39	
Re-----	3460.47	5500	232.09	.35	Cr 3460.43
Tm-----	3462.20	800	232.44	.45	Fe 3462.36
Sr-----	3464.46	95	232.89	.05	
Re-----	3464.72	4000	232.94	.30	Cr 3464.84
Cd-----	3466.20	250	233.24	1.61	Fe 3465.86
Ho-----	3474.25	600	234.85	4.94	Ce 3474.22
Ru-----	3498.94	850	239.79	4.06	Dy 3498.94
Tl-----	3519.24	2000	243.85	18.05	Zr 3519.60
Sm-----	3609.48	280	261.90	5.19	Pd 3609.55
Ti-----	3635.46	400	267.09	1.45	Mo 3635.43
Ti-----	3642.68	550	268.54	2.16	Sc 3642.79
Ti-----	3653.50	600	270.70	1.57	Tm 3653.61
Ru-----	3661.35	600	272.27	7.78	Sm 3661.36
Tm-----	3700.26	400	280.05	3.53	Tb 3700.12
Tm-----	3717.92	650	283.58	2.03	Hf 3717.80
Ru-----	3728.03	1000	285.61	6.25	Na 3728.13
Ti-----	3759.29	280	291.86	.40	Tb 3759.35
Ti-----	3761.32	240	292.26	2.88	Tm 3761.33
Tl-----	3775.72	1200	295.14	4.01	Ni 3775.57
Tm-----	3795.77	600	299.15	4.78	
Eu-----	3819.66	3400	303.93	13.13	
Sm-----	3885.29	280	317.06	12.76	Zr 3885.42
La-----	3949.10	900	329.82	4.57	Tm 3949.28
Eu-----	3971.96	2000	334.39	7.36	
W-----	4008.75	950	341.75	7.08	Pr 4008.71
K-----	4044.14	32	348.83	6.04	Fe 4043.90
W-----	4074.36	550	354.87	12.66	
Ce-----	4137.65	140	367.53	3.69	
Nd-----	4156.08	180	371.22	4.66	
Pr-----	4179.42	460	375.88	1.44	
Ce-----	4186.60	250	377.32	7.20	Dy 4186.78
Ce-----	4222.60	110	384.52	.83	Cr 4222.73
Ca-----	4226.73	1100	385.35	3.52	
U-----	4244.37	38	388.87	.50	W 4244.37
Sc-----	4246.83	1400	389.37	1.50	
Cr-----	4254.35	1700	390.87	4.09	Ho 4254.43
Cr-----	4274.80	1300	394.96	1.64	
Ca-----	4283.01	24	396.60	2.32	V 4282.91
W-----	4294.61	450	398.92	1.80	
Nd-----	4303.58	320	400.72	6.03	Pr 4303.59
La-----	4333.74	460	406.75	44.05	
Ba-----	4554.03	6500	450.80	7.84	
Cs-----	4593.18	20	458.64	2.83	
Sr-----	4607.33	650	461.47		

1. Element.
2. Wavelength, in angstroms. Mostly from Bastron and others (1960).
3. Relative intensity, National Bureau of Standards Monograph 32, "Tables of Spectral Line Intensities."
4. Distances from arbitrary starting point, in millimeters, assuming 5.0 A per millimeter for reciprocal linear dispersion.
5. Distance between spectral line and the next one, in millimeters.
6. Partial list of interfering elements. From Sol Berman, U.S. Geological Survey.

Two very different methods for attacking the problem of an uneven distribution of spectral lines in plate reading are suggested: (1) The microphotometer may be programmed to record the transmission every time it

reaches a position along the spectrum where a line is calculated to be. In this approach it cannot be assumed that all positions can be calculated from a single starting point. For various reasons there may be "stretching" errors from one spectrum to the next. These errors may be minimized experimentally or may be compensated for by the use of a number of fiducial points within the spectrum for length compensation. These points may be obtained by incorporating an internal standard element in the spectrum source. (2) One could transfer the selection problem to the computer. The microphotometer is arranged to record the transmission at equal intervals of length along the spectrum. For lines 25 μ wide, readings taken every 5 μ would supply good reading definition. Thus 101,600 readings would be required for 20 inches of spectrum. For the previously assumed time of 5 minutes for reading the entire spectrum, 339 readings per second would be required, a high but not impossible speed.

Too little space between spectral lines

In searching through table 1, column 5, for lines 2 line-width units apart or less (0.05 mm), (assuming this to be the limiting practical resolution) 5 occurrences are noted: Ni 3065 Pt, Be 3131 Tm, Hf 3135 Nd, Er 3221 Ir, and Sr 3465 Re. Table 2 shows the pertinent data on these lines given by Bastron and others (1960). If the microphotometer gave a positive indication above spectral background at 3064.7, for example, are Ni, Pt,

TABLE 2.—Close pairs of analytical lines

Element	Line wavelength (angstroms)	Concentration range (weight percent)
Ni-----	3414.76	0.0002-0.01
	3050.82	.001 - .1
	3101.55	.001 - .1
Pt-----	¹ 3064.62	.01 - .5
	2659.45	.001 - .1
	¹ 3064.71	.001 - .1
Be-----	2348.61	0.0001-0.001
	3130.42	.0005- .02
	¹ 3131.07	.001 - .05
Tm-----	¹ 3131.26	.001 - .1
	3462.20	.001 - .05
	Hf-----	2866.37
3109.12		.03 - .5
¹ 3134.72		.03 - .5
Nd-----	4303.57	.01 -1
	3328.27	.05 -3
	¹ 3134.90	.2 -5
Er-----	3230.58	0.001 -0.5
	¹ 3220.73	.01 - .5
	¹ 3220.78	.006 - .1
Sr-----	4607.33	0.0001-0.2
	¹ 3464.46	.01
	¹ 3464.72	.001 - .05
Re-----	3460.47	.005

¹ Close pairs.

or both present? This first example illustrates the advantage of the multiplicity of data. It will be noted that the above question can be answered from information supplied by the other lines for Ni and Pt, provided that there are no other interferences. For Er-Ir, according to table 2 there is no multiple choice. Actually as noted in a more extensive table (National Bureau of Standards Monograph 32) the iridium spectrum has a number of lines nearly as strong at 2544A, 2925A, 3133A, 3514A, 3800A, and so forth, with decreasing intensity. If no solution were available here to resolve the confusion between Er and Ir, a knowledge of the material being analyzed may serve as a discriminatory guide. For geologic materials, geochemical reasoning indicates that Ir is likely to be present if other elements of the platinum group are detected, that is Pt, Pd, Os, Rh, or Ru. Er is indicated if other members of the same rare-earth group or Y are present.

Interfering elements

Whether or not one spectral line interferes with another depends not only on their proximity but also on their relative intensities, kind of excitation, and nature of the sample material. The following discussion is restricted to the use of a d-c carbon arc in silicate rock analysis for which these data were compiled. A sample differing much from a normal silicate rock may require special care to avoid misinterpretation because of line interferences. A number of possible interferences are noted in the last column of table 1. As in the previous section, a definitive result almost always is available because of the multiplicity of data. For example, the first entry on table 1 indicates that Zr 2348.59A may interfere with Be 2348.61A. If this were so, the much stronger lines Zr 3273.05, Zr 3391.98, and Zr 2752.21 would show, and either of the beryllium lines 3130.42 or 3131.07 would be relied upon, depending upon the absence of other potential interferences with those lines. This is determinable by repeating the same procedure for the newly selected beryllium line.

SUMMARY

A spectrum interpretation procedure as proposed here would entail the following steps:

- (1) Record the percent transmission for (a) every 5μ of spectrum or (b) a selected set of spectral lines.
- (2) If choice 1a is made for plate reading, then pro-

gram a computer to select the required set of spectral lines resulting in a tabulation of wavelengths and percent transmissions.

(3) Correct percent transmission for spectral background and excitation errors.

(4) Select the best line for each element. This involves the complex interplay of interferences noted above.

(5) Calculate the intensity of each of the selected lines relative to an internal standard line or spectral background. Plate-calibration data are used for this to define the relation between percent transmission and intensity.

(6) Calculate concentration of the elements, using stored data to define the relation between intensity and concentration for each of the lines.

The problems of applying automatic data acquisition and computational methods to the spectrochemical determination of many elements in geologic materials stem from the large amount of data to be handled. The required plate-reading speed and accuracy have been attained in other applications, and similar data-storing, rapid-access, sorting, and calculating problems have been handled with computers.

The complete automation of spectrum-reading and interpretation appears fantastically complex because of the large number of elements, multiplicity of spectral lines, and many additional variables of interfering elements, matrix compositions, and excitation conditions. Many simplifications would be found and compromises made in a serious attack on the problem. Developments along these lines are encouraged by the possibilities of eliminating much manual labor and obtaining a better analysis, through the use of much more of the information recorded in a spectrum, than is now possible.

REFERENCES

- Anderson, F. W., and Moser, J. H., 1958, Automatic computer program for the reduction of routine emission spectrographic data: *Anal. Chemistry*, v. 30, p. 879.
- Bastron, Harry, Barnett, P. R., and Murata, K. J., 1960, A quantitative method for the determination of many constituents in a large variety of geologic materials: *U.S. Geol. Survey Bull.* 1084-G, p. 165-181.
- Schalge, A. L., Thurnan, D. H., and Miller, G. B., 1964, A digital computer method to handle emission spectrochemical data: *Appl. Spectroscopy*, v. 18, p. 30.
- Tunnelliff, D. D., and Weaver, J. R., 1964, Automatic data processing interpreting, and reporting of results of emission spectrographic analyses: *Anal. Chemistry*, v. 36, p. 2318.



A PLATINUM-LINED BOMB FOR THE HIGH-TEMPERATURE DECOMPOSITION OF REFRACTORY MINERALS

By IRVING MAY, J. J. ROWE, and RAYMOND LETNER,
Washington, D.C.

Abstract—A platinum-lined bomb is described for high-temperature acid decomposition of small mineral samples for chemical analysis. The apparatus consists of an easily removable platinum-lined Nichrome crucible which is inserted into a Morey-type bomb. As the crucible can be removed from the bomb while still sealed, there is little danger of contaminating the sample solution. No failures have occurred with runs up to 425°C and pressures of approximately 6,000 psi.

Obtaining complete decomposition is a major problem in the analysis of refractory minerals. Nearly all such minerals can be decomposed by acids at high temperatures. Such decompositions are performed best in bombs capable of withstanding not only high temperatures and pressures but also the corrosive effects of acids. Bombs suitable for these decompositions should have acid-resistant liners such as platinum or Teflon. Platinum is preferred to Teflon because it can be used at temperatures higher than the maximum of about 260°C possible with Teflon.

The platinum-lined bomb shown on figure 1 has been used by us for the decomposition with hydrofluoric acid and hydrofluoric plus sulfuric acids of small mineral samples for semimicroanalysis. The bomb is similar in some respects to one used by Von Schloemer (1962) and consists of a removable reaction vessel which is inserted into a Morey-type bomb.

A novel feature is the construction of the reaction vessel, which is a platinum-lined Nichrome crucible having an outside taper for facilitating its removal from the bomb body. The crucible can be weighed conveniently on an analytical balance before and after a run. As the crucible can be removed from the bomb without breaking the platinum seal there is little danger of contaminating the sample solution during transfer of the solution from the crucible.

The body of the crucible, made of Nichrome, protects the platinum liner from mechanical damage during in-

sertion and removal from the bomb body, made of Hasteloy, and from chemical contamination by the Hasteloy.

Removal of the crucible at the termination of a run is aided not only by its taper but also by the projection of the crucible through a hole in the bottom of the

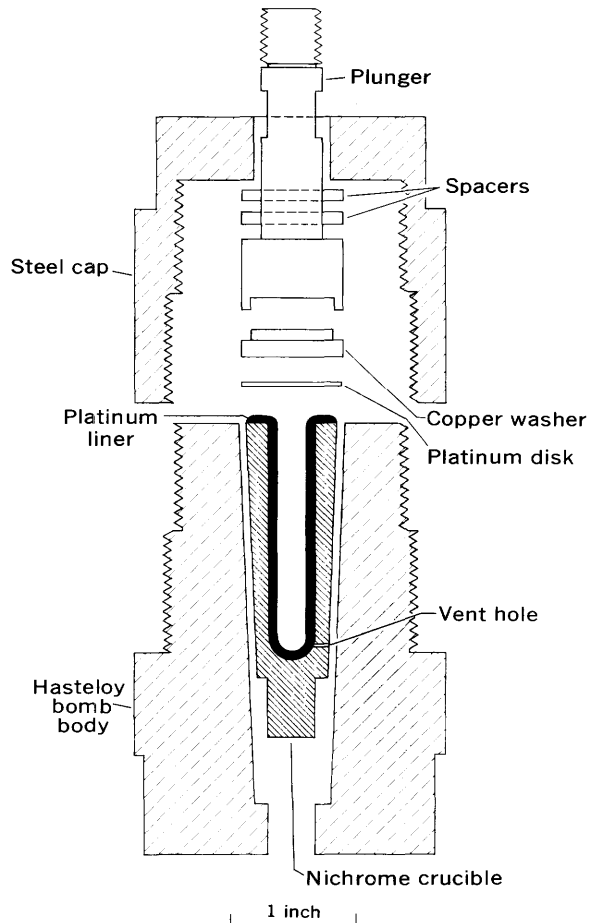


FIGURE 1.—Section through platinum-lined Morey-type bomb for high-temperature decomposition of refractory minerals.

Hasteloy body. This enables the direct application of pressure with a press for releasing the crucible.

The volume of the crucible is $3\frac{1}{2}$ milliliters, which permits the use of sample weights of as much as 100 milligrams and acid volumes of 1 to 2 ml. Temperatures as high as 425°C have been used for bomb runs with pressures estimated as high as 6,000 pounds per square inch. Pressures were estimated from the temperature and degree of filling, using Bridgman's tables.

The bomb has proven to be very reliable. No failures of the bomb nor of the platinum liner have occurred after 35 runs for periods of 16 to 24 hours each with a variety of oxide and silicate minerals.

Sealing the crucible is effected by the pressure exerted by tightening the cap against the plunger. The plunger is pushed against an annealed copper washer which transmits the thrust to the platinum sealing disk.

The body of the bomb is made of Hasteloy-C and is cylindrical except for two flat surfaces which enable its being held in a vise for sealing and opening of the bomb. The main bore has a taper of $1\frac{1}{2}^{\circ}$ included angle. Two threaded diameters (eight threads per inch) provides a doubling of thread with a given travel of the cap (Morey and Hesselgesser, 1952).

The cap, which is made of No. 4140 steel, is threaded to make a loose fit with the body. The top of the cap is cut to a $2\frac{3}{16}$ -inch hexagonal nut.

Pure platinum was used in the original liner because a massive piece was available in the laboratory. A 20-percent iridium alloy of platinum is more resistant to deformation and was used in a newly constructed crucible. The wall of the liner is $\frac{1}{16}$ inch thick, the lip is $\frac{3}{16}$ in deep, and the outside diameter of the liner is $\frac{33}{64}$ inch. The weight of the platinum is approximately 65 grams.

The inside bore of the Nichrome crucible is straight sided with a rounded bottom to make a press fit with the platinum liner. The outside diameter is tapered to match the bomb body; a shoulder on the base of the crucible makes contact with the inside shoulder of the bomb

cavity. The base of the crucible protrudes $\frac{1}{10}$ inch from the bottom of the bomb. Prior to insertion of the liner, a vent hole is drilled with a No. 80 drill through one side of the Nichrome crucible near the bottom. The vent releases air and moisture entrapped between the platinum and nichrome, thereby preventing deformation of the liner.

The plunger, made of No. 304 stainless steel, fits freely in the bomb body and is counterbored at the bottom to hold a copper washer. Near the top of the plunger are two parallel flat surfaces for easy manipulation of the plunger with a wrench. The top of the plunger is threaded for a nut which is used when necessary for extracting the plunger by turning the nut against a short piece of tubing inserted over the plunger between the cap and the nut.

The copper washer is made of oxygen-free copper and the platinum disk, 0.006 inch thick, of pure platinum. Loose-fitting stainless-steel spacers are used as required.

Before making a run, the lip of the platinum liner, the lower surface of the copper washer, and the upper surface of the platinum disk are coated with Aquadag to prevent the metal surfaces from sticking together. After a run, the bomb is permitted to cool to room temperature and the cap is removed with a wrench. The crucible is freed by setting the bomb body in a hydraulic press and gently exerting pressure until the crucible is released. The platinum disk sealing the crucible can usually be removed cleanly with gentle prying. The crucible, when being handled outside the bomb, is supported conveniently in a lightweight circular aluminum holder with a center bore to fit the lower portion of the crucible.

REFERENCES

- Morey, G. W., and Hesselgesser, J. M., 1952, The system $\text{H}_2\text{O}-\text{Na}_2\text{O}-\text{SiO}_2$ at 400°C : *Am. Jour. Sci.*, Bowen volume, p. 346.
Von Schloemer, H., 1962, Hydrothermal-synthetische gemeinsame Kristallisation von Orthoklas und Quarz: *Radex-Rundschau*, v. 3, p. 133-156.



RAPID FIELD AND LABORATORY DETERMINATION OF PHOSPHATE IN NATURAL WATER

By MARVIN J. FISHMAN and MARVIN W. SKOUGSTAD,
Denver, Colo.

Abstract.—This method is based on the formation and reduction of phosphomolybdic acid by using a single-solution reagent prepared immediately before use by dissolving a measured amount of a mixture of dry chemicals consisting of ammonium molybdate, ascorbic acid, and antimonyl potassium tartrate in dilute sulfuric acid. In the presence of phosphate an intense blue color with maximum absorbance at 882 $m\mu$ develops within 10 minutes after addition of the reagent solution. Results are accurate to $\pm 1 \mu\text{g PO}_4$.

Soluble phosphate in water is usually determined quantitatively by a phosphomolybdate or "molybdenum blue" method based on the formation of phosphomolybdic acid, which, upon reduction, produces an intensely colored blue complex (Rainwater and Thatcher, 1960). Although a solution of stannous chloride is commonly used as the reductant, its use does have several limitations and disadvantages, not the least of which are the instability of the reagent, the slow rate of color development, and the instability of the resulting color complex.

Ascorbic acid has been proposed as a preferred reducing agent (Harvey, 1948; Murphy and Riley, 1958). Even though its use provides several advantages, it has not been widely adopted, primarily because of the very slow rate of reduction and color development. More recently, Murphy and Riley (1962) described an improved procedure based on their observation that the presence of added antimony results in rapid reduction of phosphomolybdic acid. Their procedure is extremely simple, involving only the addition of a measured amount of a single-solution reagent to an aliquot of the test sample and, after 10 minutes, determining the absorbance of the intense blue-purple complex at 882 $m\mu$. The reagent is prepared by dissolving appropriate amounts of ammonium molybdate, ascorbic acid, and

potassium antimonyl tartrate in dilute sulfuric acid. This reagent solution is unstable and must be used within 24 hours.

The Murphy and Riley procedure offers several distinct advantages over methods using stannous chloride as the reductant. The authors of this paper felt that the inconvenience of preparing the reagent solution for each analysis could be overcome by a simple modification of the procedure. Moreover, the method appeared to be sufficiently simple and sensitive to be useful as a field method, when only a minimum amount of equipment is available. Thus, this paper describes a simplification of the Murphy and Riley procedure, and adapts their procedure to the field determination of phosphate in natural water samples, through the preparation of a set of permanent color standards against which test samples may be compared.

To avoid the inconvenience of preparing the single-solution reagent fresh for each set of analyses, the dry reagents, ammonium molybdate, ascorbic acid, and potassium antimonyl tartrate, are mixed in the proportions recommended by Murphy and Riley (1962). When an analysis or a series of analyses is to be made, an appropriate amount of the mixture of the dry reagents is dissolved in the required volume of dilute sulfuric acid. In actual practice, and for convenience in the field, dilute sulfuric acid is prepared in advance and stored in 100-ml bottles. The exact weight of the dry reagent mixture to be added to the dilute acid is not critical. It has been found that a small scoop which will repeatedly deliver between 0.8 and 1.2 g of the powder is satisfactory for preparation of the reagent solution. The concentration of phosphate ion in solution can be determined by using a spectrophotometer or, alternatively, by using (1) a colorimeter, or (2) visual color standards.

EQUIPMENT

Spectrophotometer, Beckman Model B (or equivalent)
 Wavelength: 882 m μ (or 700 m μ)
 Cells: 50-mm optical depth
 Phototube: Red-sensitive
 Blank: Dilution water plus reagents
 Initial sensitivity setting; 2
 Slit width: 0.10 mm (approx)

The following absorbances have been observed:

$\mu\text{g PO}_4$	Absorbance	
	882 m μ	700 m μ
0.0	0.00	0.00
12.5	.24	.18
25.0	.47	.35
37.5	.70	.52
50.0	.94	.70

Alternative 1

Colorimeter, Hach DR "Direct Reading" (or equivalent)

Filter: No. 2408 (Corning)
 Cells: 1-oz (French square) bottles

The following transmittances have been observed:

$\mu\text{g PO}_4$	Transmittance (percent)
0.0	100
12.5	86
25.0	74
37.5	62
50.0	53

Alternative 2

Visual color standards (the color complex is unstable and cannot be used for permanent color standards, but suitable stable dyes can be mixed to provide identical matching colors)

PROCEDURE

- Pipet a volume of sample containing less than 50.0 $\mu\text{g PO}_4$ (50.0 ml max) into a 100-ml beaker and adjust the volume to 50.0 ml.
- Prepare a blank and sufficient standards and adjust the volume of each to 50.0 ml.
- Add 10 ml phosphate reagent solution and mix.
- After about 10 minutes, determine phosphate in the samples and standards by one of the following methods:
 - Measure absorbance at 882 m μ , or 700 m μ .
 - Measure transmittance using colorimeter (Corning filter No. 2408).
 - Compare visually with permanent color standards.

CALCULATIONS

Spectrophotometer or colorimeter

- Determine $\mu\text{g PO}_4$ from a plot of absorbances or transmittances of standards.

$$2. \quad \text{ppm PO}_4 = \frac{1}{\text{density}} \times \frac{\mu\text{g PO}_4 \text{ in sample}}{\text{ml sample}}$$

$$\text{where density} = \frac{\text{grams of sample}}{\text{ml of sample}}$$

Report concentrations of PO_4 of <1.0 ppm to 2 decimal places, and of >1.0 ppm to 2 significant figures only.

Visual comparison

Determine ppm PO_4 by direct comparison with permanent color standards.

Report concentrations of PO_4 of <1.0 ppm to 1 decimal place, and of >1.0 ppm to 2 significant figures.

REAGENTS

Phosphate standard I, 1.00 ml=50 $\mu\text{g PO}_4$: Dissolve 71.6 mg KH_2PO_4 , dried overnight over H_2SO_4 , in demineralized water. Add 2-3 drops chloroform and dilute to 1,000 ml.

Phosphate standard II, 1.00 ml=1.0 $\mu\text{g PO}_4$: Dilute 20.0 ml phosphate standard I to 1,000 ml.

Phosphate reagent, powder: Mix thoroughly the following dry reagents: 6.0 g ammonium molybdate, 5.3 g ascorbic acid, and 0.14 g antimonyl potassium tartrate. This reagent is stable for 3 to 4 months.

Sulfuric acid, 2.5N: Add slowly, with constant stirring, 70 ml conc H_2SO_4 to about 800 ml demineralized water and dilute to 1 liter.

Phosphate reagent, solution: Dissolve 1 ± 0.2 g phosphate reagent powder in 100 ml 2.5N H_2SO_4 . The initial color will be blue. Allow to stand for about 15 minutes before using (pale yellow-green color). Prepare fresh daily.

Color standards: The preparation of permanent color standards is a trial-and-error procedure. "Castolite" transparent dyes of blue, green, and violet (The Castolite Company, Woodstock, Ill.), in proper proportions, are satisfactory for preparing an alcoholic mixture of concentrated dye of the proper shade. Permanent color standards to match the color of each phosphate standard (0.0, 0.2, 0.4, 0.6, 0.8, and 1.0 ppm PO_4) are conveniently prepared from the concentrated dye by dilution with ethyl alcohol in 1-oz (French square) bottles. Samples containing phosphate are then matched with the permanent color standards against a white background. Visual matching permits phosphate to be determined with an accuracy of ± 0.1 ppm.

DISCUSSION AND RESULTS

Quantitative preparation of the single-solution reagent from the powder is not necessary. Identical results are obtained using from 0.75 to 2.0 g of mixed powder to approximately 100 ml 2.5N H_2SO_4 .

It is not necessary to prepare a calibration curve each time phosphate is determined since the calibration curves are reproducible from day to day. The calibration curves obtained at 882 m μ are almost identical to the ones reported by Murphy and Riley (1962).

The accuracy of the method has been checked by analyzing 12 natural water samples containing 0.02 to 1.0 ppm PO_4 and comparing the results using the method of Rainwater and Thatcher (1960). The results agreed to ± 0.01 ppm (see accompanying table).

Replicate determinations are reproducible to ± 0.01 ppm.

The method is subject to the same interferences as reported by Rainwater and Thatcher (1960). These

Comparison of the accuracy of the proposed method and the method of Rainwater and Thatcher (1960)

Sample No.	Phosphate found (ppm)	
	Proposed method	Rainwater and Thatcher
1-----	0.17	0.17
2-----	.03	.04
	.04	-----
3-----	.17	.17
4-----	.93	.94
	.92	-----
5-----	.37	.39
	.36	-----
6-----	1.0	.98
7-----	.02	.02
8-----	.07	.07
	.07	-----
9-----	.04	.04
10-----	.04	.04
11-----	.02	.02
12-----	.07	.06

include barium, lead, mercury, and silver, all of which interfere by forming a precipitate; and silica, which itself forms a pale-blue color with the reagent. Nitrite interferes and must be oxidized to nitrate with hydrogen peroxide, and any residual chlorine must be removed by boiling.

REFERENCES

- Harvey, H. W., 1948, The estimation of phosphate and of total phosphorus in sea waters: *Jour. Marine Biol. Assoc. United Kingdom*, v. 27, p. 337.
- Murphy, J., and Riley, J. P., 1958, A single-solution method for the determination of soluble phosphate in sea water: *Jour. Marine Biol. Assoc. United Kingdom*, v. 37, p. 9.
- 1962, A modified single-solution method for the determination of phosphate in natural waters: *Anal. Chim. Acta*, v. 27, p. 31.
- Rainwater, F. H., and Thatcher, L. L., 1960, Methods for collection and analysis of water samples: U.S. Geol. Survey Water-Supply Paper 1454, p. 245.



LEACHABLE SILICA AND ALUMINA IN STREAMBED CLAYS

By EDWARD C. MALLORY, JR., Denver, Colo.

Abstract.—Partial dissolution of samples by boiling for 2.5 minutes in 0.5*N* NaOH gave approximate upper limits of leachable silica and alumina in 19 concentrates of streambed clays. Silica ranged from 0.8 to 19.2 and alumina from 0.5 to 5.9 weight percent of air-dried clays. These ranges seem to be caused primarily by climate and geology.

Amorphous materials commonly occur in rocks and soils (Patterson, 1962, p. 42; Aomine and Jackson, 1959, p. 210; Bates, 1960, p. 5; and Fieldes and others, 1952, p. 204–205), yet the literature contains little information on the content and geographic distribution of these materials in clay fractions of streambed sediments. This paper presents information helpful in placing approximate upper limits upon the variation of amorphous SiO₂ and amorphous Al₂O₃. The data were obtained in the course of a study of the mineralogy and exchange capacity of streambed sediments made under the supervision of V. C. Kennedy during 1961–63.

This study of the leachable components of streambed sediments involved 56 samples of sediment collected at 20 sites on 19 different streams ranging from the Juniata River at Newport, Pa., to the Mad River at Arcata, Calif. Figure 1 shows the locations and the drainage basins of these sites. Kennedy (1964) has described the clay mineralogy of streambed samples from the same sites.

From studies of differential dissolution in NaOH solution as a means of purifying clay, Hashimoto and Jackson (1960, p. 102–113) learned that by boiling the clay preparation in 0.5*N* NaOH solution for as little as 2.5 minutes, allophane and free alumina and silica could be dissolved and separated from the clay, provided the ratio of clay weight to solution volume was kept less than 100 milligrams to 100 milliliters. Some of their data are given in table 1.

The data suggest that either the two samples (kaolinite and montmorillonite) contained soluble amorphous silica and alumina or their constituents were selectively leached in the 0.5*N* NaOH solution.

TABLE 1.—Effect of boiling clay minerals in 0.5*N* NaOH for 2.5 minutes

[From Hashimoto and Jackson, 1960, p. 102–113]

	Kaolinite (Merck)	Montmorillonite (Upton, Wyo.)
Percentage SiO ₂ leached from sample	3.34	6.93
Percentage Al ₂ O ₃ leached from sample	.82	.29
Total percentage SiO ₂ in sample prior to leaching	43.1	58.7
Total percentage Al ₂ O ₃ in sample prior leaching	37.8	17.8
Ratio of SiO ₂ leached from sample to Al ₂ O ₃ leached from sample	¹ 4.1	¹ 23.9
Ratio of total SiO ₂ in sample prior to leaching to total Al ₂ O ₃ in sample prior to leaching	¹ 1.1	¹ 3.3

¹ Calculated by the author.

The samples of streambed sediment were prepared for study by first wet sieving them to separate the sand (0.062–1.0 mm) and the wet gravel (greater than 1.0 mm) fractions from clay and silt. Then the clay (less than 0.004 mm) and silt (0.004–0.062 mm) were separated by centrifugation and decantation.

The differential dissolution method of Hashimoto and Jackson (1960, p. 102–104) was used to separate the leachable silica and alumina materials from the clay fraction. By this method, 50-mg samples of air-dried clay were boiled for 2.5 minutes in 50 ml of 0.5*N* NaOH solution, and any soluble allophane and free alumina and silica present were separated from the nearly insoluble clay (table 2). Amounts of leachable silica

TABLE 2.—Results of repeat analyses of leachable silica and alumina in a single sample ¹

Analysis	Leachable silica (percentage of clay fraction)	Leachable alumina (percentage of clay fraction)
1	2.3	1.2
2	2.3	1.3
3	2.3	1.1
4	2.3	1.1
Mean values	2.3	1.2

¹ Each repeat analysis was made on a different day. Sample used was a well-mixed and lightly ground clay from the Juniata River at the Newport, Pa., sample site.

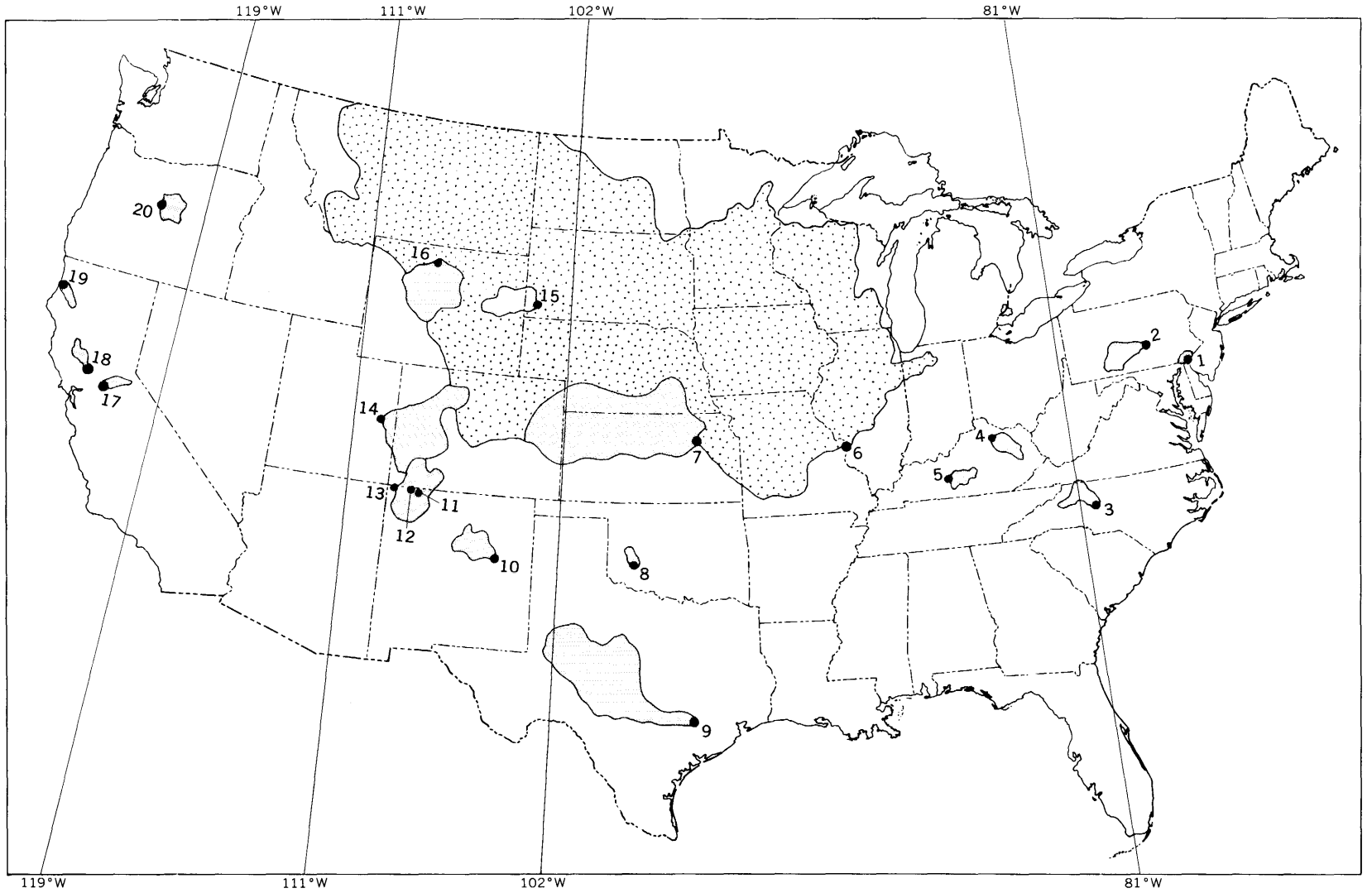


FIGURE 1.—Sediment-sampling sites used in study of silica and alumina. Information on sediment from these sites is given in table 3. Coarse stipple, the part of the Mississippi River basin referred to in this paper; fine stipple, other drainage basins referred to.

and alumina dissolved were than determined by the analytical method of Shapiro and Brannock (1956, p. 31-35). To avoid formation of an interfering precipitate at this stage of the determination, a 5-ml maximum aliquot of solution was used.

The precision of the method is good (see table 2).

Because gibbsite, small amounts of poorly crystalline material, and very fine grained clays are soluble in boiling 0.5*N* NaOH, leachable material reported in table 3 represents an upper limit of the truly amorphous material. All 56 samples studied were examined by X-ray diffraction, and only those from the Yadkin River, in North Carolina, contained gibbsite in detectable amounts.

The leachable silica content for all 56 samples averages 3.9 percent and ranges from 0.8 to 19.2 percent; the leachable alumina content averages 1.5 percent and ranges from 0.5 to 5.9 percent. The combined content of the two constituents averages 5.5 percent of sample composition and ranges from 1.9 to 20.6 percent. If the samples of streambed clay from the Crooked River, in Oregon, (No. 20 on fig. 1), which are unusually high in amorphous silica, are omitted from consideration, the data in table 3 can be summarized as follows: leachable

silica content of the clay fraction averages 3.2 percent; leachable alumina content averages 1.6 percent; the combined content of leachable silica and alumina averages 4.8 percent and ranges from 1.9 to 10.7 percent.

A general relation was noted between the amount of leachable material in streambed clays and Keller's ratios of rainfall to potential evaporation. Keller (1955, p. 67-72) showed that the intensity of weathering depends upon both precipitation and rate of evaporation of moisture; where the ratio of rainfall to evaporation is high, the degree of weathering also tends to be high. Generally, the highest content of leachable silica and alumina in streambed clays was found in streams east of long 81° W. (sites 1, 2, and 3), where the ratio of rainfall to evaporation ranges from 1.0 to 1.3 (Keller, 1955).

The next highest percentages were found in streambed clays between long 81° and 102° W. (sites 4-9), where the ratio of rainfall to evaporation ranges from 0.6 to 1.0. The lowest percentages were found between long 102° and 111° W. (sites 10-16) with ratios less than 0.6. Bed clays of streams west of long 119° W. (sites 17-20), where rainfall and evaporation vary greatly,

TABLE 3.—Amorphous silica and alumina content of streambed clays^{1 2}

Number on figure 1	Sampling site	Number of samples	Leachable silica (weight percent)		Leachable alumina (weight percent)		Total leachable silica and alumina (weight percent)	
			Average	Range	Average	Range	Average	Range
1.....	Brandywine Creek at Wilmington, Del.	5	5.5	4.8-7.0	2.8	2.6-3.1	8.3	7.4-10.1
2.....	Juniata River at Newport, Pa.....	6	4.7	2.1-8.9	1.1	.9-1.3	5.8	3.4-9.9
3.....	Yadkin River at Yadkin College, N.C.	4	4.1	3.7-4.8	5.1	4.6-5.9	9.2	8.3-10.7
4.....	Licking River at McKinneysburg, Ky.	4	2.2	2.0-2.4	1.3	1.2-1.4	3.5	3.3-3.8
5.....	Green River at Munfordville, Ky....	5	3.3	2.7-4.1	1.5	1.3-1.7	4.8	4.2-5.3
6.....	Mississippi River at St. Louis, Mo....	2	3.0	2.4-3.6	1.1	.8-1.4	4.1	3.2-5.0
7.....	Kansas River at Wamego, Kans.....	2	2.6	1.0-4.2	1.5	1.3-1.7	4.1	2.3-5.9
8.....	Elk Creek at Hobart, Okla.....	5	3.2	2.6-3.4	1.2	.8-1.5	4.4	3.4-5.0
9.....	Colorado River at Columbus, Tex....	3	3.4	2.4-5.3	.9	.8-1.0	4.3	3.4-6.2
10.....	Pecos River at Santa Rosa, N. Mex.	3	2.4	1.8-2.9	.9	.8-1.0	3.3	2.6-3.9
11.....	San Juan River at Bloomfield, N. Mex.	2	1.4	.8-1.9	1.0	.7-1.3	2.4	2.1-2.6
12.....	Animas River at Farmington, N. Mex.	1	1.9	1.9	.8	.8	2.7	2.8
13.....	San Juan River at Shiprock, N. Mex.	1	1.8	1.8	.8	.8	2.6	2.6
14.....	Colorado River near Cisco, Utah....	4	1.8	1.4-2.0	.6	.5-.7	2.4	1.9-2.7
15.....	Cheyenne River near Hot Springs, S. Dak.	1	1.7	1.7	.5	.5	2.2	2.2
16.....	Bighorn River at Kane, Wyo.....	1	1.8	1.8	.8	.8	2.6	2.6
17.....	Cosumnes River at McConnel, Calif.	1	3.7	3.7	2.0	2.0	5.7	5.7
18.....	Cache Creek at Yolo, Calif.....	1	2.0	2.0	.7	.7	2.7	2.7
19.....	Mad River near Arcata, Calif.....	2	3.2	1.1-5.4	1.0	.8-1.3	4.2	2.4-6.1
20.....	Crooked River near Post, Oreg.....	3	15.8	10.2-19.2	1.4	1.1-1.6	17.2	11.8-20.6

¹ In the Eastern United States, kaolinite, illite, and dioctahedral vermiculite (includes aluminous interlayered montmorillonite and (or) vermiculite) are the most common clay minerals in the stream sediments studied. West of the Mississippi River, montmorillonite, illite, and mixed-layer montmorillonite-illite are the major clay minerals in many of the streams studied. More detailed information

concerning clay minerals present in each of these streams can be obtained from Kennedy (1964, p. 99).

² Vermiculite is also present in many of the streams studied but commonly not in major amounts (Kennedy, oral communication, 1964).

range from less than average to above average in amount of leachable silica and alumina.

Soil studies reported in the literature also suggest a correlation between climate and amorphous material. Aomine and Jackson (1959) reported that soils developed on volcanic ash in Japan contained allophane. In a study of Hawaiian soils, Tamura and others (1953) found that soils in areas of highest rainfall contained considerable amounts of allophane. The Hawaiian soils were formed by the weathering of basalt and volcanic ash. Patterson (1962, p. 64) suggests the possibility of abundant amorphous material on the island of Maui in the Hawaiian Islands. Fieldes and others (1952, p. 205) found amorphous materials in several soils of the Cook Islands in the South Pacific. Studies by Whittig and others (1957, p. 226) indicate that soils of northwestern Oregon contain allophane. All the regions cited have a moist climate with moderate or warm temperatures.

Of the samples analyzed, streambed clays in Brandywine Creek and in the Juniata, Yadkin, Cosumnes, and Crooked Rivers (sites 1, 2, 3, 17, and 20 in table 3) contained the highest percentages of leachable silica and alumina. The first three of these rivers are in an area where the precipitation-evaporation ratio is at least 1.1, so a moderate to high degree of weathering is to be expected.

The Yadkin River clay, in North Carolina, had the highest percentage of leachable alumina. This river is in a warm humid area where gibbsite has been reported in soils (Alexander and others, 1941).

The greatest percentages of leachable silica were found in samples from the Crooked River, in Oregon, an area where intense chemical weathering would not be expected. In the part of the drainage basin above the sampling site, precipitation is approximately 10 inches a year, and the mean annual temperature is about 47°F (U.S. Weather Bureau, 1956, p. 37, 52). Streambed clays in this area, however, contain more than 17 percent of leachable material, most of it silica.

More intensive weathering may have occurred in this area at a previous time. Russell (1905, p. 34) states that "over nearly all of central Oregon, there is abundant evidence of greater precipitation and more active erosion immediately preceding the present period of aridity and weak streams."

The rocks of the area may also account for the high content of leachable silica found in samples from the Crooked River. Large deposits of volcanic tuff occur in this drainage basin (Russell, 1905) and may weather so as to form greater amounts of amorphous silica. Russell (1905, p. 19) also mentions the presence of opal grains at Opal Spring, located on the Crooked River

below the collection point. He believes that the opal is derived from the basaltic rock through which the springwater passes.

The Cosumnes River of California carries clay containing above-average amounts of leachable silica, despite the fact that it drains an area where intense chemical weathering would not be expected. The average annual precipitation of the lower part of the river basin ranges from 15 to 30 inches; that in the upper part of the basin ranges from 30 to 60 inches (Baker, 1936, p. 6). The area of greatest precipitation is at high altitude along the west slope of the Sierra Nevada, so lower temperatures would tend to decrease the degree of chemical weathering. However, in the lower part of its basin, the Cosumnes River drains an extensive area underlain by the Ione formation of Eocene age. The Ione consists of gravel, sand, clay, and lignite; the lower Ione is characterized by minerals that persist through intense weathering (Pask and Turner, 1952, p. 16-20). Allen (1929, p. 393, 403) concluded that a tropical or subtropical climate existed during Eocene time in California. Thus, although present-day conditions do not result in intense chemical weathering, above-average amounts of amorphous silica in the sediments of the Cosumnes may be accounted for by a previous cycle of intense weathering.

The data of this study suggest the following conclusions:

1. The amount of leachable silica and alumina in streambed clays is directly related to the degree of weathering induced by the climate. A warm moist climate hastens the process of chemical weathering and favors the formation of amorphous material and (or) gibbsite.

2. Source rocks may contribute anomalous amounts of leachable material in a region that does not presently have intense chemical weathering. Such rocks may have been weathered during a previous cycle when the climate was warm and moist.

REFERENCES

- Alexander, L. T., Hendricks, S. B., and Faust, G. T., 1941, Occurrence of gibbsite in some soil-forming materials: *Soil Sci. Soc. America Proc.*, v. 6, p. 52-57.
- Allen, V. T., 1929, The Ione formation of California: *California Univ. Pub., Geol. Sci. Bull.*, v. 18, no. 14, p. 374-448.
- Aomine, Shigenori, and Jackson, M. L., 1959, Allophane determination in ando soils by cation-exchange capacity delta value: *Soil Sci. Soc. America Proc.*, v. 23, p. 210-213.
- Baker, O. E., ed., 1936, Section on precipitation and humidity by J. B. Kincer U.S. Dept. Agriculture Atlas Am. Agriculture. 48 p.
- Bates, T. F., 1960, Rock weathering and clay formation in Hawaii: *Pennsylvania State Univ., Mineral Industries*, v. 29, no. 8, p. 1, 4-6.

- Fieldes, M., Swindale, L. D., and Richardson, J. P., 1952, Relation of colloidal hydrous oxides to the high cation-exchange capacity of some tropical soils of the Cook Islands: *Soil Sci.*, v. 74, p. 197-205.
- Hashimoto, Isao, and Jackson, M. L., 1960, Rapid dissolution of allophane and kaolinite-halloysite after dehydration, *in* Swineford, Ada, and Ingerson, Earl, eds., *Clays and clay minerals: Natl. Conf. Clays and Clay Minerals 7th*, Washington, October 20-23, 1958, *Proc., Earth Sci. Ser., Mon. 5*, p. 102-113; New York, Pergamon Press, 369 p.
- Jackson, M. L., 1959, Frequency distribution of clay minerals in major great soil groups as related to the factors of soil formation, *in* Swineford, Ada, and Ingerson, Earl, eds., *Clays and clay minerals: Natl. Conf. Clays and Clay Minerals 6th*, Berkeley, August 19-23, 1957, *Proc., Earth Sci. Ser., Mon. 2*, p. 133-143; New York, Pergamon Press, 411 p.
- Keller, W. D., 1955, *The principles of chemical weathering*: Columbia, Mo., Lucas Bros. Publishers, 88 p.
- Kennedy, V. C., 1964, Base-exchange capacity and clay mineralogy of some modern stream sediments: *Internat. Assoc. Sci. Hydrology, Comm. Subterranean Waters, Pub. 64*, p. 95-105.
- Pask, J. A., and Turner, M. D., 1952, *Geology and ceramic properties of the Ione formation, Buena Vista area, Amador County, California*: California Dept. Nat. Resources, Div. Mines, Spec. Rept. 19, 39 p.
- Patterson, S. H., 1962, Investigation of ferruginous bauxite deposits on Kauai and a reconnaissance of deposits on Maui: U.S. Geol. Survey open-file report, 336 p.
- Russell, I. C., 1905, *Geology and water resources of central Oregon*: U.S. Geol. Survey Bull. 252, 138 p.
- Shapiro, Leonard, and Brannock, W. W., 1956, Rapid analysis of silicate rocks: U.S. Geol. Survey Bull. 1036-C, p. 19-56.
- Tamura, T., Jackson, M. L., and Sherman, G. D., 1953, Mineral content of low humic, humic, and hydrol humic latosols of Hawaii: *Soil Sci. Soc. America Proc.*, v. 17, p. 343-346.
- U.S. Weather Bureau, 1956, *Climatic summary of the United States, Supplement for 1931 through 1952*: Washington, U.S. Govt. Printing Office, 79 p.
- Whittig, L. D., Kilmer, V. J., Roberts, R. C., and Cady, J. G., 1957, Characteristics and genesis of Cascade and Powell soils of northwestern Oregon: *Soil Sci. Soc. America Proc.*, v. 21, p. 226-232.



GROWTH OF SALT CEDAR (*TAMARIX GALLICA*) IN THE PECOS RIVER NEAR THE NEW MEXICO–TEXAS BOUNDARY

By R. U. GROZIER, San Angelo, Tex.

Abstract.—Increase in the area covered by the phreatophyte salt cedar (*Tamarix gallica*) in and along the Pecos River near the New Mexico–Texas boundary has been recorded by a series of photographs taken since 1916. Examples of the physical effects of this growth include a 35-percent reduction in channel conveyance, observed in the records of floods in August 1916 and June 1937, and a 15-percent reduction in cross section of channel from December 1932 to March 1963.

A series of photographs taken since 1916 provides striking evidence of channel changes in the Pecos River near the boundary between New Mexico and Texas. These changes have resulted from an increasing growth of salt cedar (*Tamarix gallica*) and from the deposition of silt in the channel and along the banks. Reduction in stream velocity due to ponding caused by the presence of vegetation in river bottoms is well known (Robinson, 1958, p. 28) as a cause of sedimentation in many streams in the Southwestern United States. Backwater from Red Bluff Reservoir extended into this reach of the river during several periods (June 1937 to June 1938, May 1941 to July 1943, and December 1943 to April 1944), and some siltation of the river channel probably occurred during these periods. However, conspicuous sedimentation of the river channel had been observed before completion of the reservoir early in 1937.

A stream-gaging station was maintained on the Pecos River near Angeles, Tex., from May 1914 to September 1937. A photograph taken in 1916 (fig. 1A), looking downstream from the gaging station, shows a wide channel with little vegetation. Under these conditions the flood of August 8, 1916, reached a peak discharge of 60,000 cubic feet per second at a stage of 22.5 feet.

A second photograph (fig. 1B) shows that by November 1936, before completion of the reservoir, the encroachment of salt cedar had reduced the channel appreciably. During the flood of June 1, 1937, the peak discharge, 38,900 cfs, required nearly the same stage (22.3 feet) as the flood in 1916, although the discharge

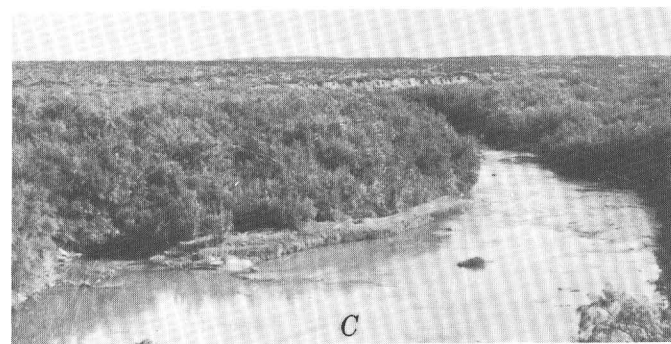
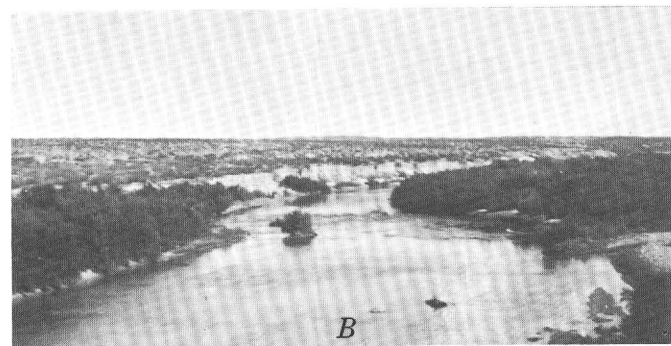
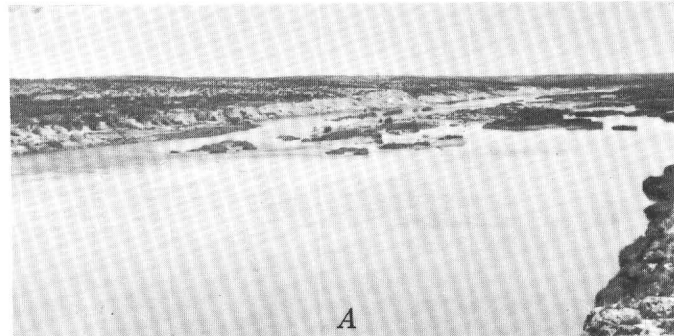


FIGURE 1.—Progressive growth of salt cedar in Pecos River channel downstream from a discontinued stream-gaging station, 8-4095 Pecos River near Angeles, Tex. Photographs taken from same vantage point: A, taken in 1916; B, in 1936; C, in 1961.

was 35 percent less than it had been in the flood 21 years earlier. This same period is reported ¹ to have been that in which the maximum rate of infestation by salt cedar occurred on the Pecos River.

A third photograph (fig. 1C), taken in October 1961, shows that growth of the salt cedar has continued to narrow the channel.

Further evidence of channel aggradation is shown by two channel cross sections (fig. 2). In 30 years the cross-sectional area at an 18-foot stage has been reduced from 6,360 to 5,380 square feet, or 15 percent. The proportional reduction of channel conveyance must have been even larger than this change suggests, because of plant growth on much of the new fill. During nonflood periods the water level is at about 3 to 4 feet at the location of the cross sections. Heavy salt cedar growth covers both banks above this stage. Photographs will be made at 5-year intervals to record channel changes.

¹ Salt Cedar Task Force for New Mexico, 1951, Report to the Salt Cedar Interagency Council: Report prepared for Salt Cedar Interagency Council (C. L. Forsling, U.S. Dept. Interior, chm.) for meeting in Albuquerque, N. Mex., July 21, 1950, p. 8.

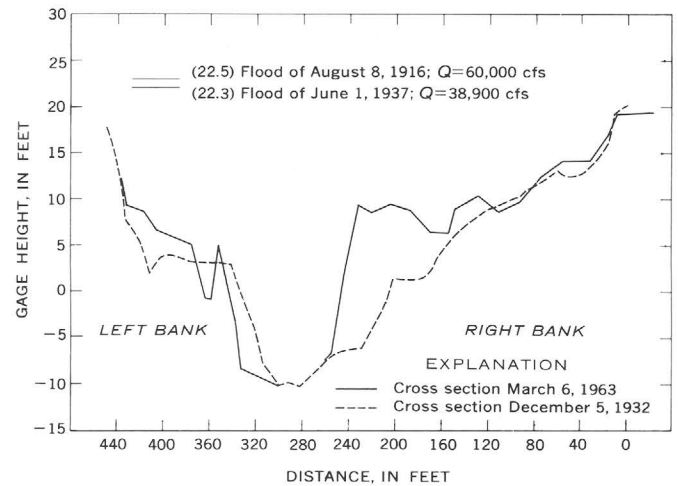


FIGURE 2.—Cross sections of Pecos River half a mile downstream from the stream-gaging station near Angeles, Tex.

REFERENCE

Robinson, T. W., 1958, Phreatophytes: U.S. Geol. Survey Water-Supply Paper 1423, 84 p.



EFFECT OF GREAT SWAMP, NEW JERSEY, ON STREAMFLOW DURING BASE-FLOW PERIODS

By E. G. MILLER, Trenton, N.J.

*Work done in cooperation with the U.S. Army Corps of Engineers
and the New Jersey Department of Conservation and Economic Development*

Abstract.—During periods of high evapotranspiration the surface drainage out of Great Swamp, N.J., is considerably less than the inflow to the swamp. Evapotranspiration from Great Swamp is believed to cause a significant reduction in yield during periods of base flow in most of the period of June through September.

Great Swamp, in the headwater part of the Passaic River basin in northern New Jersey, is one of numerous tracts of swampland which together are important in the hydrology of the basin (Vecchioli and others, 1962). Great Swamp consists of about 10 square miles of wetlands, but because of the need for ease of access to sites suitable for stream-discharge measurements the area herein termed Great Swamp is defined arbitrarily, for the purpose of this paper, as the 19 square miles within circumferential roads which encircle the swamp and some adjoining territory (fig. 1).

Vecchioli and others (1962) describe geologic and hydrologic conditions in the swamp. The regional ground-water body underlying Great Swamp is confined by relatively impermeable clay and silt beds which average about 60 feet in thickness. The artesian head in the aquifer is higher than the swamp level, indicating that the swamp is in an area of ground-water discharge. However, the quantity of water leaking upward into the swamp is estimated, on the basis of reasonable assumptions, to be only about 45,000 gallons per day (less than 0.1 cubic foot per second) in 10 square miles. Water in Great Swamp is at or near the land surface throughout most of the year, and the water table is relatively flat. Because of the slight hydraulic gradient and the low permeability of the shallow materials, lateral movement of ground water beneath the swamp is slow. Vecchioli and others (1962, p. 699–700) conclude that during the nongrowing season the storage capacity of

the shallow zone of saturation is exceeded and a considerable amount of water is ponded. At such times nearly all the precipitation that falls runs off. During the growing season, the surface of the swamp becomes dry except for the stream channels, and the water table falls to its lowest stage. Then, they postulate, much of the precipitation which falls on the swamp and some of the water stored in the swamp are dissipated by evapotranspiration.

This investigation was made, as a test of the hypothesis outlined above, by determining the effect of Great Swamp on the streamflow of the Passaic River near Millington, N.J., during periods of base flow (sustained or fair-weather flow) in the ice-free months when normal streamflow is comparatively low. Surface inflow to the swamp was measured at 36 sites near the circumferential roads on 7 different days when base flow prevailed. Measurements on Nov. 9, 1961, Apr. 20, 1962, and June 11, 1962, were made from 3 to 5 days after the preceding significant rainfall, and all the other measurements were made at least 12 days after. Surface outflow from the swamp was measured at the stream-gaging station on the Passaic River near Millington, N.J., above which the area of the basin is 55.4 square miles. For each of the 7 days the total inflow was subtracted from the total discharge from the basin at the gaging station; the difference represents the effect of the swamp on the flow of the river.

A summary of the measurements, presented in the accompanying table, compares inflow and outflow and gives the difference as the swamp contribution. On days when the outflow from the swamp was less than the inflow to the swamp, the swamp contribution is expressed as a negative value. The yield per square mile of Great Swamp is computed from the observed figures of inflow and outflow. To make the yield figures for

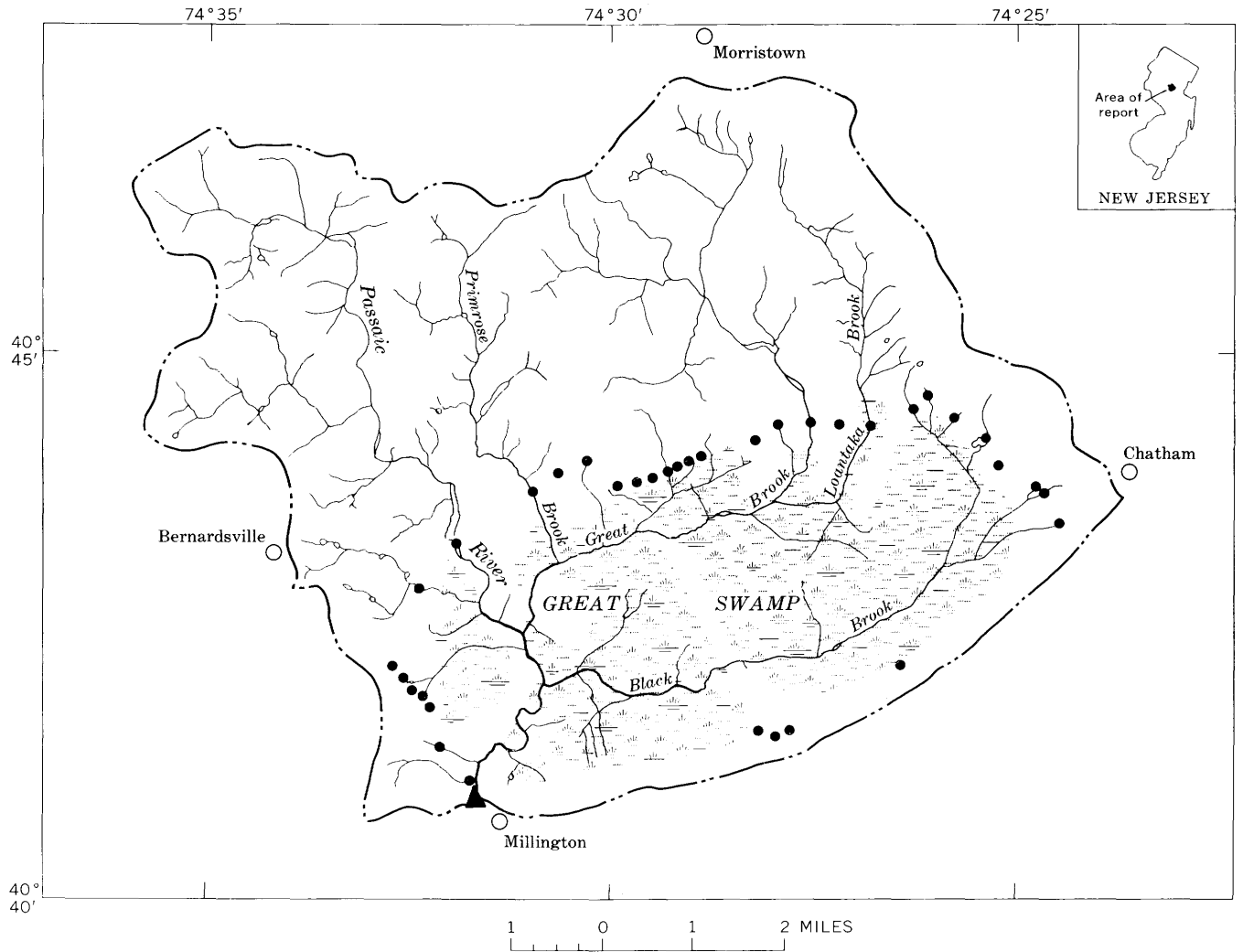


FIGURE 1.—Location of measurement sites at Great Swamp in the Passaic River basin, New Jersey. Dot, inflow measurement site; triangle, outflow measurement site.

Summary of measurements at Great Swamp, N.J.

Date	(1)	(2)	(3)	(4)	(5)	(6)	(7)	(8)	(9)
	Inflow (drainage area about 36 sq mi)			Outflow (drainage area 55.4 sq mi)			Swamp contribution (drainage area about 19 sq mi)		Ratio of swamp contribution to inflow
	Observed	Adjusted for diversion		Observed	Adjusted for diversion		(4)-(1)	cfs/sq mi	(8)/(3)
	cfs	cfs	cfs/sq mi	cfs	cfs	cfs/sq mi	cfs		
Sept. 12, 1961	5.4	6.9	0.19	4.1	5.6	0.10	-1.3	-0.07	-0.37
Nov. 9, 1961	6.7	8.1	.23	8.8	10.2	.18	2.1	.11	.48
Apr. 20, 1962	54	55.5	1.54	85	86.5	1.56	31	1.63	1.06
June 11, 1962	9.7	11.6	.32	9.2	11.1	.20	-.5	-.03	-.09
July 17, 1962	6.1	7.6	.21	1.9	3.4	.06	-4.2	-.22	-1.05
Oct. 23, 1962	10.7	12.9	.36	17	19.2	.35	6.3	.33	.92
Apr. 8, 1963	28.2	29.7	.83	47	48.5	.88	18.8	.99	1.19

the upstream area tributary to Great Swamp more suitable for comparison with those for Great Swamp, the inflow was adjusted for the net diversion of water for water supply from the main stream of the Passaic River immediately upstream from Great Swamp. The magnitude of the diversion, about 1.5 cfs, is the difference between columns 1 and 2 of the table.

The comparison of the yield per square mile of Great Swamp with the yield per square mile of the upstream area tributary to the swamp is shown as a ratio in column 9 of the table. These values show not only that the contribution of the swamp area to streamflow is variable, but that at times less water flows out of the swamp than had flowed into it. The values for the ratio of the swamp contribution to the inflow from the upstream drainage area, per square mile, range from a high of 1.19 in an April observation to a low of -1.05 in a July observation.

All the examples of diminution of streamflow through Great Swamp occurred during the period June–September, and it is reasonable to conclude that the high evapotranspiration during that season caused the reduction in base flow. Vecchioli and others (1962, p. 698) indicate that the net ground-water movement in the area is into the swamp. There is no significant use of water in the swamp area by man. The only remaining possible causes of water loss from the swamp, other than surface flow, are evaporation and transpiration. The nature of the swamp favors evapotranspiration. Water entering Great Swamp comes from rolling hills in well-defined channels, but in the swamp the water flows very slowly in response to low hydraulic gradients, and follows

meandering courses. Near the outlet of the swamp the water is virtually ponded in channels many times the size of the tributary streams, increasing the opportunity for evaporation. Moreover, Great Swamp supports a lush growth of aquatic plants and trees which must utilize large quantities of water. Finally, evaporation-pan data from Canoe Brook, N.J., about 10 miles northeast of Millington, indicate evaporation rates (for example, 0.06 to 0.28 inch per day during the period July 14–17, 1962) which, if assumed to be representative of the rates at Great Swamp, can account for the observed losses.

The measurements made in October, November, and April suggest that during the periods characterized by low evapotranspiration and by base flow, the swamp contribution per square mile may equal or even exceed the yield per square mile of the upstream region. This condition is a logical consequence of the fact that the swamp is an area of discharge for the regional ground-water body, whereas at least portions of the upstream part of the basin are areas of recharge. Thus, during periods when evapotranspiration may be neglected and when the surface-storage space in the swamp is full, the yield of Great Swamp is the precipitation plus the ground-water discharge, whereas the yield of the upstream region is the precipitation less the ground-water recharge.

REFERENCE

- Vecchioli, John, Gill, H. E., and Lang, S. M., 1962, Hydrologic role of the Great Swamp and other marshland in upper Passaic River basin: *Jour. Am. Water Works Assoc.*, v. 54, no. 6, p. 695–701.



SHORTENING AND PROTRUSION OF A WELL CASING DUE TO COMPACTION OF SEDIMENTS IN A SUBSIDING AREA IN CALIFORNIA

By J. F. POLAND and R. L. IRELAND,
Sacramento, Calif.

Abstract.—Compaction of sediments and shortening and protrusion of a heavy oil-test casing have been measured since 1962 at Westhaven in western Fresno County. Results indicate that in subsiding areas, tops of well casings are not stable bench marks, and that increased protrusion of casings is not a measure of land subsidence.

The Los Banos-Kettleman City area in the San Joaquin Valley, central California, is the most rapidly subsiding area in the United States at the present time (1964). Maximum subsidence to 1963 has been 23 feet, and the present maximum rate is 1.4 feet per year. The subsidence, which occurs over about 1,200 square miles, mostly in western Fresno County, is due chiefly to decline of artesian head and the resulting compaction of the sediments in a confined aquifer system.

In connection with its studies of land subsidence and the mechanics of aquifer systems in changing hydrologic environments, the U.S. Geological Survey in 1958 was afforded the opportunity of converting an abandoned oil-test hole into a dual water-level observation well in order to determine the artesian-head relations near the top and the base of the confined aquifer system. The well is at Westhaven, in the southern part of the Los Banos-Kettleman City area. In addition to furnishing critical information on the artesian head, the installation has also furnished data on compaction of the sediments and the vertical compression (shortening) of the oil-well casing in response to the compaction. This paper describes shortening of the casing and the implications of the shortening.

Shortening of well casings is common in areas subsiding because of fluid-pressure reduction and compaction of sediments. For example, in the Los Banos-Kettleman City area many hundreds of water wells have failed because of casing rupture due to vertical compression. Many casing breaks are repaired each year after photographs have been taken in the well cas-

ing to show the depth and nature of the breaks. Also, at the Wilmington oil field in Los Angeles County, Calif., where maximum subsidence of 27 feet had occurred by 1962, shortening of many oil-well casings as a result of compaction of the oil-producing zones has been measured by local operators. Casing-collar logs have been run periodically to determine changes in casing-joint lengths since the wells were first completed. Casing shortening of as much as 17 feet in a single well has been measured. Thus, the casing shortening reported in this paper is not unique. However, the scope of quantitative information on the rate and amount of casing shortening, casing protrusion, and compaction of the sediments, in relation to approximate land subsidence, is unique and provides evidence for certain specific conclusions.

The writers wish to acknowledge the cooperation of the Texas Co., of the California Division of Oil and Gas, and of Mr. D. A. Patterson, Manager of the Boston Ranch Co., in making this oil-test hole available for conversion to an observation well.

INSTALLATION AND MEASUREMENTS

When the oil-test hole was drilled by the Texas Co. in 1957, a surface string of 11¾-inch casing weighing 54 pounds per foot and having a wall thickness of about 0.44 inch was installed from land surface to a depth of 2,004 feet. Cement was pumped into the annular space around the casing from the bottom shoe to land surface, providing a continuous seal to prevent contamination of the fresh ground water. On abandonment of the oil test, the operator placed a cement plug beneath and in the lower part of the 11¾-inch casing, extending up to a depth of 1,930 feet.

The U.S. Geological Survey converted the blank casing to a dual water-level observation well in April 1958. As is shown on figure 1, the 11¾-inch casing was gun-

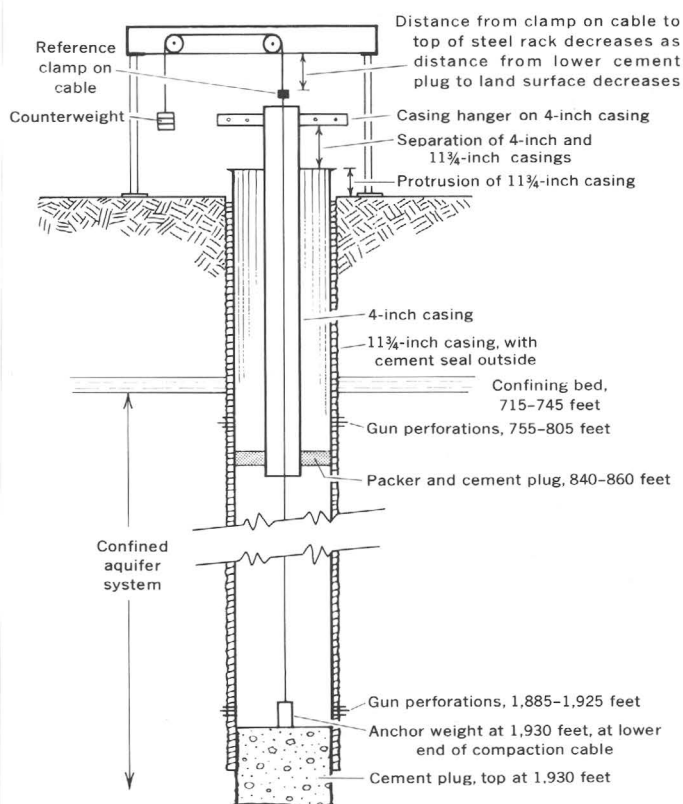


FIGURE 1.—Diagram of dual water-level observation well and equipment for measuring compaction of sediments and casing shortening, Westhaven, Calif. Not to scale. Depths are in feet below the land surface.

perforated at two depth intervals, 755 to 805 feet and 1,885 to 1,925 feet below the land surface. Four-inch standard screw pipe having a snug-fitting steel and composition packer flange at its base was then run into the 1 1/4-inch casing to a depth of 860 feet. The 4-inch pipe was suspended by a casing hanger resting on the top of the 1 1/4-inch pipe. A cement plug then was placed between the 4-inch and 1 1/4-inch casings in the depth interval between 840 and 860 feet to produce hydraulic separation of the two perforated intervals, both of which then were developed by means of air lift.

Soon after the 4-inch casing was installed, the junior author noticed that its hanger appeared to be rising off the top of the 1 1/4-inch casing, indicating shortening of the 1 1/4-inch casing between land surface and the 850-foot depth where the two casings are bonded by the cement seal. The progressive separation was measured monthly, and by August 1962, 4 1/4 years after the 4-inch casing was installed, it totalled 1.35 feet. At that time a device for measuring compaction was installed as follows: An anchor weight was lowered inside the 4-inch casing until it came to rest on the cement plug at 1,930 feet; the cable used for lowering the weight was passed over two pulleys supported on a steel rack at the land

surface, and a counterweight was attached to the end of the cable (fig. 1). This installation is similar to the compaction-measuring equipment described by Lofgren (1961, p. 49), except that land-surface movement relative to the reference clamp on the cable is measured at monthly intervals instead of continuously. It provides a measure of the total compaction or shortening of the interval between the cement plug at 1,930 feet and the land surface. Also, beginning in February 1963, protrusion of the top of the 1 1/4-inch casing above the land surface was measured. Increased protrusion represents the part of the compaction that did not result in shortening of the casing. Figure 2 illustrates the upper part of the compaction-measuring device, and the vertical separation between the two casings.

RESULTS

The measurements of progressive separation of the tops of the casings, of the shortening of the distance between the land surface and the cement plug at 1,930 feet, and of the increased protrusion of the 1 1/4-inch casing furnished the evidence for plotting the total shortening of the 1 1/4-inch casing to 1,930 feet and the shortening occurring above and below the 850-foot cement plug, as shown on figure 3.

From August 1962 to April 1964, the shortening of the distance between the land surface and the cement plug at 1,930 feet was 1.09 feet. The total shortening of the 1 1/4-inch casing and its cement jacket from the top to a depth of 1,930 feet was 1.04 feet (1.09 feet minus the casing protrusion of about 0.05 foot). The casing shortening from the top to a depth of 850 feet was 0.49 foot (measured casing separation). The shortening between depths of 850 and 1,930 feet was 0.55 foot (1.04 feet minus 0.49 foot) (fig. 3).

If it is assumed that the cement plug at 1,930 feet maintained a constant position with respect to the contiguous sediments, which seems reasonable in view of their structural bonding below the bottom of the 1 1/4-inch casing, the 1.09 feet of shortening between the land surface and the cement plug represents measured compaction of the sediments to a depth of 1,930 feet. Thus, during the 21-month period, the 1 1/4-inch casing and its cement jacket were shortened 1.04 feet in response to 1.09 feet of compaction of the surrounding sediments—that is, the casing shortening was equal to 95 percent of the compaction.

In the same time period, land subsidence, extrapolated from relevelings of nearby bench marks by the U.S. Coast and Geodetic Survey in December 1959 and March 1963, was 1.2 feet. If this extrapolated figure is correct, about 0.1 foot of compaction occurred below a depth of 1,930 feet. This amount of compaction seems

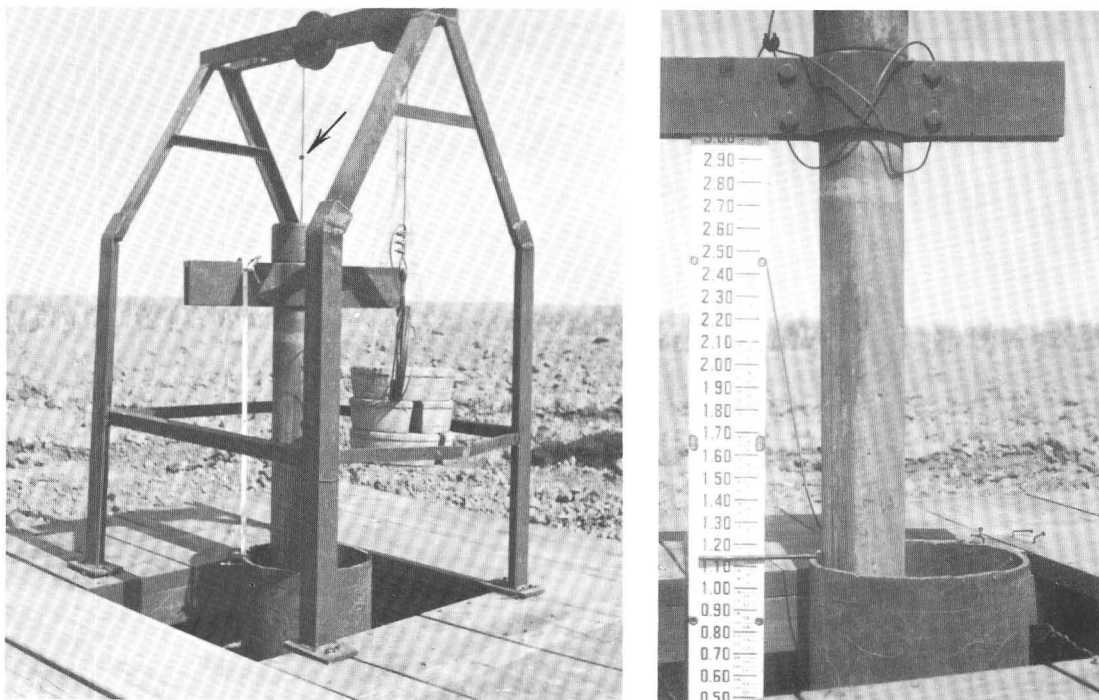


FIGURE 2.—Compaction-measuring device at well near Westhaven, Calif. *Left*, Upper part of compaction-measuring device; arrow marks reference clamp on cable. *Right*, Closeup view of casing separation; the scale shows the relative vertical movement between the top of the 1 1/4-inch casing and the bottom of the hanger on the 4-inch casing. From April 1958 to the time when the photograph was taken, June 3, 1964, the casing hanger on the 4-inch casing rose 1.85 feet above the top of the 1 1/4-inch casing.

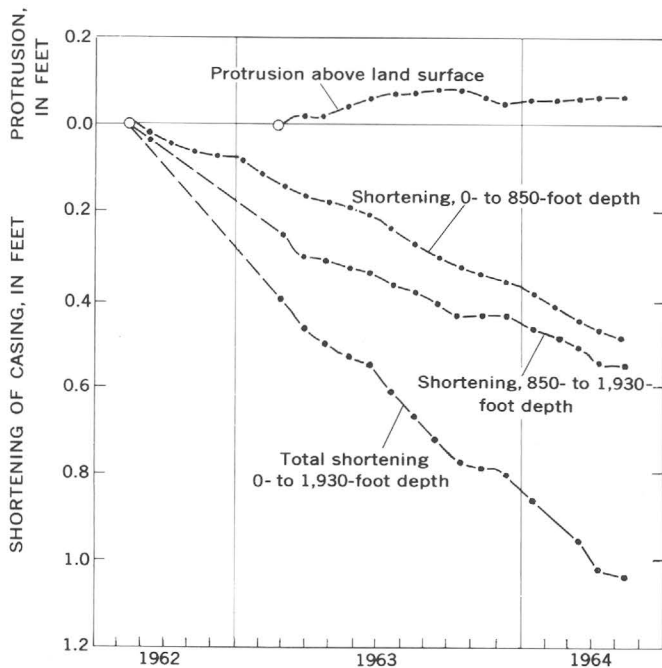


FIGURE 3.—Shortening and protrusion of 1 1/4-inch casing at Westhaven, Calif. Each dot on the plots represents an exact measurement. No dots are shown on the lower two plots from August 1962 to February 1963 because exact readings are not available for intermediate control.

reasonable in view of the fact that a few nearby water wells tap the confined aquifer system to depths as great as 2,100 feet, or 200 feet deeper than the cement plug at 1,930 feet. However, these extrapolated values for land subsidence do not affect the figures for casing shortening, which are absolute values.

CONCLUSIONS

The observations at this site indicate that even heavy oil-well casing encased in a cement jacket is too weak to resist the compressional force of the compacting sediments and is being shortened virtually in accord with the compaction. Therefore, it is concluded that in an area subsiding because of sediment compaction due to decrease in fluid pressure, the top of a well casing is not a stable reference bench mark even though the casing may extend beneath the compacting sediments.

Increased protrusion of a casing above the land surface in such a subsiding area should not be considered a reliable measure of compaction or of land subsidence. The increased protrusion of the casing at Westhaven is only about 5 percent of the compaction. On the other hand, in at least one subsiding area, Mexico City, the observed protrusion of some well casings has been approximately equal to compaction and subsidence. Here,

well casings have protruded as much as 18 feet in response to subsidence of about the same magnitude (R. J. Marsal, written communication, August 1956), showing that under favorable physical conditions, the skin friction between the compacting sediments and the well casing may not be sufficient to overcome the compressive strength of the casing. Thus, although the increased protrusion of a well casing above the land surface is evidence both for compaction of deposits within the well depth and for land subsidence, the magnitude of the protrusion affords only a minimum value that may range from only a few percent to approximately 100 percent of the subsidence.

Some of the factors influencing the response of a well casing to compacting forces in such a subsiding area are:

1. The casing depth compared to the depth range of the compacting zone.
2. The strength of the casing to resist vertical compression.
3. The magnitude of the skin friction between the compacting sediments and the well casing, which is determined in part by the type of well construction, the depth of the compacting zone, and the lithology of the compacting sediments.

The last two factors are of major influence in determining the relation of shortening to protrusion.

REFERENCE

- Lofgren, B. E., 1961, Measurement of compaction of aquifer systems in areas of land subsidence: Art. 24 in U.S. Geol. Survey Prof. Paper 424-B, p. B49-B52.



USE OF SODIUM IODIDE TO TRACE UNDERGROUND WATER CIRCULATION IN THE HOT SPRINGS AND GEYSERS OF THE DAISY GEYSER GROUP, YELLOWSTONE NATIONAL PARK

By J. J. ROWE, R. O. FOURNIER,
and G. W. MOREY, Washington, D.C.

Abstract.—Sodium iodide was found to be a suitable tracer in studies of water circulation in underground hot springs and geyser conduits. Subterranean interconnections linking certain hot springs and geysers were proved, and an underground reservoir containing at least 70,000 gallons of water is calculated to be present beneath the geyser group investigated. Water probably flows into and out of this reservoir at a rate of about 90 gallons per minute. Most of the discharge from the reservoir occurs below the surface, with only 10 to 15 gpm observed at the surface.

The interrelation of associated geysers, pools, and hot springs in Yellowstone National Park, Wyo., was investigated as a part of the study of the geochemistry of thermal waters in the park. Underground connections have been inferred in the past from observations of the reciprocal behavior of geysers, pools, and hot springs (Marler, 1951). Chemical tracers provide a means for proving the existence of underground connections and for determining the approximate volume of water involved in a particular system.

Ideally, a tracer suitable for studies of water movement in subterranean hot-spring conduits should fulfill the following requirements: (1) Minute quantities of the tracer should be detectable, preferably, by simple, quick analytical procedures capable of being used in the field. (2) The natural water being studied should initially not contain the tracer in quantities large enough to mask small additions from a source outside the system. (3) Once introduced, the tracer should not be removed from the water by adsorption or ion exchange with solids with which it may come into contact, or by precipitation due to chemical processes, or by decomposition. (4) The tracer should be cheap, easily obtainable, and should present no health hazard to any form of life. (5) The tracer should go into solution rapidly.

Organic dyes such as fluorescein and rhodamine B have been used in qualitative and quantitative studies of water movement (Japanese Government Agencies, 1958; Moon and others, 1957; Carpenter, 1960). However, the dyes tend to be markedly adsorbed by clays

and silica (Eugene S. Simpson, written communication, April 21, 1960), or they may decompose after being exposed for moderate lengths of time to high temperature underground.

Many stable isotopes make excellent tracers in natural waters, but they are generally expensive and require a mass spectrometer for analysis. Radioactive isotopes offer ease of recognition and analysis in the field. However, they, too, are expensive, and they constitute a potential health hazard.

It seemed likely that iodide as sodium iodide might be an effective tracer in the hot-spring waters of Yellowstone, for the following reasons: (1) Iodide is initially absent or present in only trace amounts in the waters. (2) As little as 0.1 part per million of iodide may be detected by analytical procedures which can be used in the field. (3) Because the waters contain a high content of chloride (303 ppm) and sodium (404 ppm), we can assume that iodide will not be removed by adsorption or ion exchange. (4) Sodium iodide is relatively inexpensive and presents no health hazards. (5) Sodium iodide is very soluble in water.

A test of the applicability of iodide as a tracer in hot-spring conduits was made in Yellowstone National Park at the Daisy group of geysers and hot springs during a period when none of the large geysers was active. The Daisy group consists of Comet, Splendid, and Daisy Geysers, Bonita and Brilliant Pools, a small unnamed geyser 40 feet south of Splendid, and two small pools near Splendid. These units are closely spaced within an area of 40 by 150 feet (fig. 1). The water in all the pools is boiling (about 92°C). Interconnections between most of these springs and geysers had previously been inferred by Marler (1951), who noted reciprocal behavior, as for example, simultaneous rise and fall of water levels and sympathetic geyser eruptions among members of the group.

Seven pounds of NaI was added to Splendid Geyser, and the iodide content of water in this geyser and adja-

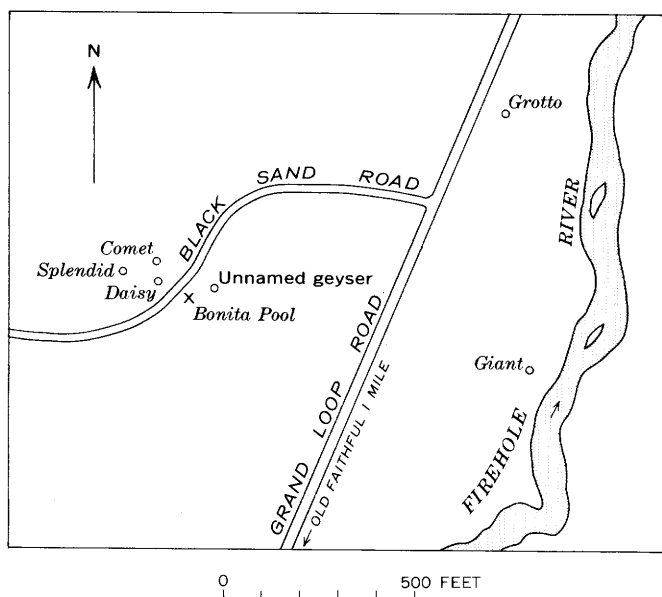
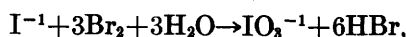


FIGURE 1.—Sketch map showing position of hot springs (x) and geysers (circle) of the Daisy geyser group and some nearby geysers.

cent pools and geysers was measured at intervals as shown in the accompanying table. A colorimetric method of analysis was used, utilizing a Lumetron photoelectric colorimeter, modified to operate in the field on a 12-volt automobile battery. Iodide was oxidized to iodate by bromine water,



after which excess bromine was either boiled out or neutralized with phenol. The iodate formed was then reacted with KI to produce six atoms of iodine for each atom of iodide originally present:



The iodine thus formed was measured by using either the blue color developed with starch (Rainwater and Thatcher, 1960, p. 181) or the violet color developed by extracting the iodine into carbon tetrachloride (Ovenston and Reece, 1951). The starch method was found to be more sensitive to small traces of iodide, but the color developed in the carbon tetrachloride was more stable than the color developed with starch. The carbon tetrachloride method is considered preferable for use in the field. These methods of analysis, though adequate, are not as simple nor as rapid as one would desire.

The iodide content of Bonita Pool before the addition of NaI to the system was 4 parts per billion, determined by Dr. W. B. Lyon, of the Oak Ridge National Laboratory, using the neutron-activation method. Such a small concentration of iodide could not be detected in the field.

Measured concentration of "tracer" iodide in hot springs and geysers after various lengths of time

Hot spring or geyser	Elapsed time after addition of iodide to Splendid Geyser	Measured concentration of iodide, in parts per million
Splendid Geyser	Before addition.	None detected.
	5 min	150
	1 hr 21 min	10.5
	2 hr 47 min	9.5
Bonita Pool	29 hr 8 min	1.0
	Before addition.	None detected.
	10 min	1.1
	25 min	1.1
Comet Geyser	1 hr 30 min	2.8
	2 hr 45 min	5.2
	29 hr 5 min	1.2
	50 min	7.4
Daisy Geyser	1 hr 3 min	.1
Geyser about 50 feet east of Bonita	40 min	0
	1 hr 33 min	0

The results of our iodide tracer measurements are shown in the accompanying table. All the geysers in the Daisy group had been dormant for several months prior to the time of the tracer study (Sept. 14–15, 1963), and they continued dormant during the course of the work reported here. However, an estimated 10 to 15 gallons per minute of water was continuously discharged from Bonita Pool and also an estimated 4 to 8 gpm from a small geyser about 50 feet east of Bonita.

The study showed that water in the surface pool at Splendid readily mixes with water underground and travels quickly to Bonita Pool, where some water is discharged from the system. The small geyser east of Bonita probably is not connected by shallow channels to the Daisy geyser group and may have no physical connection at all. The very small content of iodide (0.1 part per million) found in Daisy Geyser after about an hour indicates that, in the absence of an eruption, the water in the surficial pool of Daisy mixes slowly with water of Splendid's immediate system. On the other hand, 7.4 ppm iodide found in Comet Geyser after 50 minutes indicates that there is quick physical mixing with a relatively discrete body of water that also mixes readily with the water in the surficial pool of Splendid Geyser.

The volume of underground pools and reservoirs cannot be calculated with certainty from the results of this study. We must assume for this purpose that iodide adsorption and (or) ion exchange with underground solids was slight. There is no certainty that the added NaI ever became uniformly distributed in all the locally available underground water. Also, from the moment that the iodide was placed in the pool of Splendid, part of that iodide began to be carried away by the water circulating underground. Other thermal water was continuously added to the immediate reservoir from below to dilute the iodide locally. However, on the basis

of the relatively constant 10 ± 1 ppm iodide found in the pool of Splendid during the interval from 1 hour 21 minutes to 2 hours 47 minutes after addition of the tracer it is probable that a relatively discrete body of water of about 71,000 gallons is situated underground in the vicinity of, and directly connected with, Splendid Geyser. This same pool is more remotely connected to other members of the Daisy Geyser group.

It is known that the total amount of water ejected by Splendid Geyser during a single eruption lasting 10 minutes is approximately 30 to 40 thousand gallons (G. D. Marler, written communication, Oct. 31, 1962). Thus about half of the immediately available underground water may be ejected during an eruption of Splendid. Certainly all the water available to Splendid is not ejected during a major geyser eruption, because the water level in connecting pools such as Brilliant goes down, but the water is not completely drained.

In spite of the limitations imposed by unknown factors in the natural system and the dubiousness of certain assumptions, it is interesting and informative to write an equation of continuity for the circulation and dilution of the NaI placed in the water of the Daisy geyser group.

In the formulation of such an equation the following assumptions were made: (1) A reservoir exists beneath Splendid Geyser containing 71,000 gallons (268,000 liters) of water. (2) The 7 pounds of NaI (3,175 grams of NaI or 2,680 g of iodide) added to the water of the reservoir quickly dissolved, and thereafter the concentration of iodide remained uniform owing to convective stirring. (3) The only point of discharge from the system of water containing iodide was Bonita Pool, and an equal amount of iodide-free water continuously entered the reservoir from some underground source. The rate of flow of 10 gpm (37.85 l per min) is used in the calculation.

Let x be the number of grams of iodide in the reservoir at the end of t minutes. The concentration, C , is then

$$C = \frac{x}{268,000} \text{ g per l.}$$

In the time dt , $37.85 dt$ l of water came into the reservoir and $37.85 dt$ l of iodide solution was discharged from Bonita. Hence the change in the amount of iodide in the reservoir is

$$dx = -37.85 C dt = -\frac{37.85 x}{268,000} dt.$$

The amount of iodide in the reservoir expected to be

present after 29 hours (1,750 minutes) is then determined by

$$\int_{2,680}^x \frac{dx}{x} = -\frac{37.85}{268,000} \int_0^{1,750} dt,$$

and

$$\ln \frac{x}{2,680} = -0.247.$$

Solving for x yields a value of 2,094 g of iodide in 268,000 l of water, or about 7.8 ppm. However, the measured concentration after 29 hours was 1 ppm. Even if the overflow of Bonita Pool was underestimated by two-thirds (overflow 30 gpm rather than 10), the expected concentration of iodide in the reservoir after 29 hours would be about 4.8 ppm. In order to decrease the iodide concentration to 1 ppm in 29 hours a rate of movement of water through the system of about 90 gpm would be needed.

Admittedly, the above calculations are crude, and the assumptions upon which they are based are difficult to evaluate. The results are, however, compatible with the interpretation that most of the iodide has been lost from the system by underground circulation. Much of this iodide may have been discharged in the water flowing from pools and geysers outside the Daisy geyser group. On the basis of observations of apparent reciprocal behavior of Giant and Splendid Geysers in 1952, when both of these geysers were active, George D. Marler (written communication, Oct. 31, 1962) suggested that the Giant Geyser group (including Grotto Geyser) is connected to the Daisy geyser group. Thus, a good place to have looked for far-traveling iodide during the tracer study would have been Grotto Geyser, which is located about 1,100 feet N. 70° E. of Splendid Geyser, and which erupted several times during the course of the study.

REFERENCES

- Carpenter, J. H., 1960, Tracer for circulation and mixing in natural waters: Public Works, v. 91, p. 110-112.
- Japanese Government Agencies, 1958, Oceanographic research on waste disposal off the coast of Tokai-Mura: Internat. Conf. Peaceful Uses Atomic Energy, 2d, Geneva, Sept. 1958, Proc., v. 18, paper 1355, p. 404-409.
- Marler, G. D., 1951, Exchange of function as a cause of geyser irregularity: Am. Jour. Sci., v. 249, p. 329-342.
- Moon, F. W., Jr., Bretschneider, C. L., and Wood, D. W., 1957, A method for measuring eddy diffusion in coastal embayments: Inst. Marine Sci., v. 4, no. 2, p. 13-21.
- Ovenston, T. C. J., and Reece, W. T., 1951, Note on the spectrophotometric determination of iodine by extraction with organic solvents: Anal. Chim. Acta. v. 5, p. 123.
- Rainwater, F. H., and Thatcher, L. L., 1960, Methods for collection and analysis of water samples: U.S. Geol. Survey Water-Supply Paper 1454, 301 p.

THE ALGEBRA OF STREAM-ORDER NUMBERS

By ADRIAN E. SCHEIDEGGER, Urbana, Ill.

Abstract.—In studies of river morphology in which the concept of stream order is used, it is commonly assumed that where two rivers of order N join, they form a river of order $N+1$. No general rule is followed, however, for finding the order X of a stream formed by two rivers of different orders N and M . The order X can be computed according to the equation $X = \log_2(2^N + 2^M)$.

In many studies of the morphology of river systems, streams are classified on the basis of order, proceeding downstream from the headwaters. For example, first-order streams are those which (on a map of given scale) have no tributaries, and second-order streams are those which receive as tributaries only streams of the first order. Horton (1945), who developed the concept of stream order now widely used in the United States and who based a theory of similarity of river systems on stream order, considered that the main stream should be denoted by the same ordinal number all the way to its headwaters, and hence he renumbered one of the first-order streams (usually either the longest or the one which seems the most direct upstream continuation of the main stream) as second order. The procedure was then repeated with higher-order streams, so that the N th-order stream extends headward to the beginning

of the longest tributary. Thus, as a stream-order map was prepared, Horton renumbered one of the lower-order streams every time two channels of equal order joined one another. Strahler (1957) applied the term "order" only to channel segments. He assumed that two channel segments of order N which join form a channel of order $N+1$. Both Horton and Strahler ignored the junction of an N th-order channel with lower-order channels in assigning order numbers. Figure 1 illustrates the application of these stream-ordering systems to a hypothetical stream.

Rzhanitsyn (1964) expanded Horton's similarity theory. He (1964, p. 3-5) stated that the characteristics of each river reach depend on its order (the order signifying a stream that has definite physical characteristics), and on its position along the length of the stream, and that similarity conditions can be expressed that are specific for each order. To determine design equations for channel works, the characteristics pertaining to the various orders must be related to each other.

Rzhanitsyn (1964) followed a procedure similar to that of Horton and of Strahler, in assuming stream order to increase by 1 if a stream is joined by another

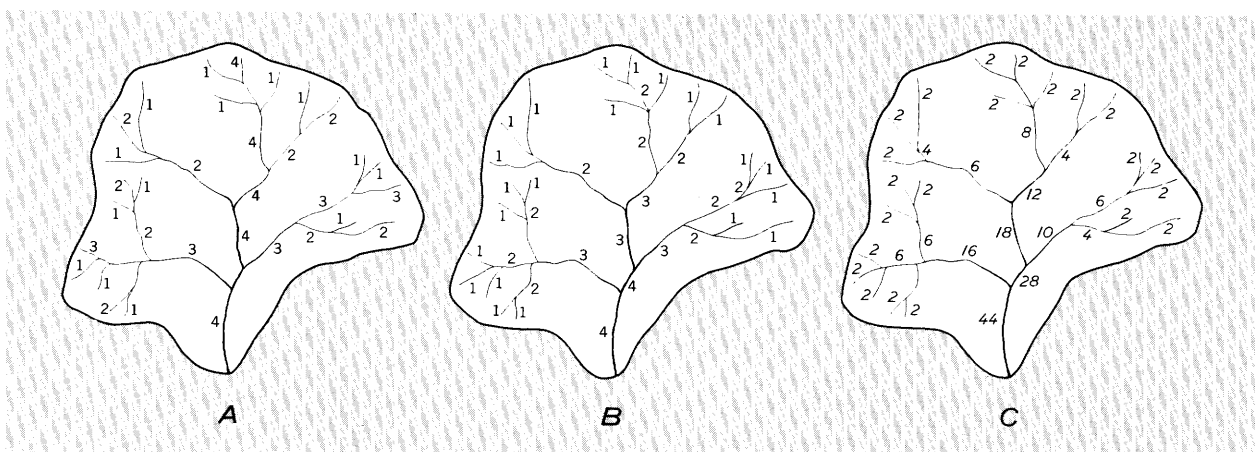


FIGURE 1.—Stream-ordering systems of Horton (A), Strahler (B), and this report (C), as applied to a hypothetical stream (in part after Bowden and Wallis, 1964). In C, the italic numbers = 2^N where N = stream order.

U.S. GEOL. SURVEY PROF. PAPER 525-B, PAGES B187-B189

of the same order. This assumption is meaningful in an idealized river system which is very regular, such as an idealized river network which consists only of the confluence of streams of the same order, combining to form a stream of the next higher order. However, real streams are more complex; many of them receive numerous tributaries of lower order. What, then, should be the order of a combined stream? As was noted above, the lower-order tributaries are ignored under the ordering systems of Horton and of Strahler. Rzhnitsyn (1964, p. 26) stated that because "... the change of the characteristics of a stream of a given order to those of the next higher order increases the numerical values of the characteristics . . . there is good reason to consider that the river changes in order also in the case when, for instance, two rivers of the III order enter consecutively into a river of IV order, so that below the inflow of the second III order stream the river changes to a V order."

The purpose of the present paper is to define a consistent algebra of stream-order numbers which will take into account the effect on the order of a stream of the inflow of lower-order tributaries.

EXPLICIT LAW FOR THE COMPOSITION OF STREAM ORDERS

The basic property of stream-order numbers is that if two "orders" N be combined [operation denoted by an asterisk (*)] the resulting stream is of order $N+1$. Hence

$$N * N = N + 1.$$

This relates algebraically the operation of combination and the operation of addition [denoted as usual by plus (+)], with respect to channels of the same order.

Other rules are needed for the combination of channels of unequal orders. Rzhnitsyn's assumption that the confluence of two streams of order $N-1$ with an N th order stream increases the order of the latter to $N+1$ is shown below to lead to a consistent algebra of stream-order numbers. The effect of other streams of still lower order must also be taken into account.

Therefore it is postulated that

$$N * (N-1) * (N-1) = N + 1.$$

Furthermore, in order that the distributive law be valid (that is, that the order in which the rivers join is immaterial), it is postulated that

$$[N * (N-1)] * (N-1) = N * [(N-1) * (N-1)];$$

and so that the commutative law be satisfied (since the

result must be the same whether an M -order river joins an N -order one, or vice versa) it is postulated that

$$N * M = M * N.$$

The above postulates define completely the algebra of combination of stream-order numbers.

Any integral N can be expressed in terms of smaller orders:

$$N = (N-1) * (N-1) = (N-2) * (N-2) * (N-2) * (N-2) \\ = M * M * M * \dots * M,$$

where the number of "factors" M is equal to 2^{N-M} . Thus we may write

$$N = M * 2^{N-M}$$

where the asterisk in the "exponent" indicates that the "multiplications" (that is combinations denoted by *) refer to confluences of streams of the indicated order.

Continuing the algebraic analysis to include hypothetical zero-order streams (which do not exist in nature),

$$N = 0 * 2^N$$

and

$$N * M = 0 * 2^N * 0 * 2^M = 0 * (2^N + 2^M).$$

Also,

$$N * M = 0 * 2^{(N * M)}.$$

Hence, setting

$$X = N * M$$

we have, from a combination of the three previous equations:

$$2^X = 2^N + 2^M$$

or

$$M * N = X = \frac{\log(2^N + 2^M)}{\log 2} \equiv \log_2(2^N + 2^M).$$

This is the general law for the composition of stream-order numbers, derived from the fundamental postulates for integer values of N and M ; by analytic continuation, it may be extended to noninteger values.

One problem facing the geomorphologist who uses stream order in his studies lies in the identification of first-order streams, which depends on the scale of the topographic map used. A stream classified from map interpretation as being of the first order might be seen in the field to be a second- or third-order stream. The stream-order composition law derived above does not depend significantly on the choice of stream to be designated as being of the first order. If the second-order streams are treated as first-order streams, then all orders

are simply reduced by one:

$$(M-1) * (N-1) = \frac{\log(2^{N-1} + 2^{M-1})}{\log 2} = \frac{\log(2^N + 2^M)}{\log 2} - 1 \\ = (M * N) - 1.$$

ANALYTICAL IMPLICATIONS OF THE STREAM-ORDERING METHODS

As was noted above, the effect of lower-order tributaries on the order of larger streams is generally neglected, and the order of a stream is assumed to change only if the stream is joined by another of the same order (fig. 1A, B). This procedure is expressed in the following algebraic statements (in which confluence is denoted by an asterisk, as previously):

$$N * M = N \text{ if } N > M \\ = M \text{ if } N < M; \text{ and} \\ = N + 1 \text{ if } N = M.$$

But these statements represent an algebra for which the distributive law does not hold. Thus,

$$[(M-1) * (M-1)] * M = M * M = M + 1 \\ (M-1) * [(M-1) * M] = (M-1) * M = M$$

In other words, two rivers of order $(M-1)$ must first combine if their confluence with an M -order river is to increase the latter's order.

Another feature of the generally accepted schemes is that "factorization" is not uniquely possible. A stream of a given order (>1) can in theory be created in an infinity of ways by combinations of lower-order streams. In nature the situation is much simpler because in most

places only a relatively small number of lower-order tributaries flow into a stream of N -order before it joins another N -order stream. Nonetheless, if the hydraulic characteristics of a river reach are to be tied to its order, it seems desirable, as Rzhnitsyn suggested, to take into account the effect of all the tributaries on the order of the main stream.

The new composition law for stream orders produces the ordering shown on figure 1C. The italic number beside each stream segment was obtained by addition of the corresponding numbers of the segments whose confluence creates the segment in question. The order of the segment is the logarithm to the base 2 of the italic number. That is, the italic number equals 2^N where N is the order of the stream. First-order streams are assigned the number 2 because where $N=1$, $2^N=2$. Once the first-order stream segments have been marked on the stream-order map, the numbers for the other segments are obtained by simple additions, and the orders by taking logarithms to the base 2.

REFERENCES

- Bowden, K. L., and Wallis, J. R., 1964, Effect of stream-ordering technique on Horton's law of drainage composition: *Geol. Soc. America Bull.*, v. 75, p. 767-774.
- Horton, R. E., 1945, Erosional development of streams and their drainage basins; hydrophysical approach to quantitative morphology: *Geol. Soc. America Bull.*, v. 56, no. 3, p. 275-370.
- Rzhnitsyn, N. A., 1964, Morphological and hydrological regularities of the structure of the river net: Translated from Russian by D. R. Krimgold, Washington, U.S. Govt. Printing Office (for U.S. Dept. Agriculture), 380 p.
- Strahler, A. N., 1957, Quantitative analysis of watershed geomorphology: *Am. Geophys. Union Trans.* v. 38, no. 6, p. 913-920.



PHOTOGRAPHIC COPYING USING REFLECTION-TRANSMISSION ILLUMINATION

By ERNEST P. KRIER, Denver, Colo.

Abstract.—Detail lost in shadow areas on photographic prints can be salvaged, for reproduction, by a copy process using transmitted light or a combination of transmitted and reflected light.

Quality and detail in photographic copies of prints can be improved by using a combination of transmitted and reflected light. Most photographic copy negatives made from prints are made with reflected light and at best can show only the same detail as the original prints viewed in reflected light. Much additional detail is apparent on many prints when they are viewed with predominantly transmitted light; black shadow areas become lighter, and contrasting tones appear. Prints made from copy negatives photographed with transmitted or a balanced combination of transmitted and reflected light generally have more detail in shadow areas than the original prints (Denstman and Schultz, 1963, p. 103).

When reflected light is used, contrasting tones on a photographic print are obtained by a two-stage process of absorption by silver grains in the emulsion: first as light travels through the emulsion toward the paper backing, and second as it is reflected from the paper back through the emulsion and toward the viewer. The effect is thus proportional to the square of the absorption by the silver image (fig. 1). When transmitted light is used, this absorption occurs only once, and the apparent density is reduced by a factor proportional to the amount of absorption. Thus, the use of transmitted light (or a combination of transmitted and reflected light) opens up shadow areas but retains detail in light areas and is ideal for the best rendition of tones and detail in a copy print.

Equipment for copying by the use of both reflected and transmitted light is easily arranged by combining a source for transmitted light—such as a contact printer, light table, or viewing box—with a source for reflected light—photoflood lamps (fig. 2). Voltage regulators can be used to balance the light sources.

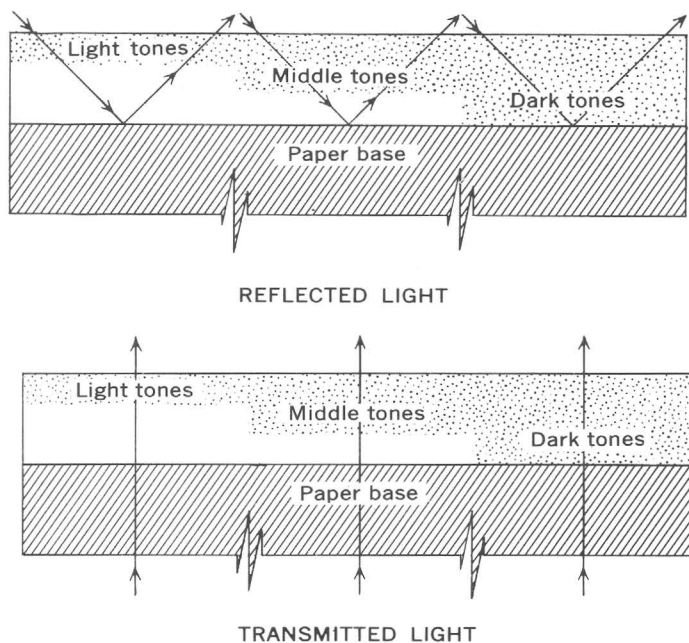


FIGURE 1—Schematic diagrams showing reflection of light from a photographic print (top) and transmission of light through a photographic print (bottom).

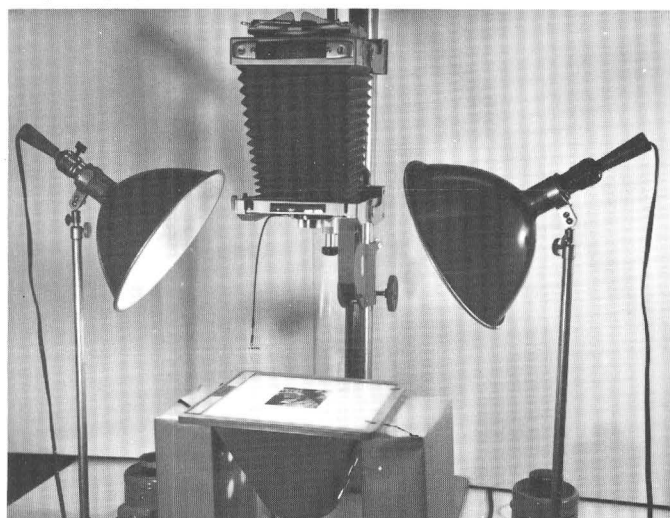


FIGURE 2.—Setup for photocopying with reflected or transmitted light or a combination of both.

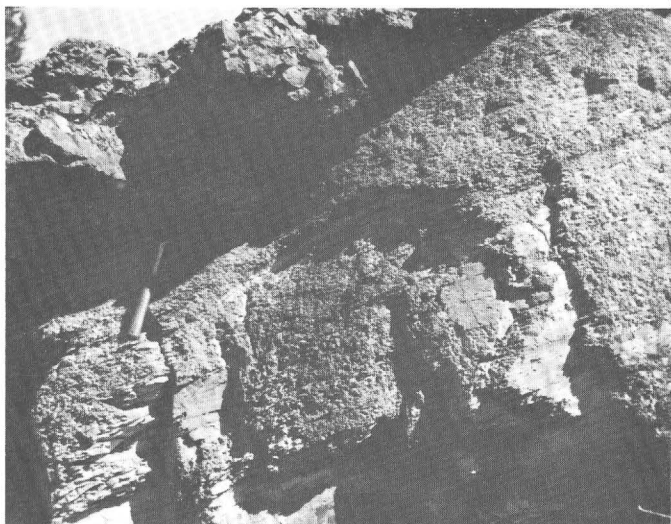


FIGURE 3.—Photocopy made with reflected light only.

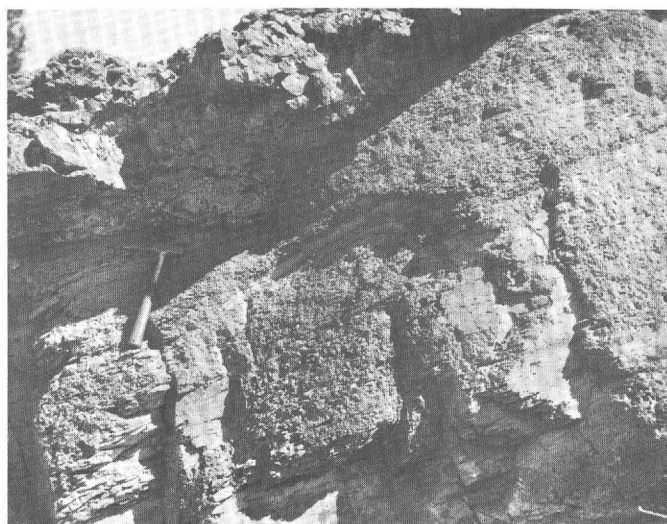


FIGURE 4.—Photocopy made with transmitted light only.

A minimum of experimenting will ordinarily produce excellent results. A copy (fig. 3) made with reflected light is a faithful reproduction of the original as viewed in reflected light. A second copy (fig. 4) made with only transmitted light shows added detail in shadow areas and is more suitable for reproduction. The copy negatives were made on the same type film, were processed similarly, and were printed on the same type of paper. With the setup shown on figure 2, either transmitted light or transmitted and reflected light together can be used to bring out the detail in photographic copies of prints. If the material to be copied is opaque, only reflected light can be used; if it is highly translucent, transmitted light alone may be used. Because most photographic prints are neither opaque nor highly translucent, a combination of reflected and trans-

mitted light usually will give the best results. Obviously, the technique is limited to use of translucent prints that have no markings on the back. Use of a "transparentizing" solution may improve the transmitted image. The technique is particularly valuable in copying Polaroid prints, for which no negatives are available. It can greatly improve the quality of reproduction not only in field photographic laboratories but also in the platemaking stage when prints are screened for reproduction.

REFERENCE

Denstman, Harold, and Schultz, M. J., 1963, *Photographic reproduction*: New York, McGraw-Hill.



SUBJECT INDEX

[For major headings such as "Economic geology," "Geophysics," "Paleontology," see under State names or refer to table of contents]

A	Page	D	Page	L	Page
Acid decomposition, refractory minerals, new apparatus.....	B165	Decomposition, refractory minerals, new apparatus.....	B165	Land subsidence, as a cause of earth cracks....	B122
Age determinations, K-Ar, Alaska.....	108				
K-Ar and Rb-Sr, Utah.....	104	E		M	
Alaska, coal, northwestern part.....	34	Electronmicroprobe analyses, copper in meteorites.....	101	Magnetic susceptibility, use in identifying basalt flows.....	142
geochronology, southeastern coast.....	108	Evaporites. <i>See</i> Salt, Gypsum.		Maryland, gravel resources, Montgomery and Prince Georges Counties.....	39
glacial geology, Alaska Range.....	112	F		<i>Mathevia</i> , Cambrian, Nevada-California.....	73
stratigraphy, northwestern part.....	34	Feldspar ratios, use in classification of igneous rocks.....	79	Mercury, Idaho, Big Creek-Yellow Pine area.....	23
Alumina, leachable, in streambed clay.....	170	Florida, petrography, land-pebble phosphate district.....	91	Meteorites, stony, metallic copper content.....	101
Antimony, Idaho, Big Creek-Yellow Pine area.....	23	G		Microanalysis, X-ray fluorescence, of silicates.....	155
Appalachian Mountains, paleobotany, Pennsylvania.....	64	Gamma activation device, for beryllium analysis.....	151	Mississippian, Alaska, coal.....	34
structural geology, southern part.....	49	Georgia, structural geology, northern part.....	49	Mohorovicic discontinuity, relation to basalt-eclogite transformation zone.....	1
Arizona, geomorphology, southern part.....	122	Geysers, water circulation, tracing.....	184	Mollusks, Cambrian, Nevada-California.....	73
Automation, of spectrochemical analysis.....	160	Glaciers, rate of movement of Teton Glacier, Wyo.....	137	Montana, stratigraphy, southwestern part....	54
		rock, Alaska.....	112		
B		Glacial troughs, age and origin, Washington..	132	N	
Basalt-eclogite transformation, crust, Western United States.....	1	Glass, silicic, in ash-flow sheet.....	85	Nevada, paleontology, southern part.....	73
Basalt flows, identification by magnetic properties.....	142	Gold Flat Member, Thirsty Canyon Tuff, Nevada, petrology.....	85	petrology, Nevada Test Site.....	85, 142, 146
Basin-range structure, effect on calderas.....	43	Gravel deposits, dissected, Chile.....	117	structural geology, Nevada Test Site.....	43
Beryllium, quantitative analysis, new device.....	151	Maryland, Montgomery and Prince Georges Counties.....	39	New Jersey, surface water, Great Swamp....	177
Biotite, age determination, Utah.....	104	Gravity studies, Colorado.....	9		
Bomb, for decomposition of minerals, new design.....	165	Gullying, earth cracks as a cause.....	122	O	
Bone Valley Formation, Florida, phosphate ..	91	Gypsum, occurrence and origin, Virginia.....	29	Ohio, glacial geology, Cincinnati area.....	126
		H		Ostracodes, classification of Healdiacea.....	69
C		Hawaii, seismology, island of Hawaii.....	13		
Calderas, gravity studies, Colorado.....	9	Hawthorn Formation, Florida, phosphate.....	91	P	
structural geology, Nevada.....	43	Healdiacea, ostracode superfamily, classification.....	69	Paintbrush Tuff, Nevada, determining porosity.....	146
California, paleontology, southeastern part ..	73	Hot springs, water circulation, tracing.....	184	Paleozoic, Alaska, geochronology.....	108
petrology, southern part.....	96			<i>See also</i> Cambrian, Mississippian.	
Cambrian, Nevada-California, paleontology..	73	I		Pantellerite ash-flow sheet, Nevada.....	85
Carmel Formation, Utah, geochronology.....	104	Idaho, economic geology, Big Creek-Yellow Pine area.....	23	Patuxent Formation, Maryland, gravel deposits.....	39
Cenozoic, Chile, geomorphology.....	117	Igneous rocks, method of classification.....	79	Pennsylvania, paleobotany, south-central part.....	64
<i>See also</i> Tertiary, Pleistocene, Recent.				Phosphate, in natural waters, field and laboratory determination.....	167
Chile, geomorphology, northern part.....	117	J		precipitation and recycling.....	91
Chondrites, metallic copper content.....	101	Jurassic, Utah, geochronology.....	104	Phosphomolybdic acid, in the determination of phosphate in natural water....	167
Cinnabar. <i>See</i> Mercury.				Photographs, copies, new process to increase detail.....	190
Classification, paleontologic, ostracodes.....	69	K		Pleistocene, Ohio-Kentucky, glacial geology..	126
petrologic, igneous rocks.....	79	Kentucky, glacial geology, northern part.....	126	Washington, glacial geology.....	132
Clay, streambed, silica and alumina content..	170	structural geology, southeastern part.....	49	Pollen, Cretaceous, use in dating clay.....	64
Clinchport thrust fault, southern Appalachian Mountains, redefinition.....	49			Porosity, of tuff, determining best value.....	146
Coal, Alaska, Lisburne Peninsula.....	34			Potassium-argon age determinations.....	104, 108
Colorado, geophysics, Bonanza mining area...	9			<i>Pseudophanasymmetria</i> , ostracode genus, classification.....	69
Computers, potential use in spectrochemical analysis.....	160				
Conasauga Group, facies changes, Tennessee and Virginia.....	49				
Copies, photographic, new process to increase detail.....	190				
Copper, metallic, in stony meteorites.....	101				
Cretaceous, Pennsylvania, paleobotany.....	64				
Montana, stratigraphy.....	54				
Crustal studies, Western United States.....	1				

R	Page
Recent, Alaska, rock glaciers.....	B112
Reflection-transmission illumination, use in copying photographs.....	190
Refractory minerals, acid decomposition.....	165
Rivers, new system of numbering stream order.....	187
Rock glaciers, Alaska.....	112
Rubidium-strontium age determinations.....	104

S	Page
Salt, occurrence and origin, Virginia.....	29
Salt cedar, effect on river channels.....	175
Seismic studies, island of Hawaii.....	13
Silica, leachable, in streambed clay.....	170
Silicates, X-ray fluorescence analysis.....	155
Silicic igneous rocks, classification.....	79
Sodium iodide, use as tracer in water.....	184
Southern California batholith, tantalum distribution.....	96
Spectrochemical analysis, suggested automation.....	160
Spores, Cretaceous, use in dating clay.....	64
Stibnite. <i>See</i> Antimony.	

	Page
Stream order, new numbering system.....	B187
Streambed sediments, leachable silica and alumina.....	170
Streamflow, effect of swamps.....	177
Swamps, effect on streamflow.....	177

T

Tantalum, distribution in igneous rocks.....	96
Tennessee, stratigraphy, Mascot-Jefferson City mining district.....	17
structural geology, eastern part.....	49
zinc, Mascot-Jefferson City mining district.....	17
Tertiary, Colorado, geophysics.....	9
Montana, stratigraphy.....	54
Nevada, petrology.....	85, 142
structural geology.....	43
Texas, surface water, western part.....	175
Thirsty Canyon Tuff, Nevada, petrology.....	85
Transmission-reflection illumination, use in copying photographs.....	190
Tuff, lapilli, determining porosity.....	146

U

	Page
Utah, geochronology, eastern and southwestern parts.....	B104

V

Virginia, salt and gypsum, southwestern part.....	29
stratigraphy, southwestern part.....	29
structural geology, southwestern part.....	49

W

Washington, glacial geology, Puget Sound.....	132
West Virginia, structural geology, southeastern part.....	49
Western United States, crustal studies.....	1
Wyoming, geochemistry, Yellowstone Park.....	184
glaciology, Teton Glacier.....	137

X, Z

X-ray fluorescence analysis, of silicates.....	155
Zinc, correlation of abundance with rock thickness.....	17

AUTHOR INDEX

A	Page
Altschuler, Z. S.	B91
B	
Brett, Robin	101
Brew, D. A.	108
Byers, F. M., Jr.	43
C	
Christiansen, R. L.	43
Cramer, W. G.	151
Crandell, D. R.	132
Cuttitta, Frank	155
D	
Dinnin, J. I.	96
Duke, M. B.	101
E	
Endo, E. T.	13
F	
Fishman, M. J.	167
Foster, H. L.	112
Fournier, R. O.	184
G	
Gottfried, David	96
Grozier, R. U.	175
H	
Harris, L. D.	49
Helz, A. W.	160
Holmes, G. W.	112

K	Page
Kam, William	B122
Karig, D. E.	9
Koyanagi, R. Y.	13
Krier, E. P.	190
L	
Lanphere, M. A.	108
Larson, R. R.	155
Leighton, M. M.	126
Leonard, B. F.	23
Letner, Raymond	165
Lipman, P. W.	43
Loney, R. A.	108
M	
McAllister, J. F.	73
Mallory, E. C., Jr.	170
Manger, G. E.	146
Marie, J. R.	17
Marvin, R. F.	104
May, Irving	165
Miller, E. G.	177
Morey, G. W.	184
Mullineaux, D. R.	132
N	
Noble, D. C.	85
O	
O'Connor, J. T.	79
Orkild, P. P.	43
P	
Pakiser, L. C.	1

R	Page
Ray, L. L.	B126
Reed, J. C., Jr.	137
Reso, Anthony	73
Roberts, A. E.	54
Rose, H. J., Jr.	155
Rowe, J. J.	165, 184
S	
Sargent, K. A.	142
Scheidegger, A. E.	187
Seegerstrom, Kenneth	117
Sharp, W. N.	151
Skougstad, M. W.	167
Sohn, I. G.	69
T	
Tailleur, I. L.	34
Tschudy, R. H.	64
V	
Vaughn, W. W.	151
W	
Waldron, H. H.	132
Walthall, F. G.	104
Wedow, Helmut, Jr.	17
Withington, C. F.	29, 39
Wright, J. C.	104
Y	
Yochelson, E. L.	73

